# SYNTHESIS AND PRECLINICAL EVALUATION OF PEPTIDE RECEPTOR-TARGETED DIAGNOSTIC AND THERAPEUTIC RADIOPHARMACEUTICALS FOR PROSTATE CANCER

---

A Dissertation

presented to

the Faculty of the Graduate School

at the University of Missouri-Columbia

---

In partial fulfillment of the requirements for the degree

Doctor of Philosophy

---

Submitted by

**NKEMAKONAM CHUKWUEBUKA OKOYE**

Under the Supervision of

Professor Silvia S. Jurisson and Professor Timothy J. Hoffman

MAY 2019

The undersigned, appointed by the dean of the Graduate School at the University of Missouri-Columbia, have examined the dissertation entitled

***Synthesis and Preclinical Evaluation of Peptide Receptor-targeted Diagnostic and Therapeutic Radiopharmaceuticals for Prostate Cancer***

presented by Nkemakonam C. Okoye, a candidate for the degree of Doctor of Philosophy in Chemistry, and hereby certify that, in their opinion, it is worthy of acceptance.

_____

Professor Silvia S. Jurisson

_____

Professor Timothy J. Hoffman

_____

Professor Heather M. Hennkens

_____

Professor J. David Robertson

_____

Professor Gary A. Baker

# Dedication

This dissertation is dedicated to my lovely parents, Sir Josiah Okoye and Lady Charity Okoye, for their selfless sacrifice in ensuring that I got a good education.

# Acknowledgments

I am very grateful to my advisors, Dr. Silvia Jurisson and Dr. Timothy Hoffman for their incredible support, encouragement, mentorship and guidance throughout my graduate studies. I owe the success of the research described in this dissertation to their dedication in nurturing me into a competent scientist by patiently teaching me the skills and expertise needed to be successful in my research. I will like to specially acknowledge Tammy Rold for her contributions towards the *in vitro* cell studies and *in vivo* mice studies described in this dissertation. Also, special thanks to Ashley Berendzen for her contributions to the mice SPECT/CT imaging studies. Tammy and Ashley made the times I spent over in the Hoffman research labs at the Harry S. Truman VA Hospital very memorable and I am truly grateful. The members of my graduate committee, Dr. Heather Hennkens, Dr. J. David Robertson and Dr. Gary Baker, provided very thoughtful insights that assisted me in critically thinking about my research. I will also like to thank other individuals that contributed to the success of my research including Dr. Fabio Gallazzi (LC-MS facility), James Guthrie (ICP-MS facility at MURR), Dr. John Lydon (help with HPGe studies and $^{105}$Rh production), Dr. Wei Wycoff (NMR facility), and members of the radiopharmaceutical group at MURR (Mary Embree, Marina Kuchuk and Daniel Oconnor). Also, I will like to acknowledge present and past members of the Jurisson research group for their support and for providing an intellectually stimulating environment during my studies. Thank you to the University of Missouri-Columbia (MU), MU Department of Chemistry, MU Research Reactor (MURR), and the Research Division at the Harry S. Truman Memorial VA Hospital for providing the necessary facilities, equipment and financial support for my research. The work described here was supported

in part by grant funding from The United States Department of Veterans Affairs (VA Merit Award # 1I01BX001699 and VA Research Career Scientist Award to Timothy Hoffman), The National Cancer Institute (NCI-RO1 Award # CA222293) and The Society of Nuclear Medicine and Molecular Imaging (2018 Bradley-Alavi Student Fellowship to Nkemakonam Okoye).

To my parents, Sir Josiah Okoye and Lady Charity Okoye, thank you for your constant love, support, and prayers. I am grateful to my siblings (Chisom, Jideofor, Olisa and Ezinne) and my amazing friends for their encouragement and moral support. I also acknowledge Dr. Kenneth Okafor and his family for their incredible support and for being my family in the United States. Finally, I am grateful to God for His grace and for blessing me with life, good health, and a sound mind, without which I would not have done any of this work.

# Table of Contents

# List of Illustrations

## List of Figures

## Chapter 3

## Chapter 4

# List of Tables

**Page**

**Chapter 2**



**Chapter 3**

# List of Schemes



# List of Equations

# Academic Abstract

The overexpression of certain peptide receptors on cancers cells can be exploited for the development of radiopharmaceuticals that are selectively delivered to cancer cells for diagnostic imaging or therapeutic purposes. Parts of this dissertation explore the development and preclinical evaluation of a radiolabeled antagonist peptide conjugate (RM2 = DOTA-4-amino-1-carboxymethyl-piperidine-D-Phe-Gln-Trp-Ala-Val-Gly-His-Sta-Leu-$NH_2$) that targets the bombesin receptor (BB2r) overexpressed in human prostate cancer. Two radionuclides, $^{203}$Pb and $^{212}$Pb, were selected due to their uniqueness as a chemically identical theranostic matched pair. Lead-203 ($t_{1/2}$ = 51.9 hours) decays by electron capture to stable $^{203}$Tl, with the emission of 278 keV gamma rays (81% intensity) suitable for single-photon emission computed tomography (SPECT) imaging. On the other hand, $^{212}$Pb ($t_{1/2}$ = 10.6 hours) decays by beta emission into $^{212}$Bi ($t_{1/2}$ = 60.6 minutes), which subsequently decays into stable $^{208}$Pb through a branched decay chain consisting of one alpha particle and one beta particle emission in each decay pathway. Hence, $^{212}$Pb is of interest as an *in vivo* generator of $^{212}$Bi for targeted alpha therapy. The fundamental chemistry and radiochemistry involved in the synthesis, purification and characterization of both [$^{203}$Pb]Pb-RM2 and [$^{212}$Pb]Pb-RM2 is described. Additionally, *in vivo* preclinical evaluation of the radiolabeled peptide conjugates was performed in male mouse models inoculated with PC3 human prostate cancer cells.

The last portion of the work described in this dissertation focuses on $^{105}$Rh as a potential therapeutic radionuclide. Rhodium-105 ($t_{1/2}$ = 35.4 hours) is a moderate energy beta-emitting radionuclide [$\beta^-_{avg}$ = 152 keV], with low energy gamma emissions [319 keV (19%) and 306 keV (5%)]. The production of $^{105}$Rh from recycled $^{104}$Ru metal target via

the $^{104}Ru$ (p, n) $^{105}Ru$ ➔ $^{105}Rh$ reaction was reported. In addition, a microwave-assisted procedure for the synthesis of Rh(III) complexes without the addition of refluxing ethanol or $SnCl_2$ as reducing agents is described.

# CHAPTER 1: General Introduction

## 1.1. Radiopharmaceuticals as a Tool in Cancer Diagnosis and Therapy

Simply put, a radiopharmaceutical is a radioactive drug. Radiopharmaceuticals have emerged as a very useful tool for physicians in the fight against cancer by revolutionizing the ability to non-invasively detect, stage, treat, and monitor the progression of cancer. Similar to other pharmaceutical drugs, the development of a new radiopharmaceutical is a long and complex process that involves a great deal of interdisciplinary research. This process typically includes understanding the disease at a molecular level, identifying molecular targets specific to the disease, designing a lead compound that has a desired influence on the identified molecular target, optimizing the lead compound to meet minimal toxicity and favorable pharmacokinetics, and performing numerous preclinical and clinical trials to ascertain the safety and efficacy of the drug in humans.

Nevertheless, the radiopharmaceutical drug development process is uniquely different from that of a conventional pharmaceutical drug. This difference stems mainly from the fact that the key component in a radiopharmaceutical is the radionuclide, whose nuclear properties (e.g., half-life, type of radioactive decay, etc.) determine the clinical utility of the drug. Unfortunately, scientists have no control over the nuclear properties of a radionuclide; hence the choices for clinically-relevant radionuclides are limited. In some cases, the initial chemical form of the radionuclide may create additional challenges that would not have been otherwise encountered for conventional pharmaceutical development.

Despite these challenges, several radiopharmaceuticals have been successfully developed and are currently being used in patient care.

For a new radiopharmaceutical to be successful, it must fulfill one of two clinical needs: (1) be used as diagnostic agent or (2) be used as a therapeutic agent. Diagnostic radiopharmaceuticals require radionuclides that emit either gamma ($\gamma$) rays or positrons ($\beta^+$). Gamma rays are electromagnetic radiation, which minimally interact with body tissues and can easily penetrate the body, enabling them to be externally detected by radiation detectors. Gamma ray-emitting radionuclides (e.g., $^{99m}$Tc, $^{111}$In, $^{201}$Tl, $^{203}$Pb, etc.) are useful for single photon emission computed tomography (SPECT), where the gamma rays are detected by a single or a pair of lead-collimated radiation detectors (typically NaI(Tl) scintillation detectors).[1] On the other hand, positrons are positively charged electrons emitted from the nucleus of proton-rich nuclides. Positrons interact with negatively charged electrons through a process called positron annihilation to produce two coincident 511 keV photons approximately 180° apart. Positron-emitting radionuclides (e.g., $^{18}$F, $^{89}$Zr, $^{68}$Ga, etc.) are useful for positron emission tomography (PET), where the 511 keV annihilation photons are detected in coincidence by a ring of scintillation radiation detectors (e.g., lutetium oxyorthosilicate, LSO), which allows for the use of electronic collimation to distinguish between true and interfering photons.[1] In both SPECT and PET imaging modalities, mathematical algorithms are utilized to reconstruct a 3D image showing the distribution of the radionuclide in the body.[1]

In contrast, therapeutic radiopharmaceuticals require radionuclides that emit ionizing particulate radiation, such as alpha ($\alpha$) particles, beta ($\beta^-$) particles, or Auger electrons. Alpha particles are the same as a helium nucleus consisting of two protons, two

neutrons and have a +2 charge. Alpha particles are predominantly emitted by high mass radionuclides ($A \geq 210$). Beta particles are negative electrons ejected from a neutron-rich nucleus. Auger electrons are low energy (0.1 – 1 keV) orbital electrons that are emitted by radionuclides that decay by either electron capture or internal conversion. Alpha particles, beta particles and Auger electrons all strongly interact with target tissues (e.g., cancerous tumor) and lead to extensive localized ionization, which can damage chemical bonds in DNA molecules and potentially induce cytotoxicity.[2]

For most nuclear medicine applications, it is desired that a diagnostic radiopharmaceutical be coupled with a therapeutic radiopharmaceutical. This concept is commonly known as "theranostics".[3] It is important that the chemical and pharmacokinetic behaviors of both the diagnostic and therapeutic radiopharmaceuticals match. Ideally, the diagnostic and therapeutic radionuclides are a chemically identical radioisotope pair (also known as "matched pair"). The most well-known matched pair for theranostic radiopharmaceutical application is the $^{123}$I/$^{131}$I pair, where $^{123}$I-labeled compounds (e.g., [$^{123}$I]NaI capsules) are used for diagnosis, while $^{131}$I-labeled compounds (e.g., [$^{131}$I]NaI capsules) are used for therapy. Another promising theranostic matched pair is the $^{203}$Pb/$^{212}$Pb pair, which is the focus of Chapters 2 and 3, respectively. Alternatively, radionuclide pairs from different elements can be utilized for theranostic radiopharmaceutical development provided that their chemistry is very similar (e.g., $^{99m}$Tc/$^{186/188}$Re) and there is no significant difference in the pharmacokinetic behavior between the diagnostic and therapeutic analogues. A good example is the $^{68}$Ga/$^{177}$Lu pair, where $^{68}$Ga is used for diagnosis and $^{177}$Lu is used for therapy. The $^{68}$Ga/$^{177}$Lu pair has been utilized in the development of two FDA-approved radiopharmaceuticals, [$^{68}$Ga]Ga-

Dotatate (NETSPOT™)[4] and [$^{177}$Lu]Lu-Dotatate (LUTATHERA®)[5], for the diagnosis and treatment of gastroenteropancreatic neuroendocrine tumors, respectively.

## 1.2. Radiopharmaceutical Design

Some radionuclides possess an intrinsic affinity to certain organs/tissues due to their physiological properties. These radionuclides can therefore be used as radiopharmaceuticals by direct administration of the anionic or cationic salt. For example, iodine is primarily absorbed in the thyroid and is essential for the formation thyroid hormones. Therefore, radioactive iodine capsules ([$^{131}$I]NaI) are administered for the treatment of thyroid cancer. Similarly, radium acts as a calcium mimic and readily forms complexes with the bone mineral, hydroxyapatite. Therefore, radioactive radium salt ([$^{223}$Ra]$RaCl_2$) is used for the treatment of bone metastases. Other radiopharmaceuticals require that the radionuclide be incorporated into a biologically-active targeting molecule for it to be delivered to a specific target organ/tissue. This can be accomplished by two methods: the integrated method (also direct labeling method) and the bifunctional chelate (BFC) method. In the integrated method, the radionuclide is an integral part of the biologically-active molecule and is directly incorporated into it. This method is predominantly utilized in radiopharmaceuticals containing non-metallic radionuclides (e.g., [$^{18}$F]fluorodeoxyglucose, [$^{11}$C]choline, etc.). However, radiopharmaceuticals containing metallic radionuclides have also been developed using the integrated method (e.g., [$^{99m}$Tc]Tc-Sestamibi, [$^{99m}$Tc]Tc-methylene diphosphonate, etc.). The BFC method is predominantly utilized in radiopharmaceuticals containing metallic radionuclides. The radiometal is tightly bound to a suitable bifunctional chelator that has been covalently conjugated to a targeting vector (e.g., peptides, proteins, antibodies, etc.) through a linker

or spacer, as shown in **Figure 1-1**. The targeting vector serves as the vehicle for delivery of the radionuclide to the organ/tissue of interest. Targeting vectors localize at their biological targets through various mechanisms including receptor binding, antigen/antibody reactions, etc.

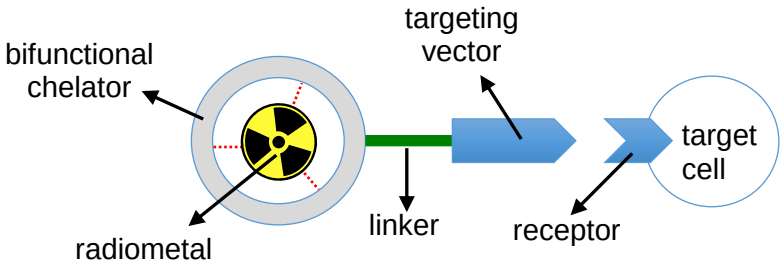


**Figure 1-1**. Schematic of the bifunctional chelate (BFC) method

## 1.3. Targeted Alpha Therapy

Out of all the therapeutic radiations (i.e., $\alpha$, $\beta^-$, and Auger electrons), alpha particles have the greatest biological effectiveness because of their high linear energy transfer (LET) properties (~100 keV/μm), which is a result of their densely ionizing track and short path length (50-100 μm) in tissues.[6-8] Due to their high LET, a few alpha particles (between 1 and 20) traversing through a cancer cell can induce irreparable double-strand DNA breakage, subsequently resulting in cell death through a number of mechanisms including apoptosis, autophagy, and necrosis.[6-7] In contrast, low LET radiation like beta particles (~0.2 keV/μm) produce mainly single-strand DNA breakage, which has a lower cytotoxic effect. The cytotoxic effect of alpha particles has been shown to be independent of dose rate and tissue oxygen levels, which makes them effective against hypoxic tumors.[6, 9]

The cytotoxic superiority of alpha particles over beta particles has been demonstrated in several preclinical studies. *In vitro* studies comparing $^{213}$Bi, an alpha-emitting radionuclide, with $^{177}$Lu, a beta-emitting radionuclide, demonstrated that $^{213}$Bi has significantly greater cytotoxic potency.[10-11] Greater DNA double-strand breaks, as quantified by immunofluorescence staining of γH2AX-foci, was observed for [$^{225}$Ac]Ac-DOTATOC compared to [$^{177}$Lu]Lu-DOTATOC.[12] Wild et al.[13] reported that the median survival time of mouse models bearing human prostate carcinoma (PC3) xenografts was increased by about 15 weeks when treated with [$^{213}$Bi]Bi-DOTA-PESIN compared to [$^{177}$Lu]Lu-DOTA-PESIN.

The first reported clinical trial for alpha particle radioimmunotherapy was performed using $^{213}$Bi-labeled HuM195 (a humanized anti-CD33 monoclonal antibody) for the treatment of myeloid leukemia, where therapeutic response in 14 out of the 15 evaluated patients was reported.[14] In another study, long-lasting therapeutic response was reported after administration of [$^{213}$Bi]Bi-DOTATOC to patients who were refractory to prior treatment with the beta-emitting compounds ([$^{90}$Y]Y-DOTATOC and [$^{177}$Lu]Lu-DOTATOC).[15] Studies using $^{211}$At-labeled antibodies have shown positive clinical outcomes for the treatment of glioblastoma[16] and ovarian cancer.[17-19] The safety and therapeutic efficacy of [$^{212}$Pb]Pb-TCMC-trastuzumab in patients with HER2-positive peritoneal malignancies has been recently demonstrated in clinical studies by Meredith et al.[20-22] Perhaps the alpha-emitting radionuclide that has gained the most attention in the past five years is $^{225}$Ac. This increased attention is partly due to the remarkable therapeutic outcomes observed after administration of [$^{225}$Ac]Ac-PSMA-617 to patients with

metastatic castration-resistant prostate cancer who failed to respond to prior treatment with [$^{177}$Lu]Lu-PSMA-617.[23-25]

In a recent phase III clinical trial, treatment with [$^{223}$Ra]$RaCl_2$ resulted in significant survival benefits in men with bone metastases resulting from castration-resistant prostate cancer.[26] This study subsequently led to the FDA approval of [$^{223}$Ra]$RaCl_2$ (Xofigo®), which is currently the only FDA-approved alpha-emitting radiopharmaceutical.

## 1.4. Alpha-emitting Radionuclides of Clinical Relevance

Based on the promising preclinical and clinical studies supporting the cytotoxic superiority of alpha particles over beta particles, there has been an increased interest for alpha-emitting radionuclides that are useful for targeted alpha therapy.[8, 27-28] The most promising clinically-relevant alpha-emitting radionuclides are discussed below.

### 1.4-1. Astatine-211

Astatine-211 ($t_{1/2}$ = 7.2 hours) decays through a branched pathway into stable $^{207}$Pb with the net emission of one alpha particle through each decay pathway (**Figure 1-2**). Astatine-211 is cyclotron produced by bombarding a bismuth target with alpha particles (~28 MeV) via the $^{209}$Bi($\alpha$, 2n)$^{211}$At reaction.[29-30] Unfortunately, very few cyclotron facilities have the capability of generating > 25 MeV alpha particles, which has greatly limited the availability of $^{211}$At. The lack of stable astatine isotopes has limited the understanding of astatine chemistry. As a member of the halogen family, the chemical properties of astatine are believed to be similar to iodine; however, astatine exhibits more metallic characteristics.[31] A major concern with $^{211}$At radiopharmaceuticals is *in vivo* stability due to the relatively weak carbon-astatine bond strength, which can lead to

deastatination and subsequent physiological accumulation of free astatine in thyroid and stomach.[32] In addition, the presence of a relatively long-lived daughter radionuclide from $^{211}$At decay ($^{207}$Bi, $t_{1/2}$ = 31.5 years) is not ideal.

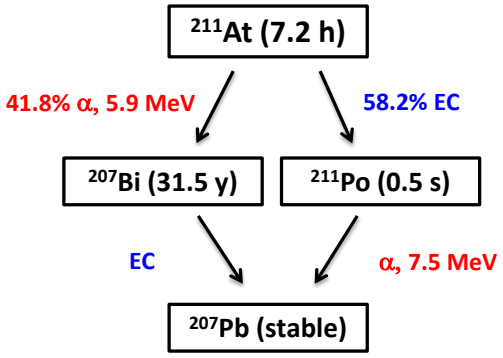


**Figure 1-2**. Astatine-211 decay chain

## 1.4-2. Radium-223

Radium-223 ($t_{1/2}$ = 11.4 days) decays into stable $^{207}$Pb through a series of intermediate daughter radionuclides, with the net emission of four alpha particles and two beta particles in its decay pathway (**Figure 1-3**). Radium-223 is obtained as a product of $^{227}$Th decay, which is the daughter radionuclide from $^{227}$Ac decay. As an alkaline earth metal, $^{223}$Ra has similar chemical properties to calcium and readily accumulates in the inorganic bone matrix through complexation to the bone mineral, hydroxyapatite.[26] This property of $^{223}$Ra was exploited for the development of [$^{223}$Ra]$RaCl_2$ (Xofigo®) for the treatment of bone metastases resulting from castration-resistant prostate cancer.[26] The application of $^{223}$Ra for the development of radiopharmaceuticals that target other diseases has been challenging due to the lack of suitable bifunctional chelators for $^{223}$Ra complexation.

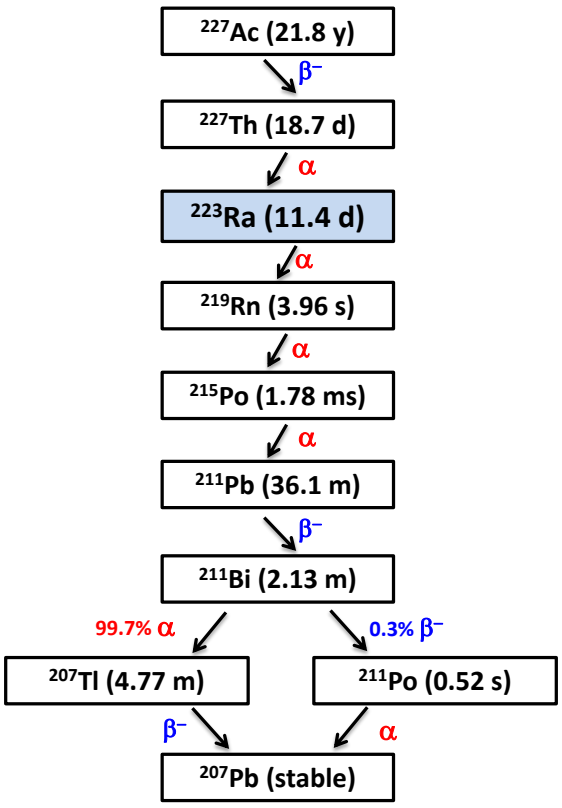


**Figure 1-3**. Radium-223 decay chain

### 1.4-3. Actinum-225 / Bismuth-213

Actinium-225 ($t_{1/2}$ = 9.9 days) is a member of the $^{233}$U decay chain (**Figure 1-4**). Actinium-225 decays into $^{213}$Bi ($t_{1/2}$ = 45.6 minutes) through two intermediate alpha-emitting daughter radionuclides ($^{221}$Fr and $^{217}$At). Bismuth-213 subsequently undergoes a branched decay into stable $^{209}$Bi, with the emission of one alpha particle and two beta particles through each decay pathway. Therefore, the decay of $^{225}$Ac into stable $^{209}$Bi results in the net emission of four alpha particles and two beta particles. Both $^{225}$Ac and $^{213}$Bi are being investigated for the development of targeted alpha radiopharmaceuticals; however, the short half-life of $^{213}$Bi poses a challenge during the radiopharmaceutical synthesis and purification process. Using $^{225}$Ac as an *in vivo* generator of $^{213}$Bi overcomes the challenges

associated with the short half-life of $^{213}$Bi. The current chelators of choice for the formation of $^{225}$Ac/$^{213}$Bi complexes are polyaminocarboxylic acid-based chelators, particularly DOTA (1,4,7,10-tetraazacyclododecane-1,4,7,10-tetraacetic acid) and its derivatives (**Figure 1-6, left**).

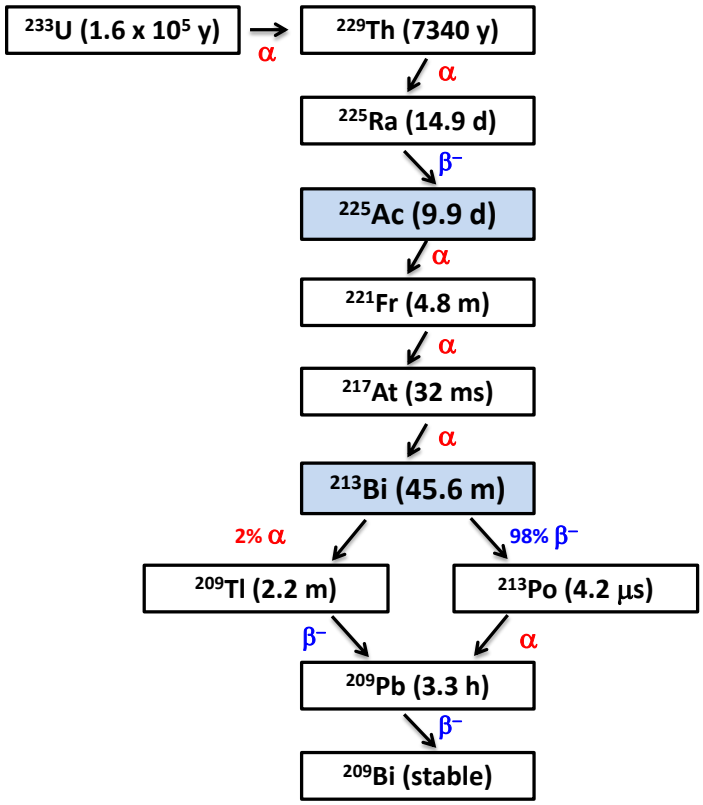


**Figure 1-4**. $^{225}$Ac / $^{213}$Bi decay chain

The primary source of $^{225}$Ac/$^{213}$Bi is from $^{229}$Th build-up resulting from $^{233}$U decay. The current estimated annual global supply of $^{225}$Ac/$^{213}$Bi from this source is 1.7 Ci (63 GBq), which will not be sufficient to meet clinical and research demands.[33] Another potential production route for $^{225}$Ac that is currently being investigated is the proton spallation of thorium targets via the $^{232}$Th(p,x)$^{225}$Ac reaction.[34-36] However, potential co-production of $^{227}$Ac ($t_{1/2}$ = 21.8 years) is of concern. Efforts have also been made to increase

the $^{229}$Th stockpile by neutron irradiation of $^{226}$Ra via the $^{226}$Ra (n,γ) $^{227}$Ra ($\beta^-$) $^{227}$Ac (n,γ) $^{228}$Ac ($\beta^-$) $^{228}$Th (n,γ) $^{229}$Th reaction.[37-38] Apostolidis et al.[39] reported the production of $^{225}$Ac in a cyclotron via the $^{226}$Ra (p, 2n) $^{225}$Ac reaction with a relatively high cross-section of 710 mb at 16.8 MeV. It is estimated that the irradiation of an ~1 g of $^{226}$Ra target with a 20 MeV proton beam at 500 μA beam current could produce a theoretical maximum of 108 Ci (4 TBq) of $^{225}$Ac per month.[33] The indirect production of $^{225}$Ac from the photonuclear transmutation of $^{226}$Ra via the $^{226}$Ra (γ, n) $^{225}$Ra ($\beta^-$) $^{225}$Ac reaction is also very promising.[40-43]

## 1.4-4. Lead-212 / Bismuth-212

Lead-212 ($t_{1/2}$ = 10.6 hours) and its daughter, $^{212}$Bi ($t_{1/2}$ = 60.6 minutes), are both members of the natural $^{232}$Th decay series (**Figure 1-5**). Lead-212 decays by beta emission into $^{212}$Bi, which subsequently undergoes a branched decay chain into stable $^{208}$Pb, with the emission of one alpha particle and one beta particle through each decay pathway. Therefore, the decay of $^{212}$Pb results in the net emission of one alpha particle and two beta particles. Similar to $^{213}$Bi, the relatively short half-life of $^{212}$Bi can be a challenging factor during the radiopharmaceutical synthesis and purification process. However, using $^{212}$Pb as an *in vivo* generator of $^{212}$Bi significantly compensates for the shorter half-life of $^{212}$Bi and allows sufficient time for the preparation, administration, and localization of the radiopharmaceutical at the target organ/tissue within the patient.[44]

The primary source for $^{212}$Pb/$^{212}$Bi is from $^{228}$Th ($t_{1/2}$ = 1.9 years), which decays into $^{224}$Ra that is subsequently used for producing $^{224}$Ra/$^{212}$Pb generators. Thorium-228 is the product of $^{232}$U decay and is also the second member of the $^{232}$Th decay series; hence, the

current availability of $^{228}$Th is dependent on $^{232}$U ($t_{1/2}$ = 68.9 years) and $^{232}$Th ($t_{1/2}$ = 1.4E10 years) stockpiles. Similar to $^{229}$Th, the availability of $^{228}$Th can potentially be increased by neutron irradiation of $^{226}$Ra via the $^{226}$Ra (n,γ) $^{227}$Ra ($\beta^-$) $^{227}$Ac (n,γ) $^{228}$Ac ($\beta^-$) $^{228}$Th reaction.[37-38, 45] Two bifunctional chelators, DOTA and TCMC [2,2',2",2"'-(1,4,7,10-tetraazacyclododecane-1,4,7,10-tetrayl)tetraacetamide], are primarily used for the complexation of $^{212}$Pb and $^{212}$Bi (**Figure 1-6**). DOTA and TCMC complexes of $^{212}$Pb and $^{212}$Bi are thermodynamically stable and do not easily dissociate at physiological pH; however, Pb-TCMC was shown to have slightly improved stability over Pb-DOTA at pH 3.5 and below.[46]

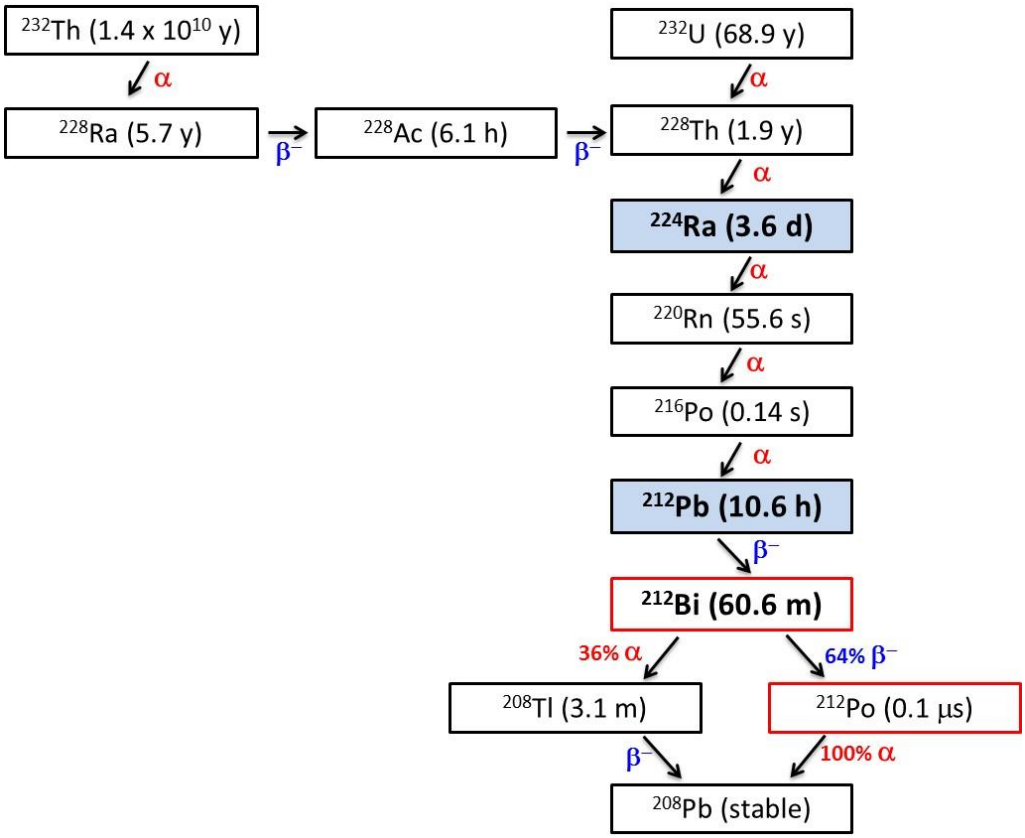


**Figure 1-5**. $^{212}$Pb / $^{212}$Bi decay chain

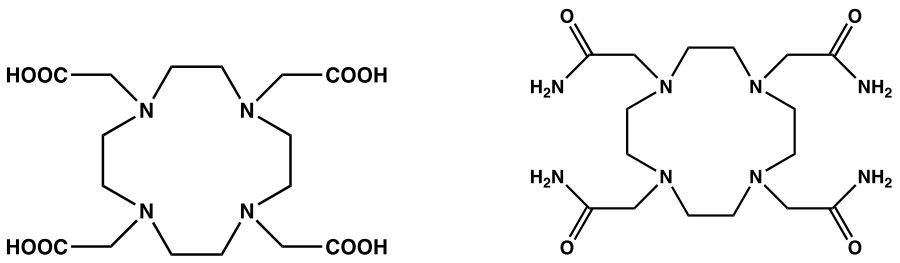


**Figure 1-6**. Chemical structures of DOTA (left) and TCMC (right)

## 1.5. Bombesin Receptors as Molecular Targets in Prostate Cancer

The gastrin-releasing peptide receptor (GRPR), also known as BB2 receptor is a cell surface transmembrane protein belonging to the family of bombesin receptors, a type of G-protein-coupled receptor possessing a seven transmembrane domain.[47] Several reports have demonstrated that the BB2 receptor is overexpressed in prostate cancer tumors.[48-52] Using *in vitro* receptor autoradiography, Körner et al. [51] observed high incidence of BB2 receptor expression in prostate carcinoma (77%, n = 60) and high grade prostatic intraepithelial neoplasia (73%, n = 55), whereas very weak expression was observed in normal prostate glands (18%, n = 111). Similarly, high BB2 receptor expression was observed in 100% (n = 30) of prostate carcinoma tissues studied by Markwalder et al. [48], with very high receptor density found in 83% of the studied tissues. The native ligand for the BB2 receptor has been identified as the gastrin-releasing peptide and was shown to bind with high affinity. The biologically active portion of the gastrin-releasing peptide is its carboxyl terminus consisting of a seven amino acid sequence (-Trp-Ala-Val-Gly-His-Leu-Met-$NH_2$). The selective overexpression of BB2 receptor in prostate cancer tumors, along with the high binding affinity of gastrin-releasing peptide analogues for the BB2 receptor, has inspired research into the development of targeted prostate cancer

theranostic radiopharmaceuticals using radiolabeled gastrin-releasing peptide analogues.[53-55]

Initial studies focused on radiolabeled gastrin-releasing peptide agonists that are internalized upon binding to BB2 receptors. Several compounds such as [$^{99m}$Tc]Tc-RP527 [56-57], [$^{177}$Lu]Lu-AMBA [58-59], [$^{177}$Lu]Lu-DOTA-PESIN,[13, 60] and [$^{111}$In]In-DOTA-X-BBN(7-14)$NH_2$ [61-62] were developed and investigated. Several clinical trials have demonstrated the safety of radiolabeled BB2 receptors agonist peptide conjugates as molecular imaging agents.[57, 63] However, in one unpublished clinical trial with [$^{177}$Lu]Lu-AMBA, side effects such as nausea, diarrhea and abdominal cramps were reported.[59] These side effects could possibly be attributed to the fact that activation of the BB2 receptor by gastrin-releasing peptide agonists can trigger a range of physiological responses like release of gastrointestinal hormones, contraction of smooth muscles in the gastrointestinal tract, and proliferation of cells.[47, 64-65] As a result, there has been a shift towards the investigation of gastrin-releasing peptide antagonists. Comparison between antagonist and agonist gastrin-releasing peptides revealed improved pharmacokinetics and tumor targeting properties with the antagonist peptides.[66-67] Of particular interest is RM2 (DOTA-4-amino-1-carboxymethyl-piperidine-D-Phe-Gln-Trp-Ala-Val-Gly-His-Sta-Leu-$NH_2$), a BB2 receptor antagonist that was shown to exhibit high and specific tumor accumulation and retention in PC3 human prostate tumor-bearing mice.[68] Clinical studies using [$^{68}$Ga]Ga-RM2 have demonstrated its high sensitivity and specificity for the detection of metastatic prostate cancer lesions in patients with biochemically recurrent disease.[69-72] Additionally, no drug related toxicity has been reported. Other BB2 receptor antagonist peptide conjugates such as NeoBOMB1 [73-74] and SB3 [75-76] have also been reported.

## 1.6. Dissertation Outline

In this work, the fundamental chemistry and radiochemistry involved in the synthesis of targeted radiopharmaceuticals are described.

Chapter 2 describes the synthesis and characterization of [$^{203}$Pb]Pb-RM2 as a potential agent for diagnostic imaging of prostate cancer. As previously mentioned, RM2 is a potent BB2 receptor antagonist peptide conjugate that binds with high affinity and specificity to the BB2 receptors overexpressed on prostate cancer cells. A method for purification of the commercially-purchased [$^{203}$Pb]$PbCl_2$ is described using a lead-selective chromatographic resin (Pb-resin). Biodistribution and *in vivo* imaging studies of [$^{203}$Pb]Pb-RM2 in male mouse models inoculated with PC3 human prostate cancer cells are also reported.

In Chapter 3, the automated synthesis of [$^{212}$Pb]Pb-RM2, the therapeutic analogue of [$^{203}$Pb]Pb-RM2, is reported. An improved method for the elution and purification of the $^{224}$Ra/$^{212}$Pb generator eluent is described. Additionally, preclinical evaluation of [$^{212}$Pb]Pb-RM2 in male mouse models inoculated with PC3 human prostate cancer cells is reported.

Finally, the fundamental chemistry, radiochemistry, and production of $^{105}$Rh from recycled $^{104}$Ru metal target via the $^{104}$Ru (p, n) $^{105}$Ru ➔ $^{105}$Rh reaction is reported in Chapter 4. A microwave-assisted method for the synthesis of Rh(III) complexes that does not require the addition of refluxing ethanol or $SnCl_2$ as reducing agents is also described.

## 1.7. References


1. Bailey, D. L.; Humm, J., *Nuclear medicine physics: a handbook for teachers and students*. IAEA: 2014.

2. Kassis, A. I.; Adelstein, S. J., Radiobiologic principles in radionuclide therapy. *Journal of Nuclear Medicine* **2005,** *46* (1 suppl), 4S-12S.

3. Yordanova, A.; Eppard, E.; Kürpig, S.; Bundschuh, R. A.; Schoenberger, S.; Gonzalez-Carmona, M.; Feldmann, G.; Ahmadzadehfar, H.; Essler, M., Theranostics in nuclear medicine practice. *OncoTargets and Therapy* **2017,** *10*, 4821.

4. Deppen, S. A.; Liu, E.; Blume, J. D.; Clanton, J.; Shi, C.; Jones-Jackson, L. B.; Lakhani, V.; Baum, R. P.; Berlin, J.; Smith, G. T., Safety and efficacy of $^{68}$Ga-DOTATATE PET/CT for diagnosis, staging, and treatment management of neuroendocrine tumors. *Journal of Nuclear Medicine* **2016,** *57* (5), 708-714.

5. Strosberg, J.; El-Haddad, G.; Wolin, E.; Hendifar, A.; Yao, J.; Chasen, B.; Mittra, E.; Kunz, P. L.; Kulke, M. H.; Jacene, H., Phase 3 trial of $^{177}$Lu-Dotatate for midgut neuroendocrine tumors. *New England Journal of Medicine* **2017,** *376* (2), 125-135.

6. Sgouros, G.; Roeske, J. C.; McDevitt, M. R.; Palm, S.; Allen, B. J.; Fisher, D. R.; Brill, A. B.; Song, H.; Howell, R. W.; Akabani, G., MIRD Pamphlet No. 22 (abridged): radiobiology and dosimetry of $\alpha$-particle emitters for targeted radionuclide therapy. *Journal of Nuclear Medicine* **2010,** *51* (2), 311-328.

7. Baidoo, K. E.; Yong, K.; Brechbiel, M. W., Molecular pathways: targeted $\alpha$-particle radiation therapy. *Clinical Cancer Research* **2013,** *19* (3), 530-537.

8. Parker, C.; Lewington, V.; Shore, N.; Kratochwil, C.; Levy, M.; Lindén, O.; Noordzij, W.; Park, J.; Saad, F., Targeted Alpha Therapy, an Emerging Class of Cancer Agents: A Review. *JAMA Oncology* **2018,** *4* (12), 1765-1772.

9. Wulbrand, C.; Seidl, C.; Gaertner, F. C.; Bruchertseifer, F.; Morgenstern, A.; Essler, M.; Senekowitsch-Schmidtke, R., Alpha-particle emitting $^{213}$Bi-anti-EGFR immunoconjugates eradicate tumor cells independent of oxygenation. *PloS One* **2013,** *8* (5), e64730.

10. Nayak, T.; Norenberg, J.; Anderson, T.; Atcher, R., A comparison of high-versus low-linear energy transfer somatostatin receptor targeted radionuclide therapy in vitro. *Cancer Biotherapy & Radiopharmaceuticals* **2005,** *20* (1), 52-57.

11. Chan, H. S.; de Blois, E.; Morgenstern, A.; Bruchertseifer, F.; de Jong, M.; Breeman, W.; Konijnenberg, M., In Vitro comparison of $^{213}$Bi-and $^{177}$Lu-radiation for peptide receptor radionuclide therapy. *PloS One* **2017,** *12* (7), e0181473.

12. Graf, F.; Fahrer, J.; Maus, S.; Morgenstern, A.; Bruchertseifer, F.; Venkatachalam, S.; Fottner, C.; Weber, M. M.; Huelsenbeck, J.; Schreckenberger, M.; Kaina, B.; Miederer, M., DNA Double Strand Breaks as Predictor of Efficacy of the Alpha-Particle Emitter Ac-

225 and the Electron Emitter Lu-177 for Somatostatin Receptor Targeted Radiotherapy. *Plos One* **2014,** *9* (2), e88239.

13. Wild, D.; Frischknecht, M.; Zhang, H.; Morgenstern, A.; Bruchertseifer, F.; Boisclair, J.; Provencher-Bolliger, A.; Reubi, J.-C.; Maecke, H. R., Alpha-versus beta-particle radiopeptide therapy in a human prostate cancer model ($^{213}$Bi-DOTA-PESIN and $^{213}$Bi-AMBA versus $^{177}$Lu-DOTA-PESIN). *Cancer Research* **2011,** *71* (3), 1009-1018.

14. Jurcic, J. G.; Larson, S. M.; Sgouros, G.; McDevitt, M. R.; Finn, R. D.; Divgi, C. R.; Ballangrud, Å. M.; Hamacher, K. A.; Ma, D.; Humm, J. L., Targeted $\alpha$ particle immunotherapy for myeloid leukemia. *Blood* **2002,** *100* (4), 1233-1239.

15. Kratochwil, C.; Giesel, F.; Bruchertseifer, F.; Mier, W.; Apostolidis, C.; Boll, R.; Murphy, K.; Haberkorn, U.; Morgenstern, A., $^{213}$Bi-DOTATOC receptor-targeted alpha-radionuclide therapy induces remission in neuroendocrine tumours refractory to beta radiation: a first-in-human experience. *European Journal of Nuclear Medicine and Molecular Imaging* **2014,** *41* (11), 2106-2119.

16. Zalutsky, M. R.; Reardon, D. A.; Akabani, G.; Coleman, R. E.; Friedman, A. H.; Friedman, H. S.; McLendon, R. E.; Wong, T. Z.; Bigner, D. D., Clinical experience with $\alpha$-particle–emitting $^{211}$At: treatment of recurrent brain tumor patients with $^{211}$At-labeled chimeric antitenascin monoclonal antibody 81C6. *Journal of Nuclear Medicine* **2008,** *49* (1), 30-38.

17. Andersson, H.; Cederkrantz, E.; Bäck, T.; Divgi, C.; Elgqvist, J.; Himmelman, J.; Horvath, G.; Jacobsson, L.; Jensen, H.; Lindegren, S., Intraperitoneal $\alpha$-particle radioimmunotherapy of ovarian cancer patients: pharmacokinetics and dosimetry of $^{211}$At-Mx35 F(ab′ )$_2$ - A phase I study. *Journal of Nuclear Medicine* **2009,** *50* (7), 1153-1160.

18. Cederkrantz, E.; Andersson, H.; Bernhardt, P.; Bäck, T.; Hultborn, R.; Jacobsson, L.; Jensen, H.; Lindegren, S.; Ljungberg, M.; Magnander, T., Absorbed doses and risk estimates of $^{211}$At-MX35 F (ab') 2 in intraperitoneal therapy of ovarian cancer patients. *International Journal of Radiation Oncology* Biology* Physics* **2015,** *93* (3), 569-576.

19. Hallqvist, A.; Bergmark, K.; Bäck, T. A.; Andersson, H.; Dahm-Kähler, P.; Johansson, M.; Lindegren, S.; Jensen, H.; Jacobsson, L.; Hultborn, R., Intraperitoneal alpha-emitting radio immunotherapy with Astatine-211 in relapsed ovarian cancer; long-term follow-up with individual absorbed dose estimations. *Journal of Nuclear Medicine* **2019**, jnumed. 118.220384.

20. Meredith, R.; Torgue, J.; Shen, S.; Fisher, D. R.; Banaga, E.; Bunch, P.; Morgan, D.; Fan, J.; Straughn, J. M., Jr., Dose escalation and dosimetry of first-in-human alpha radioimmunotherapy with $^{212}$Pb-TCMC-trastuzumab. *Journal of Nuclear Medicine* **2014,** *55* (10), 1636-42.

21. Meredith, R. F.; Torgue, J.; Azure, M. T.; Shen, S.; Saddekni, S.; Banaga, E.; Carlise, R.; Bunch, P.; Yoder, D.; Alvarez, R., Pharmacokinetics and imaging of $^{212}$Pb-TCMC-

trastuzumab after intraperitoneal administration in ovarian cancer patients. *Cancer Biotherapy & Radiopharmaceuticals* **2014,** *29* (1), 12-7.

22. Meredith, R. F.; Torgue, J. J.; Rozgaja, T. A.; Banaga, E. P.; Bunch, P. W.; Alvarez, R. D.; Straughn Jr, J. M.; Dobelbower, M. C.; Lowy, A. M., Safety and outcome measures of first-in-human intraperitoneal $\alpha$ radioimmunotherapy with $^{212}$Pb-TCMC-trastuzumab. *American Journal of Clinical Oncology* **2018,** *41* (7), 716.

23. Kratochwil, C.; Bruchertseifer, F.; Giesel, F. L.; Weis, M.; Verburg, F. A.; Mottaghy, F.; Kopka, K.; Apostolidis, C.; Haberkorn, U.; Morgenstern, A., $^{225}$Ac-PSMA-617 for PSMA-targeted $\alpha$-radiation therapy of metastatic castration-resistant prostate cancer. *Journal of Nuclear Medicine* **2016,** *57* (12), 1941-1944.

24. Kratochwil, C.; Bruchertseifer, F.; Rathke, H.; Bronzel, M.; Apostolidis, C.; Weichert, W.; Haberkorn, U.; Giesel, F. L.; Morgenstern, A., Targeted $\alpha$-Therapy of Metastatic Castration-Resistant Prostate Cancer with $^{225}$Ac-PSMA-617: Dosimetry Estimate and Empiric Dose Finding. *Journal of Nuclear Medicine* **2017,** *58* (10), 1624-1631.

25. Rahbar, K.; Ahmadzadehfar, H.; Kratochwil, C.; Haberkorn, U.; Schäfers, M.; Essler, M.; Baum, R. P.; Kulkarni, H. R.; Schmidt, M.; Drzezga, A., German multicenter study investigating $^{177}$Lu-PSMA-617 radioligand therapy in advanced prostate cancer patients. *Journal of Nuclear Medicine* **2017,** *58* (1), 85-90.

26. Parker, C.; Nilsson, S.; Heinrich, D.; Helle, S. I.; O'Sullivan, J.; Fosså, S. D.; Chodacki, A.; Wiechno, P.; Logue, J.; Seke, M., Alpha emitter radium-223 and survival in metastatic prostate cancer. *New England Journal of Medicine* **2013,** *369* (3), 213-223.

27. Kim, Y.-S.; Brechbiel, M. W., An overview of targeted alpha therapy. *Tumor Biology* **2012,** *33* (3), 573-590.

28. Mulford, D. A.; Scheinberg, D. A.; Jurcic, J. G., The promise of targeted $\alpha$-particle therapy. *Journal of Nuclear Medicine* **2005,** *46* (1 suppl), 199S-204S.

29. R Zalutsky, M.; Pruszynski, M., Astatine-211: production and availability. *Current Radiopharmaceuticals* **2011,** *4* (3), 177-185.

30. Guérard, F.; Gestin, J.-F.; Brechbiel, M. W., Production of [$^{211}$At]-astatinated radiopharmaceuticals and applications in targeted $\alpha$-particle therapy. *Cancer Biotherapy and Radiopharmaceuticals* **2013,** *28* (1), 1-20.

31. Vaidyanathan, G.; Zalutsky, M. R., Astatine radiopharmaceuticals: prospects and problems. *Current Radiopharmaceuticals* **2008,** *1* (3), 177-196.

32. Wilbur, D., [$^{211}$At]Astatine-labeled compound stability: Issues with released [$^{211}$At]astatide and development of labeling reagents to increase stability. *Current Radiopharmaceuticals* **2008,** *1* (3), 144-176.

33. Robertson, A. K.; Ramogida, C. F.; Schaffer, P.; Radchenko, V., Development of $^{225}$Ac radiopharmaceuticals: TRIUMF perspectives and experiences. *Current Radiopharmaceuticals* **2018,** *11* (3), 156-172.

34. Griswold, J. R.; Medvedev, D. G.; Engle, J. W.; Copping, R.; Fitzsimmons, J. M.; Radchenko, V.; Cooley, J.; Fassbender, M.; Denton, D. L.; Murphy, K. E., Large scale accelerator production of $^{225}$Ac: Effective cross sections for 78–192 MeV protons incident on $^{232}$Th targets. *Applied Radiation and Isotopes* **2016,** *118*, 366-374.

35. Weidner, J.; Mashnik, S.; John, K.; Ballard, B.; Birnbaum, E.; Bitteker, L.; Couture, A.; Fassbender, M.; Goff, G.; Gritzo, R., $^{225}$Ac and $^{223}$Ra production via 800 MeV proton irradiation of natural thorium targets. *Applied Radiation and Isotopes* **2012,** *70* (11), 2590-2595.

36. Weidner, J.; Mashnik, S.; John, K.; Hemez, F.; Ballard, B.; Bach, H.; Birnbaum, E.; Bitteker, L.; Couture, A.; Dry, D., Proton-induced cross sections relevant to production of $^{225}$Ac and $^{223}$Ra in natural thorium targets below 200 MeV. *Applied Radiation and isotopes* **2012,** *70* (11), 2602-2607.

37. Hogle, S.; Boll, R. A.; Murphy, K.; Denton, D.; Owens, A.; Haverlock, T. J.; Garland, M.; Mirzadeh, S., Reactor production of Thorium-229. *Applied Radiation and Isotopes* **2016,** *114*, 19-27.

38. Kuznetsov, R.; Butkalyuk, P.; Tarasov, V.; Baranov, A. Y.; Butkalyuk, I.; Romanov, E.; Kupriyanov, V.; Kazakova, E., Yields of activation products in $^{226}$Ra irradiation in the high-flux SM reactor. *Radiochemistry* **2012,** *54* (4), 383-387.

39. Apostolidis, C.; Molinet, R.; McGinley, J.; Abbas, K.; Möllenbeck, J.; Morgenstern, A., Cyclotron production of Ac-225 for targeted alpha therapy. *Applied Radiation and Isotopes* **2005,** *62* (3), 383-387.

40. Nolen, J. A.; Brown, M. A.; Rotsch, D. A.; Chemerisov, S. D.; Henning, W. F.; Song, J., Compact assembly for production of medical isotopes via photonuclear reactions. United States Patents: 2019.

41. Melville, G.; Meriarty, H.; Metcalfe, P.; Knittel, T.; Allen, B., Production of Ac-225 for cancer therapy by photon-induced transmutation of Ra-226. *Applied Radiation and Isotopes* **2007,** *65* (9), 1014-1022.

42. Melville, G.; Allen, B. J., Cyclotron and linac production of Ac-225. *Applied Radiation and Isotopes* **2009,** *67* (4), 549-555.

43. Melville, G.; Liu, S. F.; Allen, B., A theoretical model for the production of Ac-225 for cancer therapy by photon-induced transmutation of Ra-226. *Applied Radiation and Isotopes* **2006,** *64* (9), 979-988.

44. Yong, K.; Brechbiel, M. W., Towards translation of $^{212}$Pb as a clinical therapeutic; getting the lead in! *Dalton Transactions* **2011,** *40* (23), 6068-6076.

45. Mirzadeh, S., Generator-produced alpha-emitters. *Applied Radiation and Isotopes* **1998,** *49* (4), 345-349.

46. Chappell, L. L.; Dadachova, E.; Milenic, D. E.; Garmestani, K.; Wu, C.; Brechbiel, M. W., Synthesis, characterization, and evaluation of a novel bifunctional chelating agent for the lead isotopes $^{203}$Pb and $^{212}$Pb. *Nuclear Medicine and Biology* **2000,** *27* (1), 93-100.

47. Jensen, R.; Battey, J.; Spindel, E.; Benya, R., International Union of Pharmacology. LXVIII. Mammalian bombesin receptors: nomenclature, distribution, pharmacology, signaling, and functions in normal and disease states. *Pharmacological Reviews* **2008,** *60* (1), 1-42.

48. Markwalder, R.; Reubi, J. C., Gastrin-releasing peptide receptors in the human prostate relation to neoplastic transformation. *Cancer Research* **1999,** *59* (5), 1152-1159.

49. Bartholdi, M. F.; Wu, J. M.; Pu, H.; Troncoso, P.; Eden, P. A.; Feldman, R. I., In situ hybridization for gastrin‐releasing peptide receptor (GRP receptor) expression in prostatic carcinoma. *International Journal of Cancer* **1998,** *79* (1), 82-90.

50. Sun, B.; Halmos, G.; Schally, A. V.; Wang, X.; Martinez, M., Presence of receptors for bombesin/gastrin‐releasing peptide and mRNA for three receptor subtypes in human prostate cancers. *The Prostate* **2000,** *42* (4), 295-303.

51. Körner, M.; Waser, B.; Rehmann, R.; Reubi, J. C., Early over‐expression of GRP receptors in prostatic carcinogenesis. *The Prostate* **2014,** *74* (2), 217-224.

52. Ischia, J.; Patel, O.; Bolton, D.; Shulkes, A.; Baldwin, G. S., Expression and function of gastrin‐releasing peptide (GRP) in normal and cancerous urological tissues. *BJU International* **2014,** *113*, 40-47.

53. Mansi, R.; Fleischmann, A.; Mäcke, H. R.; Reubi, J. C., Targeting GRPR in urological cancers—from basic research to clinical application. *Nature Reviews Urology* **2013,** *10* (4), 235-244.

54. Baratto, L.; Jadvar, H.; Iagaru, A., Prostate cancer theranostics targeting gastrin-releasing peptide receptors. *Molecular Imaging and Biology* **2018,** *20* (4), 501-509.

55. Smith, C.; Volkert, W.; Hoffman, T., Gastrin releasing peptide (GRP) receptor targeted radiopharmaceuticals: a concise update. *Nuclear Medicine and Biology* **2003,** *30* (8), 861-868.

56. Van de Wiele, C.; Dumont, F.; Broecke, R. V.; Oosterlinck, W.; Cocquyt, V.; Serreyn, R.; Peers, S.; Thornback, J.; Slegers, G.; Dierckx, R. A., Technetium-99m RP527, a GRP analogue for visualisation of GRP receptor-expressing malignancies: a feasibility study. *European Journal of Nuclear Medicine* **2000,** *27* (11), 1694-1699.

57. Van de Wiele, C.; Dumont, F.; Dierckx, R. A.; Peers, S. H.; Thornback, J. R.; Slegers, G.; Thierens, H., Biodistribution and dosimetry of $^{99m}$Tc-RP527, a gastrin-releasing peptide (GRP) agonist for the visualization of GRP receptor–expressing malignancies. *Journal of Nuclear Medicine* **2001,** *42* (11), 1722-1727.

58. Lantry, L. E.; Cappelletti, E.; Maddalena, M. E.; Fox, J. S.; Feng, W.; Chen, J.; Thomas, R.; Eaton, S. M.; Bogdan, N. J.; Arunachalam, T., $^{177}$Lu-AMBA: Synthesis and Characterization of a Selective $^{177}$Lu-Labeled GRP-R Agonist for Systemic Radiotherapy of Prostate Cancer. *Journal of Nuclear Medicine* **2006,** *47* (7), 1144.

59. Bodei, L.; Ferrari, M.; Nunn, A.; Llull, J.; Cremonesi, M.; Martano, L.; Laurora, G.; Scardino, E.; Tiberini, S.; Bufi, G., Lu-177-AMBA bombesin analogue in hormone refractory

prostate cancer patients: a phase I escalation study with single-cycle administrations. *European Journal of Nuclear Medicine and Molecular Imaging* **2007,** *34*, S221.

60. Zhang, H.; Schuhmacher, J.; Waser, B.; Wild, D.; Eisenhut, M.; Reubi, J. C.; Maecke, H. R., DOTA-PESIN, a DOTA-conjugated bombesin derivative designed for the imaging and targeted radionuclide treatment of bombesin receptor-positive tumours. *European Journal of Nuclear Medicine and Molecular Imaging* **2007,** *34* (8), 1198-1208.

61. Hoffman, T. J.; Gali, H.; Smith, C. J.; Sieckman, G. L.; Hayes, D. L.; Owen, N. K.; Volkert, W. A., Novel series of $^{111}$In-labeled bombesin analogs as potential radiopharmaceuticals for specific targeting of gastrin-releasing peptide receptors expressed on human prostate cancer cells. *Journal of Nuclear Medicine* **2003,** *44* (5), 823-831.

62. Garrison, J. C.; Rold, T. L.; Sieckman, G. L.; Naz, F.; Sublett, S. V.; Figueroa, S. D.; Volkert, W. A.; Hoffman, T. J., Evaluation of the pharmacokinetic effects of various linking group using the $^{111}$In-DOTA-X-BBN(7− 14)$NH_2$ structural paradigm in a prostate cancer model. *Bioconjugate Chemistry* **2008,** *19* (9), 1803-1812.

63. Baum, R.; Prasad, V.; Mutloka, N.; Frischknecht, M.; Maecke, H.; Reubi, J., Molecular imaging of bombesin receptors in various tumors by Ga-68 AMBA PET/CT: first results. *Journal of Nuclear Medicine* **2007,** *48* (supplement 2), 79P-79P.

64. Bologna, M.; Festuccia, C.; Muzi, P.; Biordi, L.; Ciomei, M., Bombesin stimulates growth of human prostatic cancer cells in vitro. *Cancer* **1989,** *63* (9), 1714-1720.

65. JENSEN, R. T.; MOODY, T. W., Bombesin-related peptides and neurotensin: effects on cancer growth/proliferation and cellular signaling in cancer. In *Handbook of Biologically active peptides*, Elsevier: 2006; pp 429-434.

66. Mansi, R.; Wang, X.; Forrer, F.; Kneifel, S.; Tamma, M.-L.; Waser, B.; Cescato, R.; Reubi, J. C.; Maecke, H. R., Evaluation of a 1, 4, 7, 10-Tetraazacyclododecane-1, 4, 7, 10-Tetraacetic acid–conjugated bombesin-based radioantagonist for the labeling with single-photon emission computed tomography, positron emission tomography, and therapeutic radionuclides. *Clinical Cancer Research* **2009,** *15* (16), 5240-5249.

67. Cescato, R.; Maina, T.; Nock, B.; Nikolopoulou, A.; Charalambidis, D.; Piccand, V.; Reubi, J. C., Bombesin receptor antagonists may be preferable to agonists for tumor targeting. *Journal of Nuclear Medicine* **2008,** *49* (2), 318-326.

68. Mansi, R.; Wang, X. J.; Forrer, F.; Waser, B.; Cescato, R.; Graham, K.; Borkowski, S.; Reubi, J. C.; Maecke, H. R., Development of a potent DOTA-conjugated bombesin antagonist for targeting GRPr-positive tumours. *European Journal of Nuclear Medicine and Molecular Imaging* **2011,** *38* (1), 97-107.

69. Kähkönen, E.; Jambor, I.; Kemppainen, J.; Lehtiö, K.; Grönroos, T. J.; Kuisma, A.; Luoto, P.; Sipilä, H. J.; Tolvanen, T.; Alanen, K., In vivo imaging of prostate cancer using [$^{68}$Ga]-labeled bombesin analog BAY86-7548. *Clinical Cancer Research* **2013,** *19* (19), 5434-5443.

70. Minamimoto, R.; Hancock, S.; Schneider, B.; Chin, F.; Jamali, M.; Loening, A. M.; Vasanawala, S.; Gambhir, S. S.; Iagaru, A., Pilot Comparison of $^{68}$Ga-RM2 PET and $^{68}$Ga-PSMA PET in Patients with Biochemically Recurrent Prostate Cancer. *Journal of Nuclear Medicine* **2016**, 557-562.

71. Wieser, G.; Popp, I.; Rischke, H. C.; Drendel, V.; Grosu, A.-L.; Bartholomä, M.; Weber, W. A.; Mansi, R.; Wetterauer, U.; Schultze-Seemann, W., Diagnosis of recurrent prostate cancer with PET/CT imaging using the gastrin-releasing peptide receptor antagonist $^{68}$Ga-RM2: Preliminary results in patients with negative or inconclusive [$^{18}$F]Fluoroethylcholine-PET/CT. *European Journal of Nuclear Medicine and Molecular Imaging* **2017**, 1-10.

72. Fassbender, T. F.; Schiller, F.; Mix, M.; Maecke, H. R.; Kiefer, S.; Drendel, V.; Meyer, P. T.; Jilg, C. A., Accuracy of [$^{68}$Ga]Ga-RM2-PET/CT for diagnosis of primary prostate cancer compared to histopathology. *Nuclear Medicine and Biology* **2019,** *70*, 32-38.

73. Dalm, S. U.; Bakker, I. L.; de Blois, E.; Doeswijk, G. N.; Konijnenberg, M. W.; Orlandi, F.; Barbato, D.; Tedesco, M.; Maina, T.; Nock, B. A., $^{68}$Ga/$^{177}$Lu-NeoBOMB1, a novel radiolabeled GRPR antagonist for theranostic use in oncology. *Journal of Nuclear Medicine* **2017,** *58* (2), 293-299.

74. Nock, B. A.; Kaloudi, A.; Lymperis, E.; Giarika, A.; Kulkarni, H. R.; Klette, I.; Singh, A.; Krenning, E. P.; De Jong, M.; Maina, T., Theranostic perspectives in prostate cancer with the gastrin-releasing peptide receptor antagonist NeoBOMB1: preclinical and first clinical results. *Journal of Nuclear Medicine* **2017,** *58* (1), 75-80.

75. Maina, T.; Bergsma, H.; Kulkarni, H. R.; Mueller, D.; Charalambidis, D.; Krenning, E. P.; Nock, B. A.; de Jong, M.; Baum, R. P., Preclinical and first clinical experience with the gastrin-releasing peptide receptor-antagonist [$^{68}$Ga]SB3 and PET/CT. *European journal of nuclear medicine and molecular imaging* **2016,** *43* (5), 964-973.

76. Lymperis, E.; Kaloudi, A.; Sallegger, W.; Bakker, I. L.; Krenning, E. P.; de Jong, M.; Maina, T.; Nock, B. A., Radiometal-dependent biological profile of the radiolabeled gastrin-releasing peptide receptor antagonist SB3 in cancer theranostics: Metabolic and biodistribution patterns defined by neprilysin. *Bioconjugate chemistry* **2018,** *29* (5), 1774-1784.

# CHAPTER 2: Diagnostic Imaging of Prostate Cancer Using a $^{203}$Pb-labeled BB2 Receptor Antagonist

## 2.1. Introduction

For most cancer patients, the probability of a good prognosis increases with early disease detection. Currently, the methods employed for the diagnosis of prostate cancer include digital rectal examination (DRE), prostate-specific antigen (PSA) testing, and diagnostic anatomical imaging using magnetic resonance imaging (MRI), computed tomography (CT), or ultrasound (US). However, there is an ongoing debate as to the efficacy of these current methods due to the likelihood for overdiagnosis and the associated treatment-related harms.[1] One promising method for a more precise detection of prostate cancer tumors is through diagnostic imaging of tumor-expressed receptors using radiolabeled peptides.

The discovery that the bombesin receptor (BB2r) is overexpressed in prostate cancer cells led to its investigation as a viable target for the development of targeted diagnostic and therapeutic prostate cancer radiodiopharmaceuticals.[2-7] To this effect, several peptide analogues targeting BB2r have been evaluated.[8-11] Of particular interest is RM2 (DOTA-4-amino-1-carboxymethyl-piperidine-D-Phe-Gln-Trp-Ala-Val-Gly-His-Sta-Leu-$NH_2$, **Figure 2-1**), a BB2r antagonist peptide conjugate that has been shown to exhibit high and specific tumor targeting in BB2r-expressing prostate cancer cell line xenografts and in patients with prostate cancer.[12-17]

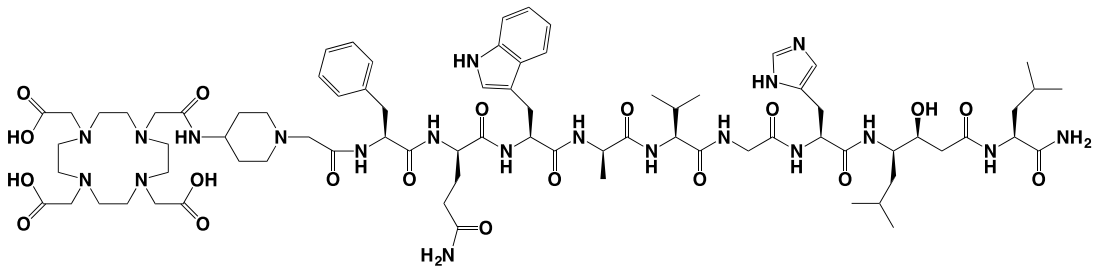

**Figure 2-1**. Chemical structure of RM2

Previous studies involving radiolabeled RM2 peptide conjugates focused mainly on [$^{68}$Ga]Ga-RM2 [12-13, 16-17] and [$^{177}$Lu]Lu-RM2 [18-19] for diagnosis and therapy, respectively. In this study, the synthesis and preclinical evaluation of [$^{203}$Pb]Pb-RM2 as the diagnostic surrogate to the therapeutic [$^{212}$Pb]Pb-RM2 is described. Lead-212 ($t_{1/2}$ = 10.6 hours) decays by beta emission into $^{212}$Bi, which subsequently decays into stable $^{208}$Pb through a branched decay pathway consisting of one alpha particle and one beta particle emission in each decay pathway. Therefore, $^{212}$Pb is of interest as an *in vivo* generator of $^{212}$Bi for targeted alpha therapy.[20-21] Lead-203 ($t_{1/2}$ = 51.9 hours) decays by electron capture to stable $^{203}$Tl, with the emission of 278 keV gamma rays (81% intensity) suitable for single-photon emission computed tomography (SPECT) imaging. The $^{203}$Pb/$^{212}$Pb pair constitute a true theranostic matched pair since there should be no difference in the chemical and pharmacokinetic properties of $^{203}$Pb- and $^{212}$Pb-labeled compounds.

The potential of $^{203}$Pb/$^{212}$Pb as a theranostic matched pair has been described in preclinical models for neuroendocrine tumors [22-23] and melanoma.[24-27] Tworowska et al.[22-23] reported promising *in vitro* and *in vivo* results for targeting somatostatin receptor-positive neuroendocrine tumors using $^{203}$Pb-labeled octreotate analogues and are planning to investigate the $^{212}$Pb-labeled analogues in clinical trials. Similarly, alpha-melanocyte-

stimulating hormone (α-MSH) peptide analogues that target the melanocortin-1 receptor have been labeled with $^{203}$Pb/$^{212}$Pb and preclinically evaluated for the development of targeted melanoma radiopharmaceuticals.[24-27] In a recent clinical study, the dosimetry estimates from a $^{203}$Pb-labeled PSMA analogue ([$^{203}$Pb]Pb-PSMA-CA012) were used to extrapolate the dosimetry of the $^{212}$Pb analogue.[28] These studies highlight the potential clinical applicability of $^{203}$Pb as a diagnostic surrogate to $^{212}$Pb. Herein, the synthesis and preclinical evaluation [$^{203}$Pb]Pb-RM2 is described.

## 2.2. Experimental

### 2.2-1. Materials and Methods

The RM2 peptide conjugate was purchased from CPC Scientific, Inc. (Sunnyvale, CA, USA) and used without further purification. [$^{203}$Pb]$PbCl_2$ was purchased from Lantheus Medical Imaging, Inc. (N. Billerica, MA, USA). [$^{59}$Fe]$FeCl_3$ was purchased from PerkinElmer (Waltham, MA, USA). [$^{125}$I]I-Tyr$^4$-BBN was purchased from PerkinElmer (Shelton, CT, USA). **CAUTION!** $^{203}$Pb, $^{59}$Fe and $^{125}$I are radioactive and must be handled in laboratories outfitted and approved for work with radioactive materials. All work involving radioactivity was approved by the Harry S. Truman VA Hospital Radiation Safety Committee prior to performance. All radioactive dose measurements were performed using a Capintec CRC-Ultra dose calibrator (Florham Park, NJ, USA). The lead-selective chromatographic resin (Pb-resin) with a particle size of 100 – 150 μm was purchased from Eichrom Technologies, LLC (Lisle, IL, USA). Fluka TraceSELECT ultrapure water, absolute ethanol, and trace metal grade HCl were obtained from Sigma-Aldrich (St. Louis, MO, USA) or Fisher Scientific (Waltham, MA, USA). Solid phase

extraction (SPE) Sep-Pak C18 Plus Light Cartridges (55-105 μm particle size) were purchased from Waters Corporation (Milford, MA, USA). Microwave synthesis was carried out in dynamic mode using a CEM Discover SP microwave synthesizer (Matthews, NC, USA). Deionized water (18.2 MΩ.cm) used for HPLC analyses was obtained from an in-house Aqua Solutions (Jasper, Georgia) water purification system. HPLC quality control of non-radiolabeled and radiolabeled peptides was performed using a Shimadzu Prominence HPLC system (Columbia, MD, USA) equipped with a UV-Vis absorbance detector (set at 220 and 280 nm) and a NaI(Tl) scintillation detector. All HPLC analyses were performed using a mobile phase consisting of solvent A (99.9% $H_2O$ and 0.1% trifluoroacetic acid [TFA]) and solvent B (99.9% $CH_3CN$ and 0.1% TFA) run on a Jupiter C-18 analytical HPLC column [5 u, 300 A, 250 × 4.6 mm purchased from Phenomenex® (Torrance, CA, USA)] maintained at a column temperature of 31 °C using an Eppendorf HPLC temperature control system. HPLC quality control was performed using a linear gradient of 10% solvent B:A increased to 70% solvent B:A over 8 minutes, followed by an additional 1 minute at 70% solvent B:A, then decreased to 10% solvent B:A over 1 minute at a flow rate of 1.5 mL/min. Electrospray Ionization Mass Spectrometry (ESI-MS) was performed at the MU Molecular Interactions Core on a Thermo Finnigan TSQ7000 triple-quadrupole instrument with an API2 source.

## 2.2-2. Synthesis of Non-radioactive Pb-RM2

Microwave-assisted synthesis of Pb-RM2 was performed by adding 130 μL of a 40 mg/mL aqueous solution of $Pb(NO_3)_2$ (5.2 mg, 15.7 μmol) into a 10 mL microwave reaction vial containing the RM2 peptide conjugate (2.6 mg, 1.6 μmol) dissolved in 1 mL of ultrapure water. The reaction vial was capped and heated in the microwave synthesizer

at 105 °C, 50 psi (max) and 150 W (max) for 5 min with stirring. Upon cooling to room temperature, the reaction mixture was loaded onto a C18 Sep-Pak cartridge preconditioned with 5 mL of absolute ethanol and 5 mL of ultrapure water. The C18 Sep-Pak cartridge was washed with 3 mL of ultrapure water to remove any unreacted $Pb(NO_3)_2$. Pb-RM2 was subsequently eluted with 2 mL of absolute ethanol. After removal of ethanol by evaporation *in vacuo*, the purified product was reconstituted in 500 μL of ultrapure water and lyophilized to obtain a white powder. HPLC and ESI-MS analysis were performed to confirm the purity of the desired product.

## 2.2-3. Purification of $[^{203}Pb]PbCl_2$

Commercially available $[^{203}Pb]PbCl_2$ was purchased with specific activity ranging from 4539 - 6629 Ci/g (168 - 245 TBq/g) and radioactivity concentrations ranging from 29.7 - 140 mCi/mL (1.09 - 5.18 GBq/mL) in 0.5 M HCl (**Table 2-1**). The $[^{203}Pb]PbCl_2$ solution supplied also contained non-radioactive metallic impurities, primarily Fe (3.58 – 8.71 μg/mL) and Pb (4.50 – 12.08 μg/mL). Prior to radiolabeling, the Fe contaminants contained in the $[^{203}Pb]PbCl_2$ stock solution were removed using a lead-selective chromatographic resin (Pb-resin) following a similar procedure previously reported by Li et al.[26] Briefly, ~50 mg of Pb-resin was packed into a fritted 1 mL polypropylene SPE column (Supelco 54220-U). The column was preconditioned with 3 mL of 0.5 M HCl, after which a 500 μL aliquot of the $[^{203}Pb]PbCl_2$ stock solution (2 - 17 mCi, 74 - 629 MBq) was loaded onto the column. Next, the column was washed with 3 mL of 0.5 M HCl to remove the metal contaminants. Finally, $^{203}Pb$ was eluted with 1 mL of 0.5 M NaOAc buffer (pH 6.5) repeatedly (using a maximum of 4 mL of NaOAc buffer) resulting in complete

recovery of $^{203}$Pb. The $^{203}$Pb solution obtained was used directly for radiolabeling experiments.

**Table 2-1.** Technical data for [$^{203}$Pb]$PbCl_2$ purchased from Lantheus

| Lot Number | Date | Specific Activity (Ci/g) | Activity Concentration (mCi/mL) | Pb (μg/mL) | Fe (μg/mL) |
|---|---|---|---|---|---|
| 101602-Pb | 10/24/2016 | 6629 | 29.7 | 4.50 | 3.58 |
| 111601-Pb | 11/14/2016 | 5697 | 55.0 | 9.68 | 7.59 |
| 011701-Pb | 01/01/2017 | 4539 | 140.5 | 12.08 | 8.71 |
| Note: Data was provided by Lantheus | | | | | |

## 2.2-4. Efficiency of Fe Separation from Pb Using Pb-resin

The efficiency of Pb-resin to separate Fe from Pb was investigated using $^{59}$Fe as a tracer. The Pb-resin column was packed and preconditioned as described above. 129 – 55 μCi (4.7 – 2.0 MBq) of $^{59}FeCl_3$ (in 0.5M HCl) was spiked into solutions containing varying amounts of $FeCl_3.6H_2O$ and $Pb(NO_3)_2$, as shown in **Table S2-1**. 500 μL of the $^{59}$Fe-spiked solutions was loaded onto different Pb-resin columns. The columns were washed with 2 mL 0.5 M HCl and the eluent was collected in 1 mL fractions and analyzed for $^{59}$Fe radioactivity using a Capintec CRC-Ultra dose calibrator.

## 2.2-5. $^{203}$Pb Labeling

The $^{203}$Pb-labeled RM2 peptide conjugate was synthesized by the addition of 80 μg (0.049 μmol) of RM2 into a reaction vial containing 2 – 5 mCi (74 – 185 MBq) of purified $^{203}$Pb in 2 mL of 0.5 M NaOAc buffer (pH 6.5). The reaction mixture was incubated in a sand bath for 50 min at 85 °C and subsequently allowed to cool to room temperature. For

purification, the radiolabeled peptide conjugate was loaded onto a C18 Sep-Pak cartridge preconditioned with 5 mL of absolute ethanol and 5 mL of ultrapure water. The C18 Sep-Pak cartridge was washed with 3 mL of ultrapure water to remove any unreacted $^{203}$Pb. [$^{203}$Pb]Pb-RM2 was eluted from the cartridge with 2 mL of absolute ethanol. The purified product was concentrated to dryness by slowly purging with a steady stream of $N_2$ at 85°C to remove the ethanol. Finally, the radiolabeled peptide was reconstituted in normal saline and passed through a 0.22 μm syringe filter (Cameo, Sanford, ME, USA) for use in animal biodistribution studies. The radiochemical purity of the radiolabeled peptide conjugate was analyzed using radio-HPLC.

## 2.2-6. Cell Culture

The PC3 human prostate cancer cell line was purchased from the American Type Cell Culture Collection (Manassas, VA, USA) and authenticated (IDEXX BioResearch, Columbia, MO, USA) prior to use. **CAUTION!** All PC3 cell work was performed following BSL-2 practices. The PC3 cells were cultured in the MU Cell and Immunobiology Core (MU CIC, Columbia, MO, USA) facility using RPMI 1640 supplemented with 10% Fetal Bovine Serum (Gibco/Life Technologies, Grand Island, NY, USA) and 50 μg/mL gentamicin (Fresenius Kabi USA, LLC; Lake Zurich, IL, USA) in a humidified environment with 5% carbon dioxide. Cells were counted using an automated cell counter (Biorad TC-20, Hercules, CA, USA), centrifuged, and resuspended in RPMI 1640 (Gibco/Life Technologies, Grand Island, NY, USA) without additives prior to use.

## 2.2-7. *In Vitro* Receptor Binding Affinity Studies

The binding affinity of non-radioactive Pb-RM2 for the BB2 receptors expressed in PC3 human prostate cancer cells was determined using a competitive displacement cell

binding assay employing [$^{125}$I]I-Tyr$^4$-BBN (Perkin Elmer Health Sciences Inc, Shelton, CT, USA), a known BB2 receptor agonist, as the displacement radioligand. Cell media consisted of RPMI 1640 media (Life Technologies, Grand Island, NY, USA) at pH 7.4 modified with 4.92 mg/mL of HEPES (Fisher BioReagents, Fair Lawn, NJ, USA) and 2 mg/mL of Bovine Serum Albumin (Fisher BioReagents, Fair Lawn, NJ, USA). For the binding assay, approximately $3\times10^4$ PC3 cells were suspended in cell media and incubated at 37 °C and 5% $CO_2$ for 45 min in the presence of 20,000 cpm [$^{125}$I]I-Tyr$^4$-BBN and increasing concentrations of Pb-RM2 ($3.33\times10^{-13}$ – $3.33\times10^{-6}$ M) in duplicate. Following incubation, cells were washed with ice-cold media three times and cell-bound radioactivity was measured by counting the washed cells in a WIPER gamma counter (Lab Technologies, Inc., Maple Park, IL, USA). The percentage of [$^{125}$I]I-Tyr$^4$-BBN bound to the cells was plotted against the concentration of Pb-RM2 to determine the respective fifty-percent inhibitory concentration ($IC_{50}$) values. Studies were performed in triplicate on three separate occasions and the final $IC_{50}$ value was calculated by averaging the results obtained in the three experiments.

## 2.2-8. Mice and Husbandry

Male CF-1 mice (4 - 5 weeks of age) were purchased from Charles Rivers Laboratories (Wilmington, MA, USA). Male ICR SCID (Institute of Cancer Research severe combined immunodeficient) mice were purchased from Taconic Farms (Germantown, NY, USA) at 4 – 5 weeks of age. All mice were housed in ventilated rack systems with up to four animals per cage containing paperchip bedding (Shepherd Specialty Papers; Chicago, IL, USA). CF-1 mice were conventionally housed with ad libitum access to rodent chow (Lab Diet 5008, Ralston Purina, St. Louis, MO, USA) and

acidified water. ICR SCID mice were housed in autoclaved cages with ad libitum access to irradiated rodent chow (Lab Diet 5053, Ralston Purina, St. Louis, MO, USA) and autoclaved acidified water. The animal room was set on a 12-h light/12-h dark schedule with temperature and humidity control. All animal studies were reviewed and approved by the Subcommittee for Animal Studies (SAS) at the Harry S. Truman VA Hospital prior to performance.

## 2.2-9. [$^{203}$Pb]$PbCl_2$ Biodistribution Studies

Normal CF-1 mice were allowed to acclimate for 10 days prior to tail vein administration of a 50 μL bolus containing 5 μCi (0.185 MBq) of [$^{203}$Pb]$PbCl_2$. Mice were sacrificed by cervical dislocation at 15 minutes, 1 hour, 4 hours, and 24 hours post injection. Selected tissues, organs, and remaining carcass were collected and weighed; the residual radioactivity was subsequently quantified in a NaI(Tl) well counter. The percent injected dose (%ID) and the percent injected dose per gram (%ID/g) of each organ or tissue were calculated. The %ID in whole blood was estimated assuming a whole blood volume equivalent to 6.5% of the measured body weight. Excreted radioactivity was reported as %ID and includes radioactivity measured in cage paper, bladder contents, and feces (collected and quantified separately at 24 hours).

## 2.2-10. [$^{203}$Pb]Pb-RM2 Biodistribution Studies

Following an on-site acclimation period of 6-11 days, SCID mice were anesthetized using isofluorane (Baxter Healthcare, Deerfield, IL, USA) administered with a non-rebreathing apparatus (Summit Medical Equipment Co., Bend, OR, USA). Anesthetized mice received bilateral subcutaneous flank injections of 100 μL containing 7 x $10^6$ PC3 cells prepared as described above. Tumors were allowed to grow 4-5 weeks until palpable

tumors (0.15 – 0.30 g) were observed. Each mouse was administered a bolus containing 8 - 29 μCi (0.296-1.073 MBq) of [$^{203}$Pb]Pb-RM2 in 100 μL via the tail vein. Mice were sacrificed by cervical dislocation at 15 minutes, 30 minutes, 1 hour, 2 hours, 4 hours, 24 hours, and 48 hours after administration. Selected tissues, organs, and remaining carcass were collected and weighed; the residual radioactivity was subsequently quantified in a NaI(Tl) well counter. The percent injected dose (%ID) and the percent injected dose per gram (%ID/g) of each organ or tissue were calculated. The %ID in whole blood was estimated assuming a whole blood volume equivalent to 6.5% of the measured body weight. Excreted radioactivity was reported as %ID and includes radioactivity measured in cage paper, bladder contents, and feces (collected and quantitated separately at 24 hours and 48 hours). Receptor blocking studies were performed by pre-injection of a 100 μL i.v. bolus via the tail vein containing 20 nmoles of unlabeled RM2 peptide conjugate in normal saline 5 minutes prior to administration of [$^{203}$Pb]Pb-RM2.

## 2.2-11. Micro SPECT/CT/MRI Imaging Studies

Micro-SPECT images were obtained using a Siemens INVEON small animal, dedicated SPECT/CT system (Siemens Medical Solutions, Malvern, PA, USA) at 24 hours post-injection of [$^{203}$Pb]Pb-RM2 or [$^{203}$Pb]$PbCl_2$. PC3 tumor-bearing mice received tail vein injections of 18-80 μCi (0.66 – 2.96 MBq) of [$^{203}$Pb]Pb-RM2, while CF-1 normal mice were injected with 25 μCi (0.93 MBq) of [$^{203}$Pb]$PbCl_2$. Mice were anesthetized using 2.5-3% isoflurane anesthesia and imaged for 30 min. The micro-SPECT images were acquired using mouse-whole-body (1.0 mm) multi-pinhole collimators, a 35 mm radius of rotation, 2 revolutions, and 60 projection/revolution. The micro-SPECT acquisition data was histogrammed using an energy window that included the 279 keV photopeak of Pb-

203 and reconstructed using a 3-dimensional ordered subset expectation maximization (OSEM-3D) algorithm applying 8 iterations and 6 subsets.

Micro-computed tomography (micro-CT) images were also obtained on the Siemens INVEON small-animal unit immediately following acquisition of the micro-SPECT imaging for the purpose of image fusion to reference the molecular data with the anatomical data. The 360 degree micro-CT images were acquired using an 80 kilovoltage peak (kVp) X-ray source with 500 μA current, 280 ms exposure at low magnification, and concurrent image reconstruction was achieved using a conebeam (Feldkamp) filtered back-projection algorithm, without downsampling, slight noise reduction, mouse beam hardening, and a Shepp-Logan filter. The raw, reconstructed micro-SPECT datasets were imported into the Siemens INVEON Research Workplace software for image smoothing employing a 3D Gaussian kernel for subsequent image fusion with the micro-CT image data and 3D visualization.

Following collection of SPECT/CT data, MRI images were obtained using a 7 Tesla small bore MRI (Bruker Biospin Corp., Billerica, MA, USA) equipped with a 35 mm inner diameter quadrature RF coil. Axial T2 weighted images (TR at 2 s and TE at 35 ms) were obtained with a slice thickness of 1 mm. MRI images were fused with SPECT imaging data using Siemens INVEON Research Workplace software.

## 2.3. Results and Discussion

### 2.3-1. Chemistry and Radiochemistry

Pb-RM2 was synthesized with an unoptimized yield of 58% (n=1). Based on HPLC analysis, the purity of Pb-RM2 conjugate was 98.2% (**Figure S2-1**). ESI-MS analysis of

Pb-RM2 revealed a high intensity peak with *m/z* of 923.86, which is consistent with the calculated *m/z* for the $[M + 2H]^{2+}$ ion (923.05) for Pb-RM2 (**Figure 2-2**). No significant impurities were observed.

The $[^{203}Pb]PbCl_2$ precursor used in this study was purchased from Lantheus Medical Imaging and contained significant amounts of Pb and Fe impurities, as shown in **Table 2-1**. A recent patent application by Lantheus reported that $^{203}Pb$ is isolated from the cyclotron waste stream as a byproduct during the production of $^{201}Tl$ via the $^{203}Tl$ (p, 3n) $^{201}Pb$ ➔ $^{201}Tl$ reaction.[29] The authors indicated that the cyclotron waste stream contains metal contaminants including Cu, Ni, Fe, and Zn.[29] Li et al.[26] reported the production of $^{203}Pb$ at Lantheus cyclotrons via the $^{205}Tl$ (p, 3n) $^{203}Pb$ reaction by bombarding 2.5 – 9 grams of natural Tl target (70.5% $^{205}Tl$ abundance) with a 26.5 MeV proton beam for 6 – 24 hours. However, $^{204}Pb$ is produced as a byproduct via the $^{205}Tl$ (p, 2n) $^{204m}Pb$ ➔ $^{204}Pb$ reaction, which could contribute to the Pb impurities contained in the $[^{203}Pb]PbCl_2$ solution. One of the reported methods for separation of Pb from Tl is through co-precipitation of Pb with macroscale amounts of $Fe(OH)_3$.[30-31] This could be another potential source of Fe impurities in the $[^{203}Pb]PbCl_2$ solution.

Prior to radiolabeling, the Fe impurities were removed using a lead-selective chromatographic resin (Pb-resin). The Fe impurities present will compete with $^{203}Pb$ for complexation to the RM2 peptide conjugate, which can result in BB2 receptor blockage by Fe-RM2. The Eichrom Pb-resin is based on a macrocylic polyether, bis-4, 4'(5')-[tert-butylcyclohexano]-18-crown-6, which was shown by Horwitz et al.[32] to have low retention for commonly encountered cations (e.g., $Ca^{2+}$, $Fe^{3+}$, $Na^{+}$, $Al^{3+}$, $Cu^{2+}$, $Zn^{2+}$). Using $^{59}Fe$ as a tracer, we demonstrated the efficiency of the Pb-resin to separate Fe from a Pb solution.

It was observed that 98 ± 1 % of $^{59}Fe$ was washed off from the Pb-resin column with two 1 mL fractions of 0.5 M HCl, as shown in **Figure 2-3**. Addition of macro-scale amounts of nonradioactive $FeCl_3$ (up to 22 μg) and $Pb(NO_3)_2$ (up to 41 μg) did not affect the retention of $^{59}Fe$ on the Pb-resin column (**Table S2-1** ).

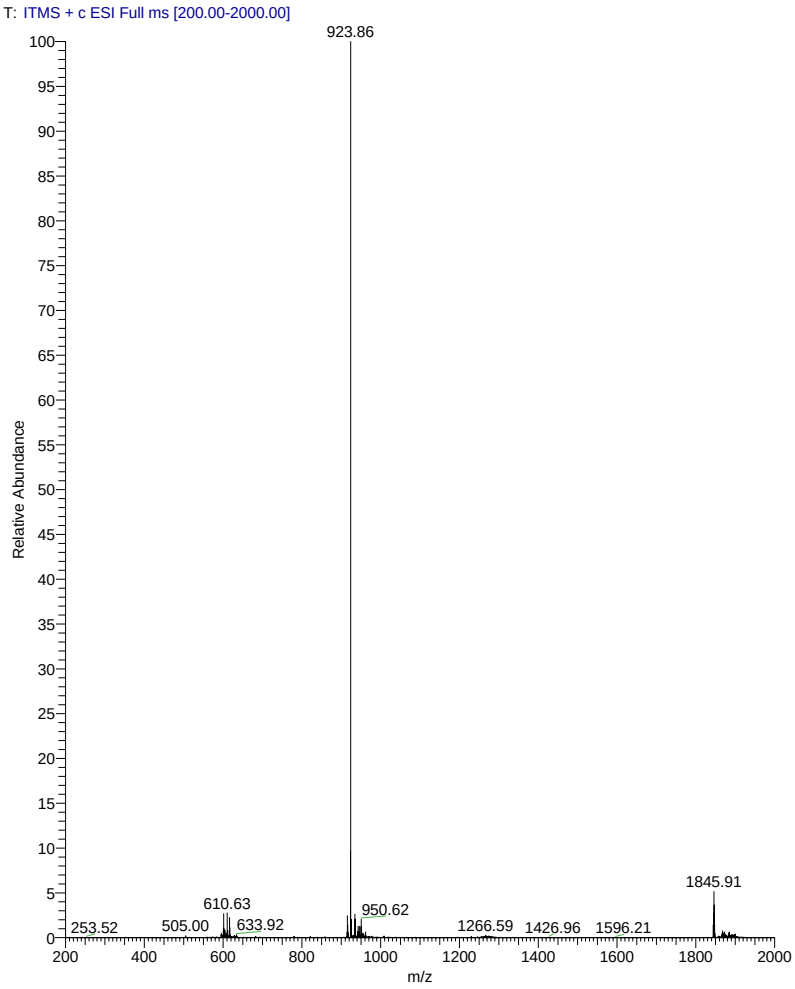


**Figure 2-2.** ESI-MS of nonradioactive Pb-RM2

Initial attempts to synthesize [$^{203}Pb$]Pb-RM2 directly from commercially purchased [$^{203}Pb$]$PbCl_2$ in acidic solution (0.5 M HCl) resulted in no radiolabeling yield. For successful radiolabeling, it was critical that the pH of the reaction solution be adjusted to ~4 using NaOAc or $NH_4OAc$. Purified $^{203}Pb^{2+}$ in 0.5 M NaOAc buffer (pH 6.5) was used

to synthesize [$^{203}$Pb]Pb-RM2 in 90 ± 3% yield (n=3), and the desired product was identified as a single species with 98.9 ± 1.5% (n=3) radiochemical purity using radio-HPLC as shown in **Figure 2-4.**

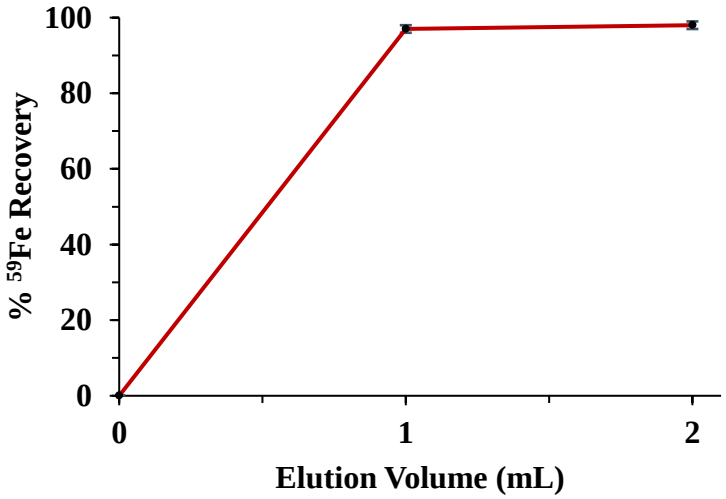


**Figure 2-3**. Efficiency of $^{59}$Fe stripping from Pb-resin (n = 9)

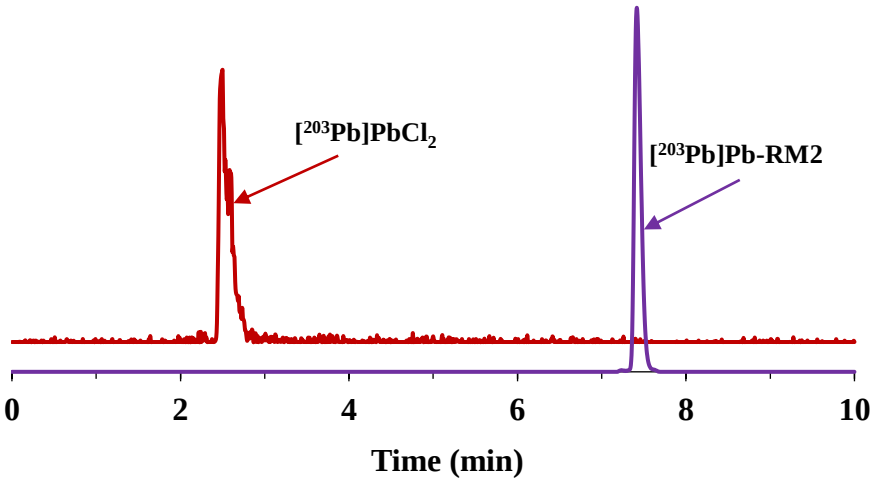


**Figure 2-4**. Radio-HPLC profiles of [$^{203}$Pb]$PbCl_2$ and [$^{203}$Pb]Pb-RM2

## 2.3-2. *In vitro* Receptor Binding Affinity Studies

*In vitro* BB2 receptor binding affinity of Pb-RM2 was determined by a competitive cell binding assay using [$^{125}$I]I-Tyr$^{4}$-BBN as a displacement radioligand. Pb-RM2 exhibited a dose dependent binding affinity for the BB2 receptors expressed in PC3 human prostate cancer cells with an $IC_{50}$ value 1.47 ± 0.05 nM, as shown in **Figure 2-5**. This is consistent with the the $IC_{50}$ value of RM2 (7.7 ± 3.3 nM) and In-RM2 (9.3 ± 3.3 nM), as reported by Mansi et al.[12], which indicates that the incorporation of Pb into RM2 peptide conjugate does not negatively impact receptor affinity. Other BB2 receptor-targeting peptide analogues, including In-DOTA-8-Aoc-BBN[7-14]$NH_2$ ($IC_{50}$ = 0.6 ± 0.1 nM)[33], Demobesin 1 ($IC_{50}$ = 0.7 ± 0.08 nM)[34], Lu-AMBA ($IC_{50}$ = 2.5 ± 0.5 nM)[35], In-RM1 ($IC_{50}$ = 14 ± 3.4 nM)[36] and Lu-NeoBOMB1 ($IC_{50}$ = 1.38 ± 0.09 nM)[37], also have low nanomolar binding affinity values comparable to that of Pb-RM2.

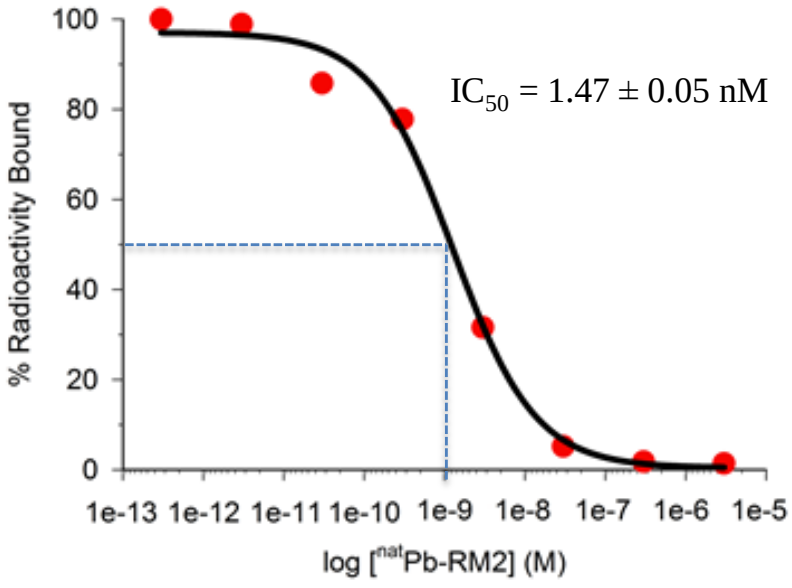


**Figure 2-5**. $IC_{50}$ curve of Pb-RM2

## 2.3-3. [$^{203}$Pb]$PbCl_2$ Biodistribution Studies

*In vivo* biodistribution data for [$^{203}$Pb]$PbCl_2$ in CF1 mice is summarized in **Table 2-2** (see **Table S2-2** for data reported as %ID). Whole-body clearance of [$^{203}$Pb]$PbCl_2$ was very slow, with only 19.82 ± 4.61% of the total injected dose cleared by 24 h post injection. Very high uptake was observed in kidney (47.32 ± 8.48% ID/g), bone (9.93 ± 2.38% ID/g), and liver (10.13 ± 1.27% ID/g) at 15 minutes post injection. The uptake in these organs remained significantly high at 24 hours post injection with 34.57 ± 4.35% ID/g in kidney, 17.23 ± 2.62% ID/g in bone, and 7.51 ± 2.26% ID/g in liver. This pattern of high uptake of [$^{203}$Pb]$PbCl_2$ in kidney, bone and liver is consistent with data previously reported by Máthé et al.[38] and Lever et al.[39], which suggests that free $^{203}Pb^{2+}$ preferentially accumulates in the kidneys, liver and bone.

**Table 2-2. [$^{203}$Pb]$PbCl_2$ biodistribution in CF1 mice**
**Data shown as mean ± SD %ID/g (n = 5 mice per time point)**

| Tissue | 15 min | 1 h | 4 h | 24 h |
|---|---|---|---|---|
| **Blood** | 3.78 ± 0.54 | 3.23 ± 0.48 | 2.62 ± 0.47 | 1.71 ± 0.20 |
| **Heart** | 0.88 ± 0.35 | 0.55 ± 0.12 | 0.46 ± 0.20 | 0.18 ± 0.03 |
| **Lung** | 3.13 ± 0.34 | 2.59 ± 0.39 | 1.85 ± 0.50 | 0.85 ± 0.17 |
| **Liver** | 10.13 ± 1.27 | 10.45 ± 0.69 | 11.87 ± 1.48 | 7.51 ± 2.26 |
| **Stomach** | 0.64 ± 0.08 | 0.78 ± 0.27 | 1.08 ± 0.23 | 0.72 ± 0.40 |
| **Sm. Intestines** | 2.10 ± 0.07 | 2.29 ± 0.26 | 2.23 ± 0.31 | 0.81 ± 0.11 |
| **Lg. Intestines** | 1.10 ± 0.37 | 1.09 ± 0.13 | 2.01 ± 0.10 | 1.22 ± 0.24 |
| **Kidney** | 47.32 ± 8.48 | 51.94 ± 11.85 | 45.17 ± 2.14 | 34.57 ± 4.35 |
| **Spleen** | 1.25 ± 0.32 | 1.69 ± 0.69 | 1.84 ± 0.47 | 1.22 ± 0.74 |
| **Brain** | 0.17 ± 0.04 | 0.17 ± 0.03 | 0.20 ± 0.09 | 0.12 ± 0.01 |
| **Pancreas** | 2.03 ± 1.13 | 2.63 ± 0.24 | 1.94 ± 0.36 | 0.95 ± 0.13 |
| **Muscle** | 0.27 ± 0.10 | 0.29 ± 0.18 | 0.13 ± 0.11 | 0.20 ± 0.18 |
| **Bone** | 9.93 ± 2.38 | 15.52 ± 6.24 | 15.01 ± 4.77 | 17.23 ± 2.62 |
| **Urine (%ID)** | 0.95 ± 0.19 | 2.05 ± 0.19 | 4.63 ± 0.86 | 10.22 ± 2.86 |
| **Excretion (%ID)** | 0.95 ± 0.19 | 2.05 ± 0.19 | 4.63 ± 0.86 | 19.82 ± 4.61 |

Note: Values for urine include radioactivity measured in cage paper

## 2.3-4. [$^{203}$Pb]Pb-RM2 Biodistribution Studies

The pharmacokinetic and BB2 receptor-targeting properties of [$^{203}$Pb]Pb-RM2 was examined in SCID mice bearing PC3 tumor xenografts, as summarized in **Table 2-3** (see **Table S2-3** for data reported as %ID). [$^{203}$Pb]Pb-RM2 exhibited substantial tumor uptake value of 6.41 ± 0.73% ID/g at 15 min post injection. The tumor uptake increased steadily with time, reaching a maximum value of 11.26 ± 2.48% ID/g at 2 hours post injection (**Figure 2-6)**. The maximum tumor uptake value reported here for [$^{203}$Pb]Pb-RM2 is comparable with maximum tumor uptake values reported for other radiolabeled RM2 peptide conjugates such as [$^{111}$In]In-RM2 (15.23 ± 4.78% ID/g)[12], [$^{68}$Ga]Ga-RM2 (14.66 ± 2.12% ID/g)[12], and [$^{177}$Lu]Lu-RM2 (11.46 ± 5.38% ID/g)[18]. A similar maximum tumor uptake value of 12.4 ± 2.3% ID/g was reported for [$^{68}$Ga]Ga-NeoBOMB1, which is another BB2 receptor antagonist peptide conjugate.[40]

Prolonged retention of [$^{203}$Pb]Pb-RM2 in the tumor was observed with 7.73 ± 2.33% ID/g remaining at 4 hours post injection, 4.36 ± 0.98% ID/g remaining at 24 hours post injection, and 3.11 ± 0.67% ID/g remaining at 48 hours post injection. The specificity of the observed tumor uptake was confirmed by conducting a blocking experiment, which involved pre-injection of 20 nmoles of unlabeled RM2 peptide conjugate prior to administration of [$^{203}$Pb]Pb-RM2. The tumor uptake was significantly lowered from 7.73 ± 2.33 % ID/g to 0.67 ± 0.15 % ID/g at 4 hours post injection of [$^{203}$Pb]Pb-RM2 (**Table 2-4)**. This represents a 91.3 % blockage ($p < 0.0001$) in tumor uptake, which demonstrates that the tumor uptake is BB2 receptor-mediated.

Rapid whole-body clearance of [$^{203}$Pb]Pb-RM2 was observed with 90.44 ± 2.92% and 94.59 ± 1.85% of the total injected dose excreted by 4 hour and 24 hours post injection,

respectively. Fast blood clearance was also observed with 0.05 + 0.01% ID/g and 0.03 ± 0.01% ID/g remaining at 4 hour and 24 hours post injection, respectively. [$^{203}$Pb]Pb-RM2 is excreted predominantly via the kidney into the urinary system. Due to the rapid clearance of [$^{203}$Pb]Pb-RM2 from the blood and nonspecifically targeted organs, high tumor to background ratios were observed, which generally increased with time through 2 hours post injection. For example, the tumor-to-blood ratio was 2.56 at 15 min post injection and increased to 187.67 at 2 hours post injection. Similarly, the tumor-to-muscle ratio increased from 8.78 at 15 min post injection to 213.67 at 2 hours post injection (**Table 2-3**).

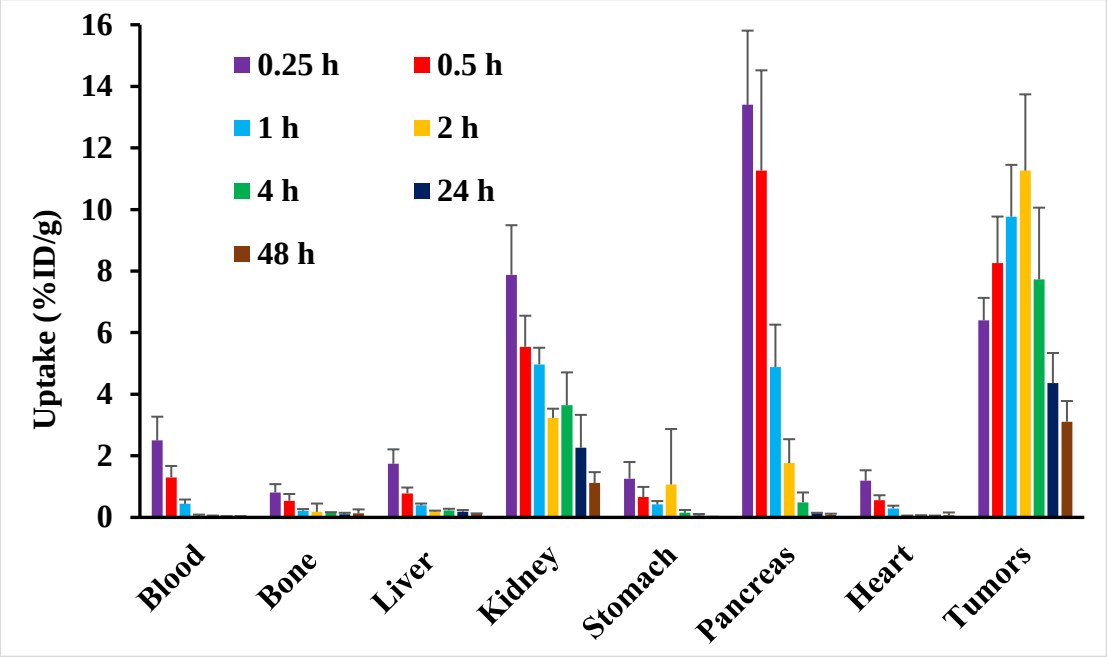


**Figure 2-6**. Biodistribution [$^{203}$Pb]Pb-RM2 in PC3 tumor bearing mice (n = 5 per time point)

**Table 2-3. [$^{203}$Pb]Pb-RM2 biodistribution in PC3 tumor-bearing mice.**
**Data shown as mean ± SD %ID/g (n = 5 mice per time point)**

| Tissue | 15 min | 30 min | 1 h | 2 h | 4 h | 24 h | 48 h |
|---|---|---|---|---|---|---|---|
| **Blood** | 2.50 ± 0.77 | 1.30 ± 0.37 | 0.44 ± 0.14 | 0.06 ± 0.03 | 0.05 ± 0.01 | 0.03 ± 0.01 | 0.02 ± 0.02 |
| **Heart** | 1.19 ± 0.34 | 0.56 ± 0.16 | 0.29 ± 0.09 | 0.05 ± 0.01 | 0.05 ± 0.02 | 0.03 ± 0.03 | 0.07 ± 0.09 |
| **Lung** | 2.41 ± 0.70 | 1.14 ± 0.26 | 0.57 ± 0.08 | 0.15 ± 0.07 | 0.12 ± 0.02 | 0.07 ± 0.05 | 0.05 ± 0.04 |
| **Liver** | 1.74 ± 0.47 | 0.78 ± 0.19 | 0.39 ± 0.06 | 0.20 ± 0.02 | 0.23 ± 0.05 | 0.18 ± 0.06 | 0.11 ± 0.02 |
| **Stomach** | 1.26 ± 0.54 | 0.66 ± 0.33 | 0.42 ± 0.11 | 1.07 ± 1.80 | 0.15 ± 0.09 | 0.06 ± 0.05 | 0.01 ± 0.01 |
| **Sm. Intestines** | 1.75 ± 0.48 | 1.33 ± 0.30 | 0.85 ± 0.08 | 2.01 ± 3.38 | 0.27 ± 0.16 | 0.17 ± 0.22 | 0.02 ± 0.00 |
| **Lg. Intestines** | 0.89 ± 0.24 | 0.57 ± 0.12 | 0.32 ± 0.08 | 0.72 ± 0.17 | 1.59 ± 1.32 | 0.14 ± 0.04 | 0.07 ± 0.03 |
| **Kidney** | 7.88 ± 1.61 | 5.54 ± 1.01 | 4.97 ± 0.54 | 3.23 ± 0.30 | 3.65 ± 1.06 | 2.26 ± 1.07 | 1.12 ± 0.35 |
| **Spleen** | 0.88 ± 0.27 | 0.37 ± 0.12 | 0.27 ± 0.08 | 0.21 ± 0.31 | 0.24 ± 0.12 | 0.12 ± 0.05 | 0.20 ± 0.30 |
| **Brain** | 0.15 ± 0.03 | 0.07 ± 0.02 | 0.03 ± 0.01 | 0.02 ± 0.01 | 0.01 ± 0.01 | 0.00 ± 0.00 | 0.01 ± 0.02 |
| **Pancreas** | 13.40 ± 2.41 | 11.26 ± 3.26 | 4.88 ± 1.38 | 1.76 ± 0.78 | 0.49 ± 0.32 | 0.13 ± 0.02 | 0.08 ± 0.04 |
| **Muscle** | 0.73 ± 0.22 | 0.41 ± 0.17 | 0.12 ± 0.03 | 0.03 ± 0.01 | 0.04 ± 0.03 | 0.06 ± 0.06 | 0.02 ± 0.02 |
| **Bone** | 0.81 ± 0.27 | 0.54 ± 0.22 | 0.22 ± 0.05 | 0.18 ± 0.27 | 0.14 ± 0.03 | 0.10 ± 0.05 | 0.13 ± 0.13 |
| **Tumors** | 6.41 ± 0.73 | 8.26 ± 1.51 | 9.77 ± 1.68 | 11.26 ± 2.48 | 7.73 ± 2.33 | 4.36 ± 0.98 | 3.11 ± 0.67 |
| **Tumor / Blood** | 2.56 | 6.35 | 22.21 | 187.67 | 154.60 | 145.33 | 155.50 |
| **Tumor / Muscle** | 8.78 | 15.63 | 53.42 | 213.67 | 160.25 | 106.83 | 320.50 |
| **Tumor / Liver** | 3.68 | 10.59 | 25.05 | 56.30 | 33.61 | 24.22 | 28.27 |
| **Tumor / Kidney** | 0.81 | 1.49 | 1.97 | 3.49 | 2.12 | 1.93 | 2.78 |
| **Tumor / Pancreas** | 0.48 | 0.73 | 2.00 | 6.40 | 15.78 | 33.56 | 38.88 |
| **Tumor / Bone** | 7.91 | 15.30 | 44.41 | 62.56 | 55.21 | 44.30 | 23.92 |
| **Urine (%ID)** | 41.66 ± 0.27 | 57.42 ± 4.40 | 79.36 ± 1.25 | 86.75 ± 8.01 | 90.44 ± 2.92 | 92.32 ± 2.06 | 91.72 ± 4.86 |
| **Excretion (%ID)** | 41.66 ± 0.27 | 57.42 ± 4.40 | 79.36 ± 1.25 | 86.75 ± 8.01 | 90.44 ± 2.92 | 94.59 ± 1.85 | 97.36 ± 0.92 |

Note: Values for urine include radioactivity measured in cage paper

A relatively high uptake of 13.40 ± 2.41% ID/g at 15 min post injection was observed in the pancreas. The pancreas is well known to be rich in BB2 receptors, and other peptide analogues that target the BB2 receptor have been shown to exhibit uptake in the pancreas.[12, 33, 36-37, 40-41] However, the clearance rate of [$^{203}$Pb]Pb-RM2 from the pancreas is rapid with 0.49 ± 0.32% ID/g and 0.13 ± 0.02% ID/g remaining at 4 hours and 24 hours post injection, respectively. This is in contrast to the prolonged retention of [$^{203}$Pb]Pb-RM2 in the tumor, which had 7.73 ± 2.33% ID/g and 4.36 ± 0.98% ID/g remaining at 4 hours and 24 hours post injection, respectively (**Figure 2-7**). Very minimal uptake was observed at every time point in critical non-target organs, including liver, bone, muscle, heart, intestines, and stomach.

**Table 2-4. [$^{203}$Pb]Pb-RM2 tumor uptake specificity**
**Data shown as mean ± SD %ID/g (n = 5 mice per time point)**

| Tissue | 4 h | 4 h Block |
|---|---|---|
| **Blood** | 0.05 ± 0.01 | 0.05 ± 0.04 |
| **Heart** | 0.05 ± 0.02 | 0.03 ± 0.02 |
| **Lung** | 0.12 ± 0.02 | 0.08 ± 0.01 |
| **Liver** | 0.23 ± 0.05 | 0.24 ± 0.02 |
| **Stomach** | 0.15 ± 0.09 | 0.15 ± 0.15 |
| **Sm. Intestines** | 0.27 ± 0.16 | 0.31 ± 0.26 |
| **Lg. Intestines** | 1.59 ± 1.32 | 1.15 ± 0.33 |
| **Kidney** | 3.65 ± 1.06 | 3.55 ± 0.43 |
| **Spleen** | 0.24 ± 0.12 | 0.22 ± 0.14 |
| **Brain** | 0.01 ± 0.01 | 0.01 ± 0.01 |
| **Pancreas** | 0.49 ± 0.32 | 0.11 ± 0.03 |
| **Muscle** | 0.04 ± 0.03 | 0.07 ± 0.05 |
| **Bone** | 0.14 ± 0.03 | 0.10 ± 0.04 |
| **Tumors** | 7.73 ± 2.33 | 0.67 ± 0.15 |
| **Excretion (%ID)** | 90.44 ± 2.92 | 94.29 ± 1.34 |

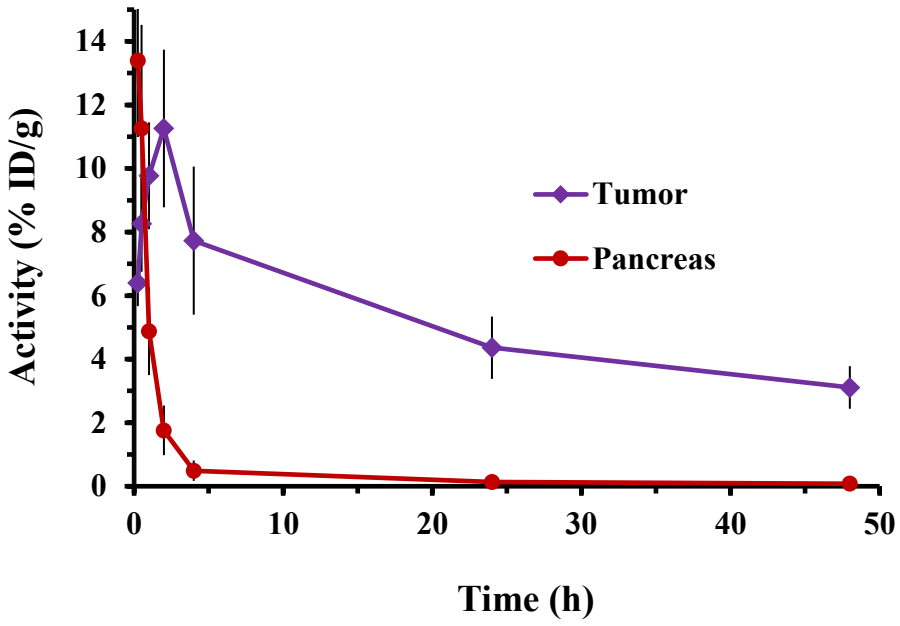


**Figure 2-7**. Comparison of [$^{203}$Pb]Pb-RM2 uptake in tumor and pancreas (n = 5 per time point)

The pharmacokinetic behavior of [$^{203}$Pb]$PbCl_2$ was distinctively different from that of [$^{203}$Pb]Pb-RM2. [$^{203}$Pb]$PbCl_2$ exhibited slow whole-body clearance and preferentially accumulated in the kidney, bone, and liver (**Table 2-2)**. In contrast, [$^{203}$Pb]Pb-RM2 exhibits rapid whole-body clearance, with very minimal uptake in the bone and liver at every time point studied (**Table 2-3)**. The [$^{203}$Pb]Pb-RM2 uptake observed in the kidney is as a result of normal clearance through the urinary system. This distinctive difference in the biodistribution of [$^{203}$Pb]Pb-RM2 in comparison to [$^{203}$Pb]$PbCl_2$ is depicted in **Figure 2-8** and is an indication of the high *in vivo* stability of [$^{203}$Pb]Pb-RM2.

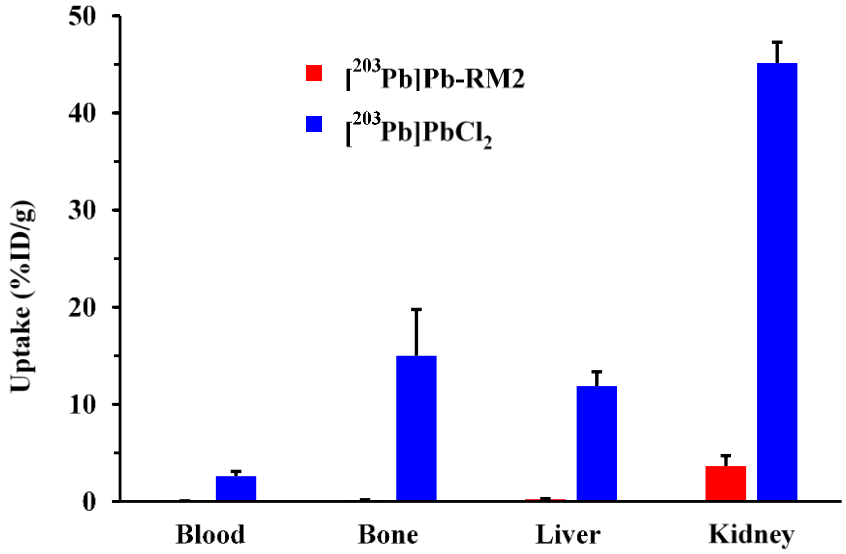


**Figure 2-8**. Comparison of [$^{203}$Pb]Pb-RM2 and [$^{203}$Pb]$PbCl_2$ uptake in select organs at 4 hours post injection (n = 5)

## 2.3-5. Micro SPECT/microCT Imaging Studies

The pharmacokinetic data is consistent with the micro-SPECT/CT images as shown in **Figures 2-9A and 2-9B**. The maximum intensity projection micro-SPECT/CT image of [$^{203}$Pb]Pb-RM2 in a PC3 tumor-bearing SCID mouse obtained at 24 hours post injection clearly shows high and selective drug accumulation in the tumors (**Figure 2-9A**). No visible [$^{203}$Pb]Pb-RM2 activity was observed in all other non-target organs except for minimal activity in the kidney, which is the predominant clearance organ for [$^{203}$Pb]Pb-RM2.

In contrast, the micro-SPECT/CT image of [$^{203}$Pb]$PbCl_2$ in a CF-1 mouse shows high drug accumulation in the kidney, liver and bone, demonstrating that free $^{203}$Pb preferentially accumulates in these organs (**Figure 2-9B, right)**. The absence of high kidney, liver and bone retention observed in the [$^{203}$Pb]Pb-RM2 (**Figure 2-9B, left)** micro-SPECT/CT image is a confirmation of the *in vivo* stability of [$^{203}$Pb]Pb-RM2.

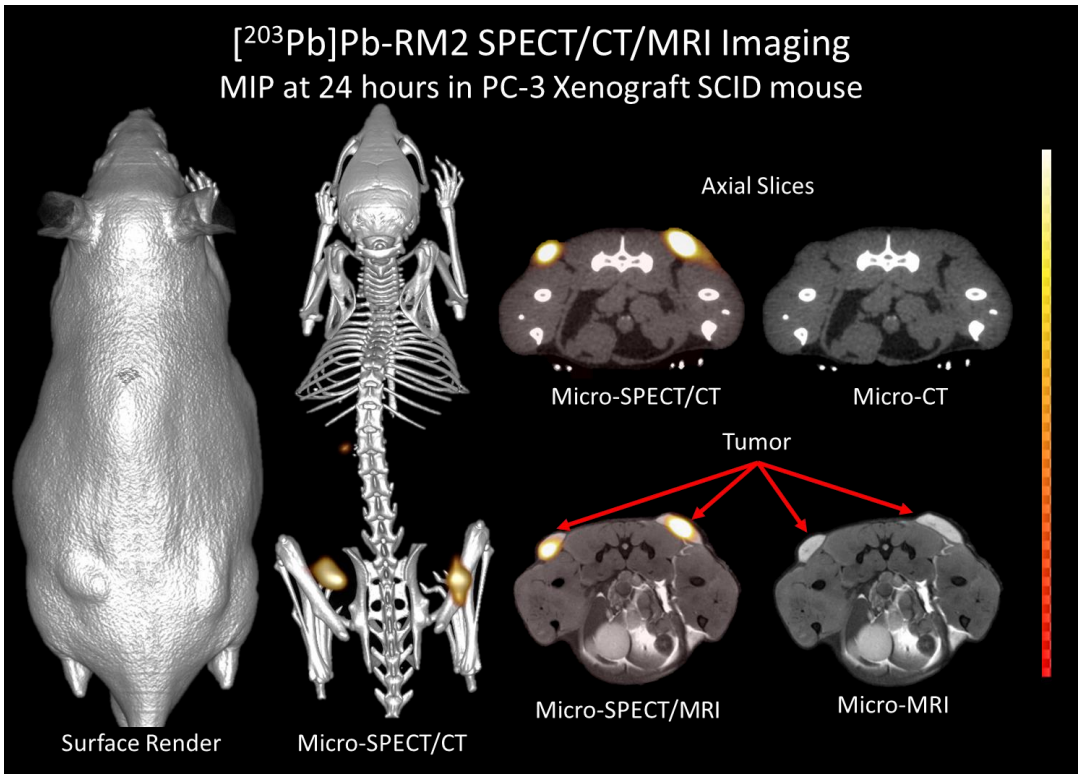


**Figure 2-9A.** MIP SPECT/CT/MRI image of [$^{203}$Pb]Pb-RM2 in PC3 xenograft SCID mouse at 24 hours post injection.

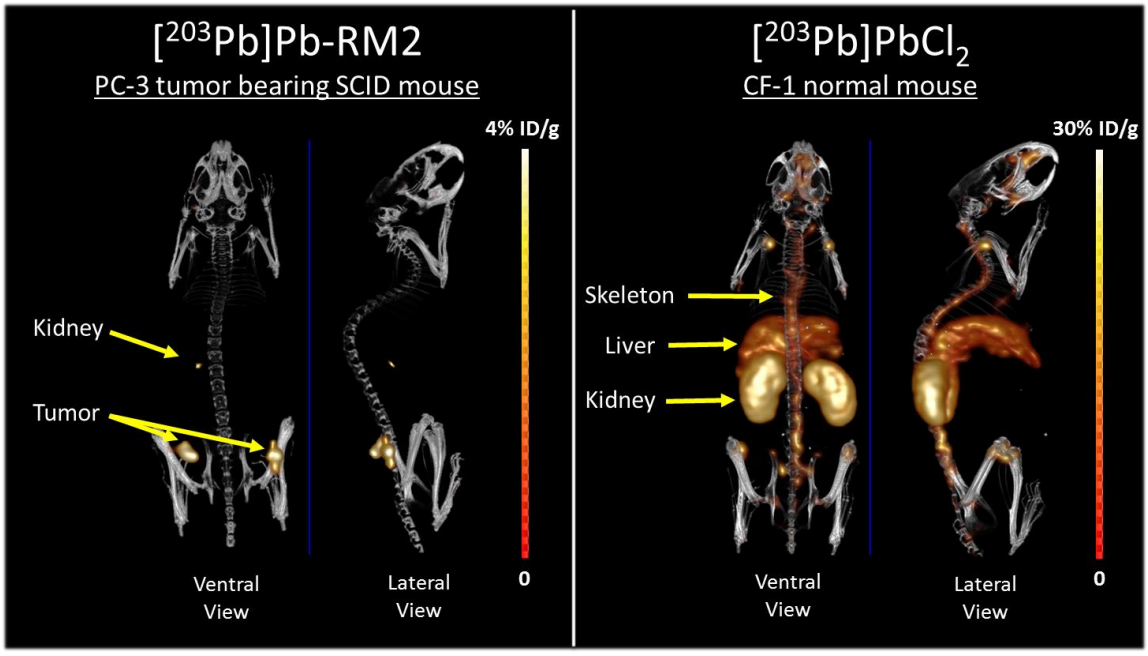


**Figure 2-9B.** Comparison between [$^{203}$Pb]Pb-RM2 (left panel) and [$^{203}$Pb]$PbCl_2$ (right panel) at 24 hours post injection

## 2.4. Conclusions

This study demonstrates the potential utility of $^{203}$Pb as a clinically relevant diagnostic radionuclide. The successful synthesis of [$^{203}$Pb]Pb-RM2, a radiolabeled antagonist peptide conjugate that targets the BB2 receptor overexpressed in prostate cancer cells, was described. [$^{203}$Pb]Pb-RM2 exhibited selective and prolonged tumor uptake in PC3 tumor-bearing SCID male mice. Additionally, we demonstrated the ability to visualize PC3 tumor xenografts in this mouse model using micro-SPECT/CT. In general, the rapid clearance of [$^{203}$Pb]Pb-RM2 from the whole body, accompanied with its high and specific uptake and retention in PC3 tumor xenografts, resulted in a favorable pharmacokinetic profile. It is worth mentioning that the presence of non-radioactive Pb in the [$^{203}$Pb]$PbCl_2$ precursor would, in theory, lower the specific activity of the administered [$^{203}$Pb]Pb-RM2 and may have led to lower uptake values in BB2-receptor expressing tissues. Based on the amount of non-radioactive Pb present in the [$^{203}$Pb]$PbCl_2$ precursor, it was calculated that the specific activity ranged from 6 – 11 mCi/μg. This indicates that only 2 – 4% of the total Pb atoms used for radiolabeling are present as $^{203}$Pb atoms, which would lead to competition between [$^{203}$Pb]Pb-RM2 and non-radioactive Pb-RM2 for the BB2 receptors.

The current action level for Pb in drinking water recommended by the United States Environmental Protection Agency (EPA) is 15 ppb (~15 μg/L). Based on the specific activity of the [$^{203}$Pb]$PbCl_2$ precursor reported here, a 25 mCi [$^{203}$Pb]Pb-RM2 patient injection (typical dose administered for [$^{99m}$Tc]Tc-Sestamibi SPECT scan) will contain ~2.2 μg of Pb, which is still below the EPA action level. However, in a high specific activity [$^{203}$Pb]$PbCl_2$ precursor with negligible non-radioactive Pb contamination, the same 25 mCi [$^{203}$Pb]Pb-RM2 patient injection would contain only ~0.09 μg of Pb, which is more

acceptable. Hence, an improved [$^{203}$Pb]$PbCl_2$ production method minimizing the amount of non-radioactive Pb contamination would be beneficial.

Comparing the biodistribution of [$^{203}$Pb]Pb-RM2 with that of other radiolabeled BB2 receptor-targeting peptides reported in literature may be challenging due to the differences in precursor specific activity and total amount of peptide conjugate used during synthesis. However, we can report that the general pharmacokinetic profile of [$^{203}$Pb]Pb-RM2 follows the same trend as what has been reported for other radiolabeled RM2 peptide conjugates including [$^{111}$In]In-RM2[12], [$^{68}$Ga]Ga-RM2[12], and [$^{177}$Lu]Lu-RM2[18]. A comparable pharmacokinetic profile was also reported for another BB2 receptor antagonist peptide conjugate, [$^{68}$Ga]Ga-NeoBOMB1.[40]

In conclusion, the BB2 receptor remains a very attractive target for developing prostate cancer radiopharmaceuticals. The favorable pharmacokinetic profile and BB2 receptor-targeting ability of [$^{203}$Pb]Pb-RM2 further highlights its potential as a diagnostic agent for prostate cancer.

## 2.5. Future Studies

As previously mentioned, the commercially purchased [$^{203}$Pb]$PbCl_2$ precursor contains significant Fe and Pb impurities. Lead-203 is typically isolated as a byproduct from the cyclotron waste stream during the production of $^{201}$Tl.[29] However, the cyclotron waste stream contains other metal contaminants, including Cu, Ni, Fe, and Zn. One of the potential sources of Pb impurities is the co-production of stable $^{204}$Pb via the $^{205}$Tl (p, 2n) $^{204m}$Pb ➔ $^{204}$Pb reaction, which is a side reaction from the desired $^{205}$Tl (p, 3n) $^{203}$Pb.[26] For routine clinical utility of $^{203}$Pb in radiopharmaceutical formulations, other $^{203}$Pb production methods that minimize Fe and Pb metallic impurities need to be developed.

One alternative $^{203}$Pb production route is via the $^{203}$Tl (p, n) $^{203}$Pb reaction. According to the TENDL-2017 nuclear data library, the maximum theoretical cross section for the $^{203}$Tl (p, n) $^{203}$Pb reaction is 111 mb at an incident proton energy of 11 MeV (**Figure 2-10**).[42] Hence, an enriched (>98%) $^{203}$Tl metal target can be irradiated with a proton beam of approximately 11 MeV. The feasibility of this production route has been demonstrated by Máthé et al.[38] The authors reported the production of 2.2 mCi (80 MBq) of $^{203}$Pb after bombardment of natural Tl metal with a proton beam of 14.5 MeV and beam current of 5 μA for 18 hours. Using more mass of enriched $^{203}$Tl metal target and a higher beam current along with a longer irradiation time would increase $^{203}$Pb production yield. However, enhanced target cooling will be needed to mitigate potential target failure due to the relatively low melting point (303.5 °C) and thermal conductivity (46.1 $W.m^{-1}\cdot K^{-1}$) of Tl. As an alternative, Tl can be electroplated or melted onto a Cu plate to enhance heat dissipation, as previously reported.[26, 43-44]

The irradiated Tl metal target can be dissolved in dilute $HNO_3$ following reported literature procedures.[26, 38] Several ion exchange resins, including Chelex 100[26, 29], AG50W-X4[44], and DOXEX[31, 38] have been used to separate $^{203}$Pb from bulk Tl metal target material. In addition, a second purification step using a Pb-resin column can be performed following the procedure reported in this study in order to further remove metallic impurities. If high specific activity [$^{203}$Pb]$PbCl_2$ is successfully produced, [$^{203}$Pb]Pb-RM2 biodistribution studies should be repeated and compared with the data reported in this study.

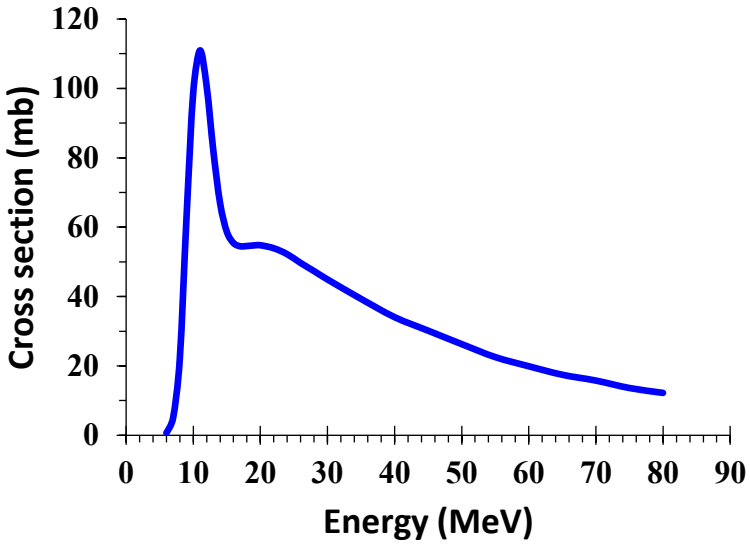


**Figure 2-10**. Calculated excitation function for the $^{203}$Tl (p, n) $^{203}$Pb nuclear reaction.[42]

## 2.6. References


1. Hayes, J. H.; Barry, M. J., Screening for prostate cancer with the prostate-specific antigen test: a review of current evidence. *Jama* **2014,** *311* (11), 1143-1149.

2. Markwalder, R.; Reubi, J. C., Gastrin-releasing peptide receptors in the human prostate relation to neoplastic transformation. *Cancer Research* **1999,** *59* (5), 1152-1159.

3. Bartholdi, M. F.; Wu, J. M.; Pu, H.; Troncoso, P.; Eden, P. A.; Feldman, R. I., In situ hybridization for gastrin‐releasing peptide receptor (GRP receptor) expression in prostatic carcinoma. *International Journal of Cancer* **1998,** *79* (1), 82-90.

4. Sun, B.; Halmos, G.; Schally, A. V.; Wang, X.; Martinez, M., Presence of receptors for bombesin/gastrin‐releasing peptide and mRNA for three receptor subtypes in human prostate cancers. *The Prostate* **2000,** *42* (4), 295-303.

5. Körner, M.; Waser, B.; Rehmann, R.; Reubi, J. C., Early over‐expression of GRP receptors in prostatic carcinogenesis. *The Prostate* **2014,** *74* (2), 217-224.

6. Ischia, J.; Patel, O.; Bolton, D.; Shulkes, A.; Baldwin, G. S., Expression and function of gastrin‐releasing peptide (GRP) in normal and cancerous urological tissues. *BJU International* **2014,** *113*, 40-47.

7. Jensen, R.; Battey, J.; Spindel, E.; Benya, R., International Union of Pharmacology. LXVIII. Mammalian bombesin receptors: nomenclature, distribution, pharmacology, signaling, and functions in normal and disease states. *Pharmacological Reviews* **2008,** *60* (1), 1-42.

8. Mansi, R.; Fleischmann, A.; Mäcke, H. R.; Reubi, J. C., Targeting GRPR in urological cancers—from basic research to clinical application. *Nature Reviews Urology* **2013,** *10* (4), 235-244.

9. Smith, C.; Volkert, W.; Hoffman, T., Gastrin releasing peptide (GRP) receptor targeted radiopharmaceuticals: a concise update. *Nuclear Medicine and Biology* **2003,** *30* (8), 861-868.

10. Baratto, L.; Jadvar, H.; Iagaru, A., Prostate cancer theranostics targeting gastrin-releasing peptide receptors. *Molecular Imaging and Biology* **2018,** *20* (4), 501-509.

11. Mansi, R.; Minamimoto, R.; Mäcke, H.; Iagaru, A. H., Bombesin-Targeted PET of Prostate Cancer. *Journal of Nuclear Medicine* **2016,** *57* (Supplement 3), 67S-72S.

12. Mansi, R.; Wang, X. J.; Forrer, F.; Waser, B.; Cescato, R.; Graham, K.; Borkowski, S.; Reubi, J. C.; Maecke, H. R., Development of a potent DOTA-conjugated bombesin antagonist for targeting GRPr-positive tumours. *European Journal of Nuclear Medicine and Molecular Imaging* **2011,** *38* (1), 97-107.

13. Kähkönen, E.; Jambor, I.; Kemppainen, J.; Lehtiö, K.; Grönroos, T. J.; Kuisma, A.; Luoto, P.; Sipilä, H. J.; Tolvanen, T.; Alanen, K., In vivo imaging of prostate cancer using

[$^{68}$Ga]-labeled bombesin analog BAY86-7548. *Clinical Cancer Research* **2013,** *19* (19), 5434-5443.

14. Wieser, G.; Popp, I.; Rischke, H. C.; Drendel, V.; Grosu, A.-L.; Bartholomä, M.; Weber, W. A.; Mansi, R.; Wetterauer, U.; Schultze-Seemann, W., Diagnosis of recurrent prostate cancer with PET/CT imaging using the gastrin-releasing peptide receptor antagonist $^{68}$Ga-RM2: Preliminary results in patients with negative or inconclusive [$^{18}$F]Fluoroethylcholine-PET/CT. *European Journal of Nuclear Medicine and Molecular Imaging* **2017**, 1-10.

15. Minamimoto, R.; Hancock, S.; Schneider, B.; Chin, F.; Jamali, M.; Loening, A. M.; Vasanawala, S.; Gambhir, S. S.; Iagaru, A., Pilot Comparison of $^{68}$Ga-RM2 PET and $^{68}$Ga-PSMA PET in Patients with Biochemically Recurrent Prostate Cancer. *Journal of Nuclear Medicine* **2016**, 557-562.

16. Minamimoto, R.; Sonni, I.; Hancock, S.; Vasanawala, S.; Loening, A.; Gambhir, S. S.; Iagaru, A., Prospective Evaluation of $^{68}$Ga-RM2 PET/MRI in Patients with Biochemical Recurrence of Prostate Cancer and Negative Conventional Imaging. *Journal of Nuclear Medicine* **2018,** *59* (5), 803-808.

17. Fassbender, T. F.; Schiller, F.; Mix, M.; Maecke, H. R.; Kiefer, S.; Drendel, V.; Meyer, P. T.; Jilg, C. A., Accuracy of [$^{68}$Ga]Ga-RM2-PET/CT for diagnosis of primary prostate cancer compared to histopathology. *Nuclear Medicine and Biology* **2019,** *70*, 32-38.

18. Breier, R. D.; Rold, T. L.; Szczodroski, A. F.; Hoffman, T. J., Evaluation of Lu-177 RM2 as a targeted radiopharmaceutical in a PC-3 xenograft model of androgen-independent prostate cancer. *Journal of Clinical Oncology* **2011,** *29* (15), e13522-e13522.

19. Donnelly, L.; Rold, T.; Richmond, K.; Szczodroski, A.; Sieckman, G.; Haddadin, S.; Hoffman, T., Combination Lu-177 BB2r antagonist/chemotherapy control of prostate cancer: A preclinical evaluation. *Journal of Nuclear Medicine* **2012,** *53* (supplement 1), 1194-1194.

20. Yong, K.; Brechbiel, M. W., Towards translation of $^{212}$Pb as a clinical therapeutic; getting the lead in! *Dalton Transactions* **2011,** *40* (23), 6068-6076.

21. Yong, K.; Brechbiel, M., Application of $^{212}$Pb for Targeted $\alpha$-particle Therapy (TAT): pre-clinical and mechanistic understanding through to clinical translation. *AIMS medical science* **2015,** *2* (3), 228.

22. Tworowska, I.; Stallons, T.; Saidi, A.; Wagh, N.; Rojas-Quijano, F.; Jurek, P.; Kiefer, G.; Delpassand, E.; Torgue, J., Image guided therapy of SSTR (+)-neuroendocrine tumors (NETs) using $^{203}$Pb-labeled octreotate analog. *Journal of Nuclear Medicine* **2018,** *59* (supplement 1), 1124-1124.

23. Tworowska, I.; Stallons, T.; Saidi, A.; Wagh, N.; Rojas-Quijano, F.; Jurek, P.; Kiefer, G.; Torgue, J.; Delpassand, E., Pb203-AR-RMX conjugates for image-guided TAT of neuroendocrine tumors (NETs). Abstract LB-259:. AACR: 2017.

24. Miao, Y.; Figueroa, S. D.; Fisher, D. R.; Moore, H. A.; Testa, R. F.; Hoffman, T. J.; Quinn, T. P., $^{203}$Pb-Labeled $\alpha$-Melanocyte–Stimulating Hormone Peptide as an Imaging Probe for Melanoma Detection. *Journal of Nuclear Medicine* **2008,** *49* (5), 823-829.

25. Miao, Y.; Hylarides, M.; Fisher, D. R.; Shelton, T.; Moore, H.; Wester, D. W.; Fritzberg, A. R.; Winkelmann, C. T.; Hoffman, T.; Quinn, T. P., Melanoma therapy via peptide-targeted $\alpha$-radiation. *Clinical Cancer Research* **2005,** *11* (15), 5616-5621.

26. Li, M.; Zhang, X.; Quinn, T. P.; Lee, D.; Liu, D.; Kunkel, F.; Zimmerman, B. E.; McAlister, D.; Olewein, K.; Menda, Y., Automated cassette-based production of high specific activity [$^{203/212}$Pb] peptide-based theranostic radiopharmaceuticals for image-guided radionuclide therapy for cancer. *Applied Radiation and Isotopes* **2017,** *127*, 52-60.

27. Yang, J.; Xu, J.; Cheuy, L.; Gonzalez, R.; Fisher, D. R.; Miao, Y., Evaluation of A Novel Pb-203-Labeled Lactam-Cyclized Alpha-Melanocyte-Stimulating Hormone Peptide for Melanoma Targeting. *Molecular Pharmaceutics* **2019**, Article ASAP.

28. dos Santos, J. C.; Schäfer, M.; Bauder-Wüst, U.; Lehnert, W.; Leotta, K.; Morgenstern, A.; Kopka, K.; Haberkorn, U.; Mier, W.; Kratochwil, C., Development and dosimetry of $^{203}$Pb/$^{212}$Pb-labelled PSMA ligands: bringing “the lead” into PSMA-targeted alpha therapy? *European Journal of Nuclear Medicine and Molecular Imaging* **2019**, 1-11.

29. Olewine, K. R. Methods and devices for isolating lead 203. United States Patent. 2017.

30. Horlock, P.; Thakur, M.; Watson, I., Cyclotron produced lead-203. *Postgraduate Medical Journal* **1975,** *51* (601), 751.

31. Qaim, S.; Weinreich, R.; Ollig, H., Production of $^{201}$Tl and $^{203}$Pb via proton induced nuclear reactions on natural thallium. *The International Journal of Applied Radiation and Isotopes* **1979,** *30* (2), 85-95.

32. Horwitz, E. P.; Dietz, M. L.; Rhoads, S.; Felinto, C.; Gale, N. H.; Houghton, J., A lead-selective extraction chromatographic resin and its application to the isolation of lead from geological samples. *Analytica Chimica Acta* **1994,** *292* (3), 263-273.

33. Hoffman, T. J.; Gali, H.; Smith, C. J.; Sieckman, G. L.; Hayes, D. L.; Owen, N. K.; Volkert, W. A., Novel series of $^{111}$In-labeled bombesin analogs as potential radiopharmaceuticals for specific targeting of gastrin-releasing peptide receptors expressed on human prostate cancer cells. *Journal of Nuclear Medicine* **2003,** *44* (5), 823-831.

34. Nock, B.; Nikolopoulou, A.; Chiotellis, E.; Loudos, G.; Maintas, D.; Reubi, J.; Maina, T., [$^{99m}$Tc] Demobesin 1, a novel potent bombesin analogue for GRP receptor-targeted tumour imaging. *European Journal of Nuclear Medicine and Molecular Imaging* **2003,** *30* (2), 247-258.

35. Lantry, L. E.; Cappelletti, E.; Maddalena, M. E.; Fox, J. S.; Feng, W.; Chen, J.; Thomas, R.; Eaton, S. M.; Bogdan, N. J.; Arunachalam, T., $^{177}$Lu-AMBA: Synthesis and

Characterization of a Selective $^{177}$Lu-Labeled GRP-R Agonist for Systemic Radiotherapy of Prostate Cancer. *Journal of Nuclear Medicine* **2006,** *47* (7), 1144.

36. Mansi, R.; Wang, X.; Forrer, F.; Kneifel, S.; Tamma, M.-L.; Waser, B.; Cescato, R.; Reubi, J. C.; Maecke, H. R., Evaluation of a 1, 4, 7, 10-Tetraazacyclododecane-1, 4, 7, 10-Tetraacetic acid–conjugated bombesin-based radioantagonist for the labeling with single-photon emission computed tomography, positron emission tomography, and therapeutic radionuclides. *Clinical Cancer Research* **2009,** *15* (16), 5240-5249.

37. Nock, B. A.; Kaloudi, A.; Lymperis, E.; Giarika, A.; Kulkarni, H. R.; Klette, I.; Singh, A.; Krenning, E. P.; De Jong, M.; Maina, T., Theranostic perspectives in prostate cancer with the gastrin-releasing peptide receptor antagonist NeoBOMB1: preclinical and first clinical results. *Journal of Nuclear Medicine* **2017,** *58* (1), 75-80.

38. Máthé, D.; Szigeti, K.; Hegedűs, N.; Horváth, I.; Veres, D. S.; Kovács, B.; Szűcs, Z., Production and in vivo imaging of $^{203}$Pb as a surrogate isotope for in vivo $^{212}$Pb internal absorbed dose studies. *Applied Radiation and Isotopes* **2016,** *114*, 1-6.

39. Lever, S.; Scheffel, U., Regional distribution of $^{203}PbCl_2$ in the mouse after intravenous injection. *Neurotoxicology* **1998,** *19* (2), 197-207.

40. Dalm, S. U.; Bakker, I. L.; de Blois, E.; Doeswijk, G. N.; Konijnenberg, M. W.; Orlandi, F.; Barbato, D.; Tedesco, M.; Maina, T.; Nock, B. A., $^{68}$Ga/$^{177}$Lu-NeoBOMB1, a novel radiolabeled GRPR antagonist for theranostic use in oncology. *Journal of Nuclear Medicine* **2017,** *58* (2), 293-299.

41. Zhang, H.; Schuhmacher, J.; Waser, B.; Wild, D.; Eisenhut, M.; Reubi, J. C.; Maecke, H. R., DOTA-PESIN, a DOTA-conjugated bombesin derivative designed for the imaging and targeted radionuclide treatment of bombesin receptor-positive tumours. *European Journal of Nuclear Medicine and Molecular Imaging* **2007,** *34* (8), 1198-1208.

42. Koning, A. J.; Rochman, D., Modern Nuclear Data Evaluation with the TALYS Code System. *Nuclear Data Sheets* **2012,** *113* (12), 2841-2934.

43. Kozlova, M.; Levin, V.; Malinin, A.; Kondratyeva, T.; Sevastyanova, A.; Kurenkov, N., The production of carrier-free lead-203. *The International Journal of Applied Radiation and Isotopes* **1982,** *33* (7), 553-555.

44. Van der Walt, T.; Strelow, F.; Haasbroek, F., Separation of lead-203 from cyclotron-bombarded thallium targets by ion-exchange chromatography. *Talanta* **1982,** *29* (7), 583-587.

# CHAPTER 3: $^{212}$Pb Targeted Alpha Therapy of BB2 Receptor Positive Prostate Cancer

## 3.1. Introduction

With about 31,620 estimated deaths in 2019, prostate cancer is currently the second leading cause of cancer-related deaths in American men, behind lung cancer.[1] For men with castration-recurrent prostate cancer, androgen deprivation therapy (ADT) has been the standard treatment for decades; however, resistance to first-line ADT can develop over time. Although subsequent therapies, including taxane-based chemotherapy (e.g., docetaxel, cabazitaxel), hormone therapy (e.g., abiraterone and enzalutamide), immunotherapy (e.g., sipuleucel-T), can be utilized upon disease progression, the duration of a response to treatment is often finite and treatment can become less effective over time, leading to patients being placed in best supportive care.[2] Therefore, additional effective treatment strategies are needed.

One promising treatment option that is being investigated is peptide receptor radionuclide therapy (PRRT). PRRT involves the complexation of a therapeutic radionuclide to a suitable chelator conjugated to a peptide that targets specific peptide receptors overexpressed on cancer cells.[3-4] In most cases, a diagnostic radionuclide can also be complexed to the same chelator, allowing for the development of a matched pair of diagnostic and therapeutic (i.e., theranostic) radiopharmaceuticals.[5] The clinical potential of PRRT was recently affirmed by the FDA approval of [$^{177}$Lu]Lu-Dotatate (Lutathera®), which is a $^{177}$Lu-labeled somatostatin agonist peptide conjugate that was shown to improve overall survival in patients with somatostatin receptor positive neuroendocrine tumors.[6] Furthermore, [$^{68}$Ga]Ga-Dotatate (Netspot®), the diagnostic analogue to [$^{177}$Lu]Lu-

Dotatate, was also approved by the FDA. The clinical successes of [$^{177}$Lu]Lu-Dotatate and [$^{68}$Ga]Ga-Dotatate demonstrate the potential of developing targeted theranostic radiopharmaceuticals for prostate cancer.

Efforts towards the development of targeted prostate cancer radiopharmaceuticals have focused on molecules that target the prostate specific membrane antigen (PSMA) or the gastrin-releasing peptide receptor (BB2r). PSMA is a type II transmembrane protein that has been shown to be overexpressed in prostate cancer cells.[7-9] Likewise, BB2r is a seven transmembrane protein that is also overexpressed in prostate cancer cells.[10-14] Hence, several PSMA-targeting molecules (e.g., PSMA-11, PSMA I&T, PSMA-617, etc.)[15-18] and BB2r-targeting molecules (e.g., RM2, AMBA, NeoBOMB1, etc.)[19-23] have been synthesized and radiolabeled with various clinically-relevant diagnostic and therapeutic radionuclides. However, there is some evidence suggesting that the levels of PSMA and BB2r can be influenced by other pharmacological compounds.[24-27] This suggests that some patients may benefit more from PSMA-targeted radiopharmaceuticals, while others may benefit more from BB2r-targeted radiopharmaceuticals. For example, Minamimoto et al.[28] recently compared the uptake of [$^{68}$Ga]Ga-PSMA and [$^{68}$Ga]Ga-RM2 in seven men with biochemically recurrent prostate cancer and reported that some prostate cancer lesions were better visualized using [$^{68}$Ga]Ga-PSMA, while others were better visualized using [$^{68}$Ga]Ga-RM2. Hence, there is need for both PSMA-targeted and BB2r-targeted radiopharmaceuticals to be developed.

The goal of this current study was to synthesize and evaluate a BB2r targeted alpha-emitting radiopharmaceutical for the treatment of prostate cancer by incorporating $^{212}$Pb into RM2 (RM2= DOTA- 4-amino-1-carboxymethyl-piperidine-D-Phe-Gln-Trp-Ala-Val-

Gly-His-Sta-Leu-$NH_2$), a potent BB2r antagonist peptide conjugate that has been shown to exhibit high and specific tumor targeting in BB2r-expressing prostate cancer cell line xenografts and in patients with prostate cancer (**Figure 2-1**).[19, 28-30] The rationale behind this study is that alpha-emitting radionuclides, when adequately targeted to cancer cells, can deliver a highly localized cytotoxic radiation dose to the cells, which would cause more irreparable double-strand DNA breakage compared to radionuclides that emit only beta particles. It is well known that alpha particles have a densely ionizing track with high linear energy transfer properties (~100 keV/μm) and short penetration range in tissues (50-100 μm).[31-34] The cytotoxic superiority of alpha-emitting radionuclides over beta-emitting radionuclides has been demonstrated in several preclinical and clinical studies.[15, 35-36]

Although not an alpha emitter, $^{212}$Pb ($t_{1/2}$ = 10.6 hours) decays by beta emission ($\beta^-_{avg}$ = 0.10 MeV) to the alpha-emitting $^{212}$Bi ($t_{1/2}$ = 60.6 minutes). Bismuth-212 subsequently decays into stable $^{208}$Pb through a branched decay chain consisting of one alpha particle emission and one beta particle emission through each decay pathway, as shown in **Figure 3-1**. Therefore, $^{212}$Pb can serve as an *in vivo* generator of $^{212}$Bi resulting in the net emission of one alpha particle and two beta particles. Using $^{212}$Pb as an *in vivo* generator of $^{212}$Bi compensates for the shorter half-life of $^{212}$Bi, and allows sufficient time for the preparation, administration, and *in vivo* accumulation of the radiopharmaceutical at its target site.[37] Additionally, the longer half-life of $^{212}$Pb is a better match for biomolecules with a longer biological half-life (e.g., antibodies). Another favorable factor that supports the clinical utility of $^{212}$Pb is the availability of a $^{224}$Ra/$^{212}$Pb generator system.

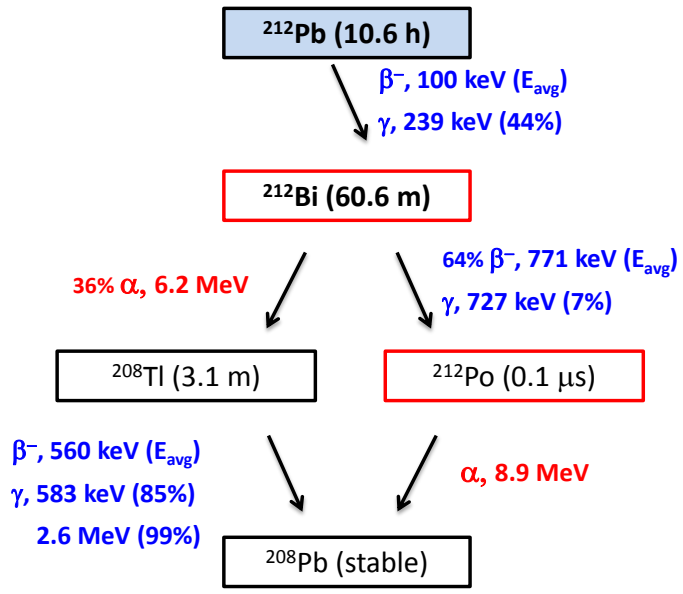


**Figure 3-1**. Lead-212 decay scheme

Several preclinical studies have demonstrated the feasibility of utilizing $^{212}$Pb for targeted alpha therapy.[38-49] The majority of these studies have been focused on $^{212}$Pb-labeled trastuzumab conjugates for targeting the human epidermal growth factor receptor type 2 (HER2) overexpressed in some cancers (e.g., ovarian, colorectal, and breast). Kasten et al.[42] reported no apparent radiation-related toxicity in the bone marrow, kidneys, and peritoneal organs after intraperitoneal injection of [$^{212}$Pb]Pb-TCMC-trastuzumab in cynomolgus monkeys. Likewise, significant therapeutic effect and no systemic toxic effect was reported by Tan et al.[41] after intravenous injection of [$^{212}$Pb]Pb-TCMC-trastuzumab in mice. These studies ultimately translated into the first-in-human clinical trial at the University of Alabama at Birmingham evaluating $^{212}$Pb targeted alpha therapy using [$^{212}$Pb]Pb-TCMC-trastuzumab.[50-52] Reports from this trial show that intraperitoneal administration of [$^{212}$Pb]Pb-TCMC-trastuzumab was well tolerated in patients even at the highest administered dose level (27 MBq/m$^2$ or 0.7 mCi/m$^2$), with no toxicity observed so

far over a >1 year follow-up period. A monoclonal antibody (376.96) targeting the B7-H3 antigen has been labeled with $^{212}$Pb and evaluated for radioimmunotherapy of ovarian and pancreatic cancers.[44-45] Miao et al.[46] reported decreased tumor growth rate in melanoma tumor-bearing mice after treatment with [$^{212}$Pb]Pb-DOTA-Re(Arg$^{11}$)CCMSH, a radiolabeled peptide targeting the melanocortin-1 receptor. Pretargeted approaches for $^{212}$Pb radioimmunotherapy have also been reported.[47-48] In general, these preclinical studies, together with the promising results from the clinical trials, demonstrate the safety and therapeutic efficacy of $^{212}$Pb. Herein, data on the synthesis and preclinical evaluation of [$^{212}$Pb]Pb-RM2 for targeted alpha therapy of prostate cancer is presented.

## 3.2. Experimental

### 3.2-1. Materials and Methods

The RM2 peptide conjugate was purchased from CPC Scientific, Inc. (Sunnyvale, CA, USA) and used without further purification. [$^{212}$Pb]$PbCl_2$ was eluted from an ~10 mCi $^{224}$Ra/$^{212}$Pb generator purchased from Oak Ridge National Laboratory (Oak Ridge, TN). **CAUTION!** $^{212}$Pb is radioactive and must be handled in laboratories outfitted and approved for work with radioactive materials. All work involving radioactivity was approved by the Harry S. Truman VA Hospital Radiation Safety Committee prior to performance. All radioactive dose measurements were performed using a Capintec CRC-Ultra dose calibrator (Florham Park, NJ, USA). Gamma spectroscopy measurements were performed using either a PerkinElmer 2480 WIZARD$^2$ gamma counter (Waltham, MA) containing a thallium-activated sodium iodide crystal or a portable Canberra model GC2018 high purity germanium detector (HPGe). The lead-selective chromatographic resin (Pb-resin) with a particle size of 100 – 150 μm was purchased from Eichrom

Technologies, LLC (Lisle, IL, USA). Fluka TraceSELECT ultrapure water, absolute ethanol, and trace metal grade HCl were obtained from Sigma-Aldrich (St. Louis, MO, USA) or Fisher Scientific (Waltham, MA, USA). Solid phase extraction (SPE) Sep-Pak C18 Plus Light Cartridges (55-105 μm particle size) were purchased from Waters Corporation (Milford, MA, USA). Radiochemical synthesis was performed using a Modular-Lab PharmTracer cassette based system (Eckert & Ziegler, Berlin, Germany). Deionized water (18.2 MΩ.cm) used for HPLC analyses was obtained from an in-house Aqua Solutions (Jasper, Georgia) water purification system. HPLC quality control of non-radiolabeled and radiolabeled peptides was performed using a Shimadzu Prominence HPLC system (Columbia, MD, USA) equipped with a UV-Vis absorbance detector (set at 220 and 280 nm) and a NaI(Tl) scintillation detector. All HPLC analyses were performed using a mobile phase consisting of solvent A (99.9% $H_2O$ and 0.1% trifluoroacetic acid [TFA]) and solvent B (99.9% $CH_3CN$ and 0.1% TFA) run on a Jupiter C-18 analytical HPLC column [5 u, 300 A, 250 × 4.6 mm purchased from Phenomenex® (Torrance, CA, USA)] maintained at a column temperature of 31 °C using an Eppendorf HPLC temperature control system. Two linear gradient protocols were developed for HPLC analyses. ***Gradient 1***: 10% solvent B:A increased to 70% solvent B:A over 8 minutes, followed by an additional 1 minute at 70% solvent B:A, then decreased to 10% solvent B:A over 1 minute at a flow rate of 1.5 mL/min. ***Gradient 2***: 22% solvent B:A increased to 25% solvent B:A over 19 minutes, followed by an additional 1 minute at 25% solvent B:A, then decreased to 22% solvent B:A over 1 minute at a flow rate of 1.5 mL/min.

### 3.2-2. Elution and Purification of $^{212}$Pb From $^{224}$Ra/$^{212}$Pb Generators

[$^{212}$Pb]$PbCl_2$ was slowly eluted from a $^{224}$Ra/$^{212}$Pb generator using 3 mL of 2 M HCl at a flow rate of ~1.5 mL/min. The amount of $^{212}$Pb radioactivity was measured using a CRC-Ultra dose calibrator set to the calibration for $^{212}$Pb (calibration # 101). Prior to radiolabeling, the [$^{212}$Pb]$PbCl_2$ solution was purified using a lead-selective chromatographic resin (Pb-resin) following the same procedure employed for the purification of [$^{203}$Pb]$PbCl_2$ as described in Chapter 2. Briefly, 50 mg of Pb-resin was packed into a fritted 1 mL polypropylene SPE column (Supelco 54220-U). The column was preconditioned with 3 mL of 2 M HCl. Next, 1 mL of the [$^{212}$Pb]$PbCl_2$ solution was loaded repeatedly onto the preconditioned column until the total volume was exhausted. The column was then washed with 3 mL of 0.5 M HCl. Finally, $^{212}$Pb was eluted from the column with 1 mL of 0.5 M NaOAc buffer (pH 6.5) repeatedly (using a maximum of 4 mL of NaOAc buffer). The radionuclide contents of the $^{212}Pb^{2+}$ solution before and after purification were determined using both an energy-calibrated PerkinElmer 2480 WIZARD$^2$ NaI(Tl) detector and a Canberra Model GC2018 portable HPGe detector.

### 3.2-3. Synthesis of [$^{212}$Pb]Pb-RM2

Synthesis of [$^{212}$Pb]Pb-RM2 was performed using the Eckert & Ziegler Modular-Lab PharmTracer automated cassette-based radiosynthesis system. A 4 mL aliquot of the purified [$^{212}$Pb]$Pb(OAc)_2$ solution (6.8 – 1.5 mCi / 251.6 – 55.5 MBq) in 0.5 M NaOAc buffer (pH 6) was added into the activity vial. The activity was subsequently transferred into the reaction vial preloaded with 60 μL of a 1 mg/mL RM2 peptide conjugate solution (60 μg, 0.037 μmol). The mixture was heated at 85 °C for 20 min. The radiolabeled peptide conjugate was transferred from the reaction vial and trapped on a C18 Sep-Pak cartridge. The Sep-Pak cartridge was washed with saline and the desired product was eluted with

80% ethanol into a product vial after filtration through a 0.22 μm syringe filter (Cameo, Sanford, ME, USA). For *in vivo* animal studies, the product was diluted with sterile saline to attain less than 10% ethanol concentration. For *in vitro* cell studies, the radiolabeled peptide conjugate trapped on the C18 Sep-Pak cartridge was eluted with ethanol. The product was concentrated to dryness by slowly purging with a steady stream of $N_2$ at 85 °C to remove the ethanol. Finally, the radiolabeled peptide conjugate was reconstituted into 2 mL of RPMI 1640 media (Gibco/Life Technologies, Grand Island, NY, USA).

## 3.2-4. Cell Culture

The PC3 human prostate cancer cell line was purchased from the American Type Cell Culture Collection (Manassas, VA, USA) and authenticated (IDEXX BioResearch, Columbia, MO, USA) prior to use. The PC3 cells were cultured in the MU Cell and Immunobiology Core (MU CIC, Columbia, MO, USA) facility using RPMI 1640 supplemented with 10% Fetal Bovine Serum (Gibco/Life Technologies, Grand Island, NY, USA) and 50 μg/mL gentamicin (Fresenius Kabi USA, LLC; Lake Zurich, IL, USA) in a humidified environment with 5% carbon dioxide. Cells were counted using an automated cell counter (Biorad TC-20, Hercules, CA, USA), centrifuged, and resuspended in RPMI 1640 (Gibco/Life Technologies, Grand Island, NY, USA) without additives prior to use.

## 3.2-5. Mice and Husbandry

Male CF-1 mice (4 – 5 weeks of age) were purchased from Charles Rivers Laboratories (Wilmington, MA, USA). Male ICR SCID (Institute of Cancer Research severe combined immunodeficient) mice were purchased from Taconic Farms (Germantown, NY, USA) at 4 – 5 weeks of age. All mice were housed in ventilated rack systems with up to four animals per cage containing paperchip bedding (Shepherd

Specialty Papers; Chicago, IL, USA). CF-1 mice were conventionally housed with ad libitum access to rodent chow (Lab Diet 5008, Ralston Purina, St. Louis, MO, USA) and acidified water. ICR SCID mice were housed in autoclaved cages with ad libitum access to irradiated rodent chow (Lab Diet 5053, Ralston Purina, St. Louis, MO, USA) and autoclaved acidified water. The animal room was set on a 12-h light/12-h dark schedule with temperature and humidity control. All animal studies were reviewed and approved by the Subcommittee for Animal Studies (SAS) at the Harry S. Truman VA Hospital prior to performance.

### 3.2-6. [$^{212}$Pb]Pb-RM2 Biodistribution Studies

Following an on-site acclimation period of 7-9 days, SCID mice were anesthetized using isofluorane (Baxter Healthcare, Deerfield, IL, USA) administered with a non-rebreathing apparatus (Summit Medical Equipment Co., Bend, OR, USA). Anesthetized mice received bilateral subcutaneous flank injections of 100 μL containing ~5 x $10^6$ PC3 cells prepared as described above. Tumors were allowed to grow 5-6 weeks until palpable tumors (0.15 – 0.40 g) were observed. Each mouse was administered a bolus containing 17 - 24 μCi (0.629 – 0.888 MBq) of [$^{212}$Pb]Pb-RM2 in 100 - 150 μL via the tail vein. Mice were sacrificed by cervical dislocation at 15 minutes, 30 minutes, 1 hour, 2 hours, 4 hours, 24 hours, and 48 hours after administration. Selected tissues, organs, and remaining carcass were collected and weighed; the residual radioactivity was subsequently quantified in a NaI(Tl) well detector. The percent injected dose (%ID) and the percent injected dose per gram (%ID/g) of each organ or tissue were calculated. The %ID in whole blood was estimated assuming a whole blood volume equivalent to 6.5% of the measured body weight. Excreted radioactivity was reported as %ID and includes radioactivity measured

in cage paper, bladder contents, and feces (collected and quantified separately at 24 hours and 48 hours). Receptor blocking studies were performed by pre-injection of a 100 μL i.v. bolus containing 2.4 nmoles of unlabeled RM2 peptide conjugate in normal saline 5 minutes prior to administration of [$^{212}$Pb]Pb-RM2.

## 3.3. Results and Discussion

### 3.3-1. [$^{212}$Pb]$PbCl_2$ Elution and Purification

The $^{224}$Ra/$^{212}$Pb generator consists of $^{224}$Ra absorbed on a macroporous cation exchange resin (BioRad AG-MP-50) and housed in a one inch thick lead pig with inlet/outlet tubes, as shown in **Figure 3-2**. Currently, the major source of $^{224}$Ra is through the decay of $^{228}$Th, which is the second product of the $^{232}$Th decay chain and is also a product of $^{232}$U decay (**Figure 1-5**). Radium-224 is separated from $^{228}$Th using an anion exchange resin and is subsequently used in the production of $^{224}$Ra/$^{212}$Pb generator.[53-54] The $^{224}$Ra/$^{212}$Pb generators used in the studies described here contain ~10 mCi (370 MBq) of $^{224}$Ra and have a shelf life of ~2 weeks. **Figure 3-3** shows the decay curve of $^{224}$Ra and $^{212}$Pb from a typical 10 mCi (370 MBq) generator calculated using the Bateman equation. It can be observed that the time for maximum ingrowth of $^{212}$Pb activity from $^{224}$Ra decay is 36.8 hours. However, in order to maximize utility, the generator was eluted every ~24 hours, which would give ~65% of the theoretical maximum $^{212}$Pb activity.

The $^{224}$Ra/$^{212}$Pb generator was eluted with 3 mL of 2 M HCl resulting in a crude generator eluent solution containing $^{212}$Pb along with its daughter radionuclides ($^{212}$Bi, $^{208}$Tl, and $^{212}$Po) as identified by gamma-ray spectroscopy. HPGe analysis of the crude [$^{212}$Pb]$PbCl_2$ eluent (**Figure S3-1**) revealed the presence of the gamma rays and X-rays

associated with $^{212}$Pb, $^{212}$Bi, and $^{208}$Tl, as listed in **Table 3-1**. No unexpected radionuclidic impurities were observed. **Figure 3-4** shows the gamma spectrum of the $^{212}$Pb generator eluent obtained using a NaI(Tl) detector. Two predominant peaks were identified; one at ~240 keV, which is associated to the gamma emission from the decay of $^{212}$Pb to $^{212}$Bi (238.6 keV, 43.6%), and the other at ~75 keV, which is associated with the K-shell X-rays emitted from $^{212}$Pb decay (74.8 keV, 10.3%; 77.1 keV, 17.1%). In addition, there is evidence of a peak at ~580 keV, which is associated with the gamma emission from the decay of $^{208}$Tl to $^{208}$Pb (583.2 keV, 30.3% corrected for branching).

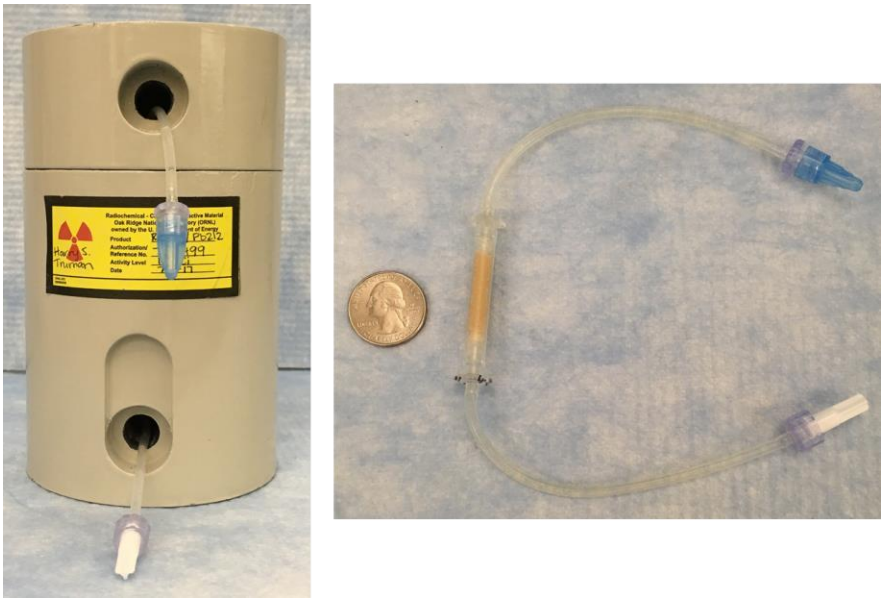

**Figure 3-2.** Picture of a $^{224}$Ra/$^{212}$Pb generator housed in a lead pig (left) and disassembled to show the cation exchange resin column (right)

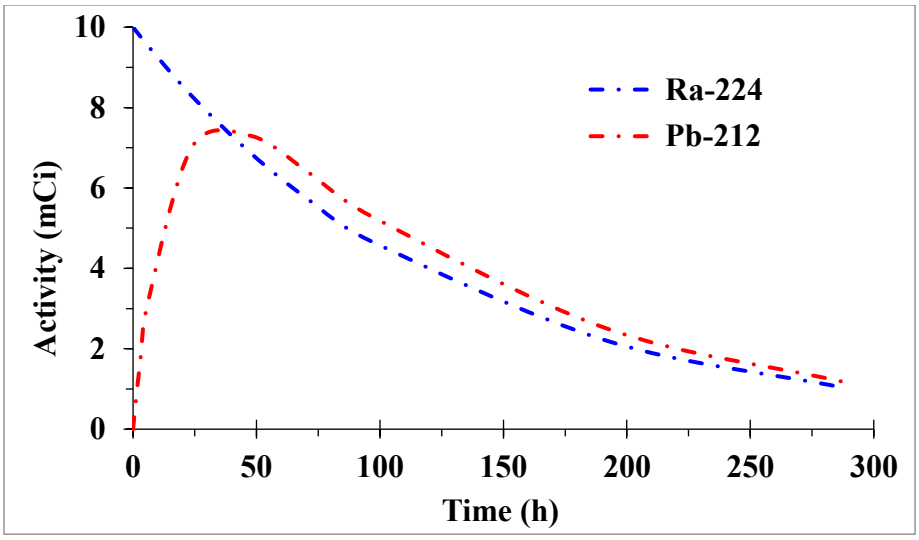


**Figure 3-3.** Decay curve of $^{224}$Ra and $^{212}$Pb from a 10 mCi $^{224}$Ra/$^{212}$Pb generator

Prior to use in radiolabeling, the crude [$^{212}$Pb]$PbCl_2$ generator eluent was purified using the Eichrom Pb-resin, which has been shown to selectively retain Pb in acidic solutions.[55-56] This purification step was performed to improve specific activity by removing nonradioactive metal impurities and minimizing the amount of radiometal impurities from $^{212}$Pb daughter radionuclides ($^{212}$Bi, $^{208}$Tl, and $^{212}$Po). The crude [$^{212}$Pb]$PbCl_2$ generator eluent was loaded onto the Pb-resin column and washed with 0.5 M HCl. Subsequently, $^{212}$Pb was eluted from the column as [$^{212}$Pb]$Pb(OAc)_2$ using 0.5 M NaOAc buffer (pH 6.5). When compared to the crude [$^{212}$Pb]$PbCl_2$ generator eluent, HPGe analysis of the purified [$^{212}$Pb]$Pb(OAc)_2$ shows a reduction in the gamma peaks areas associated $^{212}$Bi and $^{208}$Tl (**Figure S3-2**). Likewise, the NaI(Tl) gamma spectrum of the purified [$^{212}$Pb]$Pb(OAc)_2$ show a reduction in the intensity of the 580 keV peak associated with the decay of $^{208}$Tl to $^{208}$Pb, as shown in **Figure 3-4:**. Thallium-208 rapidly establishes transient equilibrium with $^{212}$Bi in about 13 minutes; hence the 583.2 keV gamma peak from $^{208}$Tl decay can be used to track the presence $^{212}$Bi.

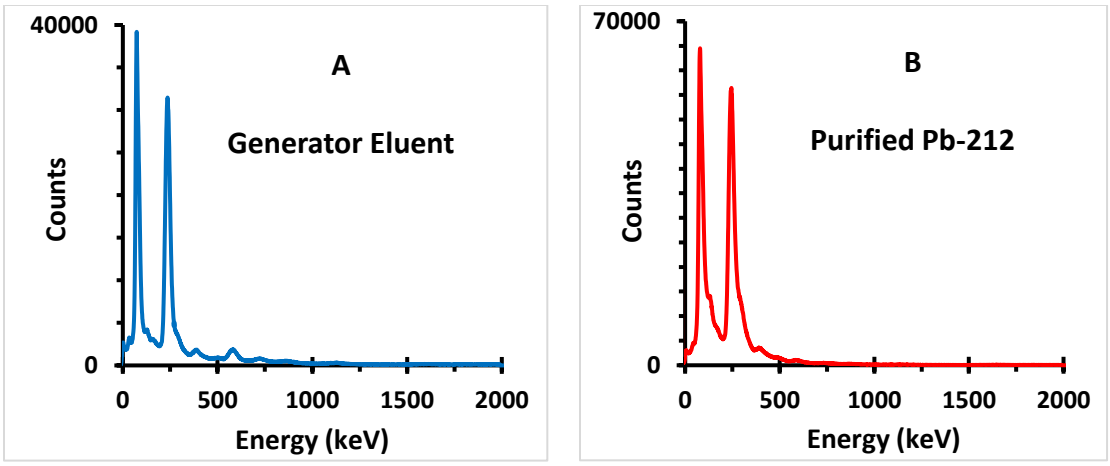


**Figure 3-4.** Gamma spectrum of crude $^{212}$Pb generator eluent (A) and after purification using Pb-resin (B)

The conventional method reported in the literature for the synthesis of $^{212}$Pb-labeled biomolecules typically includes the following steps: (1) evaporation of the [$^{212}$Pb]$PbCl_2$ generator eluent to dryness, (2) digestion with 8 M $HNO_3$ and subsequent reconstitution in 0.1 M $HNO_3$, (3) neutralization to pH ~5 with 5 M $NH_4OAc$, (4) radiolabeling, and (5) purification (**Figure 3-5, left**).[39, 41, 57-59] It has been reported that this conventional method takes about 3.5 hours before an injectable dose can be prepared.[58] Additionally, this conventional method does not allow for the initial separation of $^{212}$Bi, $^{208}$Tl, and $^{212}$Po from the [$^{212}$Pb]$PbCl_2$ generator eluent. In contrast, the method described here for the elution and purification of $^{212}$Pb takes less than 1.5 hours for the preparation and quality control of an injectable dose (**Figure 3-5, right**). This method also enables the separation of $^{212}$Bi, $^{208}$Tl, and $^{212}$Po from the [$^{212}$Pb]$PbCl_2$ generator eluent and eliminates the need for undesirable processes like evaporation to dryness and digestion with 8 M $HNO_3$. Most importantly, this method can be adopted to automated radiosynthesis modules, following recently published procedures.[55, 60] This will make it more convenient for GMP formulation

in well-equipped radiopharmacies and potentially minimize radiation exposure to personnel.

| **Table 3-1.** The significant X-rays and γ-rays associated with $^{212}$Pb and its daughter radionuclides | |
|---|---|
| **Radionuclide** | **Energy (keV)** |
| $^{212}$Pb | 74.8 (10.2%), 77.1 (17.1%), 86.8 (2.07%), 87.3 (3.97%), 89.8 (1.46%), 115.2 (0.6%), **238.6 (43.6%)**, 300.1 (3.3%), |
| $^{212}$Bi | 288.07 (0.1%)§, 327.9 (0.04%), 452.4 (0.1%), **727.3 (4.2%)***, 785.3 (0.7%)*, 893.4 (0.2%)*, 952.1 (0.1%)*, 1078.62 (0.36%)*, 1512.7 (0.18%)*, 1620.5 (0.9%)* |
| $^{208}$Tl | 74.9 (1.2%)*, 277.3 (2.3%)*, 510.7 (8.1%)*, **583.2 (30.3%)***, 763.1 (0.6%)*, 860.6 (4.4%)*, 927.6 (0.04)*, 982.7 (0.07)*, 1093.9 (0.15%)*, 2614.5 (35.8%)* |
| § Corrected for 64.06% branch decay<br>* Corrected for 35.94% branch decay | |

## 3.3-2. Synthesis and *In Vitro* Stability of [$^{212}$Pb]Pb-RM2

Synthesis of [$^{212}$Pb]Pb-RM2 was accomplished by reacting purified [$^{212}$Pb]Pb(OAc)$_2$ with RM2 peptide conjugate using the Eckert & Ziegler Modular-Lab PharmTracer automated cassette-based radiosynthesis system. The radiolabeling yields obtained after C18 Sep-Pak purification were always above 100% due to the continuous in-growth of $^{212}$Bi, $^{208}$Tl, and $^{212}$Po from the decay of $^{212}$Pb. The radiochemical purity was determined using radio-HPLC. **Figure 3-6A** shows a typical radio-HPLC chromatogram of [$^{212}$Pb]Pb-RM2 compared to that of [$^{212}$Pb]PbCl$_2$ obtained using gradient 1 (10% to 70% ACN:H$_2$O over 10 minutes at 1.5 mL/min). It can be observed that the desired product (retention time ~6.3 minutes) was obtained in over 94% radiochemical purity with very

minor impurities from free $^{212}Pb/^{212}Bi$ (retention time ~2.3 minutes). For a more robust analysis of the radiochemical purity, gradient 2 (22% to 25% ACN:$H_2O$ over 20 minutes at 1.5 mL/min) was developed to better differentiate between [$^{212}Pb$]Pb-RM2 and [$^{212}Bi$]Bi-RM2 by comparing the radio-HPLC chromatogram with the non-radioactive Pb-RM2 and Bi-RM2 standards (**Figure 3-6B**). Using gradient 2 conditions, it can be observed that [$^{212}Pb$]Pb-RM2 has a retention time of ~13.5 minutes while [$^{212}Bi$]Bi-RM2 has a retention time of ~12 minutes. Apart from free $^{212}Pb/^{212}Bi$ (retention time ~2.4 minutes), no other radiochemical impurities were observed.

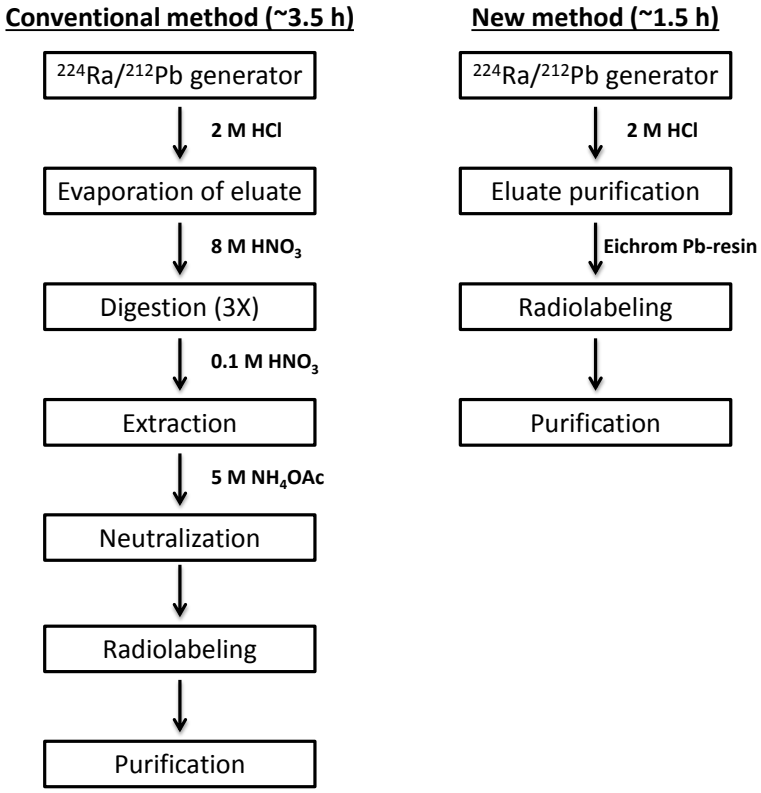


**Figure 3-5**. A flow chart comparing the conventional method for the synthesis of $^{212}Pb$-labeled biomolecules with the new method developed in this study

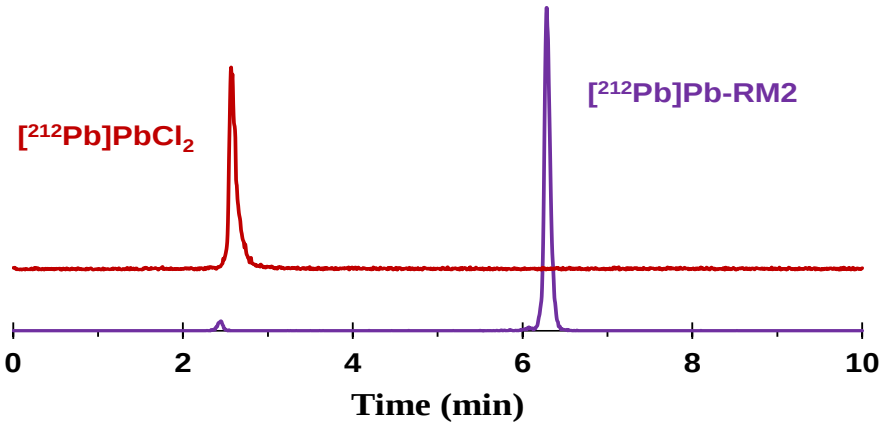


**Figure 3-6A.** Radio-HPLC profiles of [$^{212}$Pb]$PbCl_2$ and [$^{212}$Pb]Pb-RM2 using gradient 1 (10% to 70% ACN:$H_2O$ over 10 minutes)

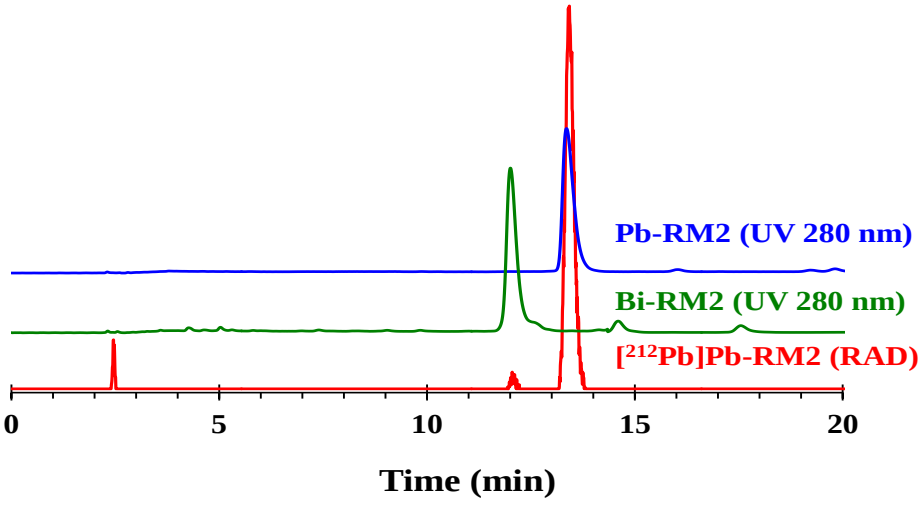


**Figure 3-6B.** HPLC profiles of [$^{212}$Pb]Pb-RM2, Pb-RM2, and Bi-RM2 using gradient 2 (22% to 25% ACN:$H_2O$ over 20 minutes)

Aliquots (1.6 mL, 0.49 mCi) of Sep-Pak purified [$^{212}$Pb]Pb-RM2 were mixed with either saline (400 µL) or 0.03 M gentisic acid solution in saline (400 µL). The solutions were incubated at room temperature and 15 µL aliquots were taken for radio-HPLC analysis at 1 hour, 2 hours, 4 hours and 24 hours using gradient 2. The percentage of

[$^{212}$Pb]Pb-RM2, [$^{212}$Bi]Bi-RM2 and free $^{212}$Pb/$^{212}$Bi present at each time point was determined by integrating the area under each peak. The amount of free $^{212}$Pb/$^{212}$Bi observed at 24 hours was less than 15% for all solutions analyzed (**Table 3-2A and 3-2B**). The addition of gentisic acid as a radiolysis stabilizer had no significant effect in improving stability (**Figure 3-7**).

Su et al.[48] investigated the *in vitro* stability of [$^{212}$Pb]Pb-DOTA-biotin and reported 30.8% and 34.9% free $^{212}$Pb/$^{212}$Bi at 4 hours and 24 hours, respectively, using radio-HPLC. Similarly Mirzadeh et al.[61] reported that about 35% of free $^{212}$Bi is released from the decay of [$^{212}$Pb]Pb-DOTA using Chelex-100 columns for the separation of free metal from metal complex species. In contrast, the current study reported here for [$^{212}$Pb]Pb-RM2 does not show the same level of instability, with less than 15% of free $^{212}$Pb/$^{212}$Bi observed at 24 hours. Perhaps, the initial purification of the [$^{212}$Pb]$PbCl_2$ generator eluent prior to use in radiolabeling, along with Sep-Pak purification after synthesis, contributed to the improved stability for [$^{212}$Pb]Pb-RM2 reported here.

**Table 3-2A.** [$^{212}$Pb]Pb-RM2 *in vitro* stability in saline*

| Time (h) | Free $^{212}$Pb/$^{212}$Bi (%) | [$^{212}$Bi]Bi-RM2 (%) | [$^{212}$Pb]Pb-RM2 (%) |
|---|---|---|---|
| 0 | 2.60 | 4.80 | 92.50 |
| 1 | 5.85 ± 0.65 | 7.55 ± 0.55 | 86.50 ± 0.10 |
| 2 | 8.30 ± 0.80 | 8.40 ± 1.1 | 83.30 ± 0.35 |
| 4 | 9.35 ± 0.05 | 9.50 ± 0.50 | 81.15 ± 0.45 |
| 24 | 11.45 ± 1.65 | 11.55 ± 0.65 | 77.05 ± 2.25 |

* n = 2

| **Table 3-2B.** [$^{212}$Pb]Pb-RM2 *in vitro* stability in saline with gentisic acid * | | | |
|---|---|---|---|
| Time (h) | Free $^{212}$Pb/$^{212}$Bi (%) | [$^{212}$Bi]Bi-RM2 (%) | [$^{212}$Pb]Pb-RM2 (%) |
| 0 | 2.80 | 5.16 | 92.04 |
| 1 | 6.75 ± 0.35 | 8.65 ± 0.25 | 84.60 ± 0.10 |
| 2 | 8.70 ± 0.40 | 9.50 ± 0.20 | 81.80 ± 0.20 |
| 4 | 10.30 ± 0.40 | 8.55 ± 0.05 | 81.20 ± 0.50 |
| 24 | 13.45 ± 0.35 | 9.20 ± 1.60 | 77.35 ± 1.95 |
| * n = 2 | | | |

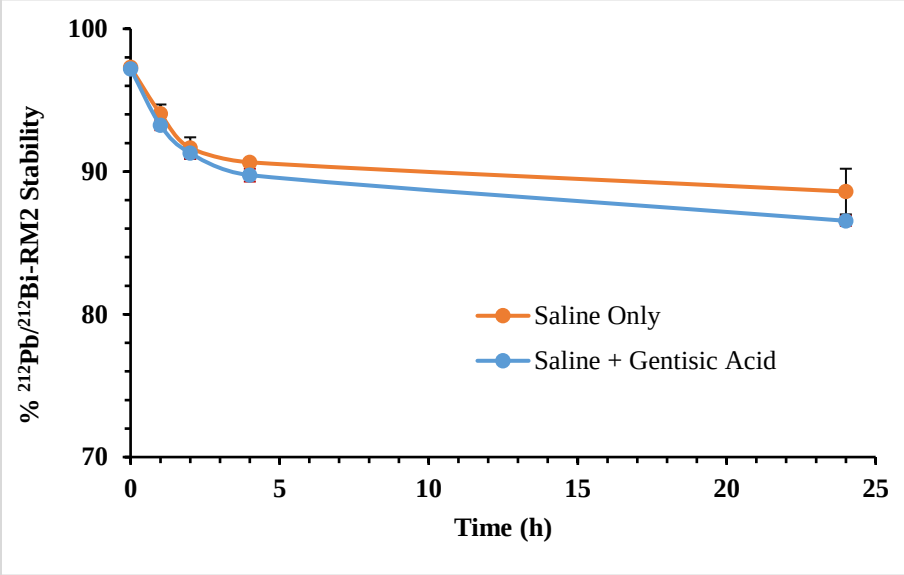


**Figure 3-7.** Stability of [$^{212}$Pb]Pb-RM2 in saline and 0.03 M gentisic acid solution in saline (n = 2 per time point)

## 3.3-3. [$^{212}$Pb]Pb-RM2 Biodistribution Studies

The pharmacokinetic profile of [$^{212}$Pb]Pb-RM2 was examined in SCID mice bearing PC3 tumor xenografts, as summarized in **Table 3-3** (see **Table S3-1** for data reported as %ID). [$^{212}$Pb]Pb-RM2 exhibited substantial tumor uptake values at the early time points, with a maximum value of 4.81 ± 1.59% ID/g at 1 hour post injection. Prolonged retention of [$^{212}$Pb]Pb-RM2 in the tumor was observed, with 3.98 ± 0.70% ID/g,

3.52 ± 0.83% ID/g and 2.62 ± 0.31% ID/g at 2 hours, 4 hours and 24 hours post injection, respectively. The specificity of the observed tumor uptake was confirmed by conducting a blocking experiment, which involved pre-injection of 2.4 nmoles of unlabeled RM2 prior to administration of [$^{212}$Pb]Pb-RM2. The tumor uptake was reduced from 3.52 ± 0.83% ID/g to 1.43 ± 0.31% ID/g at 4 hours post injection of [$^{212}$Pb]Pb-RM2. This represents a 59.4% blockage ($p < 0.0001$) in tumor uptake, indicating that the tumor uptake is BB2 receptor-mediated. The reduction in the tumor blockage observed for [$^{212}$Pb]Pb-RM2 (59.4 %) compared to [$^{203}$Pb]Pb-RM2 (91.3%) is as a result of the ~10 fold decrease in amount of pre-injected unlabeled RM2 peptide conjugate between both studies (2.4 nmoles vs 20 nmoles, respectively).

It has been widely reported that the BB2 receptor is expressed in the pancreas.[19, 22-23, 62-64] Therefore, the early [$^{212}$Pb]Pb-RM2 pancreas uptake value of 23.64 ± 12.70% ID/g at 15 min post injection was expected. However, rapid pancreas clearance was observed, with 1.62 ± 1.15% ID/g and 0.34 ± 0.12% ID/g remaining at 2 hours and 4 hours post injection, respectively **Figure 3-8**. Additionally, rapid whole-body clearance of [$^{212}$Pb]Pb-RM2 was observed with 93.76 ± 1.40% and 96.89 ± 0.38% of the total injected dose excreted by 4 hour and 24 hours post injection, respectively. Fast blood clearance was also observed with 0.03 + 0.04% ID/g and 0.02 ± 0.02% ID/g remaining at 4 hour and 24 hours post injection, respectively. [$^{212}$Pb]Pb-RM2 is excreted predominantly via the kidney into the urinary system. Additionally, no substantial retention of [$^{212}$Pb]Pb-RM2 activity was observed in all non-specifically targeted organs. Due to the rapid clearance of [$^{212}$Pb]Pb-RM2 from the blood and non-specifically targeted organs, high tumor to background ratios were observed, which generally increased with time. For example, the tumor-to-blood ratio

was 1.20 at 15 min post injection and increased to 42.77 at 2 hours post injection. Similarly, the tumor-to-muscle ratio increased from 6.70 at 15 min post injection to 108.32 at 2 hours post injection (**Table 3-3**).

As already discussed in Chapter 2, free $Pb^{2+}$ is preferentially accumulated and retained in the kidney, bone, and liver. [$^{212}$Pb]Pb-RM2 exhibited very minimal uptake in the bone and liver at every time point studied. The [$^{212}$Pb]Pb-RM2 activity observed in the kidney is as a result of normal clearance through the urinary system, which steadily decreased over time. The very minimal accumulation of [$^{212}$Pb]Pb-RM2 activity in the bone and liver is an indication of its high *in vivo* stability.

In theory, the pharmacokinetic behavior of [$^{212}$Pb]Pb-RM2 should be identical to the biodistribution of [$^{203}$Pb]Pb-RM2 since there should be no difference in the chemical behavior of the two compounds. Generally, [$^{212}$Pb]Pb-RM2 and [$^{203}$Pb]Pb-RM2 exhibited similar pharmacokinetic trends, with rapid clearance from the blood and non-specifically targeted organs predominantly through the urinary system via the kidneys. Additionally, specific uptake was observed in the BB2 receptor expressing organs/tissues (pancreas and PC3 tumor xenografts). However, some discrepancies were observed in the maximum uptake values between [$^{212}$Pb]Pb-RM2 and [$^{203}$Pb]Pb-RM2. For example, the maximum [$^{203}$Pb]Pb-RM2 tumor uptake value observed was 11.26 ± 2.48% ID/g, while the maximum [$^{212}$Pb]Pb-RM2 tumor uptake value observed was 4.81 ± 1.59% ID/g (**Figure 3-9A)**. Similarly, the maximum [$^{203}$Pb]Pb-RM2 activity observed in the pancreas was 13.40 ± 2.41% ID/g, while the maximum [$^{212}$Pb]Pb-RM2 activity observed in the pancreas was 23.64 ± 12.70% ID/g (**Figure 3-9B)**.

**Table 3-3. [$^{212}$Pb]Pb-RM2 biodistribution in PC3 tumor bearing mice**
**Data shown as mean ± SD %ID/g (n = 6 mice per time point)**

| Tissue | 15 min | 30 min | 1 h | 2 h * | 4 h* | 24 h | 48 h |
|---|---|---|---|---|---|---|---|
| **Blood** | 3.89 ± 0.26 | 1.66 ± 0.35 | 0.59 ± 0.21 | 0.06 ± 0.03 | 0.03 ± 0.04 | 0.02 ± 0.02 | 0.06 ± 0.10 |
| **Heart** | 1.40 ± 0.23 | 0.65 ± 0.09 | 0.15 ± 0.10 | 0.05 ± 0.01 | 0.10 ± 0.12 | 0.12 ± 0.15 | 0.31 ± 0.67 |
| **Lung** | 2.44 ± 0.31 | 1.35 ± 0.22 | 0.50 ± 0.13 | 0.16 ± 0.08 | 0.11 ± 0.08 | 0.09 ± 0.10 | 0.21 ± 0.43 |
| **Liver** | 2.61 ± 0.33 | 1.57 ± 0.65 | 1.01 ± 0.32 | 0.41 ± 0.09 | 0.22 ± 0.08 | 0.05 ± 0.01 | 0.05 ± 0.06 |
| **Stomach** | 1.24 ± 0.39 | 0.57 ± 0.17 | 0.73 ± 0.30 | 0.38 ± 0.39 | 0.13 ± 0.05 | 0.03 ± 0.07 | 0.11 ± 0.17 |
| **Sm. Intestines** | 2.29 ± 0.85 | 1.08 ± 0.43 | 0.97 ± 0.30 | 0.41 ± 0.30 | 0.14 ± 0.06 | 0.05 ± 0.02 | 0.03 ± 0.03 |
| **Lg. Intestines** | 1.04 ± 0.30 | 0.44 ± 0.10 | 0.40 ± 0.09 | 0.84 ± 0.50 | 0.73 ± 0.18 | 0.35 ± 0.27 | 0.10 ± 0.11 |
| **Kidney** | 15.61 ± 2.94 | 12.31 ± 2.92 | 11.42 ± 2.43 | 6.34 ± 1.85 | 3.54 ± 1.10 | 1.01 ± 0.26 | 1.42 ± 0.35 |
| **Spleen** | 1.32 ± 0.43 | 0.81 ± 0.22 | 0.32 ± 0.13 | 0.13 ± 0.13 | 0.17 ± 0.11 | 0.12 ± 0.11 | 0.33± 0.54 |
| **Brain** | 0.15 ± 0.02 | 0.09 ± 0.03 | 0.04 ± 0.06 | 0.01 ± 0.01 | 0.02 ± 0.04 | 0.01 ± 0.01 | 0.07 ± 0.15 |
| **Pancreas** | 23.64 ± 12.70 | 7.89 ± 3.69 | 6.61 ± 3.23 | 1.62 ± 1.15 | 0.34 ± 0.12 | 0.07 ± 0.06 | 0.06 ± 0.09 |
| **Muscle** | 0.70 ± 0.11 | 0.37 ± 0.10 | 0.09 ± 0.05 | 0.04 ± 0.05 | 0.04 ± 0.04 | 0.04 ± 0.04 | 0.23 ± 0.30 |
| **Bone** | 1.27 ± 0.06 | 0.63 ± 0.20 | 0.26 ± 0.12 | 0.09± 0.07 | 0.11 ± 0.12 | 0.09 ± 0.14 | 0.26 ± 0.40 |
| **Tumors** | 4.69 ± 0.82 | 4.36 ± 0.73 | 4.81 ± 1.59 | 3.98 ± 0.70 | 3.52 ± 0.83 | 2.62 ± 0.31 | 1.58 ± 0.35 |
| **Tumor / Blood** | 1.20 | 6.95 | 8.10 | 42.77 | 102.11 | 154.97 | 25.54 |
| **Tumor / Muscle** | 6.70 | 11.81 | 53.42 | 108.32 | 86.59 | 74.49 | 6.90 |
| **Tumor / Liver** | 1.79 | 2.77 | 4.77 | 9.76 | 16.22 | 49.13 | 29.09 |
| **Tumor / Kidney** | 0.30 | 0.35 | 0.42 | 0.62 | 0.99 | 2.59 | 3.71 |
| **Tumor / Pancreas** | 0.19 | 0.55 | 0.72 | 2.45 | 10.50 | 39.23 | 26.68 |
| **Tumor / Bone** | 3.70 | 6.59 | 18.45 | 44.66 | 32.03 | 29.98 | 6.15 |
| **Urine (%ID)** | 33.67 ± 11.23 | 62.93 ± 8.67 | 76.73 ± 2.16 | 89.87 ± 2.04 | 93.76 ± 1.40 | 92.92 ± 3.17 | 88.28± 10.58 |
| **Excretion (%ID)** | 33.67 ± 11.23 | 62.93 ± 8.67 | 76.73 ± 2.16 | 89.87 ± 2.04 | 93.76 ± 1.40 | 96.89 ± 0.38 | 98.11± 1.18 |

* n = 7

Note: Values for urine include radioactivity measured in bladder and cage paper

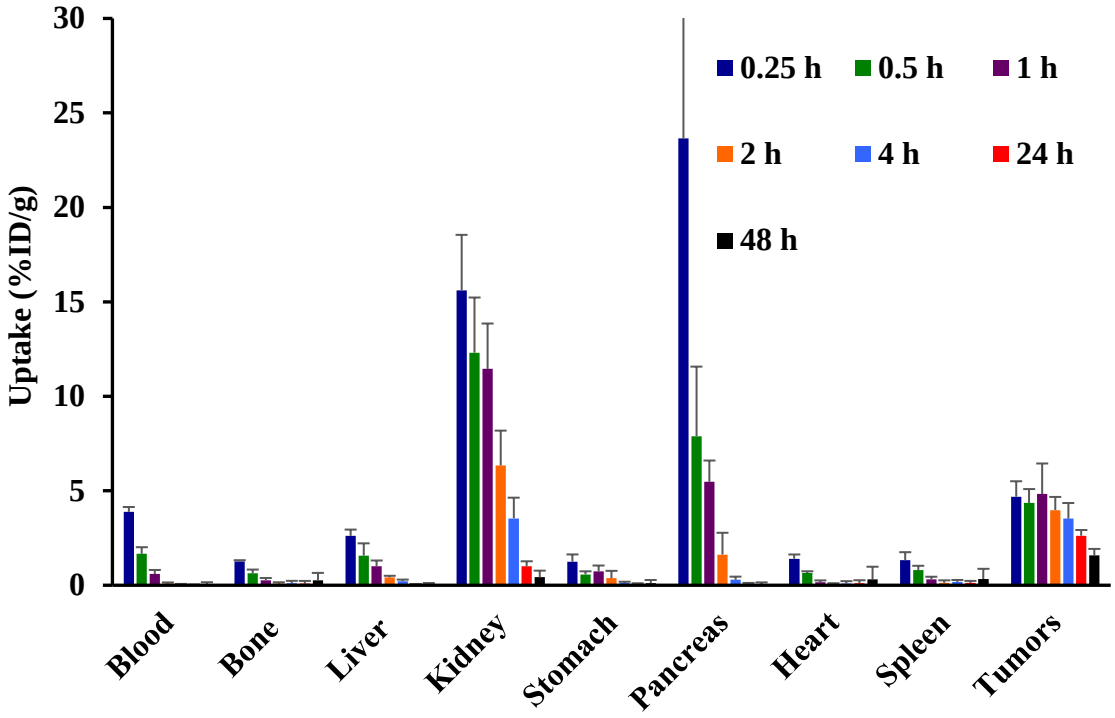


**Figure 3-8**. Biodistribution of [$^{212}$Pb]Pb-RM2 in PC3 tumor bearing mice

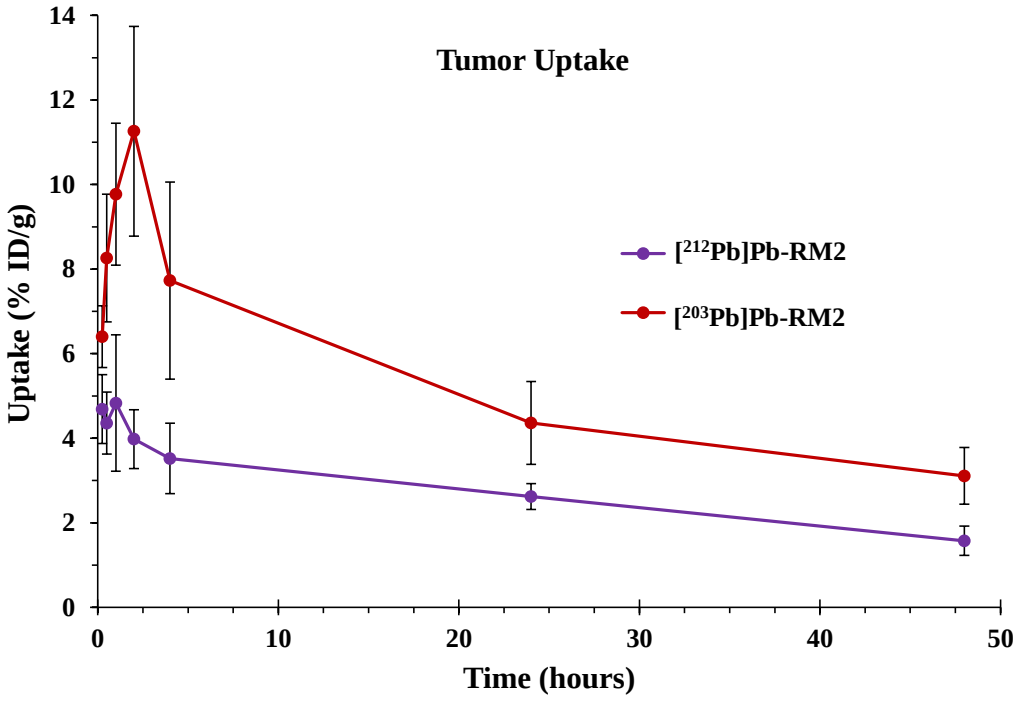


**Figure 3-9A**. Comparison of [$^{212}$Pb]Pb-RM2 and [$^{203}$Pb]Pb-RM2 uptake in PC3 tumor (n = 6 per time point)

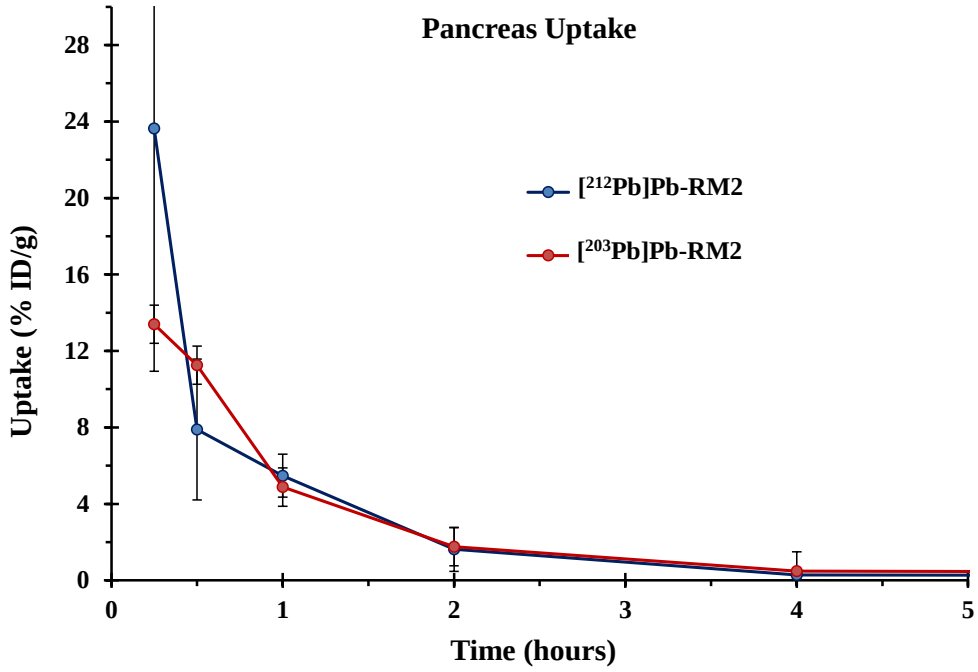


**Figure 3-9B**. Comparison of [$^{212}$Pb]Pb-RM2 and [$^{203}$Pb]Pb-RM2 uptake in pancreas (n = 6 per time point)

One possible explanation for the discrepancies observed in the BB2 receptor expressing organs/tissues between [$^{203}$Pb]Pb-RM2 and [$^{212}$Pb]Pb-RM2 is potential differences in the specific activity of the [$^{203}$Pb]$PbCl_2$ and [$^{212}$Pb]$PbCl_2$ precursor. As described in Chapter 2, the [$^{203}$Pb]$PbCl_2$ precursor contained substantial amounts of non-radioactive Pb, which would lead to competition between [$^{203}$Pb]Pb-RM2 and non-radioactive Pb-RM2 for the same BB2 receptors, resulting in lower [$^{203}$Pb]Pb-RM2 uptake values in BB2 receptor-expressing organs/tissues. In theory, the [$^{212}$Pb]$PbCl_2$ precursor should have high specific activity since it is obtained from a $^{224}$Ra/$^{212}$Pb generator and should contain very minimal Pb impurities. To rule out the presence of metallic impurities in the [$^{212}$Pb]$PbCl_2$ generator eluent, 200 µL aliquots were collected and analyzed by ICP-MS after decay of $^{212}$Pb. Surprisingly, it was observed that the [$^{212}$Pb]$PbCl_2$ generator

eluent contained significant amounts of metallic contaminants, predominantly Pb, Fe and Zn (**Table S3-2**).

The Fe and Zn contamination was significantly reduced after purification using Pb-resin, as shown in **Figures 3-10A to 3-10C**. Based on the amount of non-radioactive Pb observed in the [$^{212}$Pb]$PbCl_2$ generator eluent, it was calculated that the specific activity is ~28 mCi/μg on the first day of eluting the $^{224}$Ra/$^{212}$Pb generator. This indicates that 2% of the total Pb atoms are present as $^{212}$Pb, which is comparable to what was determined in the [$^{203}$Pb]$PbCl_2$ precursor as described in Chapter 2. Based on this information, it can be concluded that the difference in the specific activities (with respect to total non-radioactive Pb atoms) between the [$^{203}$Pb]$PbCl_2$ and [$^{212}$Pb]$PbCl_2$ precursor is not significant enough to explain the discrepancies in the uptake values observed in the BB2 receptor expressing organs/tissues between [$^{203}$Pb]Pb-RM2 and [$^{212}$Pb]Pb-RM2.

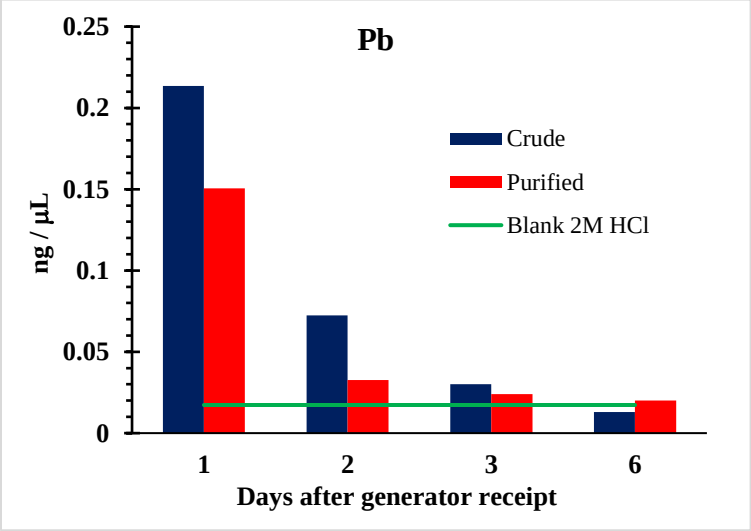


**Figure 3-10A.** Comparison of Pb contamination in [$^{212}$Pb]$PbCl_2$ generator eluent before and after purification (n = 1, generator #4)

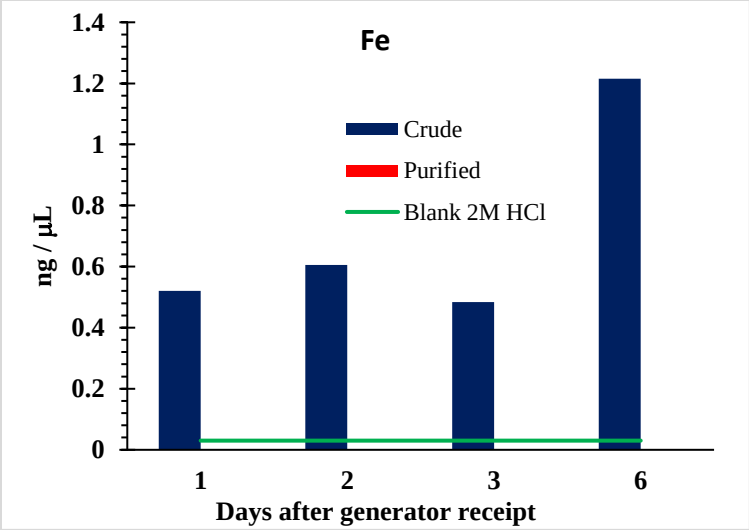


**Figure 3-10B.** Comparison of Fe contamination in [$^{212}$Pb]$PbCl_2$ generator eluent before and after purification (n = 1, generator #4)

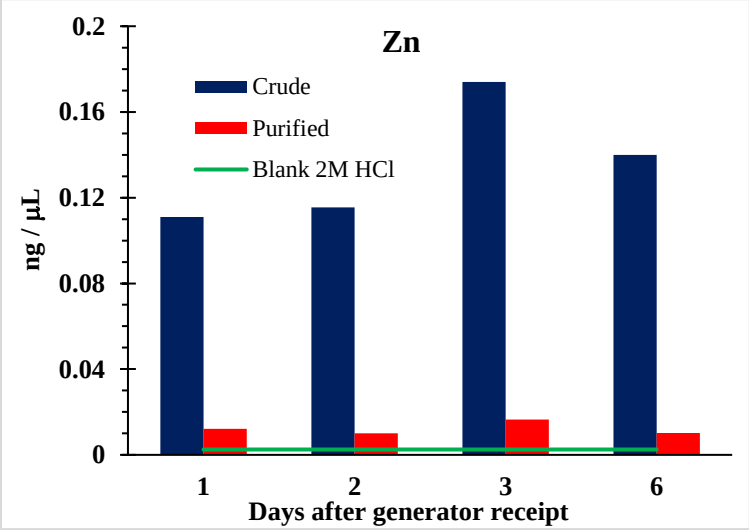


**Figure 3-10C.** Comparison of Zn contamination in [$^{212}$Pb]$PbCl_2$ generator eluent before and after purification (n = 1, generator #4)

Variations in specific activity with respect to the total amount of peptide used for radiolabeling and variations in the activity concentration administered to the animals can influence the uptake values observed in the BB2 receptor-expressing organs/tissues (**Table**

**3-4)**. As expected, the total [$^{212}$Pb]$PbCl_2$ activity eluted from the $^{224}$Ra/$^{212}$Pb generator decreases over time, thereby resulting in a decrease in the [$^{212}$Pb]Pb-RM2 activity over time. Therefore, the activity concentration and specific activity per μmol RM2 was different depending on the day the radiolabeling experiment was performed (**Table 3-5**). Considering that ~ 20 μCi (0.7 MBq) of [$^{212}$Pb]Pb-RM2 in a ~100 μL bolus is typically administered to each mouse, the [$^{212}$Pb]Pb-RM2 activity required more dilution in the earlier days than in the later during the biodistribution study. Thus, a greater amount of unlabeled RM2 peptide conjugate was injected into each mouse in the later days during the biodistribution study, which possibly contributed to the observed decrease in [$^{212}$Pb]Pb-RM2 uptake in the BB2 receptor-expressing organs/tissues. The influence of the total amount of injected peptide on pancreas uptake was also reported by Dalm et al.[22] for [$^{177}$Lu]Lu-NeoBOMB, which is another BB2 receptor antagonist peptide conjugate. The authors observed a pancreas uptake value of 105 ± 13% ID/g with the injection of 1 MBq/10 pmol of [$^{177}$Lu]Lu-NeoBOMB whereas, the pancreas uptake value was 19.8 ± 6.9% ID/g with the injection of 1 MBq/200 pmol of [$^{177}$Lu]Lu-NeoBOMB. Similar peptide related influence on the uptake values in BB2 receptor-expressing organs was reported for [$^{111}$In]In-AMBA, which is a BB2r agonist peptide conjugate.[65] Effect of peptide mass on pharmacokinetics have also been reported for radiolabeled peptide conjugates targeting the somatostatin receptor.[66]

| **Table 3-4.** Variations in [$^{212}$Pb]Pb-RM2 pancreas and tumor uptake with the date of synthesis | | | | |
|---|---|---|---|---|
| | **10/27/2017** | **10/31/2017** | **11/01/2017** | **11/06/2017** |
| | **15 min** | | | |
| **Pancreas** | 34.66 ± 6.25 * | 12.63 ± 0.48 * | | |
| **Tumor** | 5.20 ± 0.71 * | 4.18 ± 0.48 * | | |
| | **30 min** | | | |
| **Pancreas** | | | 12.41 ± 2.36 ǂ | 5.63 ± 0.61 # |
| **Tumor** | | | 4.71 ± 0.87 ǂ | 4.18 ± 0.64 # |
| | **1 hour** | | | |
| **Pancreas** | 8.60 ± 3.67 * | 4.26 ± 0.86 * | | |
| **Tumor** | 4.91 ± 2.26 * | 4.72 ± 0.62 * | | |
| | **2 hours** | | | |
| **Pancreas** | 3.09 ± 1.21 ǂ | 1.22 ± 0.33 * | | 0.75 ± 0.01ǂ |
| **Tumor** | 4.72 ± 0.18 ǂ | 4.06 ± 0.44 * | | 3.12 ± 0.12 ǂ |
| **ǂ n = 2, * n = 3, # n = 4** | | | | |

| **Table 3-5.** Variations in [$^{212}$Pb]Pb-RM2 specific activity and activity concentration with the date of synthesis | | | | |
|---|---|---|---|---|
| Date | Activity after Sep-Pack purification (mCi) | RM2 (μmol) | Specific Activity (mCi/ μmol RM2) | Activity concentration (mCi/mL)* |
| 10/27/2017 | 5.74 | 0.037 | 149.5 | 2.73 |
| 10/31/2017 | 2.96 | 0.037 | 80.9 | 1.48 |
| 11/01/2017 | 2.26 | 0.037 | 61.7 | 1.13 |
| 11/06/2017 | 0.93 | 0.037 | 25.4 | 0.46 |
| * assuming final volume of 2 mL | | | | |

## 3.4. On-going Studies

### 3.4-1. *In-vitro* Evaluation of [$^{212}$Pb]Pb-RM2 Therapeutic Efficacy

The *in vitro* evaluation of the therapeutic efficacy of [$^{212}$Pb]Pb-RM2 is currently underway in various prostate cancer cell lines including PC3, 22RV1, DU-145, LNCAP, LNCAP C42B, LNCAP C42, and VCAP. The cells were exposed to increasing doses of [$^{212}$Pb]Pb-RM2 (0.5 μCi, 1 μCi, 2 μCi and 4 μCi). Subsequently, the therapeutic efficacy was determined by assessing cell viability using the MTT assay, cell survival and proliferation using the clonogenic assay, and DNA damage using immunofluorescence staining of 53BPI and γH2AX markers.

Initial data on cell survival (using clonogenic assay) obtained in two cell lines (PC3 and LNCAP) after exposure to [$^{212}$Pb]Pb-RM2 and [$^{177}$Lu]Lu-RM2 show significantly improved therapeutic efficacy (as indicated by the lower survival fraction) with [$^{212}$Pb]Pb-RM2, as shown in **Figure 3-11**.

### 3.4-2. Evaluation of [$^{212}$Pb]Pb-RM2 Maximum Tolerated Dose and *In Vivo* Toxicity

Studies to evaluate the maximum tolerated dose of [$^{212}$Pb]Pb-RM2 in CF-1 normal mice are currently underway. Three treatment groups and one control group are being investigated. The treatment groups received an intravenous injection of [$^{212}$Pb]Pb-RM2 at three dose levels (50 μCi, 100 μCi and 200 μCi), with 26 mice per dose level. A control group of 21 mice received an intravenous injection of saline. Body weight (BW), complete blood counts (CBC), and body condition score (BCS) were recorded prior to injection of either [$^{212}$Pb]Pb-RM2 or saline. After injection, BW, CBC, and BCS will be monitored weekly for a duration of 30 weeks. A subset of the animals in each study group will be

sacrificed at day 30, 50, 70 and 90 (n = 4 per time point) for tissue histopathological examination and toxicity evaluation by monitoring serum chemistry markers for liver function [e.g., alanine aminotransferase (ALT), alkaline phosphatase (ALP), aspartate aminotransferase (AST), and bilirubin], kidney function [blood urea nitrogen (BUN), calcium, albumin, and creatinine], pancreas function [amylase and lipase] and general metabolic function [glucose, inorganic phosphorus and total cholesterol].

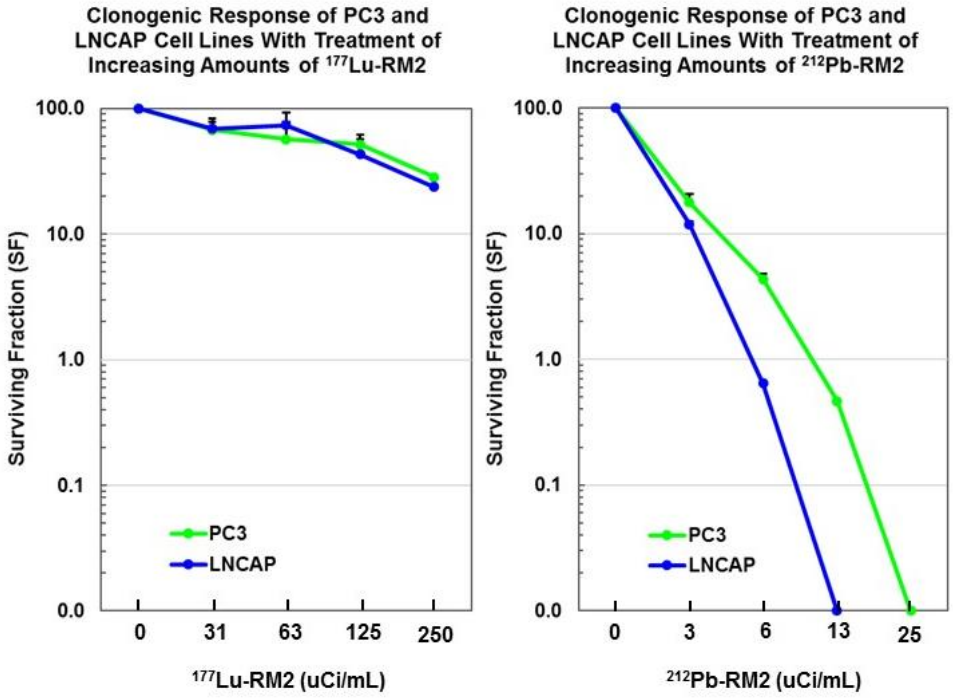


**Figure 3-11**. Comparison of clonogenic response of PC3 and LNCAP cells lines to [$^{177}$Lu]Lu-RM2 treatment (left) and [$^{212}$Pb]Pb-RM2 (right)

As at week 10 into the maximum tolerated dose studies, no deaths in any of the treatment groups and no adverse effects on body weight have been observed. In fact, the average body weight has steadily increased over time in all study groups (**Figure 3-12**). Additionally, no apparent signs of hematological toxicity have been observed through

week 10 into the maximum tolerated dose studies, with no significant differences in the average white blood cell counts (**Figure 3-13**) and average platelets counts (**Figure 3-14**) between the control and treatment groups. Furthermore, the absence of a significant decrease in white blood cell and platelet counts is an indication of normal bone marrow activity and lack of myelosuppression.

## 3.5. Conclusions

The method described in this study for the synthesis of [$^{212}$Pb]Pb-RM2 incorporates a step for the purification of the [$^{212}$Pb]$PbCl_2$ generator eluent using the Eichrom Pb-resin, which cuts down the synthesis time to ~1.5 hours compared to the ~3.5 hours that has been traditionally reported for $^{212}$Pb labeling.[58] We demonstrated that this purification step significantly reduces the amount of radiometal impurities from $^{212}$Pb daughter radionuclides ($^{212}$Bi, $^{208}$Tl, and $^{212}$Po). ICP-MS analysis of the crude [$^{212}$Pb]$PbCl_2$ generator eluent revealed the presence of significant amounts of Pb, Fe and Zn metal contamination; however, the Pb-resin purification step reduced the Fe and Zn contamination to negligible amounts.

A major concern with alpha-emitting radionuclides is the recoil energy imparted to the daughter radionuclide upon alpha decay as a result of conservation of momentum. This recoil energy is typically around 100 keV and is significantly greater that the bond energies for most common bonds (e.g., C–O = 3.6 eV; C–C = 3.6 eV; C–N = 3.0 eV; C≡O = 11.2 eV). Therefore, there is a possibility that the chemical bonds in any chelator used for the complexation of an alpha-emitting radionuclide would break as a result of the recoil energy, resulting in possible redistribution of the daughter radionuclide. However, it is worth mentioning the decay of $^{212}$Pb into $^{212}$Bi occurs by beta emission.

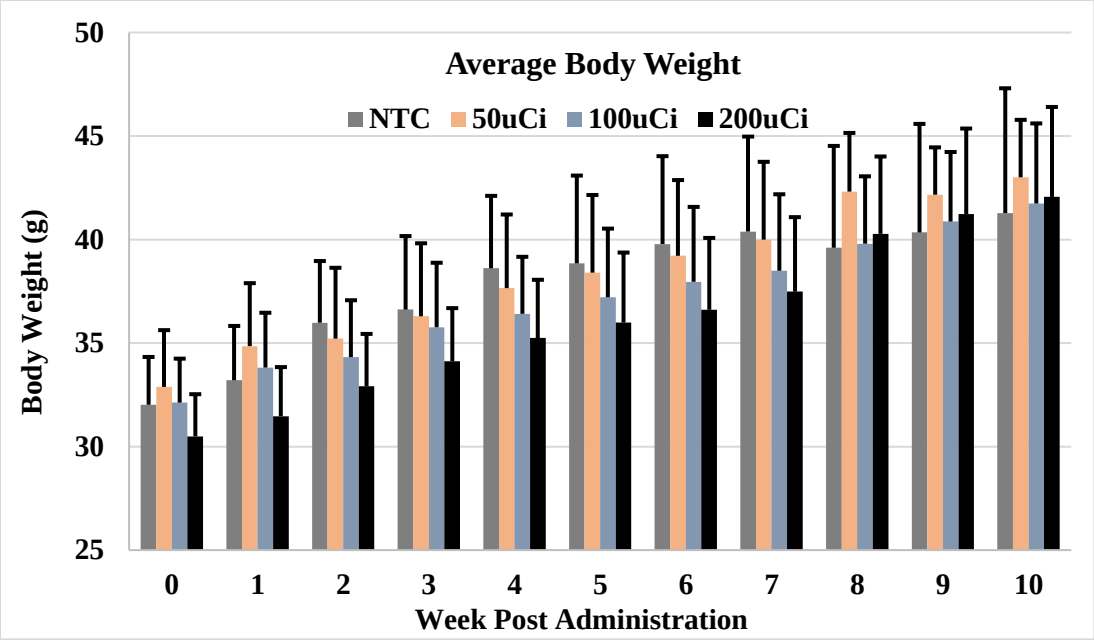


**Figure 3-12.** Effect of [$^{212}$Pb]Pb-RM2 administration on body weight in CF-1 mice

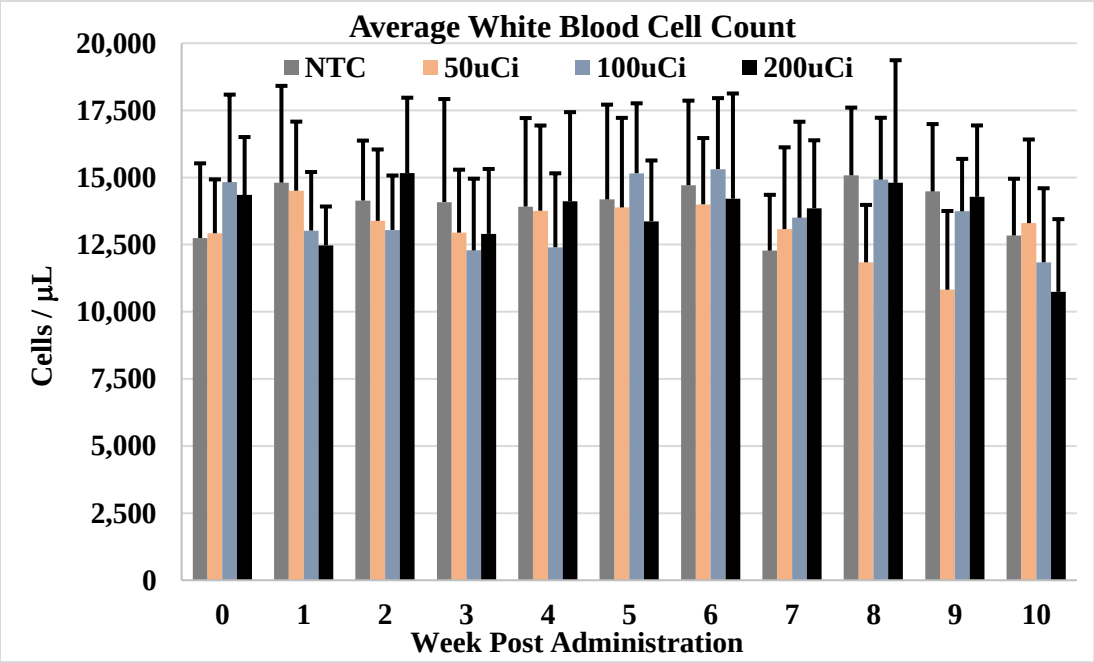


**Figure 3-13.** Effect of [$^{212}$Pb]Pb-RM2 administration on white blood cells in CF-1 mice

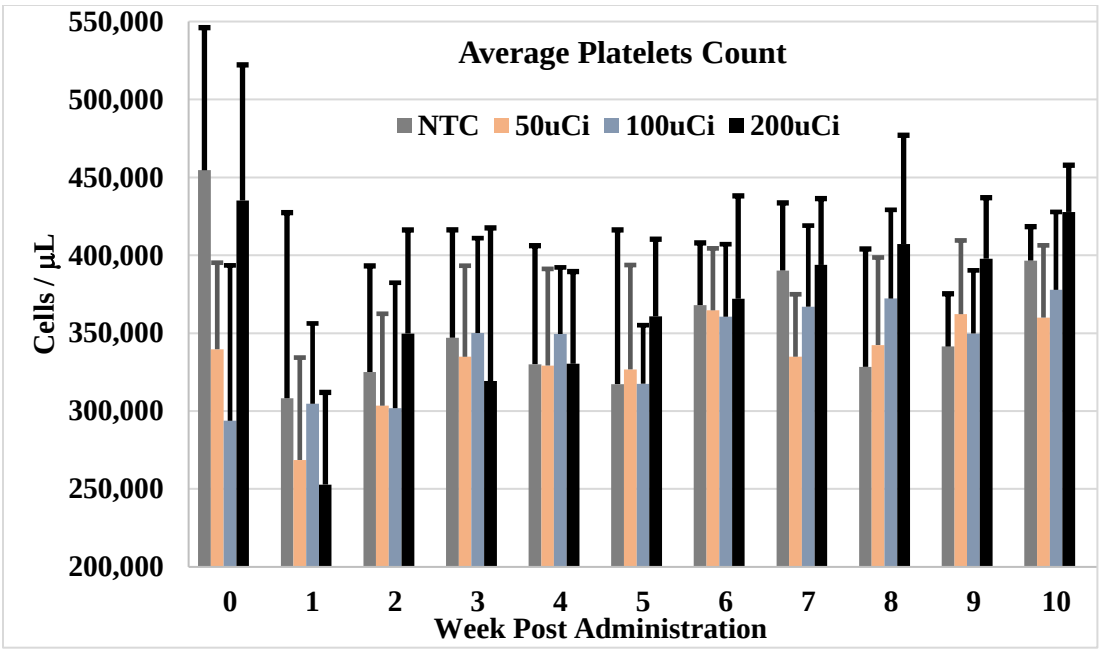


**Figure 3-14:** Effect of [$^{212}$Pb]Pb-RM2 administration on platelets count in CF-1 mice

The effective recoil energy from $^{212}$Pb beta decay is on the order of 1 eV, which is not sufficient to disrupt the chemical integrity of the [$^{212}$Pb]Pb-DOTA conjugate.[61] Although electronic excitation of the metal-chelator conjugate can occur from internal conversion and emission of X-rays following beta decay, we expect that this will have a much less severe effect compared to the recoil energy from a direct alpha particle emission. For example, the recoil energy from the 5.9 MeV alpha particle emission in $^{225}$Ac decay is 104 keV. [$^{212}$Pb]Pb-RM2 was found to be relatively stable at room temperature, with less than 15% of free $^{212}$Pb/$^{212}$Bi observed at 24 hours after incubation in either saline or 0.03 M gentisic acid solution in saline. This is an improvement from the ~35% instability previous reported.[48, 61] This improved stability could be attributed to the initial purification of the [$^{212}$Pb]$PbCl_2$ generator eluent prior to radiolabeling, along with Sep-Pak purification of [$^{212}$Pb]Pb-RM2 after synthesis.

[$^{212}$Pb]Pb-RM2 exhibited specific tumor targeting in PC3 tumor-bearing SCID mice. Additionally, rapid clearance from the blood and non-target organs were observed primarily through the urinary system. Most importantly, negligible [$^{212}$Pb]Pb-RM2 activity was observed in the bone and liver at every time point studied. The is an indication of the high *in vivo* stability [$^{212}$Pb]Pb-RM2 because redistribution of free $^{212}$Pb/$^{212}$Bi should result in accumulation of activity in the bone and liver. The [$^{212}$Pb]Pb-RM2 activity concentration and specific activity per μmol of RM2 was found to be related to its uptake in BB2 receptor-expressing organs/tissues (pancreas and PC3 tumor), with lower specific activity (mCi/ μmol RM2) resulting in lower uptake values. Preliminary data from ongoing *in vitro* studies show that exposure of [$^{212}$Pb]Pb-RM2 to PC3 and LNCAP cells caused significant cell death. Additionally, no radiation-related toxicity has been observed as at week 10 in ongoing [$^{212}$Pb]Pb-RM2 maximum tolerated dose studies in CF-1 normal mice.

In conclusion, the favorable pharmacokinetic profile of [$^{212}$Pb]Pb-RM2, together with the preliminary demonstration of *in vitro* therapeutic efficacy and lack of toxicity in ongoing MTD studies, highlight its potential as a therapeutic radiopharmaceutical for prostate cancer. As with other radionuclides of interest in targeted alpha therapy, a major factor that could hinder future routine clinical utility of $^{212}$Pb-based radiopharmaceuticals is the availability of GMP grade $^{224}$Ra/$^{212}$Pb generators. The completion of a $^{212}$Pb generator production facility (Laboratoire Maurice Tubiana) in France was recently announced by Orano Med, although no information on the production method was provided. A potential method for increasing the availability of $^{224}$Ra/$^{212}$Pb generators is to develop new production routes for $^{228}$Th other than through the natural decay of $^{232}$U and $^{232}$Th. Thorium-228 is the parent isotope of $^{224}$Ra; hence, increasing the production of $^{228}$Th

would lead to increased availability of $^{224}$Ra for producing the $^{224}$Ra/$^{212}$Pb generators. One potential production route for $^{228}$Th is by neutron irradiation of $^{226}$Ra via the $^{226}$Ra (n,γ) $^{227}$Ra ($\beta^-$) $^{227}$Ac (n,γ) $^{228}$Ac ($\beta^-$) $^{228}$Th reaction.[67-68] Interestingly, the neutron irradiation of $^{226}$Ra has been primarily investigated for the production of $^{229}$Th as a means of increasing the availability of $^{225}$Ac (**Figure 3-15**). However, more $^{228}$Th is produced from the neutron irradiation of $^{226}$Ra. For example, Hogle et al.[67] reported that the production yield of for $^{228}$Th and $^{229}$Th was 1450 ± 110 kBq/μg and 74.0 ± 7.4 Bq/μg, respectively, after an ~26 days irradiation of $^{226}$Ra target. Additionally, the co-production of Ac-227 does not constitute a major concern since there are established methods to separate Ac from Th.[67-68] Furthermore, the data presented in this study show that the incorporation of a final purification step for the $^{224}$Ra/$^{212}$Pb generator eluent using the Eichrom Pb-resin is successful in removing residual radionuclidic contamination prior to radiolabeling.

## 3.6. Future Studies

The data obtained upon completion of the [$^{212}$Pb]Pb-RM2 MTD studies will be used to initiate therapy studies to evaluate the *in vivo* therapeutic efficacy of [$^{212}$Pb]Pb-RM2 in SCID mice bearing PC3 prostate tumor xenografts. The therapy doses will be administered at levels that did not induce radiation related toxicity based on the MTD studies. Four study groups will be investigated: (1) non-tumor bearing control group receiving an intravenous administration of saline, (2) tumor bearing control group receiving an intravenous administration of saline, (3) tumor bearing therapy group receiving an intravenous administration of [$^{212}$Pb]Pb-RM2, and (4) tumor bearing therapy group receiving an intravenous administration of non-radioactive Pb-RM2. Each study group will consist of 15 mice. Similar to the MTD studies, BW, CBC, and BCS will be monitored weekly for a

duration of 30 weeks. Additionally, tumor volumes will be measured weekly for the same duration using calipers.

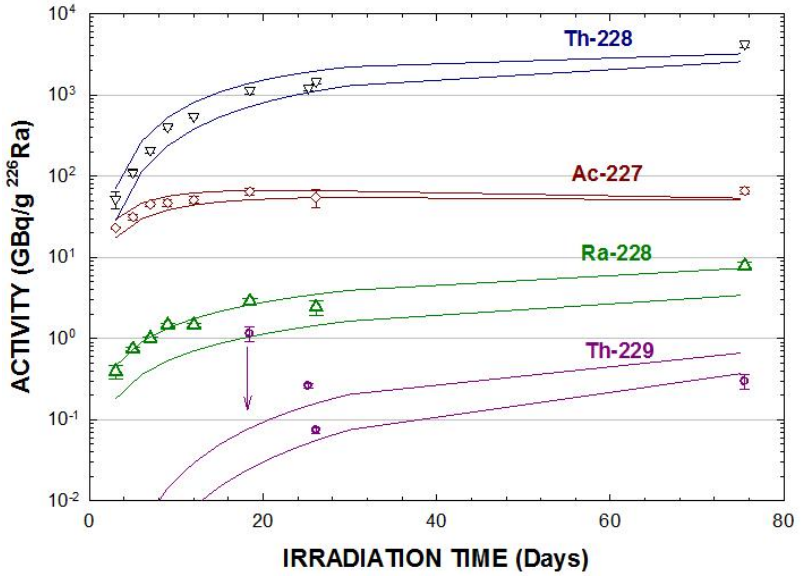


**Figure 3-15.** Experimental and theoretical yields of $^{228}$Th, $^{227}$Ac, $^{228}$Ra and $^{229}$ Th from $^{226}$Ra irradiation at ORNL HFIR. Reproduced with permission from Hogle at al.[67]

## 3.7. References


1. American Cancer Society. Cancer Facts & Figures 2019. American Cancer Society; 2019.

2. Mohler, J.; Antonarakis, E.; Armstrong, A., NCCN Guidelines, version 2.2017: Prostate Cancer Updates. 2017.

3. Reubi, J. C.; Macke, H. R.; Krenning, E. P., Candidates for peptide receptor radiotherapy today and in the future. *Journal of Nuclear Medicine* **2005,** *46* (1 suppl), 67s-75s.

4. Dash, A.; Chakraborty, S.; Pillai, M. R. A.; Knapp Jr, F. F., Peptide receptor radionuclide therapy: an overview. *Cancer Biotherapy and Radiopharmaceuticals* **2015,** *30* (2), 47-71.

5. Cutler, C. S.; Hennkens, H. M.; Sisay, N.; Huclier-Markai, S.; Jurisson, S. S., Radiometals for Combined Imaging and Therapy. *Chemical Reviews* **2013,** *113* (2), 858-883.

6. Strosberg, J.; El-Haddad, G.; Wolin, E.; Hendifar, A.; Yao, J.; Chasen, B.; Mittra, E.; Kunz, P. L.; Kulke, M. H.; Jacene, H., Phase 3 trial of $^{177}$Lu-Dotatate for midgut neuroendocrine tumors. *New England Journal of Medicine* **2017,** *376* (2), 125-135.

7. Silver, D. A.; Pellicer, I.; Fair, W. R.; Heston, W.; Cordon-Cardo, C., Prostate-specific membrane antigen expression in normal and malignant human tissues. *Clinical Cancer Research* **1997,** *3* (1), 81-85.

8. Tsourlakis, M. C.; Klein, F.; Kluth, M.; Quaas, A.; Graefen, M.; Haese, A.; Simon, R.; Sauter, G.; Schlomm, T.; Minner, S., PSMA expression is highly homogenous in primary prostate cancer. *Applied Immunohistochemistry & Molecular Morphology* **2015,** *23* (6), 449-455.

9. Bostwick, D. G.; Pacelli, A.; Blute, M.; Roche, P.; Murphy, G. P., Prostate specific membrane antigen expression in prostatic intraepithelial neoplasia and adenocarcinoma: a study of 184 cases. *Cancer: Interdisciplinary International Journal of the American Cancer Society* **1998,** *82* (11), 2256-2261.

10. Markwalder, R.; Reubi, J. C., Gastrin-releasing peptide receptors in the human prostate relation to neoplastic transformation. *Cancer Research* **1999,** *59* (5), 1152-1159.

11. Bartholdi, M. F.; Wu, J. M.; Pu, H.; Troncoso, P.; Eden, P. A.; Feldman, R. I., In situ hybridization for gastrin‐releasing peptide receptor (GRP receptor) expression in prostatic carcinoma. *International Journal of Cancer* **1998,** *79* (1), 82-90.

12. Sun, B.; Halmos, G.; Schally, A. V.; Wang, X.; Martinez, M., Presence of receptors for bombesin/gastrin‐releasing peptide and mRNA for three receptor subtypes in human prostate cancers. *The Prostate* **2000,** *42* (4), 295-303.

13. Körner, M.; Waser, B.; Rehmann, R.; Reubi, J. C., Early over‐expression of GRP receptors in prostatic carcinogenesis. *The Prostate* **2014,** *74* (2), 217-224.

14. Ischia, J.; Patel, O.; Bolton, D.; Shulkes, A.; Baldwin, G. S., Expression and function of gastrin‐releasing peptide (GRP) in normal and cancerous urological tissues. *BJU International* **2014,** *113*, 40-47.

15. Kratochwil, C.; Bruchertseifer, F.; Giesel, F. L.; Weis, M.; Verburg, F. A.; Mottaghy, F.; Kopka, K.; Apostolidis, C.; Haberkorn, U.; Morgenstern, A., $^{225}$Ac-PSMA-617 for PSMA-targeted $\alpha$-radiation therapy of metastatic castration-resistant prostate cancer. *Journal of Nuclear Medicine* **2016,** *57* (12), 1941-1944.

16. Afshar-Oromieh, A.; Hetzheim, H.; Kratochwil, C.; Benesova, M.; Eder, M.; Neels, O. C.; Eisenhut, M.; Kübler, W.; Holland-Letz, T.; Giesel, F. L., The theranostic PSMA ligand PSMA-617 in the diagnosis of prostate cancer by PET/CT: Biodistribution in humans, radiation dosimetry, and first evaluation of tumor lesions. *Journal of Nuclear Medicine* **2015,** *56* (11), 1697-1705.

17. Weineisen, M.; Schottelius, M.; Simecek, J.; Baum, R. P.; Yildiz, A.; Beykan, S.; Kulkarni, H. R.; Lassmann, M.; Klette, I.; Eiber, M., $^{68}$Ga-and $^{177}$Lu-labeled PSMA I&T: optimization of a PSMA-targeted theranostic concept and first proof-of-concept human studies. *Journal of Nuclear Medicine* **2015,** *56* (8), 1169-1176.

18. Sterzing, F.; Kratochwil, C.; Fiedler, H.; Katayama, S.; Habl, G.; Kopka, K.; Afshar-Oromieh, A.; Debus, J.; Haberkorn, U.; Giesel, F. L., $^{68}$Ga-PSMA-11 PET/CT: a new technique with high potential for the radiotherapeutic management of prostate cancer patients. *European Journal of Nuclear Medicine and Molecular Imaging* **2016,** *43* (1), 34-41.

19. Mansi, R.; Wang, X. J.; Forrer, F.; Waser, B.; Cescato, R.; Graham, K.; Borkowski, S.; Reubi, J. C.; Maecke, H. R., Development of a potent DOTA-conjugated bombesin antagonist for targeting GRPr-positive tumours. *European Journal of Nuclear Medicine and Molecular Imaging* **2011,** *38* (1), 97-107.

20. Minamimoto, R.; Sonni, I.; Hancock, S.; Vasanawala, S.; Loening, A.; Gambhir, S. S.; Iagaru, A., Prospective Evaluation of $^{68}$Ga-RM2 PET/MRI in Patients with Biochemical Recurrence of Prostate Cancer and Negative Conventional Imaging. *Journal of Nuclear Medicine* **2018,** *59* (5), 803-808.

21. Lantry, L. E.; Cappelletti, E.; Maddalena, M. E.; Fox, J. S.; Feng, W.; Chen, J.; Thomas, R.; Eaton, S. M.; Bogdan, N. J.; Arunachalam, T., $^{177}$Lu-AMBA: Synthesis and Characterization of a Selective $^{177}$Lu-Labeled GRP-R Agonist for Systemic Radiotherapy of Prostate Cancer. *Journal of Nuclear Medicine* **2006,** *47* (7), 1144.

22. Dalm, S. U.; Bakker, I. L.; de Blois, E.; Doeswijk, G. N.; Konijnenberg, M. W.; Orlandi, F.; Barbato, D.; Tedesco, M.; Maina, T.; Nock, B. A., $^{68}$Ga/$^{177}$Lu-NeoBOMB1, a novel radiolabeled GRPR antagonist for theranostic use in oncology. *Journal of Nuclear Medicine* **2017,** *58* (2), 293-299.

23. Nock, B. A.; Kaloudi, A.; Lymperis, E.; Giarika, A.; Kulkarni, H. R.; Klette, I.; Singh, A.; Krenning, E. P.; De Jong, M.; Maina, T., Theranostic perspectives in prostate cancer

with the gastrin-releasing peptide receptor antagonist NeoBOMB1: preclinical and first clinical results. *Journal of Nuclear Medicine* **2017,** *58* (1), 75-80.

24. Kranzbühler, B.; Salemi, S.; Umbricht, C. A.; Müller, C.; Burger, I. A.; Sulser, T.; Eberli, D., Pharmacological upregulation of prostate‐specific membrane antigen (PSMA) expression in prostate cancer cells. *The Prostate* **2018,** *78* (10), 758-765.

25. Qiao, J.; Grabowska, M. M.; Forestier, I. S.; Mirosevich, J.; Case, T. C.; Chung, D. H.; Cates, J. M.; Matusik, R. J.; Manning, H. C.; Jin, R., Activation of GRP/GRP-R signaling contributes to castration-resistant prostate cancer progression. *Oncotarget* **2016,** *7* (38), 61955.

26. Heinrich, E.; Probst, K.; Michel, M. S.; Trojan, L., Gastrin‐releasing peptide: Predictor of castration‐resistant prostate cancer? *The Prostate* **2011,** *71* (6), 642-648.

27. Serda, R. E.; Bisoffi, M.; Thompson, T. A.; Ji, M.; Omdahl, J. L.; Sillerud, L. O., 1$\alpha$, 25‐Dihydroxyvitamin D3 down‐regulates expression of prostate specific membrane antigen in prostate cancer cells. *The Prostate* **2008,** *68* (7), 773-783.

28. Minamimoto, R.; Hancock, S.; Schneider, B.; Chin, F.; Jamali, M.; Loening, A. M.; Vasanawala, S.; Gambhir, S. S.; Iagaru, A., Pilot Comparison of $^{68}$Ga-RM2 PET and $^{68}$Ga-PSMA PET in Patients with Biochemically Recurrent Prostate Cancer. *Journal of Nuclear Medicine* **2016**, 557-562.

29. Kähkönen, E.; Jambor, I.; Kemppainen, J.; Lehtiö, K.; Grönroos, T. J.; Kuisma, A.; Luoto, P.; Sipilä, H. J.; Tolvanen, T.; Alanen, K., In vivo imaging of prostate cancer using [$^{68}$Ga]-labeled bombesin analog BAY86-7548. *Clinical Cancer Research* **2013,** *19* (19), 5434-5443.

30. Wieser, G.; Popp, I.; Rischke, H. C.; Drendel, V.; Grosu, A.-L.; Bartholomä, M.; Weber, W. A.; Mansi, R.; Wetterauer, U.; Schultze-Seemann, W., Diagnosis of recurrent prostate cancer with PET/CT imaging using the gastrin-releasing peptide receptor antagonist $^{68}$Ga-RM2: Preliminary results in patients with negative or inconclusive [$^{18}$F]Fluoroethylcholine-PET/CT. *European Journal of Nuclear Medicine and Molecular Imaging* **2017**, 1-10.

31. Sgouros, G.; Roeske, J. C.; McDevitt, M. R.; Palm, S.; Allen, B. J.; Fisher, D. R.; Brill, A. B.; Song, H.; Howell, R. W.; Akabani, G., MIRD Pamphlet No. 22 (abridged): radiobiology and dosimetry of $\alpha$-particle emitters for targeted radionuclide therapy. *Journal of Nuclear Medicine* **2010,** *51* (2), 311-328.

32. Baidoo, K. E.; Yong, K.; Brechbiel, M. W., Molecular pathways: targeted $\alpha$-particle radiation therapy. *Clinical Cancer Research* **2013,** *19* (3), 530-537.

33. Parker, C.; Lewington, V.; Shore, N.; Kratochwil, C.; Levy, M.; Lindén, O.; Noordzij, W.; Park, J.; Saad, F., Targeted Alpha Therapy, an Emerging Class of Cancer Agents: A Review. *JAMA Oncology* **2018,** *4* (12), 1765-1772.

34. Kim, Y.-S.; Brechbiel, M. W., An overview of targeted alpha therapy. *Tumor Biology* **2012,** *33* (3), 573-590.

35. Nayak, T.; Norenberg, J.; Anderson, T.; Atcher, R., A comparison of high-versus low-linear energy transfer somatostatin receptor targeted radionuclide therapy in vitro. *Cancer Biotherapy & Radiopharmaceuticals* **2005,** *20* (1), 52-57.

36. Chan, H. S.; de Blois, E.; Morgenstern, A.; Bruchertseifer, F.; de Jong, M.; Breeman, W.; Konijnenberg, M., In Vitro comparison of $^{213}$Bi-and $^{177}$Lu-radiation for peptide receptor radionuclide therapy. *PloS One* **2017,** *12* (7), e0181473.

37. Yong, K.; Brechbiel, M. W., Towards translation of $^{212}$Pb as a clinical therapeutic; getting the lead in! *Dalton Transactions* **2011,** *40* (23), 6068-6076.

38. Yong, K. J.; Milenic, D. E.; Baidoo, K. E.; Brechbiel, M. W., $^{212}$Pb-radioimmunotherapy induces G2 cell-cycle arrest and delays DNA damage repair in tumor xenografts in a model for disseminated intraperitoneal disease. *Molecular Cancer Therapeutics* **2012,** *11* (3), 639-648.

39. Milenic, D. E.; Garmestani, K.; Brady, E. D.; Albert, P. S.; Ma, D.; Abdulla, A.; Brechbiel, M. W., $\alpha$-Particle radioimmunotherapy of disseminated peritoneal disease using a $^{212}$Pb-labeled radioimmunoconjugate targeting HER2. *Cancer Biotherapy & Radiopharmaceuticals* **2005,** *20* (5), 557-568.

40. Milenic, D. E.; Baidoo, K. E.; Kim, Y. S.; Barkley, R.; Brechbiel, M. W., Targeted alpha-Particle Radiation Therapy of HER1-Positive Disseminated Intraperitoneal Disease: An Investigation of the Human Anti-EGFR Monoclonal Antibody, Panitumumab. *Translational Oncology* **2017,** *10* (4), 535-545.

41. Tan, Z.; Chen, P.; Schneider, N.; Glover, S.; Cui, L.; Torgue, J.; Rixe, O.; Spitz, H. B.; Dong, Z., Significant systemic therapeutic effects of high-LET immunoradiation by $^{212}$Pb-trastuzumab against prostatic tumors of androgen-independent human prostate cancer in mice. *International Journal of Oncology* **2012,** *40* (6), 1881-1888.

42. Kasten, B. B.; Azure, M. T.; Schoeb, T. R.; Fisher, D. R.; Zinn, K. R., Imaging, biodistribution, and toxicology evaluation of $^{212}$Pb-TCMC-trastuzumab in nonhuman primates. *Nuclear Medicine and Biology* **2016,** *43* (7), 391-396.

43. Schneider, N.; Lobaugh, M.; Tan, Z.; Sandwall, P.; Chen, P.; Glover, S.; Cui, L.; Murry, M.; Dong, Z.; Torgue, J., Biodistribution of $^{212}$Pb conjugated trastuzumab in mice. *Journal of Radioanalytical and Nuclear Chemistry* **2013,** *296* (1), 75-81.

44. Kasten, B. B.; Arend, R. C.; Katre, A. A.; Kim, H.; Fan, J.; Ferrone, S.; Zinn, K. R.; Buchsbaum, D. J., B7-H3-targeted $^{212}$Pb radioimmunotherapy of ovarian cancer in preclinical models. *Nuclear Medicine and Biology* **2017,** *47*, 23-30.

45. Kasten, B. B.; Gangrade, A.; Kim, H.; Fan, J.; Ferrone, S.; Ferrone, C. R.; Zinn, K. R.; Buchsbaum, D. J., $^{212}$Pb-labeled B7-H3-targeting antibody for pancreatic cancer therapy in mouse models. *Nuclear Medicine and Biology* **2018,** *58*, 67-73.

46. Miao, Y.; Hylarides, M.; Fisher, D. R.; Shelton, T.; Moore, H.; Wester, D. W.; Fritzberg, A. R.; Winkelmann, C. T.; Hoffman, T.; Quinn, T. P., Melanoma therapy via peptide-targeted $\alpha$-radiation. *Clinical Cancer Research* **2005,** *11* (15), 5616-5621.

47. Shah, M.; Zhang, X.; Rossin, R.; Robillard, M. S.; Fisher, D.; Bueltmann, T.; Hoeben, F. J.; Quinn, T., Metal-free Cycloaddition Chemistry Driven Pretargeted Radioimmunotherapy Using $\alpha$ -Particle Radiation. *Bioconjugate Chemistry* **2017**.

48. Su, F.-M.; Beaumier, P.; Axworthy, D.; Atcher, R.; Fritzberg, A., Pretargeted radioimmunotherapy in tumored mice using an in vivo $^{212}$Pb/$^{212}$Bi generator. *Nuclear Medicine and Biology* **2005,** *32* (7), 741-747.

49. Saidib, A.; Maalanda, A.; Torgueb, J.; Heyerdahla, H.; Dahlea, J., Targeted Alpha Therapy with $^{212}$Pb-NNV003 for the Treatment of CD37 Positive B-Cell Chronic Lymphocytic Leukemia (CLL) and Non-Hodgkin Lymphoma (NHL). American Society of Hematology: 2018.

50. Meredith, R. F.; Torgue, J. J.; Rozgaja, T. A.; Banaga, E. P.; Bunch, P. W.; Alvarez, R. D.; Straughn Jr, J. M.; Dobelbower, M. C.; Lowy, A. M., Safety and outcome measures of first-in-human intraperitoneal $\alpha$ radioimmunotherapy with $^{212}$Pb-TCMC-trastuzumab. *American Journal of Clinical Oncology* **2018,** *41* (7), 716.

51. Meredith, R.; Torgue, J.; Shen, S.; Fisher, D. R.; Banaga, E.; Bunch, P.; Morgan, D.; Fan, J.; Straughn, J. M., Jr., Dose escalation and dosimetry of first-in-human alpha radioimmunotherapy with $^{212}$Pb-TCMC-trastuzumab. *Journal of Nuclear Medicine* **2014,** *55* (10), 1636-42.

52. Meredith, R. F.; Torgue, J.; Azure, M. T.; Shen, S.; Saddekni, S.; Banaga, E.; Carlise, R.; Bunch, P.; Yoder, D.; Alvarez, R., Pharmacokinetics and imaging of $^{212}$Pb-TCMC-trastuzumab after intraperitoneal administration in ovarian cancer patients. *Cancer Biotherapy & Radiopharmaceuticals* **2014,** *29* (1), 12-7.

53. Atcher, R. W.; Friedman, A. M.; Hines, J., Isotopic generator for bismuth-212 and lead-212 from radium. U.S. Patent No. 4,663,129.: 1987.

54. Mirzadeh, S., Generator-produced alpha-emitters. *Applied Radiation and Isotopes* **1998,** *49* (4), 345-349.

55. Li, M.; Zhang, X.; Quinn, T. P.; Lee, D.; Liu, D.; Kunkel, F.; Zimmerman, B. E.; McAlister, D.; Olewein, K.; Menda, Y., Automated cassette-based production of high specific activity [$^{203/212}$Pb] peptide-based theranostic radiopharmaceuticals for image-guided radionuclide therapy for cancer. *Applied Radiation and Isotopes* **2017,** *127*, 52-60.

56. Horwitz, E. P.; Dietz, M. L.; Rhoads, S.; Felinto, C.; Gale, N. H.; Houghton, J., A lead-selective extraction chromatographic resin and its application to the isolation of lead from geological samples. *Analytica Chimica Acta* **1994,** *292* (3), 263-273.

57. Milenic, D.; Baidoo, K.; Brechbiel, M., Bench to bedside: stability studies of GMP produced trastuzumab-TCMC in support of a clinical trial. *Pharmaceuticals* **2015,** *8* (3), 435-454.

58. Baidoo, K. E.; Milenic, D. E.; Brechbiel, M. W., Methodology for labeling proteins and peptides with lead-212 ($^{212}$ Pb). *Nuclear Medicine and Biology* **2013,** *40* (5), 592-599.

59. Milenic, D. E.; Molinolo, A. A.; Solivella, M. S.; Banaga, E.; Torgue, J.; Besnainou, S.; Brechbiel, M. W.; Baidoo, K. E., Toxicological studies of $^{212}$Pb intravenously or intraperitoneally injected into mice for a phase 1 trial. *Pharmaceuticals* **2015,** *8* (3), 416-434.

60. Torgue, J.; Maquaire, P.; Young, J.; Andreoletti, G.; Bourdet, P. Method and apparatus for the production of lead 212 for medical use. United States Patent. 2015.

61. Mirzadeh, S.; Kumar, K.; Gansow, O. A., The chemical fate of $^{212}$Bi-DOTA formed by $\beta^-$ decay of $^{212}$Pb(DOTA)$^{2-}$. *Radiochimica Acta* **1993,** *60* (1), 1-10.

62. Mansi, R.; Wang, X.; Forrer, F.; Kneifel, S.; Tamma, M.-L.; Waser, B.; Cescato, R.; Reubi, J. C.; Maecke, H. R., Evaluation of a 1, 4, 7, 10-Tetraazacyclododecane-1, 4, 7, 10-Tetraacetic acid–conjugated bombesin-based radioantagonist for the labeling with single-photon emission computed tomography, positron emission tomography, and therapeutic radionuclides. *Clinical Cancer Research* **2009,** *15* (16), 5240-5249.

63. Hoffman, T. J.; Gali, H.; Smith, C. J.; Sieckman, G. L.; Hayes, D. L.; Owen, N. K.; Volkert, W. A., Novel series of $^{111}$In-labeled bombesin analogs as potential radiopharmaceuticals for specific targeting of gastrin-releasing peptide receptors expressed on human prostate cancer cells. *Journal of Nuclear Medicine* **2003,** *44* (5), 823-831.

64. Zhang, H.; Schuhmacher, J.; Waser, B.; Wild, D.; Eisenhut, M.; Reubi, J. C.; Maecke, H. R., DOTA-PESIN, a DOTA-conjugated bombesin derivative designed for the imaging and targeted radionuclide treatment of bombesin receptor-positive tumours. *European Journal of Nuclear Medicine and Molecular Imaging* **2007,** *34* (8), 1198-1208.

65. De Blois, E.; Schroeder, R.; De Ridder, C.; Van Weerden, W.; Breeman, W.; De Jong, M., Improving radiopeptide pharmacokinetics by adjusting experimental conditions for bombesin receptor-mediated imaging of prostate cancer. *Quarterly Journal of Nuclear Medicine and Molecular Imaging* **2013,** *57*, 1-9.

66. Nicolas, G. P.; Mansi, R.; McDougall, L.; Kaufmann, J.; Bouterfa, H.; Wild, D.; Fani, M., Biodistribution, pharmacokinetics, and dosimetry of $^{177}$Lu-, $^{90}$Y-, and $^{111}$In-labeled somatostatin receptor antagonist OPS201 in comparison to the agonist $^{177}$Lu-DOTATATE: the mass effect. *Journal of Nuclear Medicine* **2017,** *58* (9), 1435-1441.

67. Hogle, S.; Boll, R. A.; Murphy, K.; Denton, D.; Owens, A.; Haverlock, T. J.; Garland, M.; Mirzadeh, S., Reactor production of Thorium-229. *Applied Radiation and Isotopes* **2016,** *114*, 19-27.

68. Kuznetsov, R.; Butkalyuk, P.; Tarasov, V.; Baranov, A. Y.; Butkalyuk, I.; Romanov, E.; Kupriyanov, V.; Kazakova, E., Yields of activation products in $^{226}$Ra irradiation in the high-flux SM reactor. *Radiochemistry* **2012,** *54* (4), 383-387.

# CHAPTER 4: Microwave-assisted Synthesis of Rh(III) Complexes and Radiochemical Evaluation of $^{105}$Rh Produced from Recycled $^{104}$Ru Metal Target

## 4.1. Introduction

Grazman and Troutner[1-2] first identified $^{105}$Rh as a potential therapeutic radionuclide. Rhodium-105 (half-life = 35.4 hours) is a moderate energy beta emitting radionuclide [$\beta^-_{max}$ = 567 keV (75%), $\beta^-_{avg}$ = 152 keV], with low energy gamma emissions [319 keV (19%) and 306 keV (5%)]. The beta energy of $^{105}$Rh is comparable to the beta energies of $^{177}$Lu ($\beta^-_{avg}$ = 134 keV) and $^{131}$I ($\beta^-_{avg}$ = 182 keV), which are currently used in the production of FDA-approved therapeutic radiopharmaceuticals.

Rhodium-105 is produced at the University of Missouri Research Reactor Center (MURR) by thermal neutron (~9.78 x $10^{13}$ n/cm$^2$/s) irradiation of an enriched (>98%) $^{104}$Ru metal target to give $^{105}$Ru (half-life = 4.4 hours), which subsequently decays by beta particle emission to $^{105}$Rh, as previously reported by Grazman and Troutner (**Equation 4-1**).[1-2] A 24 hour wait period is allowed to ensure the decay of $^{105}$Ru into $^{105}$Rh. Rhodium-105 is separated from the bulk $^{104}$Ru metal target by oxidation of $^{104}$Ru metal to [$^{104}$Ru]$RuO_4$ using hypochlorite generated *in situ* by bubbling $Cl_2$ into a 2 M NaOH solution containing the $^{104}$Ru metal target (**Figure 4-1**). [$^{104}$Ru]$RuO_4$ is distilled off at elevated temperature (~ 90 °C) and trapped in a 3 M HCl solution for future recovery, leaving behind $^{105}$Rh in the original target dissolution vial. Rhodium-105 is acidified with 1 M HCl to yield a mixture of $^{105}$Rh chloride species such as [$^{105}$Rh]$RhCl_3(OH_2)_3$, [$^{105}$Rh]$RhCl_4(OH_2)_2^{1-}$, [$^{105}$Rh]$RhCl_5(OH_2)_2^{2-}$, and [$^{105}$Rh]$RhCl_6^{3-}$, as previously determined by electrophoresis analysis.[1-3]

$$^{104}\text{Ru} \xrightarrow{n} {}^{105}\text{Ru} \xrightarrow[t_{1/2} = 4.4\ \text{h}]{\beta^-} {}^{105}\text{Rh}$$

**Equation 4-1.** Production of $^{105}$Rh

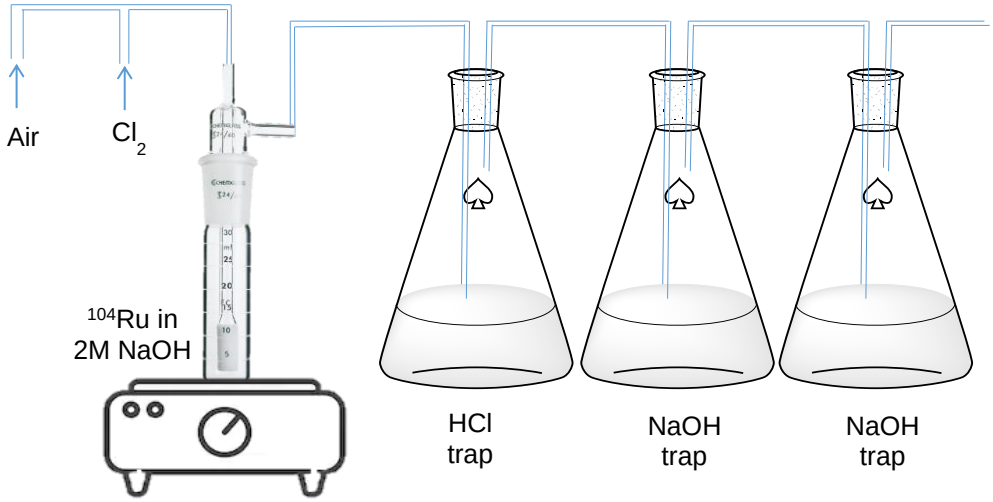


**Figure 4-1.** Schematic for $^{105}$Rh separation

Due to the high cost of the enriched $^{104}$Ru metal target, it is necessary that the target material be recycled for reuse in order to make routine $^{105}$Rh production economically feasible. In addition, less than 1% of the total $^{104}$Ru atoms are converted to $^{105}$Ru atoms following neutron irradiation; hence, the $^{104}$Ru metal target can be reused multiple times if successfully recovered. Recent research by Phelps and colleagues at the University of Missouri have demonstrated the possibility of recycling and reusing $^{104}$Ru trapped in 3 M HCl as ruthenate ($[^{104}\text{Ru}]RuO_4^{2-}$) during the $^{105}$Rh production process.[4] The target recycling process involves concentrating the 3 M HCl solutions to dryness to yield hydrated ruthenium chloride ($[^{104}\text{Ru}]RuCl_3 \cdot xH_2O$), dehydrating $[^{104}\text{Ru}]RuCl_3 \cdot xH_2O$ with Ar at 525 °C, and subsequently reducing to $^{104}$Ru metal with $H_2$ at 800 °C. ICP-MS analysis revealed that the isotopic enrichment of the recycled metal target was 98.9% $^{104}$Ru.[4] Neutron

activation analysis on the recycled $^{104}$Ru metal target produced mainly $^{105}$Ru, with very minimal amounts of $^{24}$Na (0.3% of total $^{105}$Ru) produced from neutron activation of minor NaCl contaminants in the recycled $^{104}$Ru metal.[4]

A very attractive chemical property of Rh is the kinetic inertness of Rh(III) complexes, which favors a low spin octahedral $d^6$ arrangement.[5] This suggests that $^{105}$Rh(III) complexes should exhibit high *in vivo* stability since they should be stable to transchelation by serum proteins. Therefore, several researchers have investigated $^{105}$Rh(III) complexes as potential radiotherapeutic agents.[6-13] Initial studies were done using polyamine chelates, especially derivatives of cyclam and cyclen.[6] Troutner and his research group investigated several diethylenetriamine,[7, 10] amine oxime,[11] and porphyrin,[9] ligands and their derivatives. Li et al.[8] evaluated the *in vivo* pharmacokinetics of a series of $^{105}$Rh-labeled tetradentate thiamacrocyclic ligands in rats. The authors observed very minimal *in vivo* degradation of the radiolabeled complexes and clearance through both the hepatobiliary and urinary systems was also observed depending on the ligand structure and derivatization.[8]

More recently, efforts on the development of chelators for $^{105}$Rh complexation have focused on tetrathioether frameworks.[12-14] Goswami et al.[12] investigated how the number of carbon chain length [ethylene ($222S_4$), propylene ($333S_4$), or a combination of both ($232S_4$)] between the sulfur atoms in the tetrathioether ligand backbone affected the conformation of the final Rh(III) complex. The authors found that the smaller backbone chain length ($222S_4$) favored the formation of the *cis*-dichloro isomer, while the larger backbone chain length ($333S_4$) favored the formation of the *trans*-dichloro isomer.[12] Similar results were also reported by Dame[15] and Crenshaw[16] using tetrathioether ligand

frameworks containing pendant methyl acetate groups, shown in **Figure 4-2A and 4-2B**. The intermediate backbone chain length ($232S_4$) gave a mixture of both the *cis*-dichloro and *trans*-dichloro isomers.[12] Goswami et al.[13] subsequently evaluated the *in vivo* pharmacokinetics of $^{105}$Rh-labeled tetrathioether ligands ($222S_4$, $232S_4$, and $333S_4$) containing pendant carboxylic acid groups. The $^{105}$Rh complexes effectively cleared from the blood and tissues primarily through the urinary system; however, the [$^{105}$Rh]Rh-$222S_4$ complex was shown to exhibit slightly superior stability and lesser hepatobiliary clearance than the [$^{105}$Rh]Rh-$333S_4$ complex.[13] Akgun et al.[17] investigated Rh(III) complexes derived from a series of diaminedithioether ligands and found that the ligand with 232 carbon backbone chain length with *gem*-dimethyl groups was preferred.

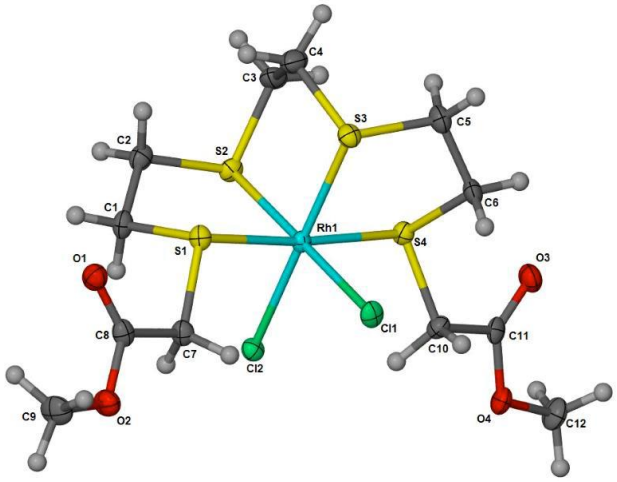


**Figure 4-2A.** Crystal structure of *cis*-[$RhCl_2$-$222S_4$diAcOMe]$PF_6$ as reported by Dame.[15]

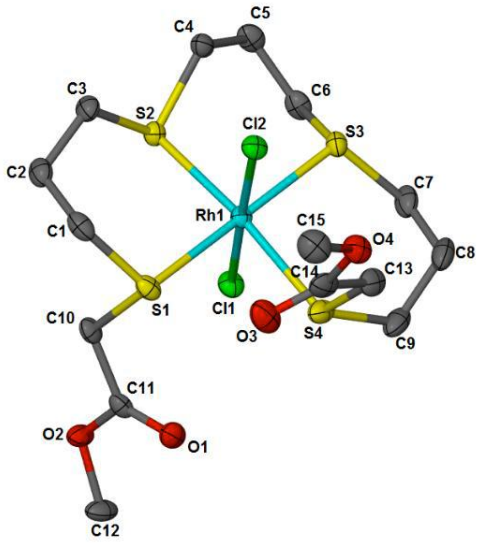


**Figure 4-2B.** Crystal structure of *trans*-[$RhCl_2$-333$S_4$diAcOMe]$PF_6$ as reported by Crenshaw.[16]

Recently, Carroll[18] performed $^{105}$Rh-labeling studies using 333-$S_4$-8Aoc-BBN(7-14)$NH_2$, which is a bifunctional chelate containing the 333$S_4$diAcOH tetrathioether ligand conjugated to the bombesin(7-14) agonist peptide for targeting the gastrin-releasing peptide receptor. Carroll reported very low radiolabeling yields (<10%) and observed the formation of multiple radiolabeled species. The multiple radiolabeled species were attributed to acid catalyzed esterification of the pendant carboxylic acid groups on the tetrathioether ligand because the reaction was carried out under acidic conditions (pH 4 – 5) in the presence of refluxing ethanol. In addition, the pendant carboxylic acid groups were found to directly coordinate with the Rh(III) core.[14] To avoid the formation of acid catalyzed esterification products, Crenshaw[16] and Dame[15] investigated the formation of Rh(III) complexes of 333$S_4$ and 222$S_4$ tetrathioether ligands respectively, using $SnCl_2$ as reducing agent instead of refluxing ethanol. It has been widely reported that the catalytic reduction of $Rh^{+3}$ to $Rh^{+1}$, with subsequent re-oxidation to $Rh^{+3}$ by atmospheric oxygen, is

necessary for the formation of Rh(III) complexes.[14, 19-20] Hence refluxing alcohols, particularly ethanol, have been traditionally used as reducing agents for the formation of Rh(III) complexes.[3, 8, 12-13]

This study reports the synthesis of Rh(III) complexes using two tetrathioether ligands (***222S$_4$diAcOMe*** and ***222S$_4$diAcOH***) and a tetradentate thiamacrocyclic ligand (***16S$_4$-diol***) without refluxing ethanol or $SnCl_2$ as a reducing agent. A rapid microwave-assisted synthesis procedure for Rh(III) complexes was developed and an improved HPLC method for distinguishing the various product species is reported. Additionally, we report the production of $^{105}$Rh from recycled $^{104}$Ru targets. Finally, $^{105}$Rh-labeling studies using [$^{105}$Rh]$RhCl_3$ produced from both new and recycled $^{104}$Ru metal target materials are reported.

## 4.2. Experimental

### 4.2-1. Materials and Methods

1,5,9,13-tetrathiacyclohexadecane-3,11-diol (***16S$_4$-diol***; *cis/trans* mixture) was purchased from Sigma-Aldrich and used without further purification. All other chemicals and reagents were purchased from Sigma-Aldrich or Fisher Scientific and used without further purification. Plastic-backed silica gel TLC plates were purchased from Sigma-Aldrich or Fisher Scientific and were used for radio TLC. Only 18 MΩ water was used. [$^{105}$Rh]$RhCl_3$ was produced at the University of Missouri Research Reactor Center (MURR) by the bombardment of enriched $^{104}$Ru metal targets (2 – 5 mg) encapsulated in a quartz vial with thermal neutron irradiation (~9.78 x $10^{13}$ n/cm$^2$/s) for ~90 hours at the reflector position. **CAUTION!** $^{105}$Rh is radioactive and must be handled in laboratories outfitted and approved for work with radioactive materials. $^1$H and $^{13}$C NMR spectra were

obtained using a 500 MHz or a 600 MHz Bruker ARX spectrometer. Microwave synthesis was carried out in dynamic mode using a CEM Discover SP microwave synthesizer (Matthews, NC). Electrospray Ionization Mass Spectrometry (ESI-MS) was performed on a Thermo Finnigan TSQ7000 triple-quadrupole instrument with an API2 source. Inductively coupled plasma mass spectrometry (ICP-MS) was performed using a PerkinElmer NexION 300X Model equipped with a glass cyclonic spray chamber and glass concentric nebulizer and operated in KED mode. An Eckert & Ziegler Bioscan AR-2000 Imager using LabLogic Win-Scan imaging scanner software was used for scanning radioTLC plates. High-performance liquid chromatography (HPLC) was performed using a Shimadzu Prominence HPLC system equipped with a UV-Vis absorbance detector (set at 254 and 280 nm), and a NaI(Tl) scintillation detector. All HPLC analyses were performed using a mobile phase consisting of solvent A [99.9% $H_2O$ and 0.1% trifluoroacetic acid (TFA)] and solvent B [99.9% $CH_3CN$ (ACN) and 0.1% TFA] run on a Thermo Scientific Beta Basic Column (C18, 5μ, 150 × 4.6 mm). Three different linear gradient systems were developed for HPLC analyses. ***Gradient 1***: 10% solvent B:A increased to 80% solvent B:A over 18 minutes, followed by an additional 1 minute at 80% solvent B:A, then decreased to 10% solvent B:A over 1 minute. ***Gradient 2***: 2% solvent B:A increased to 5% solvent B:A over 10 minutes, followed by an additional 5 minute at 5% solvent B:A, then increased to 80% solvent B:A over 9 minutes, and finally decreased to 2% solvent B:A over 1 minute. ***Gradient 3***: 5% solvent B:A increased to 20% solvent B:A over 15 minutes, followed by an additional 2 minutes at 20% solvent B:A, then decreased to 5% solvent B:A over 3 minutes.

### 4.2-2. Synthesis of methyl 2-((2-chloroethyl)thio)acetate [$C_5H_9ClO_2S$], *intermediate 1*

***Intermediate 1*** was synthesized following a slightly modified literature procedure.[13, 15, 18] 1,2-dichloroethane (88.6 mL, 1.12 mol) and triethylamine (17.2 mL, 0.12 mol) were added into a one-necked round bottom flask and heated to 90 °C. While stirring at 90 °C, methyl thioglycolate (10 mL, 0.11 mol) was added drop wise. The reaction was refluxed overnight (~ 18 hours) at 90 °C under $N_2$. The reaction progress was monitored using silica gel TLC, with 1:1 hexane / ethyl ether as the mobile phase. Upon reaction completion, the reaction mixture was cooled to room temperature and ethyl ether (~ 70 mL) was added to precipitate the trimethylammonium salts. The mixture was filtered and the solid residues were washed with ethyl ether. The filtrate was concentrated to minimal volume using a rotary evaporator. The condensed filtrate was then transferred to a smaller round bottom flask. Any remaining 1,2-dichloroethane was removed by vacuum distillation (~13 mbar) beginning at 60 °C and gradually increased to 115 °C. The distillation apparatus was replaced with clean glassware. The desired product was finally obtained as a colorless oily liquid by vacuum distillation (~13 mbar) between 135 °C to 145 °C. Yield, 12.81 g, 69%. $^1$H NMR (500 MHz, $CDCl_3$) δ ppm: 2.97 (t, $CH_2C\mathbf{H}_2S$, 2H), 3.25 (s, $SC\mathbf{H}_2COO$, 2H), 3.65 (t, $CH_2C\mathbf{H}_2Cl$, 2H), 3.72 (s, $COOC\mathbf{H}_3$, 3H). $^{13}$C NMR (500 MHz, $CDCl_3$) δ ppm: 33.80 ($\mathbf{C}H_2$), 34.98 ($S\mathbf{C}H_2$), 42.88 ($\mathbf{C}H_2$), 52.84 ($O\mathbf{C}H_3$), 170.86 (**C**OOMe).

### 4.2-3. Synthesis of dimethyl 3,6,9,12-tetrathiatetradecanedioate [$C_{12}H_{22}O_4S_4$], *222S4diAcOMe*

***222S4diAcOMe*** was synthesized following a slightly modified literature procedure.[13, 15, 18] ***Intermediate 1*** (5 g, 30 mmol), triethylamine (5 mL, 36 mmol), and 1,2-

ethanedithiol (1.13 mL, 13 mmol) was added into a round bottom flask and refluxed overnight (> 18 hours) at 95 °C under $N_2$. The reaction progress was monitored using silica gel TLC, with dichloromethane as the mobile phase. Upon reaction completion, the reaction mixture was cooled to room temperature and ethyl ether (~ 70 mL) was added to precipitate the trimethylammonium salts. The solution was filtered and the filtrate was concentrated to dryness using a rotary evaporator to afford white solids. The white solids were dissolved in hot ethyl ether and 15 mL of hexane was added to the mixture. The mixture was place in a dry ice bath to precipitate the desired product as white solids. Yield, 2.37 g, 51%. $^1$H NMR (600 MHz, $CDCl_3$) δ ppm: 2.78 – 2.88 (m, SC**H**$_2$CH$_2$, 12H), 3.26 (s, SC**H**$_2$COO, 4H), 3.74 (s, OC**H**$_3$, 6H). $^{13}$C NMR (600 MHz, $CDCl_3$) δ ppm: 31.64 (**C**H$_2$), 32.22 (**C**H$_2$), 32.63 (**C**H$_2$), 33.36 (S**C**H$_2$COOMe), 52.52 (**C**H$_3$), 170.72 (**C**OOMe).

### 4.2-4. Synthesis of 3,6,9,12-tetrathiatetradecanedioic acid [$C_{10}H_{18}O_4S_4$], *222S$_4$diAcOH*

***222S$_4$diAcOH*** was synthesized following a slightly modified literature procedure.[13, 15] ***222S$_4$diAcOMe*** (0.37 g, 1.03 mmol) was dissolved in methanol (15 mL) inside a 35 mL quartz microwave reaction vial. Potassium hydroxide (0.36 g, 6.4 mmol) was dissolved in 1 mL of deionized $H_2O$ and added into the reaction vial. The reaction was heated at 100 °C for 15 minutes using a CEM Discover SP microwave synthesizer in dynamic mode. The mixture was allowed to cool to room temperature to afford a white precipitate. The precipitate was filtered and washed with cold methanol. The precipitate was dissolved in deionized $H_2O$ and acidified by dropwise addition of 3 M HCl to afford the desired product as a white solid. Yield, 0.20 g, 59%. $^1$H NMR (500 MHz, $CD_3CN$) δ ppm: 2.78 – 2.87 (m, SC**H**$_2$CH$_2$, 12H), 3.30 (s, SC**H**$_2$COO, 4H). $^{13}$C NMR (500 MHz,

$CD_3CN$) δ ppm: 31.01 (**C**$H_2$), 31.68 (**C**$H_2$), 32.25 (**C**$H_2$), 32.71 (S**C**$H_2$COOH), 170.99 (**C**OOH). ESI-MS (*m/z*): 329.02 (330.01 calculated for $C_{10}H_{18}O_4S_4[M - H]^-$).

## 4.2-5. Synthesis of [Rh(III)$Cl_2$-*222$S_4$diAcOMe*]X (X = $Cl^-$ or $PF_6^-$)

The Rh(III) complex of ***222$S_4$diAcOMe*** was synthesized following a modified procedure.[12, 15] In summary, $RhCl_3 \cdot xH_2O$ (40 – 15 mg) was dissolved in 1 mL of deionized $H_2O$. ***222$S_4$diAcOMe*** (50 – 13 mg) was dissolved in acetonitrile. The molar ratio between ***222$S_4$diAcOMe*** and $RhCl_3$ was 1:1.2. The $RhCl_3$ solution and the ***222$S_4$diAcOMe*** solution were combined into a 10 mL a quartz microwave reaction vial and the mixture was heated at 100 °C for at least 15 minutes using a CEM Discover SP microwave synthesizer in dynamic mode. Several reaction conditions, as indicated in **Scheme 4-1**, were investigated to determine the different product species formed. Upon reaction completion, the original color of the reaction solution changed from wine red to bright yellow. The solution was filtered using a 0.2 μm syringe filter. The desired product was obtained as the $Cl^-$ salt by concentrating the filtrate to dryness in a rotary evaporator to afford a yellow solid. The $PF_6^-$ salt was obtained by adding 1 mL of a 0.1 g/mL aqueous solution of $NH_4PF_6$ and additional 2 mL deionized $H_2O$ to the filtrate to afford a yellow precipitate. The solution was centrifuged and the supernatant was removed. The precipitate was washed twice with cold ethanol and then dissolved in acetonitrile. The solution was concentrated to dryness in a rotary evaporator to afford the desired product as a yellow solid. The identity and purity of the product was analyzed using NMR, HPLC and ESI-MS.

$RhCl_3$ + $222S_4diAcOMe$ $\xrightarrow[\text{microwave, 100 °C, 10 min}]{\text{ACN (0.5 mL), } H_2O \text{ (1.5 mL)}}$ $[RhCl_2\text{-}222S_4diAcOMe]Cl$ …. **(1)**

$RhCl_3$ + $222S_4diAcOMe$ $\xrightarrow[\text{microwave, 100 °C, 5 min}]{\text{ACN (0.5 mL), } H_2O \text{ (1.5 mL)}}$ $[RhCl_2\text{-}222S_4diAcOMe]Cl$ …. **(2)**

$RhCl_3$ + $222S_4diAcOMe$ $\xrightarrow[\text{microwave, 80 °C, 10 min}]{\text{ACN (0.5 mL), } H_2O \text{ (1.5 mL)}}$ $[RhCl_2\text{-}222S_4diAcOMe]Cl$ …. **(3)**

$RhCl_3$ + $222S_4diAcOMe$ $\xrightarrow[\text{microwave, 60 °C, 10 min}]{\text{ACN (0.5 mL), } H_2O \text{ (1.5 mL)}}$ $[RhCl_2\text{-}222S_4diAcOMe]Cl$ …. **(4)**

$RhCl_3$ + $222S_4diAcOMe$ $\xrightarrow[\text{microwave, 100 °C, 10 min}]{\text{EtOH (1 mL), } H_2O \text{ (1 mL)}}$ $[RhCl_2\text{-}222S_4diAcOMe]Cl$ …. **(5)**

$RhCl_3$ + $222S_4diAcOMe$ $\xrightarrow[\text{microwave, 100 °C, 15 min}]{\text{ACN (0.5 mL) , EtOH (0.5 mL), } H_2O \text{ (1 mL)}}$ $[RhCl_2\text{-}222S_4diAcOMe]Cl$ …. **(6)**

$RhCl_3$ + $222S_4diAcOMe$ $\xrightarrow[\text{microwave, 100 °C, 10 min}]{\text{ACN (0.5 mL), } H_2O \text{ (1 mL), 0.5M HCl (1 mL)}}$ $[RhCl_2\text{-}222S_4diAcOMe]Cl$ …. **(7)**

$RhCl_3$ + $222S_4diAcOMe$ $\xrightarrow[\text{microwave, 100 °C, 15 min}]{\text{ACN (0.5 mL), } H_2O \text{ (1 mL), sat. NaCl (0.5 mL)}}$ $[RhCl_2\text{-}222S_4diAcOMe]Cl$ …. **(8)**

$RhCl_3$ + $222S_4diAcOMe$ $\xrightarrow[\text{microwave, 100 °C, 10 min}]{\text{ACN (0.5 mL), } H_2O \text{ (2 mL), } SnCl_2 \text{ (7.8 mg)}}$ $[RhCl_2\text{-}222S_4diAcOMe]Cl$ …. **(9)**

**Scheme 4-1.** Reaction conditions for the synthesis of [$RhCl_2$-***222S$_4$diAcOMe***]Cl

## 4.2-6. Synthesis of [Rh(III)$Cl_2$-*222S$_4$diAcOH*]Cl

The Rh(III) complex of ***222S$_4$diAcOH*** was synthesized following a modified procedure.[12-13, 15] In summary, $RhCl_3{\cdot}xH_2O$ (25 – 15 mg) was dissolved in 1 mL of deionized $H_2O$. ***222S$_4$diAcOH*** (35 – 13 mg) was dissolved in acetonitrile or deionized $H_2O$. The molar ratio between ***222S$_4$diAcOH*** and $RhCl_3$ was 1:1.2. The $RhCl_3$ solution and the ***222S$_4$diAcOH*** solution were combined into a 10 mL a quartz microwave reaction vial and the mixture was heated at 90 °C for 10 minutes using a CEM Discover SP microwave synthesizer in dynamic mode. Several reaction conditions, as indicated in **Scheme 4-2**, were investigated to determine the different product species formed. Upon reaction completion, the original color of the reaction solution changed from wine red to bright yellow. The solution was filtered using a 0.2 μm syringe filter and subsequently evaporated

to dryness to obtain a yellow solid. The identity and purity of the product was analyzed using HPLC and ESI-MS.

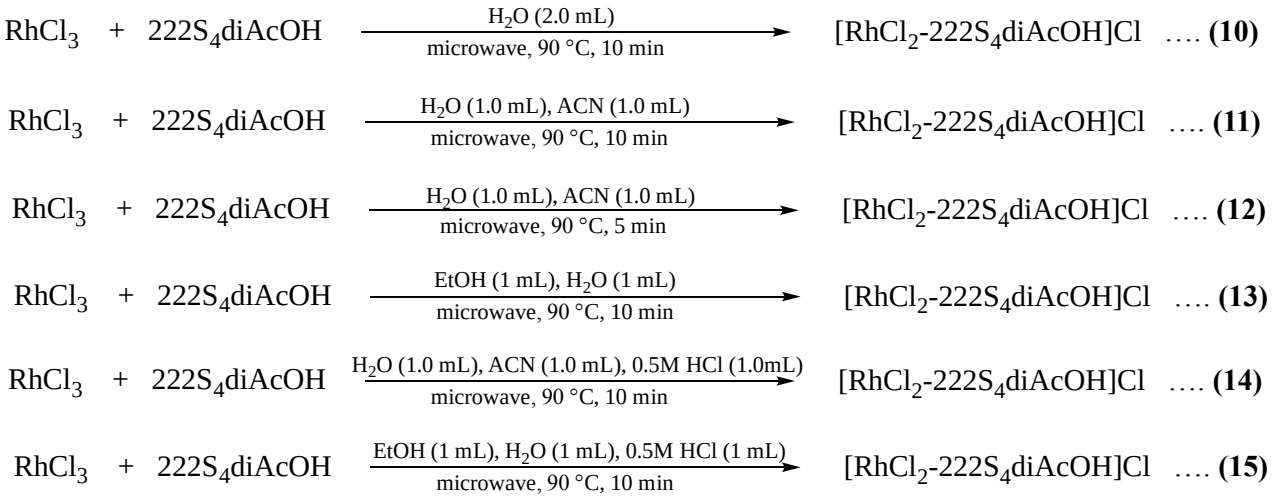


**Scheme 4-2.** Reaction conditions investigated for the synthesis of [$RhCl_2$-222$S_4$diAcOH]Cl

## 4.2-7. Synthesis of [Rh(III)$Cl_2$-*16$S_4$diol*]Cl

The Rh(III) complex of ***16$S_4$diol*** was synthesized following a modified procedure described by Venkatesh et al.[3] In summary, $RhCl_3 \cdot xH_2O$ (30 – 5 mg) was dissolved in 1 mL of deionized $H_2O$. ***16$S_4$diol*** (50 – 8 mg) was dissolved in either ethanol or acetonitrile. The molar ratio between ***16$S_4$diol*** and $RhCl_3$ was 1:1.2. The $RhCl_3$ solution and the ***16$S_4$diol*** solution were combined into a 10 mL a quartz microwave reaction vial and the mixture was heated using a CEM Discover SP microwave synthesizer in dynamic mode. The color of the reaction solution changed from wine red to bright yellow. A comprehensive detail of the various reaction conditions investigated is listed in **Scheme 4-3**. Upon reaction completion, the reaction solution was filtered using a 0.2 μm syringe filter. The identity and purity of the product was analyzed using HPLC and ESI-MS.

$RhCl_3$ + $16S_4$diol $\xrightarrow[\text{microwave, 90 °C, 10 min}]{\text{ACN (0.5 mL), } H_2O \text{ (1.5 mL)}}$ [$RhCl_2$-$16S_4$diol]Cl …. **(16)**

$RhCl_3$ + $16S_4$diol $\xrightarrow[\text{microwave, 90 °C, 10 min}]{\text{EtOH (0.5 mL), } H_2O \text{ (1.5 mL)}}$ [$RhCl_2$-$16S_4$diol]Cl …. **(17)**

$RhCl_3$ + $16S_4$diol $\xrightarrow[\text{microwave, 110 °C, 5 min}]{\text{ACN (1 mL), } H_2O \text{ (1 mL)}}$ [$RhCl_2$-$16S_4$diol]Cl …. **(18)**

$RhCl_3$ + $16S_4$diol $\xrightarrow[\text{microwave, 110 °C, 5 min}]{\text{EtOH (1 mL), } H_2O \text{ (1 mL)}}$ [$RhCl_2$-$16S_4$diol]Cl …. **(19)**

$RhCl_3$ + $16S_4$diol $\xrightarrow[\text{microwave, 110 °C, 5 min}]{\text{ACN (0.5 mL), } H_2O \text{ (1 mL), } SnCl_2 \text{ (5.6 mg)}}$ [$RhCl_2$-$16S_4$diol]Cl …. **(20)**

$RhCl_3$ + $16S_4$diol $\xrightarrow[\text{microwave, 110 °C, 5 min}]{\text{ACN (1 mL), 0.5M HCl (1 mL)}}$ [$RhCl_2$-$16S_4$diol]Cl …. **(21)**

**Scheme 4-3.** Reaction conditions investigated for the synthesis of [$RhCl_2$-$16S_4$diol]Cl

## 4.2-8. Production of $^{105}$Rh from Recycled $^{104}$Ru Metal Target

Ruthenium-104 trapped in 3 M HCl as ruthenate ([$^{104}$Ru]$RuO_4^{2-}$) from previous $^{105}$Rh productions at MURR over a period of more than two decades was recovered and recycled by Phelps and colleagues.[4] The target recycling process involved concentrating the 3 M HCl solutions to dryness to yield hydrated ruthenium chloride ([$^{104}$Ru]$RuCl_3 \cdot xH_2O$), dehydrating [$^{104}$Ru]$RuCl_3 \cdot xH_2O$ with Ar at 525 °C, and subsequently reducing to $^{104}$Ru metal with $H_2$ at 800 °C.[4]

Three separate neutron irradiations of the recycled $^{104}$Ru metal and one irradiation of new $^{104}$Ru metal were performed at MURR as summarized in **Table 4-1**. Briefly, $^{104}$Ru metal target was encapsulated in a 4 x 6 mm quartz vial and irradiated for ~90 hours with thermal neutrons (~9.78 x $10^{13}$ n/cm$^2$/s) at the MURR neutron reflector position (G1 or H1). A 24-hour wait period was allowed to ensure the decay of $^{105}$Ru into $^{105}$Rh. After the wait period, the total activity of the irradiated target in the quartz vial was measured. Subsequently, the quartz vial was scored and broken, and the irradiated target was

transferred into a 30 mL glass midget impinger containing 2 mL of 2 M NaOH. The impinger was connected to one 3 M HCl (500 mL) and two 5 M NaOH (500 mL) traps using teflon-lined tubing as shown in **Figure 4-1**.

Rhodium-105 was separated from the bulk $^{104}$Ru metal target by oxidation of $^{104}$Ru metal to [$^{104}$Ru]$RuO_4$ using hypochlorite generated *in situ*, and subsequent distillation of [$^{104}$Ru]$RuO_4$ at elevated temperatures. To accomplish this, $Cl_2$ at ~ 30 mL/min (50 seconds for production 1 and 2, 2 minutes for production 3, and 5 minutes for production 4) was bubbled into the impinger containing the irradiated $^{104}$Ru metal target in 2 mL of 2 M NaOH. The impinger was heated at 40 °C for 1 hour under constant airflow (~30 mL/min). Additional $Cl_2$ at ~ 30 mL/min (12 minutes for productions 1 and 2, and 25 minutes for productions 3 and 4) was bubbled into the impinger followed by heating at 90 °C for 1 hour under constant airflow (~30 mL/min). The target solution was filtered through a 0.8 μm syringe filter into a clean midget impinger. The solution was heated for an additional 30 minutes at 90 °C under constant airflow (~30 mL/min). Finally, 0.25 mL of 1 M HCl was added to the solution and heated for 30 minutes at 90 °C without airflow. The radionuclidic purity of the final $^{105}$Rh stock solution was evaluated using an HPGe gamma spectrometer. Additionally, a 200 μL aliquot of the $^{105}$Rh stock solution was analyzed by inductively coupled plasma mass spectrometry (ICP-MS) after decay of $^{105}$Rh.

## 4.2-9. $^{105}$Rh-labeling

[$^{105}$Rh]$RhCl_3$ (22 - 3 mCi / 814 - 111 MBq) in ~ 2 mL 1 M HCl (pH 0.5 – 1) was obtained from MURR. 200 μL of deionized $H_2O$ was added to a 400 μL aliquot of the $^{105}RhCl_3$ stock solution and the pH was carefully adjusted to ~3.5 using 1M NaOH (20 μL) and 0.5M NaOH (20 μL).

The $^{105}$Rh complex of ***222S$_4$diAcOMe*** was synthesized by adding 100 μL (550 – 100 μCi / 20.4 - 3.7 MBq) of the pH-adjusted [$^{105}$Rh]RhCl$_3$ solution to a solution containing 100 μL (10 μg) of a 0.1 mg/mL (0.3 mM) ***222S$_4$diAcOMe*** ligand solution in acetonitrile, 200 μL of $H_2O$ and 100 μL of 50% ACN : $H_2O$. The resultant solution was heated for 1 hour at 90 °C in a water bath. Upon cooling to room temperature, the reaction solution was analyzed using radio-HPLC and TLC.

The $^{105}$Rh complex of ***222S$_4$diAcOH*** was synthesized by adding 100 μL (550 - 100 μCi / 20.4 - 3.7 MBq) of the pH-adjusted [$^{105}$Rh]RhCl$_3$ solution to a solution containing 100 μL (10 μg) of 0.1 mg/mL (0.3 mM) ***222S$_4$diAcOH*** ligand in 50% acetonitrile : $H_2O$, 200 μL of $H_2O$ and 100 μL of 50% ACN : $H_2O$. The resultant solution was heated for 1 hour at 90 °C in a water bath. Upon cooling to room temperature, the reaction solution was analyzed using radio-HPLC and TLC.

The $^{105}$Rh complex of ***16S$_4$-diol*** was synthesized by adding 100 μL (550 - 100 μCi / 20.4 - 3.7 MBq) of the pH-adjusted [$^{105}$Rh]RhCl$_3$ solution to a solution containing 100 μL (10 μg) of 0.1 mg/mL (0.3 mM) 16S$_4$-diol ligand in 50% ethanol : $H_2O$, 200 μL of $H_2O$ and 100 μL of 50% ethanol : $H_2O$. The resultant solution was heated for 1 hour at 90 °C in a water bath. Upon cooling to room temperature, the reaction solution was analyzed using radio-HPLC and TLC.

## 4.2-10. Radiochemical Analyses

The radiochemical purity of the $^{105}$Rh complexes was determined using radio-HPLC and silica gel TLC. The TLC plates for all $^{105}$Rh complexes were developed in three different mobile phases (0.9% saline, acetonitrile and 0.4M $NaBPh_4$ in acetonitrile). Three

different linear gradient systems (***Gradient 1***, ***Gradient 2***, and ***Gradient 3*** described in materials and methods) were used for radio-HPLC analyses.

## 4.3. Results and Discussion

The synthesis of ***222S$_4$diAcOMe*** and ***222S$_4$diAcOH*** was accomplished following modified literature procedures, as shown in **Figure 4-3**.[13, 15] NMR characterization of these tetrathioether ligands is consistent with previously reported data, as shown in **Figure 4-4A through 4-6C**.[13, 15] Additionally, ***222S$_4$diAcOH*** was identified as the $[M-H]^-$ ion [*m/z* = 329.02 (found), 330.01 (calculated)] based on ESI-MS analysis, as shown in **Figure 4-7**. A key detail in the purification of ***Intermediate 1*** is to ensure that the vacuum distillation glassware has no air leaks and that strong vacuum (~ 13 mbar) is constantly applied throughout the distillation process. The vacuum distillation method described here eliminates the need for silica gel column separation, as reported by Dame.[15]

A microwave synthesizer was utilized for the synthesis of all Rh(III) complexes reported in this study. Previously, it was reported that at least a 1 hour reaction time was required for the formation of Rh(III) complexes of both tetrathioether ligands and tetradentate thiamacrocyclic ligands.[3, 12-13] The microwave-assisted synthesis procedure reported in this study significantly reduced the reaction time to 10 minutes or less, while also reducing the formation of unwanted byproducts.

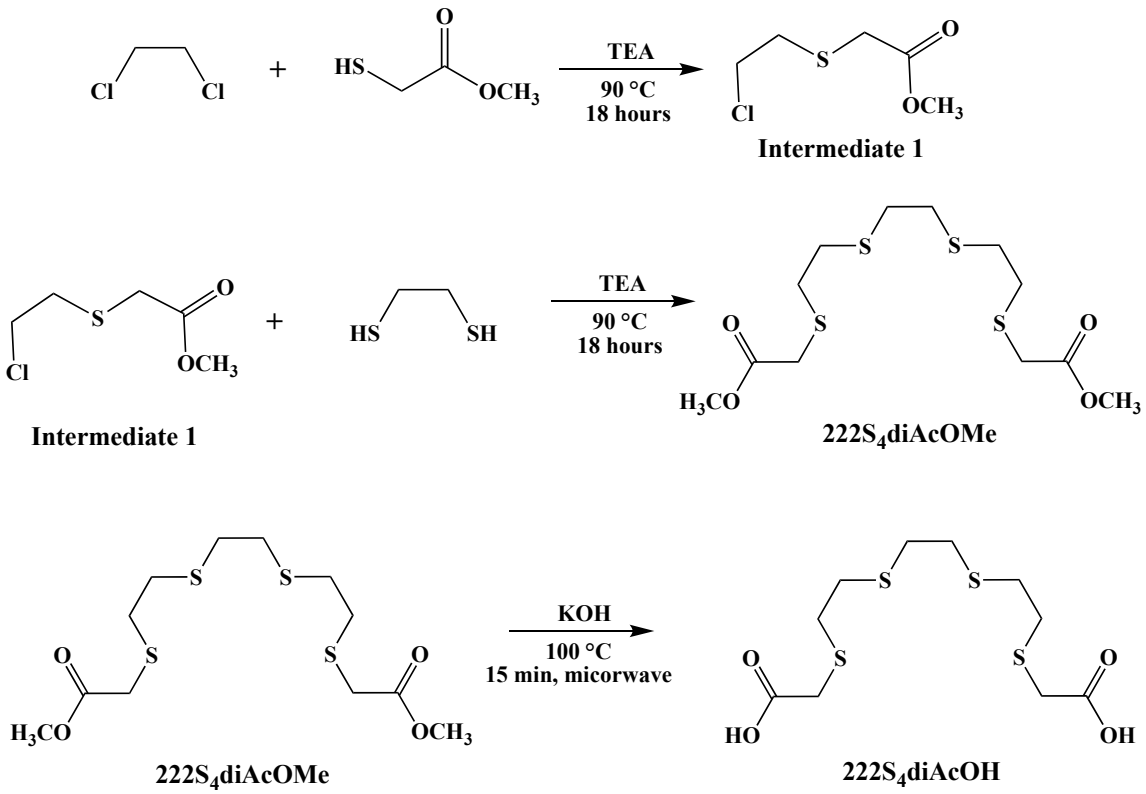


**Figure 4-3.** Synthesis of *222S4diAcOMe* and *222S4diAcOH*

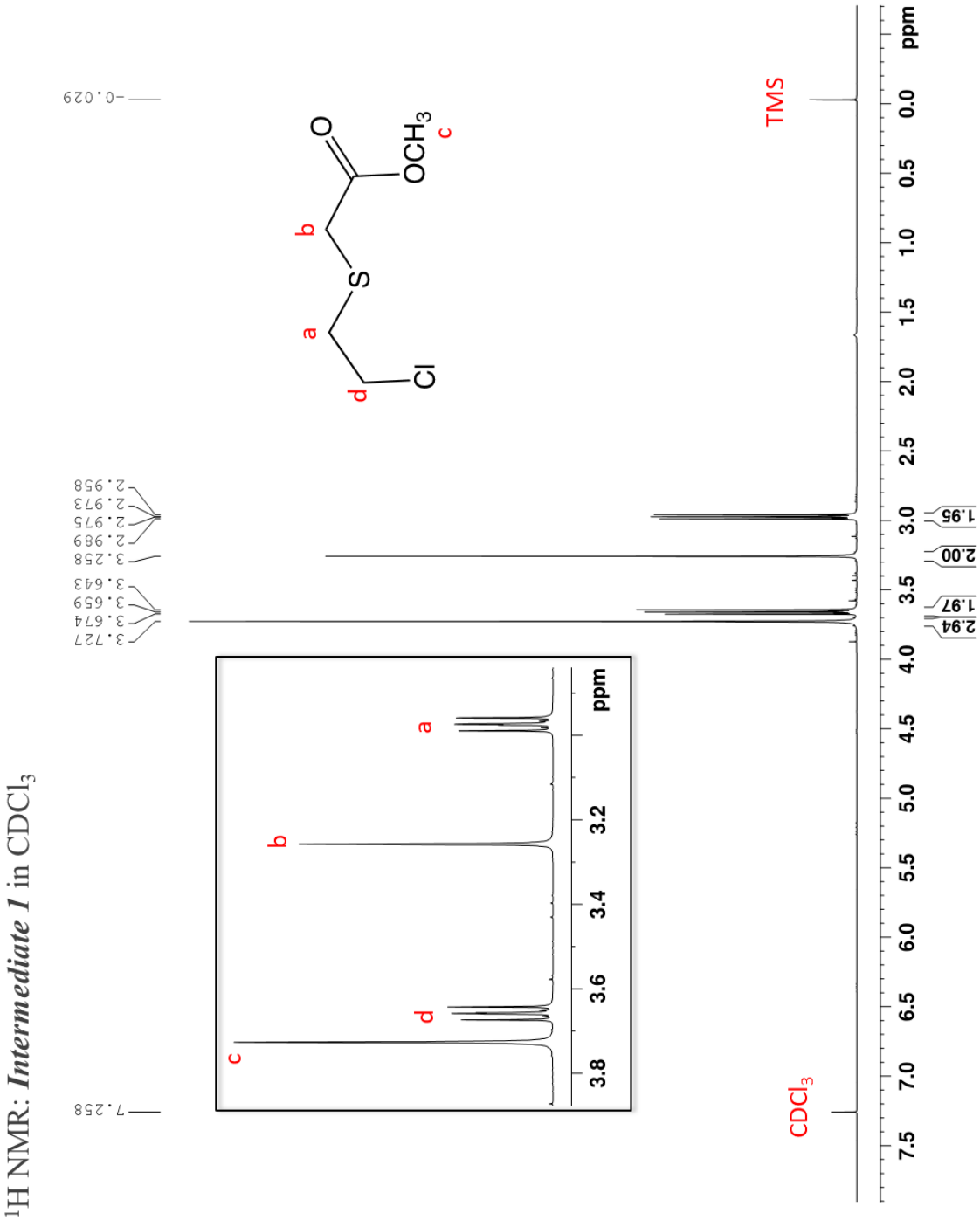


**Figure 4-4A.** $^1$H NMR spectrum of *Intermediate 1*

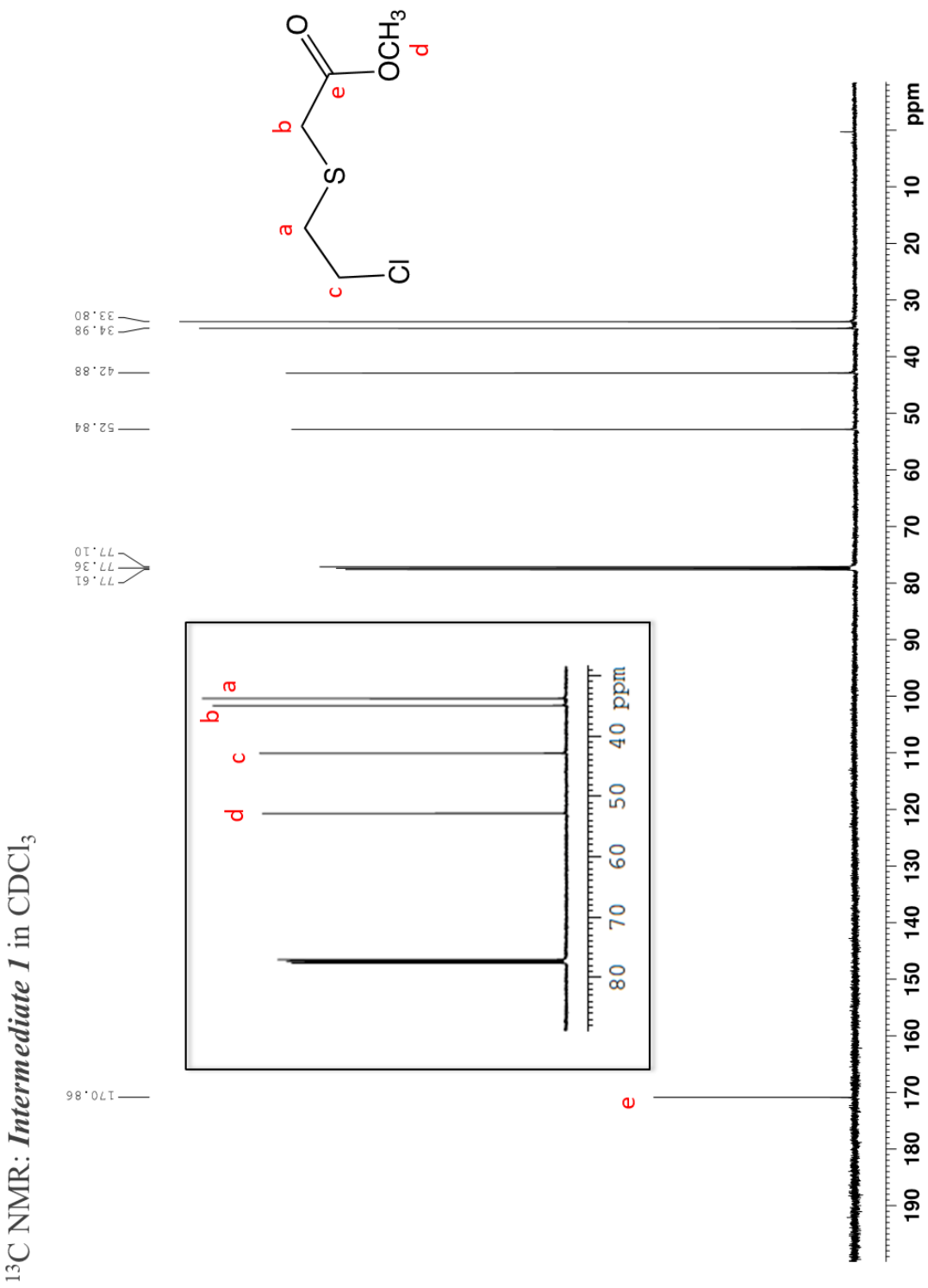


**Figure 4-4B.** $^{13}$C NMR spectrum of *Intermediate 1*

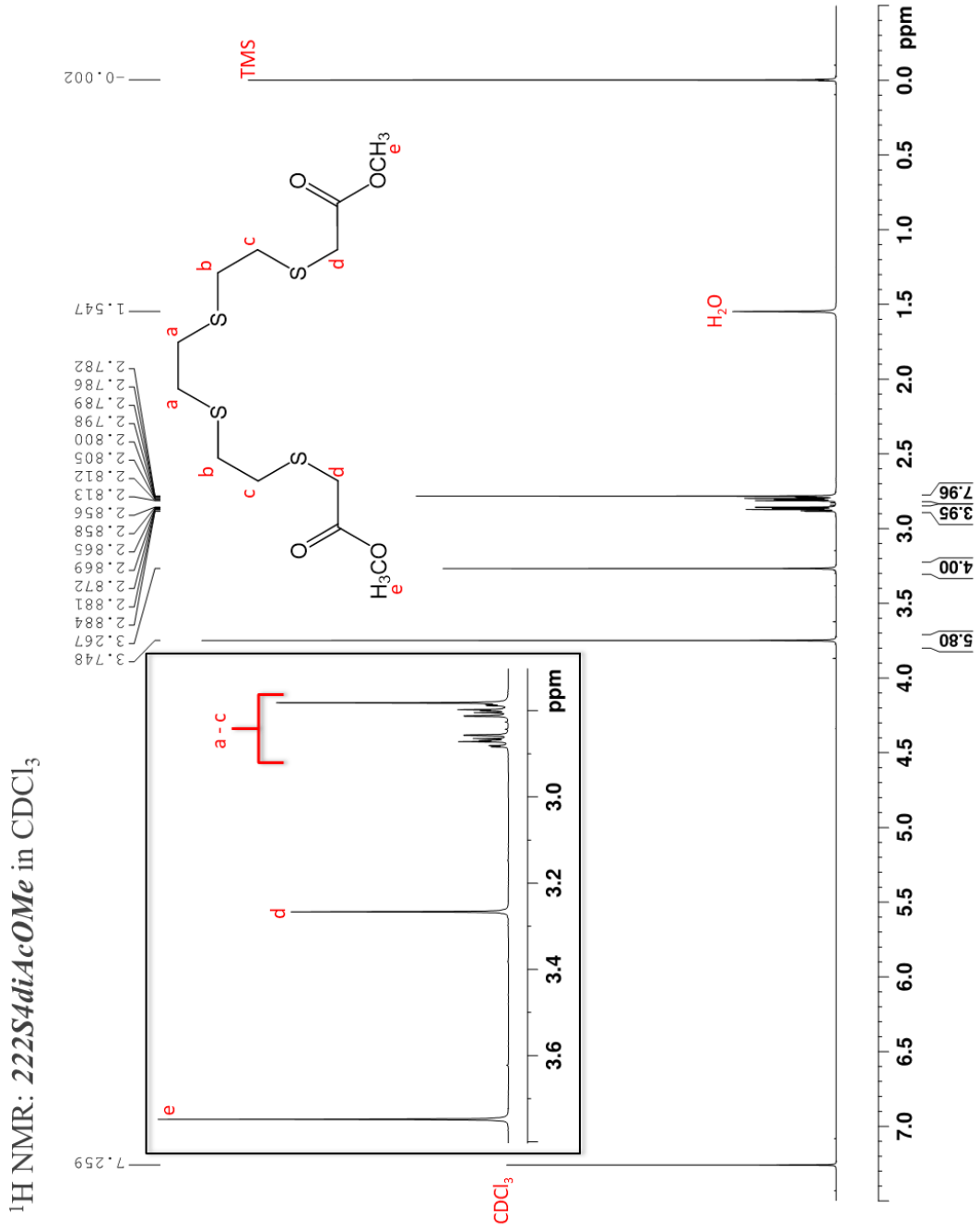


**Figure 4-5A.** $^1$H NMR spectrum of *222S$_4$diAcOMe*

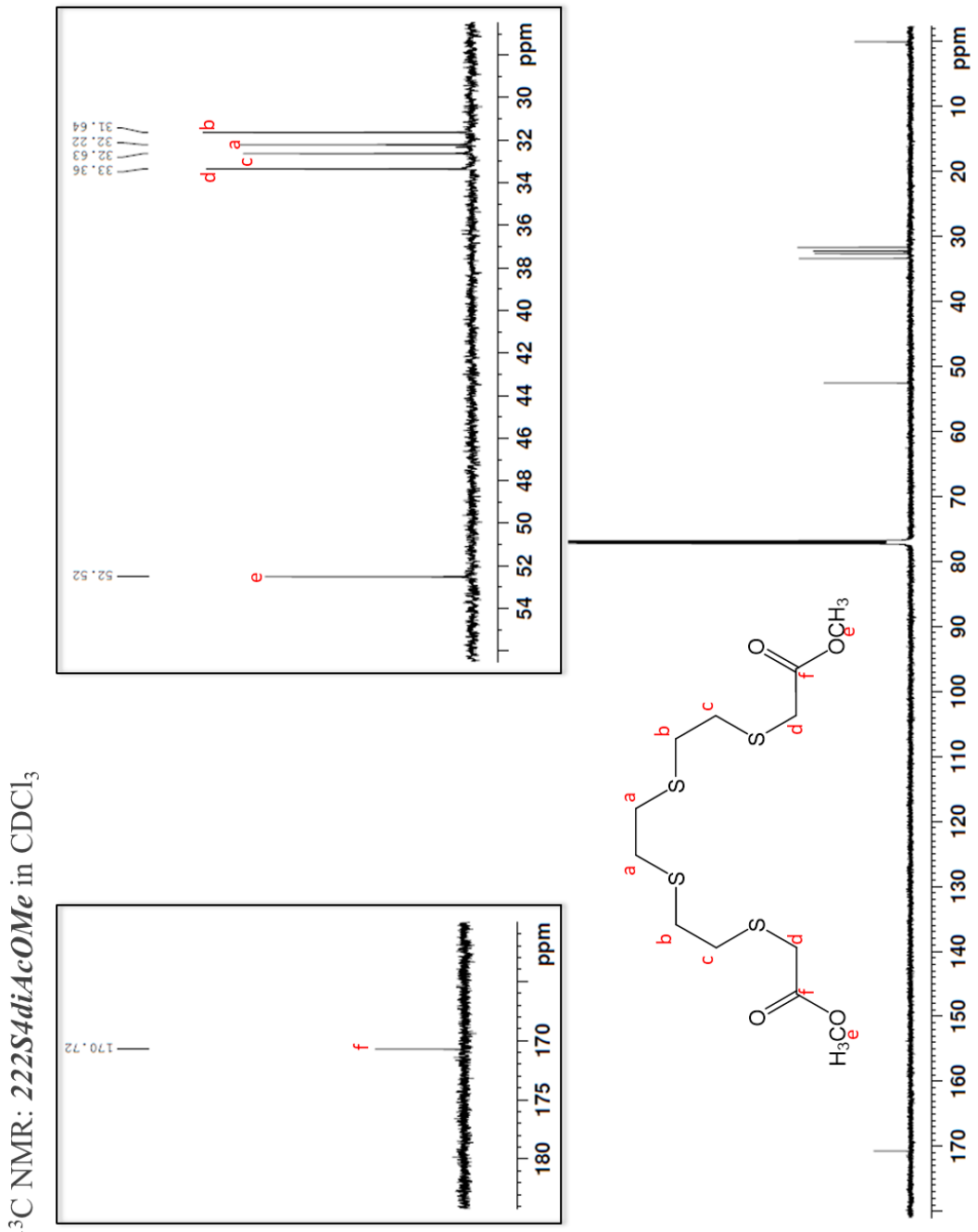


**Figure 4-5B.** $^{13}$C NMR spectrum of *222S$_4$diAcOMe*

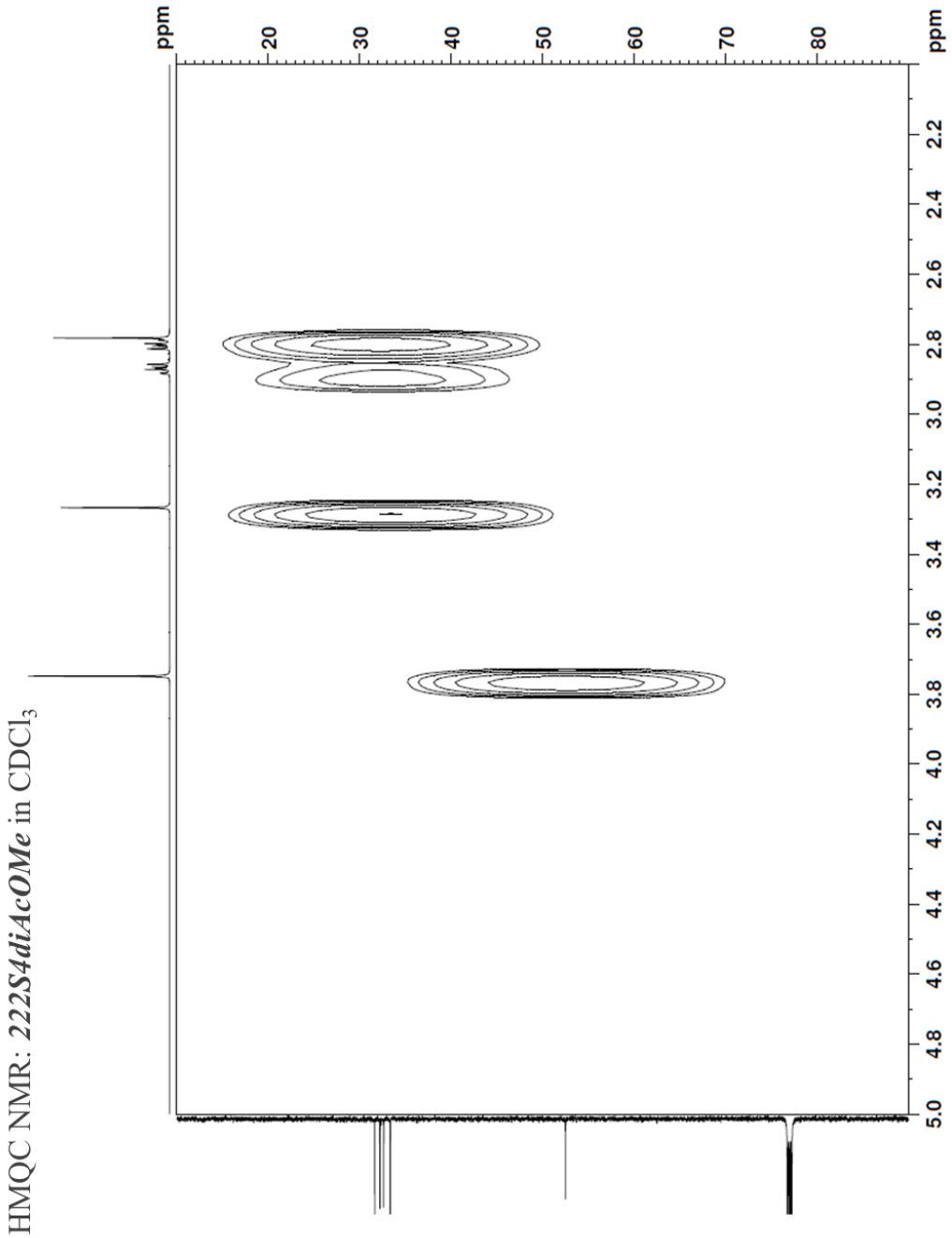


**Figure 4-5C.** HMQC NMR spectrum of *222S$_4$diAcOMe*

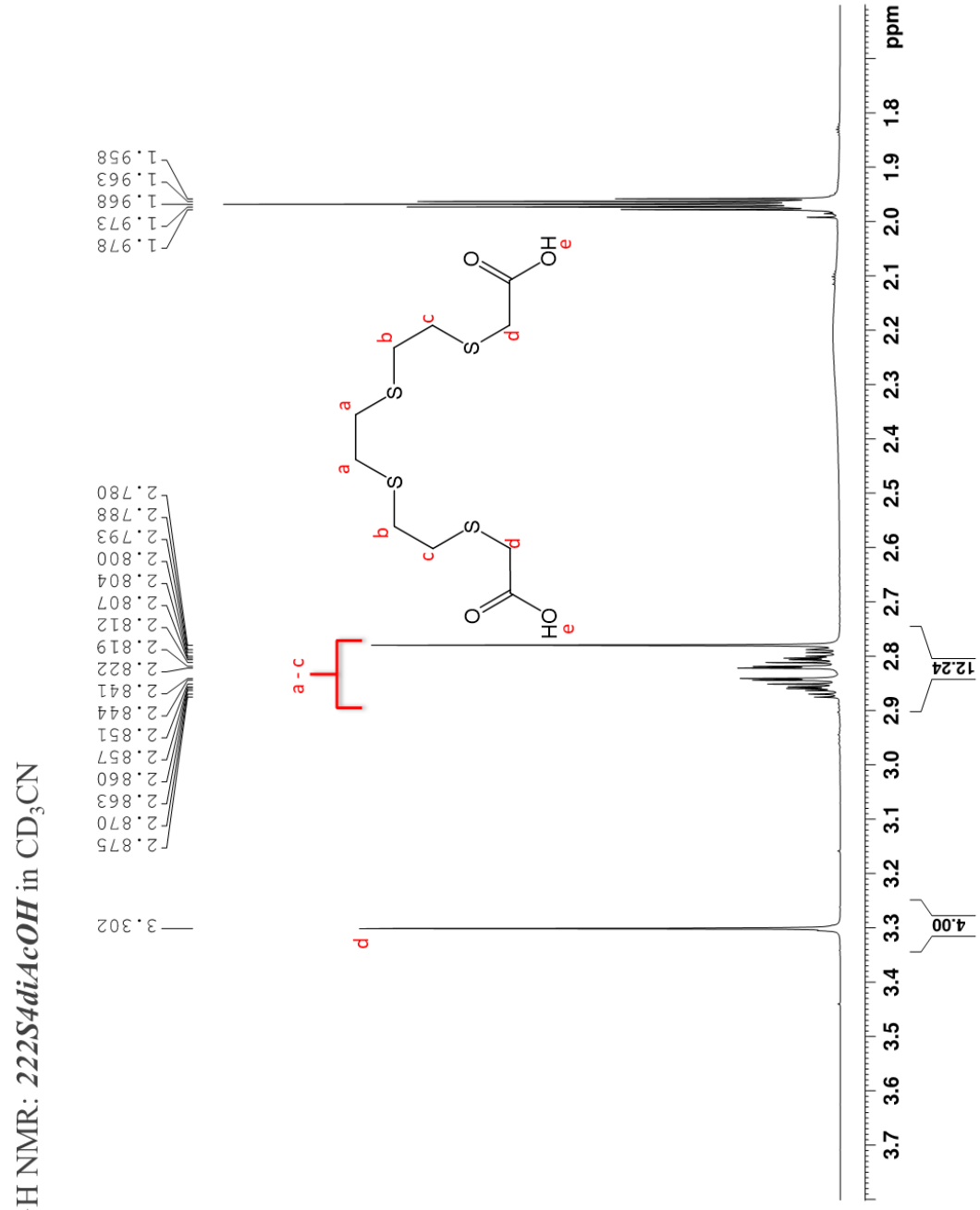


**Figure 4-6A.** $^1$H NMR spectrum of *222S₄diAcOH*

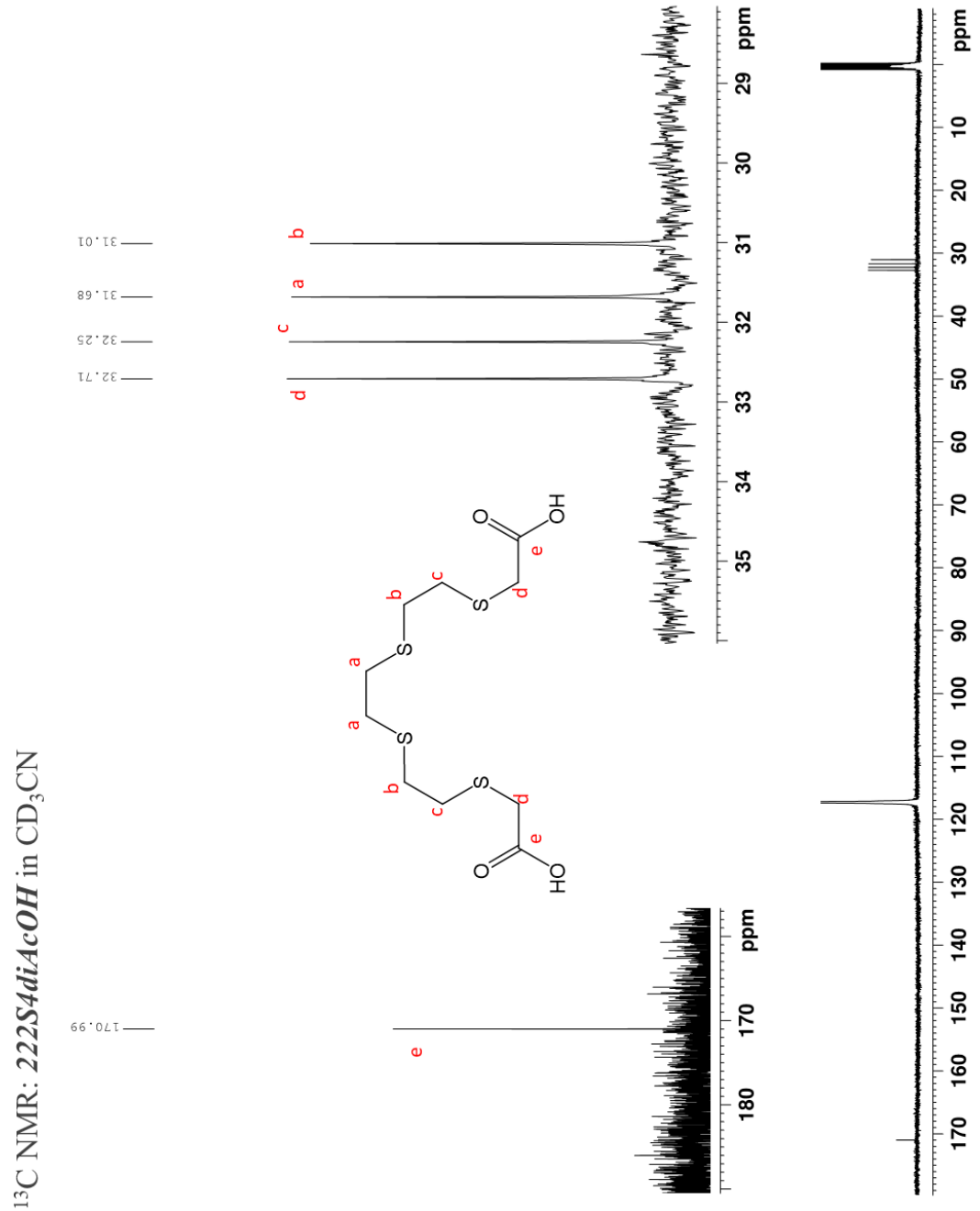


**Figure 4-6B.** $^{13}C$ NMR spectrum of *222S₄diAcOH*

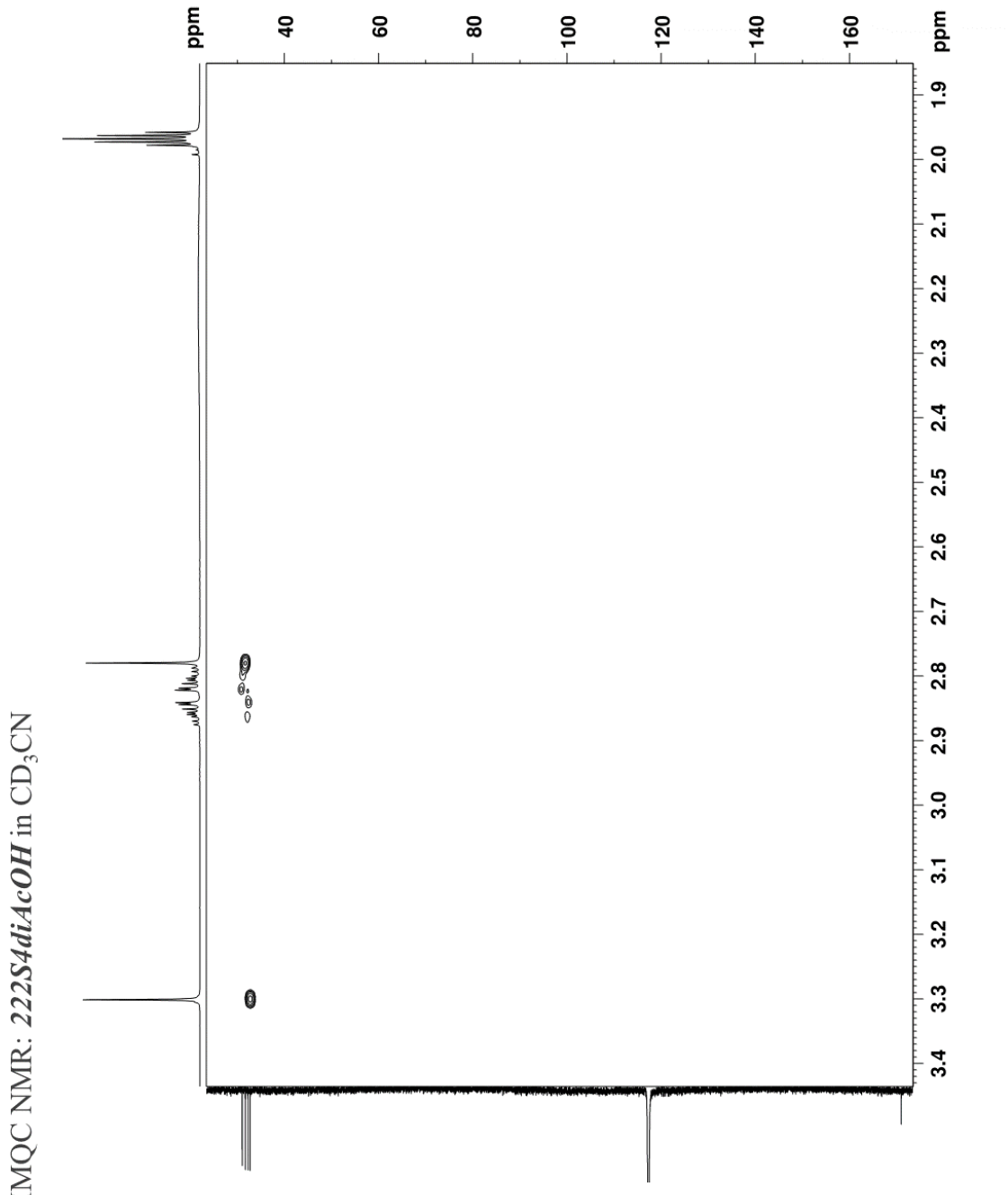


**Figure 4-6C:** HMQC NMR spectrum of *222S$_4$diAcOH*

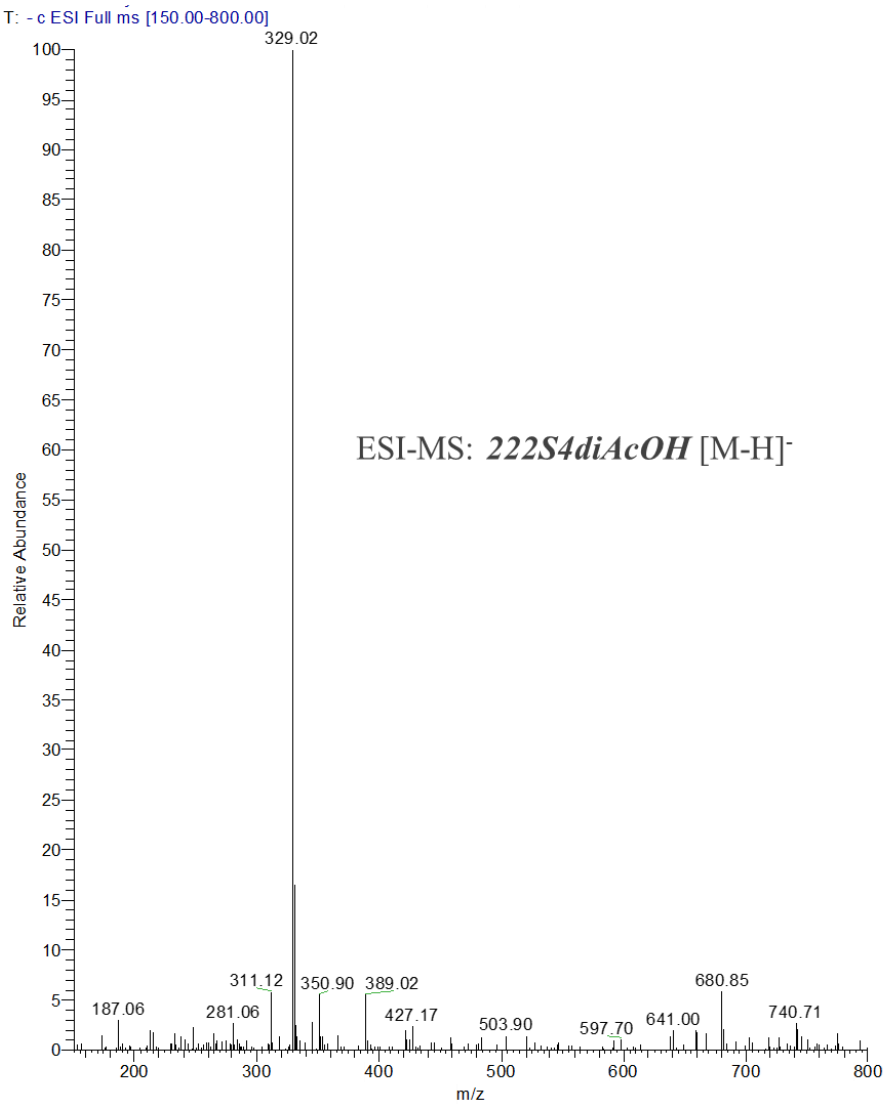


**Figure 4-7.** ESI-MS of *222S$_4$diAcOH*

## 4.3-1. Rh(III) Complexes With 222S$_4$diAcOMe Chelate System

**[Rh(III)Cl$_2$-*222S$_4$diAcOMe*]Cl** was synthesized by reacting $RhCl_3$ with ***222S$_4$diAcOMe*** using a microwave synthesizer. Based on the crystal structures reported by Dame[15] (**Figure 4-2A**) and Goswami et al.[12], we expected the formation of the *cis*-dichloro isomer, where Rh(III) is coordinated to two chlorides and to the four sulfur atoms in the ***222S$_4$diAcOMe*** tetrathioether ligand.

Ten different reaction conditions were investigated as shown in **Scheme 4-1**. Reactions 1 – 4 were performed in acetonitrile and water only. HPLC analysis of these reactions revealed a predominant peak (peak area ~ 88%) at approximately 8.2 minutes using ***Gradient 1*** (10% solvent B:A increased to 80% solvent B:A over 18 minutes, followed by an additional 1 minute at 80% solvent B:A, then decreased to 10% solvent B:A over 1 minute), as shown in **Figures S4-1A to S4-1I**. ESI-MS analysis of this peak indicates the presence of a strong signal for the $M^+$ ion of *cis*-**[Rh(III)$Cl_2$-*222$S_4$diAcOMe*]**$^+$ [*m/z* = 530.85 (found), 530.88 (calculated for $C_{12}H_{22}Cl_2O_4RhS_4^+$)], as shown in **Figure 4-8**. There was no significant difference in the HPLC profile between reactions 1 – 4 (no ethanol or $SnCl_2$ used) and reactions 5 - 6 (ethanol used) or reaction 9 ($SnCl_2$ used). To the best of our knowledge, this is the first report of a Rh(III) tetrathioether complex synthesized without using ethanol or $SnCl_2$ for the catalytic reduction of $Rh^{+3}$ to $Rh^{+1}$, as previously reported.[3, 12-13, 15-16, 18-19]

Two other minor product species were identified in reactions 1 – 4; one with a retention time of approximately 6.5 minutes, and the other with a retention time of approximately 4.4 minutes, as shown in **Figures S4-1A to S4-1I**. ESI-MS analysis revealed that the peak at approximately 6.5 minutes is consistent with the species where one of the pendant methyl acetate groups has been hydrolyzed to a carboxylic acid group [*m/z* = 516.90 (found), 516.87 (calculated for $C_{11}H_{20}Cl_2O_4RhS_4^+$)], as shown in **Figure 4-9**. The *m/z* of the peak at approximately 4.4 minutes is consistent with the species where one of the pendant methyl acetate groups has been hydrolyzed to a carboxylic acid and is directly coordinated to the Rh(III) center along with one chloride atom [*m/z* = 480.93 (found), 480.89 (calculated for $C_{11}H_{19}ClO_4RhS_4^+$)], as shown in **Figure 4-10**.

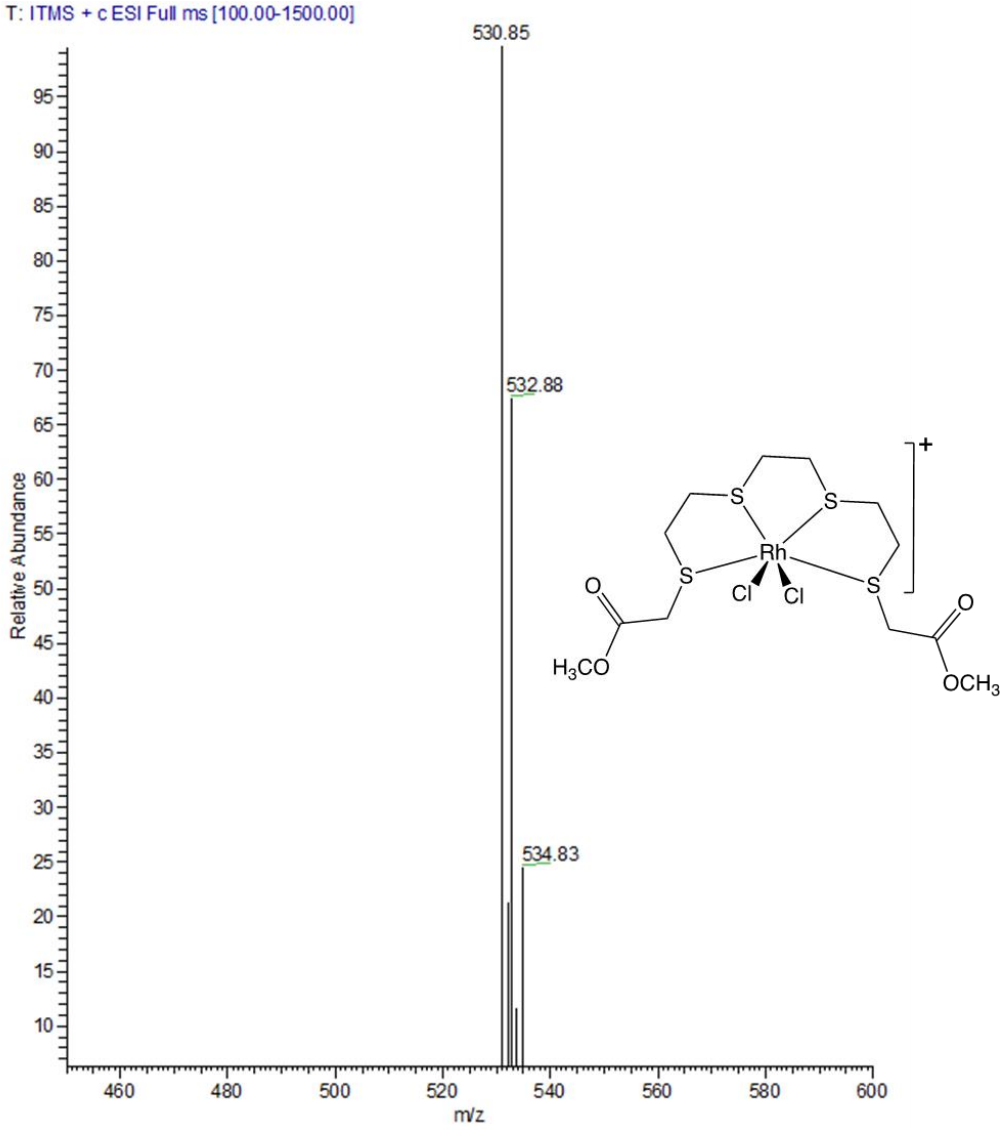


**Figure 4-8.** ESI-MS of *cis*-**[Rh(III)Cl$_2$-*222S$_4$diAcOMe*]$^+$**

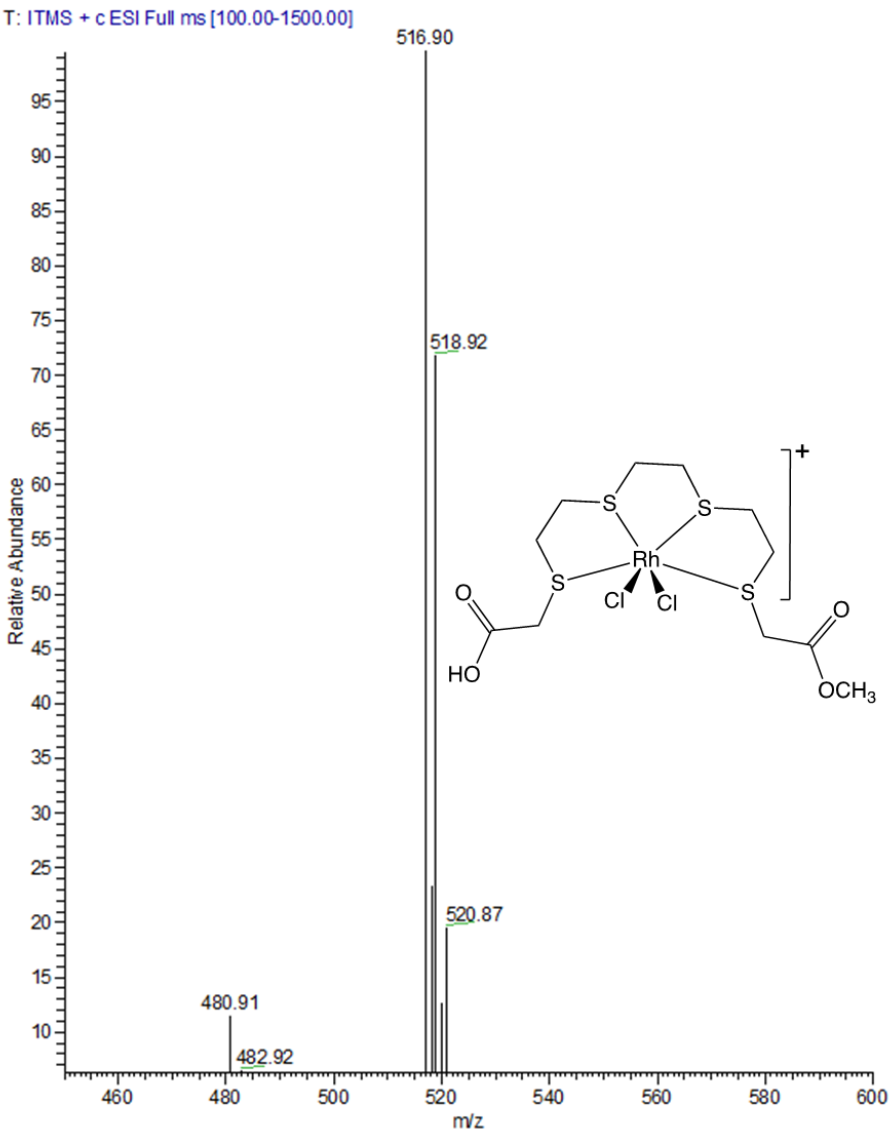


**Figure 4-9.** ESI-MS of $C_{11}H_{20}Cl_2O_4RhS_4^+$

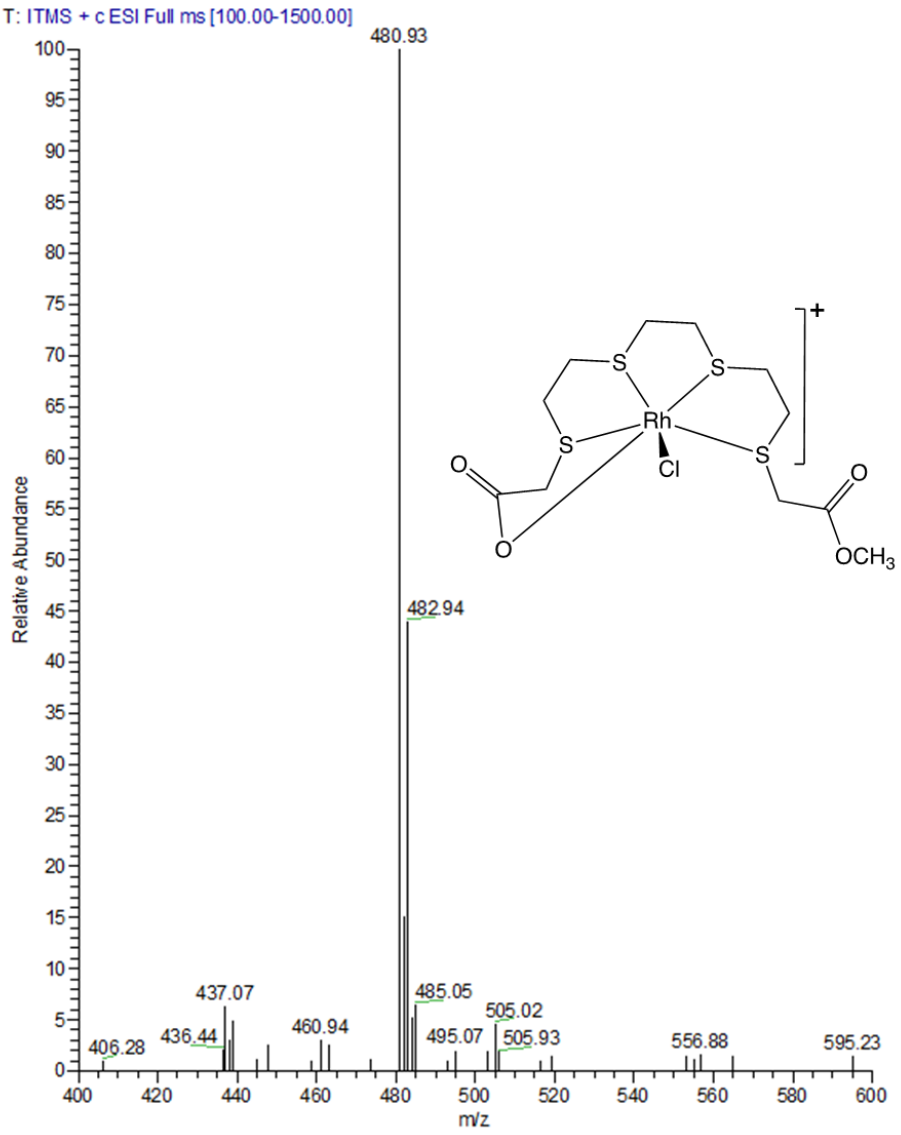


**Figure 4-10.** ESI-MS of $C_{11}H_{19}ClO_4RhS_4^+$

Reaction 7 was performed in acetonitrile and water, with the addition of 1 mL 0.5 M HCl. In addition to the peaks at 8.2 minutes, 6.5 minutes, and 4.4 minutes described above, a new and intense peak (peak area ~ 46%) was observed at 2.2 minutes (**Figure S4-1G)**. ESI-MS analysis revealed that this new peak is consistent with the species where both of the pendant methyl acetate groups have been hydrolyzed to carboxylic acid groups and are both directly coordinated to the Rh(III) center [*m/z* = 430.94 (found), 430.90 (calculated

for $C_{10}H_{16}O_4RhS_4^+$)], as shown in **Figure 4-11**. This reaction condition is more representative of the reaction condition at the radiotracer scale because $^{105}RhCl_3$ is obtained in a 1 M HCl solution; hence, it is likely the acid hydrolysis of the pendant methyl acetate groups in ***222S4diAcOMe*** will occur at the radiotracer scale.

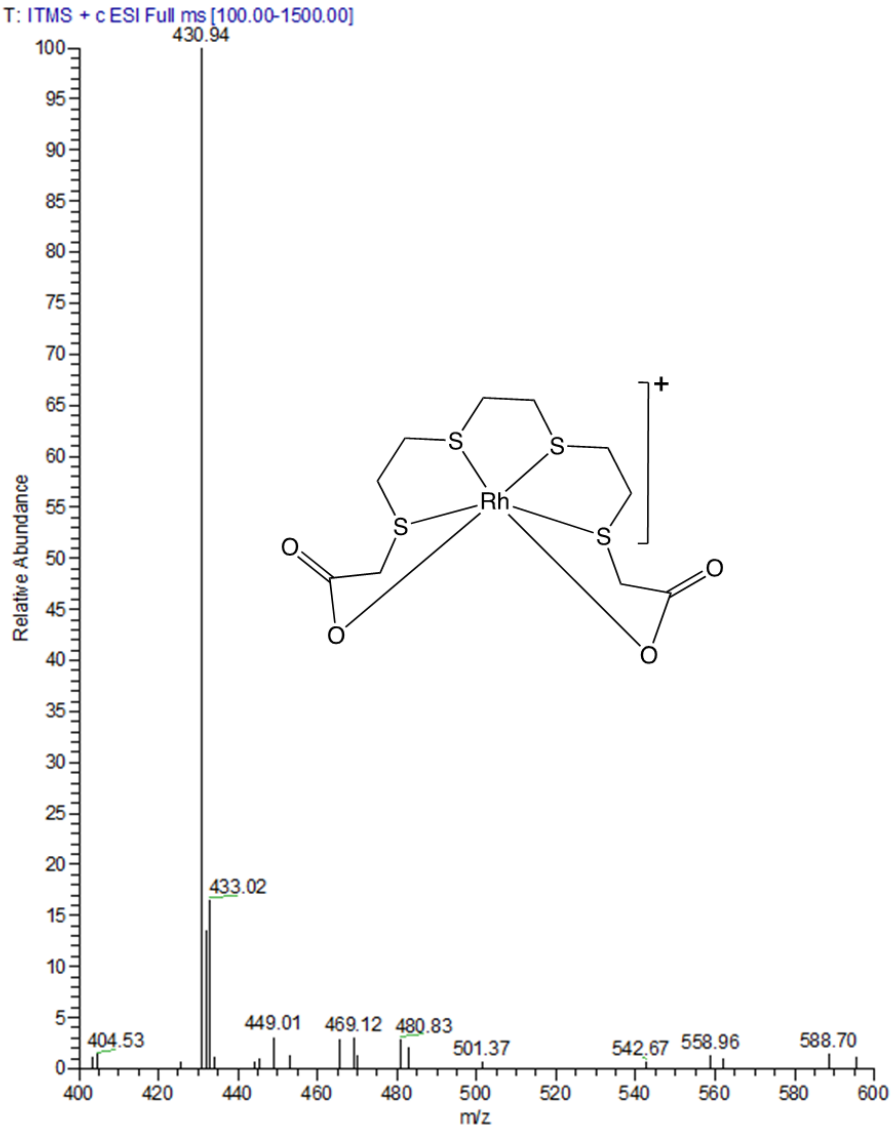


**Figure 4-11.** ESI-MS of $C_{10}H_{16}O_4RhS_4^+$

$^{13}C$ NMR of **[Rh(III)Cl$_2$-*222S$_4$diAcOMe*]Cl** (**Figure 4-12A**) shows four $CH_2$ signals (36.85 – 41. 52 ppm) and one $CH_3$ signal (53.90 ppm), which is indicative of the

presence of a single isomer. If more than one isomer were present, additional $CH_2$ signals would have been observed, similar to data reported by Goswami et al.[12] The $^1H$ NMR of **[Rh(III)Cl$_2$-*222S$_4$diAcOMe*]Cl** (**Figure 4-12B**) is not as straightforward to interpret as the $^{13}C$ NMR. Each sulfur atom on the ***222S$_4$diAcOMe*** ligand becomes a chiral center upon complexation with Rh(III); hence, different enantiomeric isomers are possible, which explains the complexity of the $^1H$ NMR. However, two-dimensional $^{13}C$ - $^1H$ heteronuclear multiple-quantum correlation (HMQC) NMR allowed the assignment of the multiple $^1H$ peaks between 2.5 – 4.5 ppm to their corresponding $^{13}C$ peak, as shown in **Figure 4-12C**.

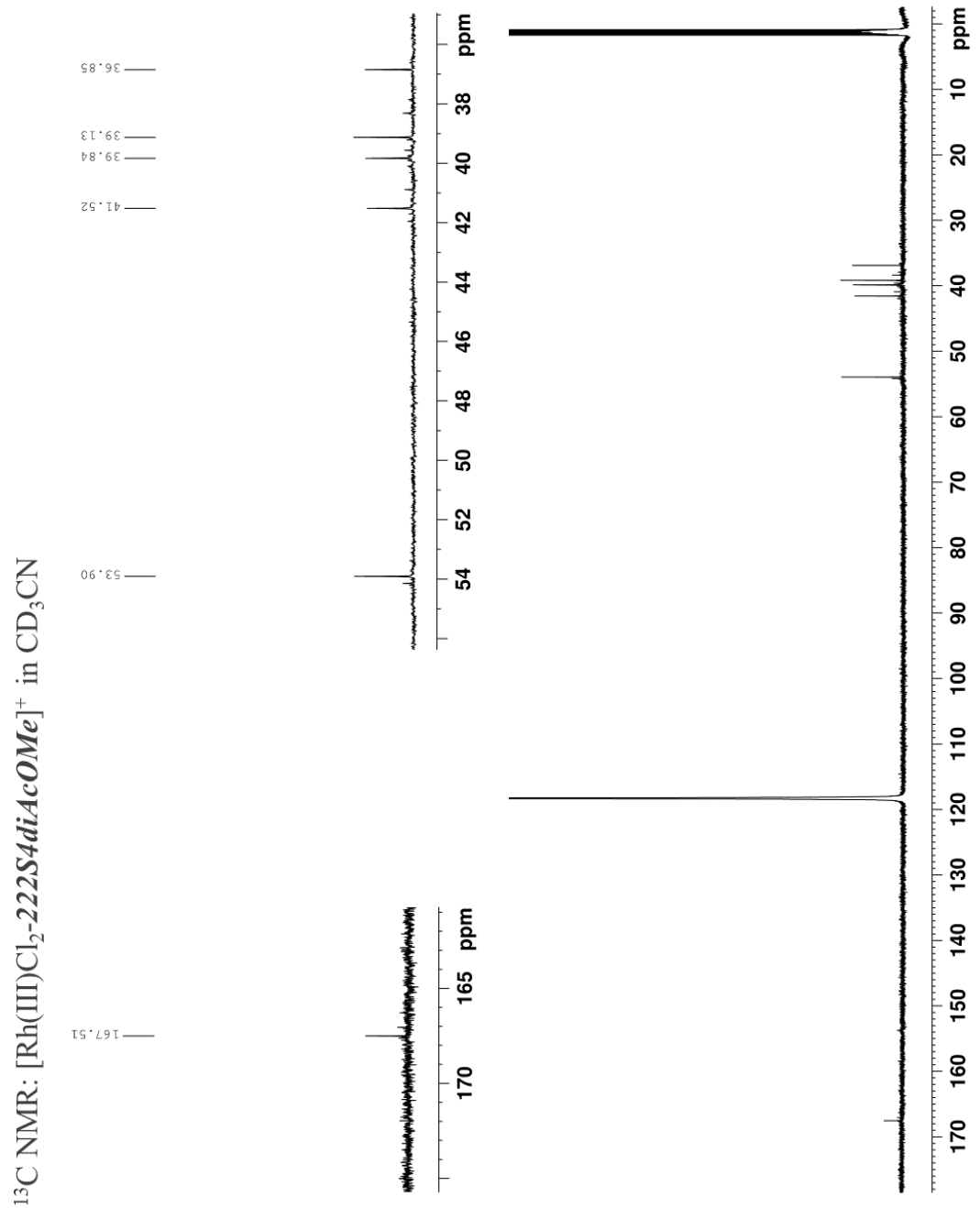


**Figure 4-12A.** $^{13}$C NMR spectrum of [Rh(III)Cl$_2$-*222S$_4$diAcOMe*]Cl

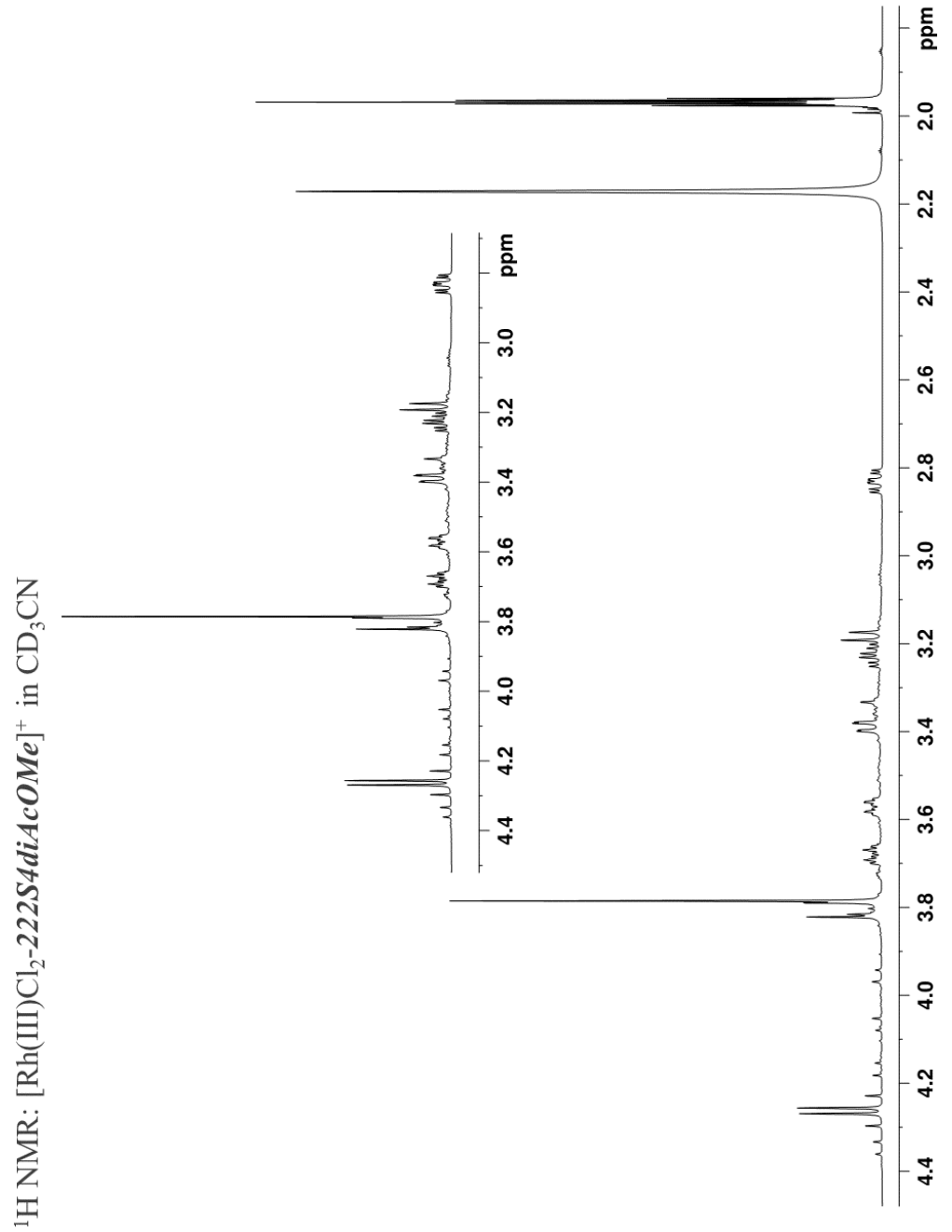


**Figure 4-12B.** $^1$H NMR spectrum of [Rh(III)Cl$_2$-*222S$_4$diAcOMe*]Cl

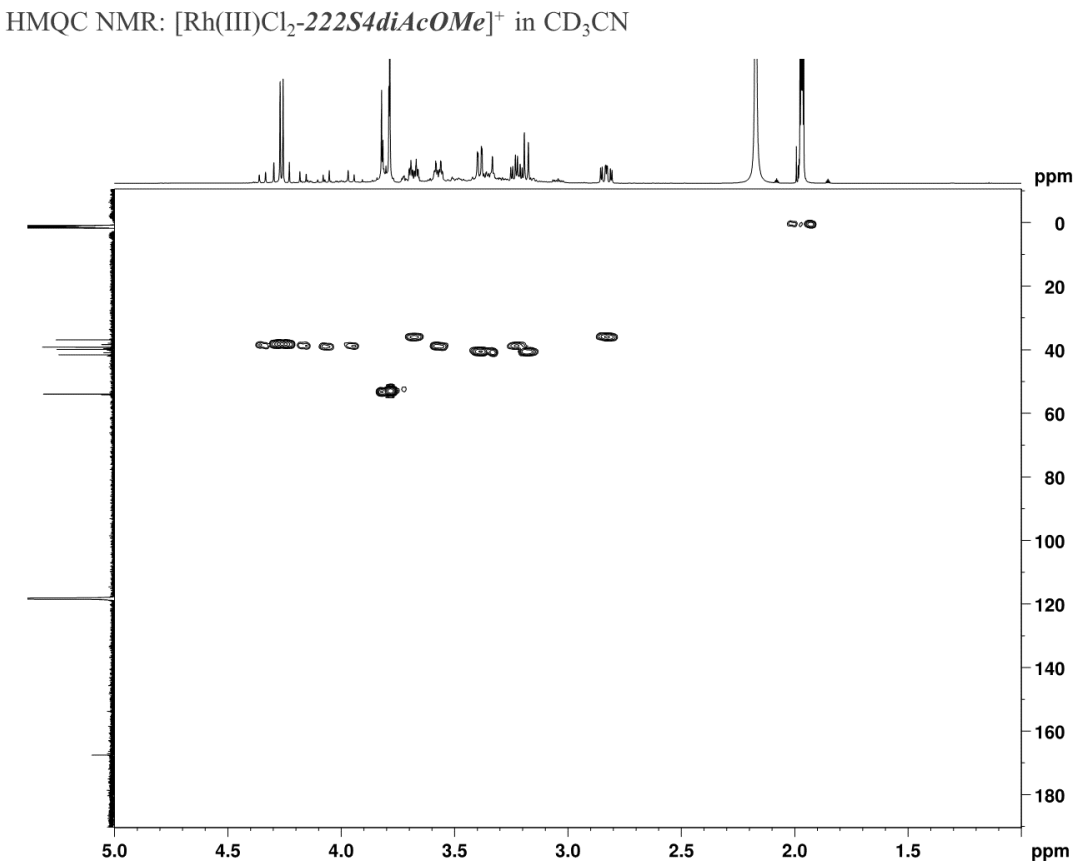


**Figure 4-12C.** HMQC NMR spectrum of [Rh(III)$Cl_2$-*222$S_4$diAcOMe*]Cl

## 4.3-2. Rh(III) Complexes With *222$S_4$diAcOH* Chelate System

Six different reaction conditions were investigated for the synthesis of **Rh(III)$Cl_2$-*222$S_4$diAcOH*]Cl**, as shown in **Scheme 4-2**. HPLC analysis of these reactions revealed a predominant peak with a retention time of approximately 7.5 minutes (**Figure S4-2A to S4-2D**) using ***Gradient 2*** (2% solvent B increased to 5% solvent B over 10 minutes, followed by an additional 5 minute at 5% solvent B, then increased to 80% solvent B over 9 minute, and finally decreased to 2% solvent B over 1 minute). ESI-MS analysis revealed that this peak is consistent with the species where one of the pendant carboxylic acid group

and one chloride group is directly coordinated to the Rh(III) center [*m/z* = 466.96 (found), 466.88 (calculated for $C_{10}H_{17}ClO_4RhS_4^+$)], as shown in **Figure 4-13**.

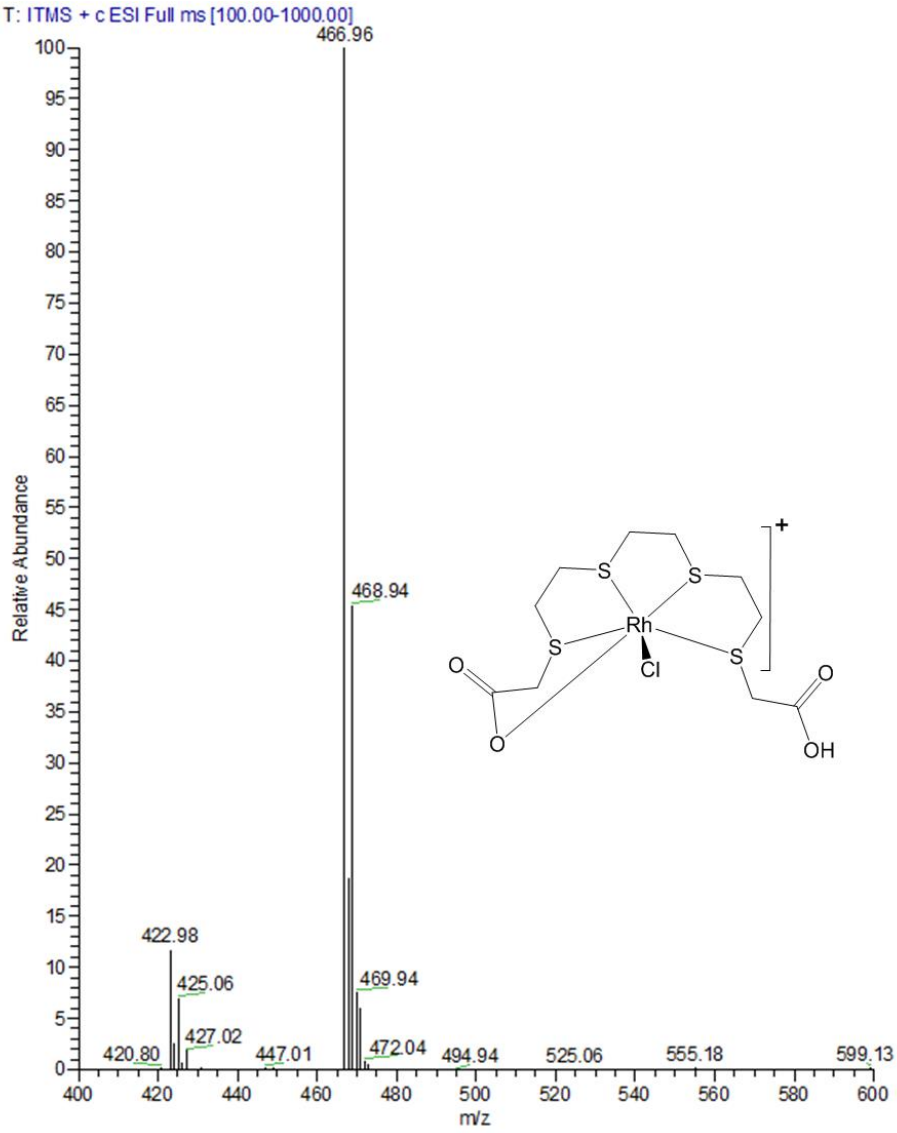


**Figure 4-13.** ESI-MS of $C_{10}H_{17}ClO_4RhS_4^+$

Two other product species were observed with retention times of approximately 2.3 minutes and 11.8 minutes. The *m/z* of the peak at approximately 2.3 minutes is consistent with the species where both of the pendant carboxylic acid groups are directly coordinated

to the Rh(III) center [*m/z* = 430.78 (found), 430.90 (calculated for $C_{10}H_{16}O_4RhS_4^+$)], as shown in **Figure 4-14**. The *m/z* of the peak at approximately 11.8 minutes is consistent with the species where two chloride atoms are directly coordinated to the Rh(III) center [*m/z* = 502.88 (found), 502.85 (calculated for $C_{10}H_{18}Cl_2O_4RhS_4^+$)], as shown in **Figure 4-15**.

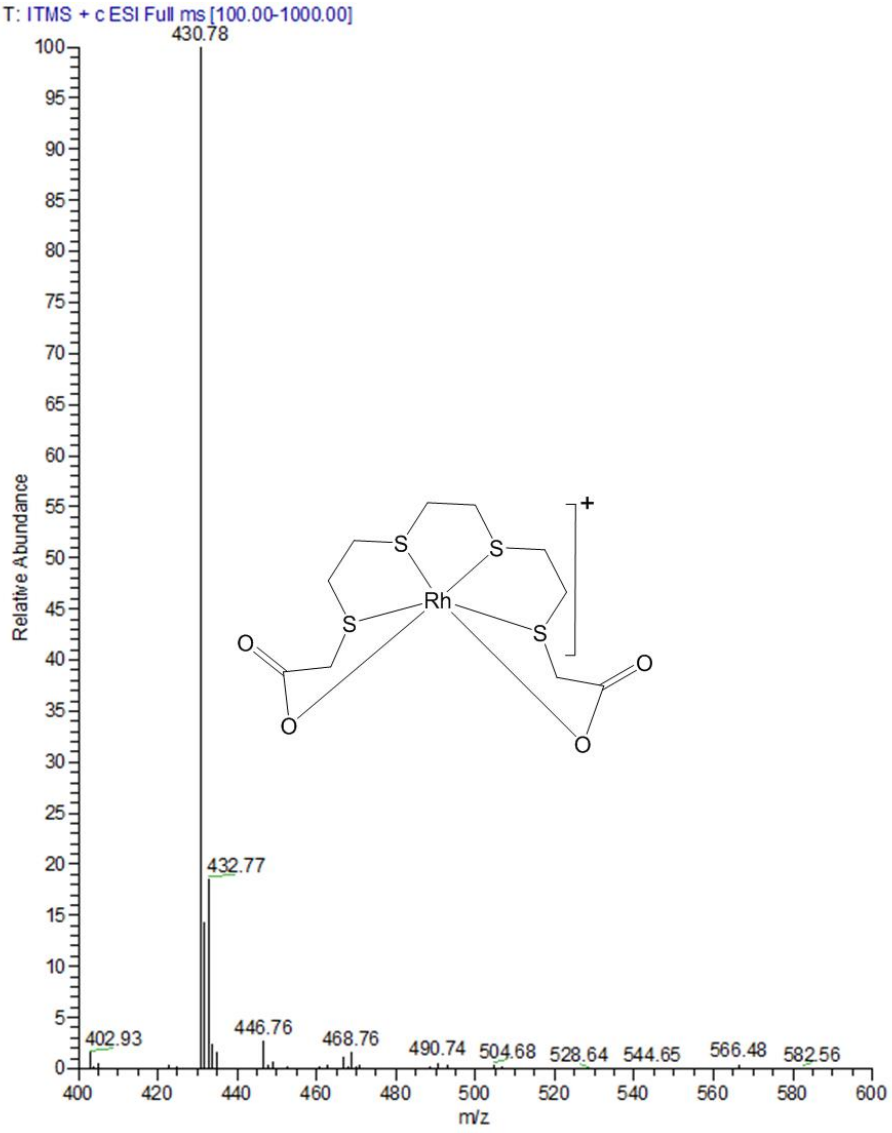


**Figure 4-14.** ESI-MS of $C_{10}H_{16}O_4RhS_4^+$

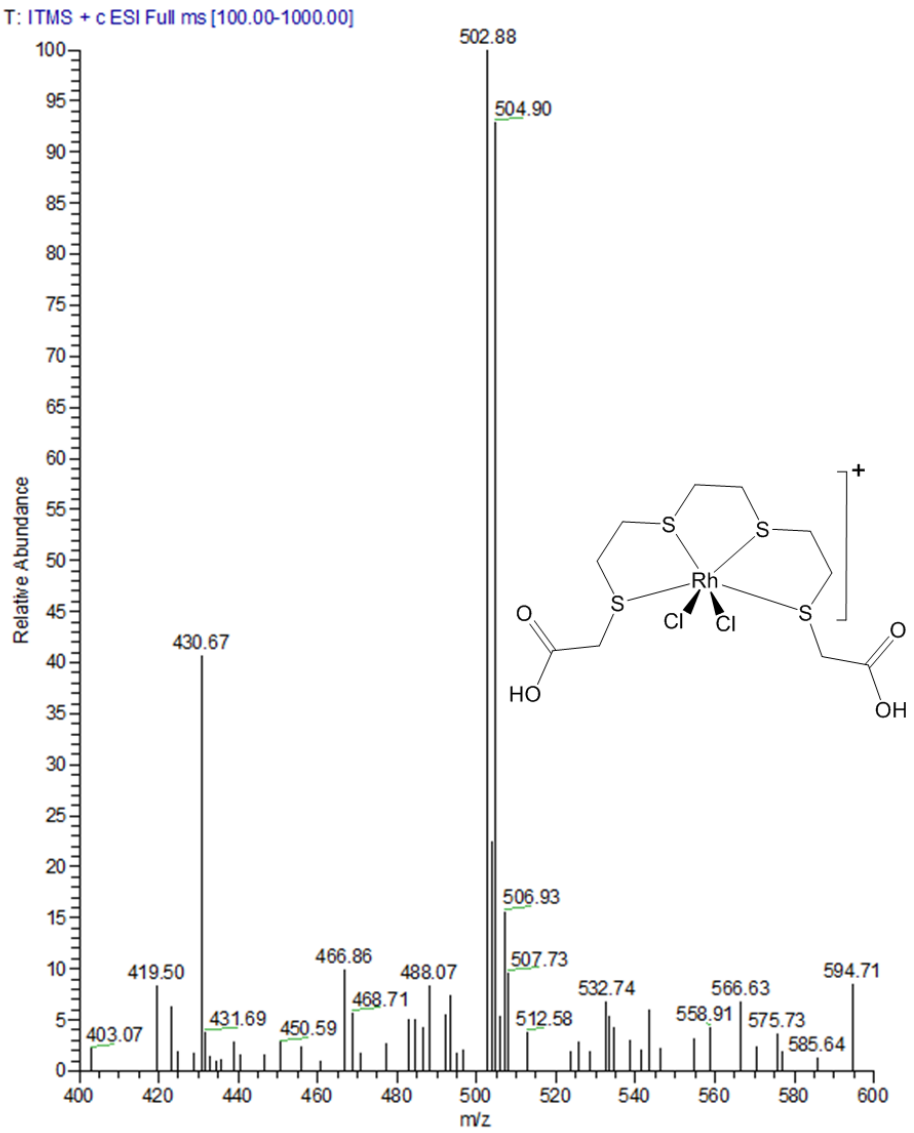


**Figure 4-15.** ESI-MS of for $C_{10}H_{18}Cl_2O_4RhS_4^+$

## 4.3-3. Rh(III) Complexes With 16S4diol Chelate System

***16S4-diol*** is generally used as the chelate of choice for quick assessment of $^{105}$Rh-labeling efficiency. Hence, non-radioactive Rh(III) complexes formed with ***16S4-diol*** were evaluated as a standard for comparing Rh(III) coordination chemistry with other chelators at the tracer scale. **[Rh(III)Cl2-*16S4-diol*]Cl** was synthesized by reacting $RhCl_3$ with ***16S4-diol*** using a microwave synthesizer. The crystal structure previously reported by Venkatesh

et al.[3] indicates that Rh(III) was coordinated to four S atoms in a square planar geometry, with two Cl atoms bound to the Rh(III) core in the *trans* axial positions. However, two isomers were identified, which resulted from the diol oxygens being in either the *cis* or *trans* position. This result was expected because the ***16S$_4$-diol*** ligand was purchased as the *cis/trans* mixture.

Six different reaction conditions were investigated as shown in **Scheme 4-3**. HPLC analysis of reactions 16 and 17 revealed 5 predominant peaks with retention times of approximately 10.5 minutes, 9.7 minutes, 8.5 minutes, 8.0 minutes, and 7.3 minutes using ***Gradient 3*** (5% solvent B increased to 20% solvent B over 15 minutes, followed by an additional 2 minutes at 20% solvent B, then decreased to 5% solvent B over 3 minutes), as shown in (**Figure S4-3A to S4-3F)**. ESI-MS analysis revealed that the peaks at approximately 10.5 minutes and 9.7 minutes (combined peak area ~ 80%) are consistent with the $M^+$ ion of **[Rh(III)Cl$_2$-*16S$_4$diol*]**$^+$ [*m/z* = 501.12 (found), 500.91 (calculated for $C_{12}H_{24}Cl_2O_2RhS_4^+$)], as shown in **Figure 4-16**. We can conclude that these two isomers result from the diol oxygens being in either the *cis* or *trans* position since the ***16S$_4$-diol*** ligand was purchased as the *cis/trans* mixture. In addition, similar results were reported by Venkatesh et al.[3]

The peaks at 8.5 minutes and 8.0 minutes correspond to the species where two hydroxyl groups (OH) are directly coordinated to the Rh(III) metal center instead of two chlorides [*m/z* = 465.08 (found), 464.98 (calculated for $C_{12}H_{26}O_4RhS_4^+$)], as shown in **Figure 4-17**. Similar product species were observed by Carroll[18]. No significant difference was observed in the HPLC profile between reaction 16 (no ethanol used) and reaction 17

(ethanol used), which further suggests that Rh(III) complexes can be formed without the addition of ethanol for the catalytic reduction of $Rh^{+3}$ to $Rh^{+1}$.

Interestingly, the product species with a retention time of approximately 10.5 minutes was preferentially formed when the reaction temperature was increased to 110 °C (reactions 18 – 21). No significant difference was observed in the HPLC profile between reaction 18 (no ethanol used), reaction 19 (ethanol used), and reaction 20 ($SnCl_2$ used).

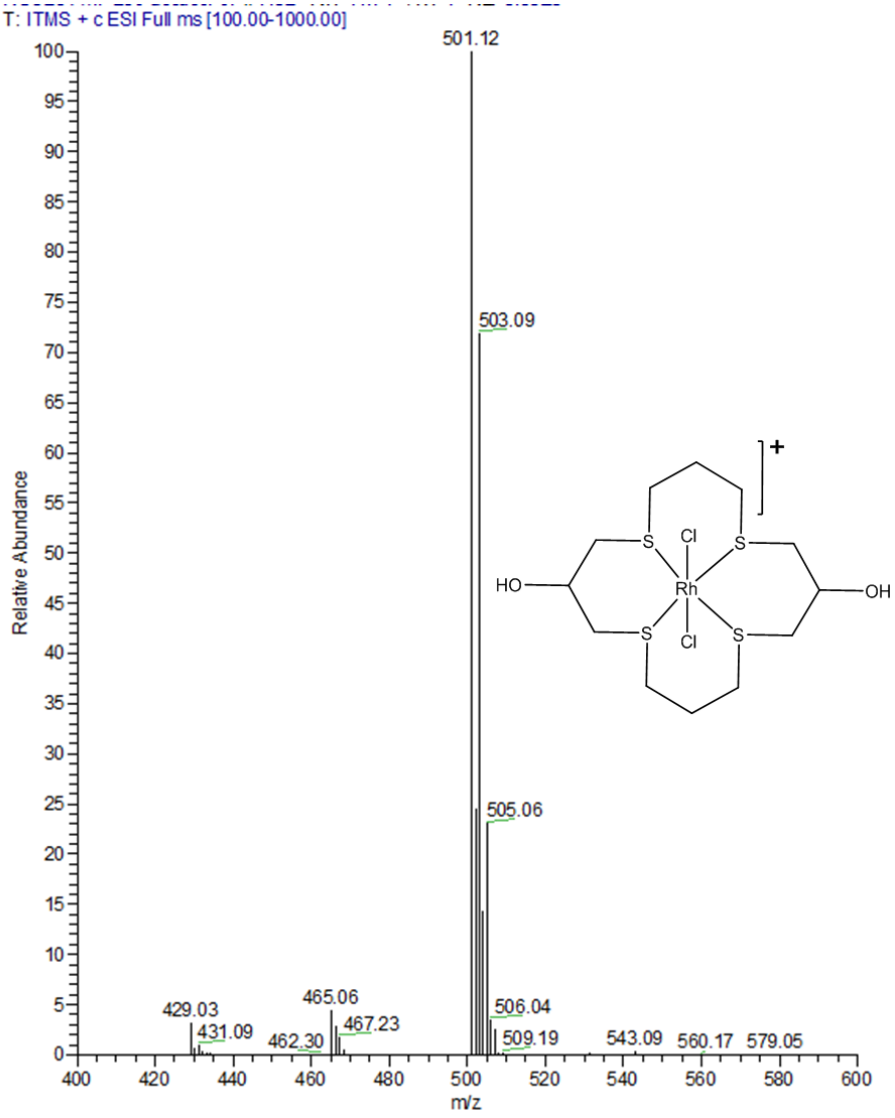


**Figure 4-16.** ESI-MS of for [Rh(III)$Cl_2$-*16S4diol*]$^+$

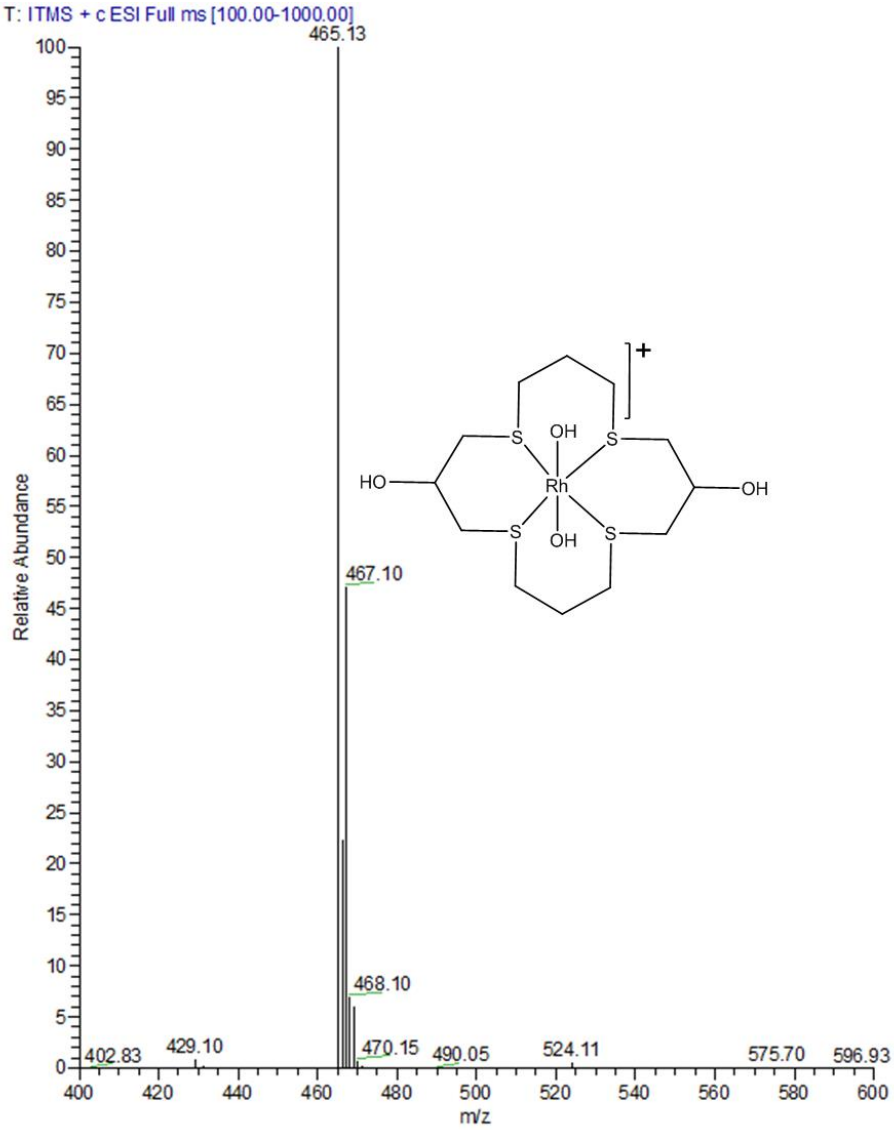


**Figure 4-17.** ESI-MS of for [Rh(III)$OH_2$-*16S4diol*]$^+$

## 4.3-4. Production of $^{105}$Rh from Recycled $^{104}$Ru Metal Target

Three separate neutron irradiations of the recycled $^{104}$Ru metal (production 1, 3 and 4) and one irradiation of new $^{104}$Ru metal (production 2) were performed at MURR as summarized in **Table 4-1**. The $^{105}$Rh recovery in productions 3 and 4 (57.9% and 57.6%, respectively) was significantly higher than the $^{105}$Rh recovery from productions 1 and 2 (22.9% and 15.1%, respectively). To the best of our knowledge, the ~ 57% $^{105}$Rh recovery

reported here for productions 3 and 4 is the highest that has been reported for $^{105}$Rh production. The time for $Cl_2$ bubbling during the target processing procedure in productions 3 and 4 was more than double that used in productions 1 and 2. Bubbling more $Cl_2$ into NaOH solution would potentially generate more hypochlorite *in situ*, which would facilitate the dissolution of the $^{104}$Ru target and the release of $^{105}$Rh into the solution. This might explain why the $^{105}$Rh recovery was higher in productions 3 and 4, which had more time for $Cl_2$ bubbling.

**Table 4-1**: $^{105}$Rh production from recycled $^{104}$Ru metal target at MURR

| | Pull Date | $^{104}$Ru Target* (mg) | Irradiation time (h) | Initial $^{105}$Rh activity (mCi) | Recovered $^{105}$Rh activity (mCi) | % $^{105}$Rh recovery (decay corrected) |
|---|---|---|---|---|---|---|
| Production 1 | 4/17/2018 | 1.44 | 90.02 | 7.17 | 1.50 | 22.9 |
| Production 2 | 5/17/2018 | 3.24 | 89.15 | 23.90 | 3.30 | 15.1 |
| Production 3 | 6/11/2018 | 4.78 | 89.67 | 38.20 | 19.79 | 57.9 |
| Production 4 | 8/6/2018 | 4.46 | 90.02 | 36.60 | 19.10 | 57.6 |

*Recycled $^{104}$Ru metal target was used except for production 2 where new $^{104}$Ru metal target was used

Although high $^{105}$Rh recovery was achieved in productions 3 and 4, visual inspection of the midget impinger during the dissolution of the recycled $^{104}$Ru target revealed that the target did not completely dissolve, given that some very fine black particles were still observed after heating in *in situ* generated hypochlorite for 1 hour at 40 °C. It is possible that the high temperatures required during the target recycling process might have affected the particle size of the metal powder, thereby making it more difficult to dissolve. Additionally, there is a possibility that passivation of the $^{104}$Ru metal target

occurred during the recycling process that included a long storage period of [$^{104}$Ru]$RuO_4$ in 3 M HCl.[21]

HPGe gamma spectrometry analysis of the final $^{105}$Rh stock solutions revealed the predominant gamma peaks associated with $^{105}$Rh (318 and 306 keV). However, very minimal impurities from $^{24}$Na (< 0.1%) at 1368 keV were observed. The $^{24}$Na impurity is most likely from the neutron activation of NaCl contaminants contained in the recycled $^{104}$Ru metal. The $^{24}$Na impurities reported here are consistent with previous results reported by Phelps.[4] No other radionuclide impurities were identified.

ICP-MS analysis was performed on a 200 μL aliquot of decayed $^{105}$Rh stock solution to determine the separation efficiency between $^{104}$Ru metal target and $^{105}$Rh during the target processing procedure. The $^{105}$Rh stock solution is usually obtained in a total volume of ~2 mL; hence, the amount of metallic impurities obtained from the 200 μL ICP-MS analysis aliquot was multiplied by 10 to get an estimate of the total amount of metallic impurities in the stock solution. For all four $^{105}$Rh productions, the amount of $^{104}$Ru remaining after separation was less than 0.05% of the original amount of irradiated $^{104}$Ru metal target (**Table 4-2**). This is assuming that all signals at mass 104 are due to Ru with an isotopic composition identical to the 98.9% enriched $^{104}$Ru metal target. Other metals identified during the ICP-MS analysis include $^{105}$Pd, $^{106}$Pd and $^{103}$Rh. Pallidium-105 is produced from the beta decay of $^{105}$Rh. Pallidium-106 is produced from the beta decay of $^{106}$Rh, which is produced from the neutron capture reaction on $^{105}$Rh as shown in **Equation 4-2**. Given the very high thermal neutron capture cross section for $^{105}$Rh (11,000 barns), there is a high probability for neutron activation of $^{105}$Rh produced from the beta decay of $^{105}$Ru during the neutron irradiation of $^{104}$Ru metal target. Rhodium-103 is produced from

the beta decay of $^{103}$Ru, which is produced from the neutron activation of $^{102}$Ru impurity in the $^{104}$Ru metal target as shown in **Equation 4-3**. Phelps previously reported that the $^{104}$Ru metal target contains about 0.5% $^{102}$Ru impurities, which would explain the formation of $^{103}$Rh.[4]

$$^{105}\text{Rh} \xrightarrow{n,\gamma} {}^{106}\text{Rh} \xrightarrow{\beta^-} {}^{106}\text{Pd}$$

**Equation 4-2.** Possible production route for $^{106}$Pd

$$^{102}\text{Ru} \xrightarrow{n,\gamma} {}^{103}\text{Ru} \xrightarrow{\beta^-} {}^{103}\text{Rh}$$

**Equation 4-3.** Possible production route for $^{103}$Rh

**Table 4-2:** ICP-MS analysis of metals in decayed $^{105}$Rh stock solution*

| | $^{104}$Ru Metal Target (ng) | Total $^{105}$Pd (ng) | Total $^{106}$Pd (ng) | Total $^{103}$Rh (ng) | Total $^{104}$Ru remaining (ng) | % $^{104}$Ru remaining |
|---|---|---|---|---|---|---|
| Production 1 | 1.44 E+06 | 4.5 | 0.71 | 0.95 | 52.9 | 0.004 |
| Production 2 | 3.24 E+06 | 23.5 | 4.05 | 0.10 | 35.4 | 0.001 |
| Production 3 | 4.78 E+06 | 46.4 | 6.32 | 8.42 | 745 | 0.016 |
| Production 4 | 4.46 E+06 | 40.7 | 6.03 | 7.48 | 2130 | 0.048 |

*Based on 2 mL of $^{105}$Rh stock solution

## 4.3-5. $^{105}$Rh-labeling

Prior to radiolabeling, the pH of the [$^{105}$Rh]$RhCl_3$ solution was carefully adjusted to ~ 3.5 using 1 M NaOH (20 μL) and 0.5 M NaOH (20 μL). Previous studies have shown that $Rh^{+3}$ tends to hydrolyze under basic conditions to form $Rh(OH)_3$ ($K_{sp} = 4.8 \times 10^{-23}$), which may form dimers or bridged species.[22] Once $Rh(OH)_3$ is formed, it is almost

impossible to convert back to $Rh^{+3}$. Hence, it is critical that $^{105}$Rh-labeling experiments be performed under acidic conditions (pH < 5). Care should be taken when adjusting the pH of the [$^{105}$Rh]$RhCl_3$ solution to avoid going above pH 7. The $R_f$ value of [$^{105}$Rh]$RhCl_3$ developed using 0.9% saline is 0.05 when the pH of the [$^{105}$Rh]$RhCl_3$ solution is above 7 (**Figure S4-4)** as opposed to 1.0 when the pH is ~4 (**Figure S4-5)**. This indicates that [$^{105}$Rh]$Rh(OH)_3$ (formed when pH > 7) remains at the origin, while [$^{105}$Rh]$RhCl_3$ moves to the solvent front in 0.9% saline. Radiolabeling experiments that were performed in pH > 7 resulted in no radiolabeling yields based on TLC analysis, with all radioactivity remaining in the origin.

$^{105}$Rh-labeling was performed using ***222S$_4$diAcOMe***, ***222S$_4$diAcOH,*** and **16S$_4$-diol**. The pH-adjusted [$^{105}$Rh]$RhCl_3$ solution was incubated with the ligand solutions for 1 hour at 90 °C in a water bath. Silica gel TLC analysis was performed using three mobile phases; 0.9% saline, acetonitrile, and 0.4 M $NaBPh_4$ in acetonitrile. The $R_f$ values of [$^{105}$Rh]$RhCl_3$, [**$^{105}$Rh]$RhCl_2$-*222S$_4$diAcOMe***, [**$^{105}$Rh]$RhCl_2$-*222S$_4$diAcOH***, and [**$^{105}$Rh]$RhCl_2$-*16S$_4$diol*** in the three mobile phases are tabulated in **Table 4-3** and the images of the TLC scan are shown in **Figures S4-4 to S4-16**.

**Table 4-3.** Silica gel TLC analysis of $^{105}$Rh complexes

| Compound | $R_f$ (0.9% Saline) | $R_f$ (ACN) | $R_f$ (0.4 M $NaBPh_4$ in ACN) |
|---|---|---|---|
| [$^{105}$Rh]$RhCl_3$ | 1.0 | 0.05 | 0.05 |
| [**$^{105}$Rh]$RhCl_2$-*222S$_4$diAcOMe*** | ~0.8 | ~0.6 | 0.3-0.7 |
| [**$^{105}$Rh]$RhCl_2$-*222S$_4$diAcOH*** | ~0.8 | ~0.6 | 0.3-0.7 |
| [**$^{105}$Rh]$RhCl_2$-*16S$_4$diol*** | 0.3 | 0.2-0.4 | 0.9 |

The radiolabeling yield for [$^{105}$**Rh]RhCl$_2$-*16S$_4$diol*** was 80.9 ± 0.4% (n = 3), which was determined using the TLC scans developed in saline as the mobile phase. The radiolabeling yields for [$^{105}$**Rh]RhCl$_2$-*222S$_4$diAcOMe*** and [$^{105}$**Rh]RhCl$_2$-*222S$_4$diAcOH*** were 92.5 ± 2.0% (n = 3) and 91.0 ± 1.5% (n = 3), respectively, which were determined using the TLC scans developed in acetonitrile as the mobile phase. The TLC scans from [$^{105}$**Rh]RhCl$_2$-*222S$_4$diAcOMe*** and [$^{105}$**Rh]RhCl$_2$-*222S$_4$diAcOH*** were almost identical in all three mobile phases. It is likely that the pendant methyl acetate groups in the ***222S$_4$diAcOMe*** ligand would be hydrolyzed to carboxylic acid groups given the acidic reaction conditions used for radiolabeling. This would result in identical product species with the ***222S$_4$diAcOH*** ligand. Acid hydrolysis of the pendant methyl acetate groups in ***222S$_4$diAcOMe*** was also observed during the macro-scale synthesis of **Rh(III)Cl$_2$-*222S$_4$diAcOMe*** with the addition of 1 mL of 0.5 M HCl.

## 4.4. Conclusions

Rh-105 remains an attractive radioisotope for the development of therapeutic radiopharmaceuticals due to its favorable nuclear properties (half-life = 35.4 hours, $\beta^-_{avg}$ = 152 keV). Historically, it has been reported that the catalytic reduction of $Rh^{+3}$ to $Rh^{+1}$, with subsequent re-oxidation to $Rh^{+3}$ by atmospheric oxygen, is necessary for the ligand exchange and formation of Rh(III) complexes.[14, 19-20] Hence refluxing alcohols, particularly ethanol, have been traditionally used as reducing agents for the formation of Rh(III) complexes.[3, 8, 12-13] However, the studies reported here demonstrates that Rh(III) complexes can be synthesized without the addition of ethanol or $SnCl_2$ as reducing agents. Additionally, a microwave-assisted synthesis method for Rh(III) complexes was reported. The use a microwave significantly reduced the reaction time to 10 minutes or less

compared to the over 1 hour reaction time reported using the conventional bench top synthesis method.[15, 18] An improved HPLC method was developed to identify the various Rh(III) product species, which were subsequently characterized using ESI-MS.

We also report the production of $^{105}$Rh using recycled $^{104}$Ru metal target. Subsequently, $^{105}$Rh-labeling experiments were performed using three ligands (***16S$_4$-diol***, ***222S$_4$diAcOMe***, and ***222S$_4$diAcOH***). To the best of our knowledge, the is the first reported synthesis of Rh(III) complexes using $^{105}$Rh produced from recycled $^{104}$Ru metal targets. Additionally, $^{105}$Rh-labeling of ***222S$_4$diAcOMe***, and ***222S$_4$diAcOH*** was achieved without ethanol or $SnCl_2$ as reducing agents.

## 4.5. Future Studies

Although the production of $^{105}$Rh using recycled $^{104}$Ru metal target was successful, there is room to improve the target processing procedure. The use of $Cl_2$ to generate hypochlorite *in situ* for the oxidation of $^{104}$Ru metal creates room for possible inconsistencies between different batches of target processing. This is because the amount of $Cl_2$ used may vary due to changes in tubing length or pressure in the $Cl_2$ tank. The data reported here shows that the amount of $^{105}$Rh recovered is influenced by the amount of $Cl_2$ (i.e., increased $Cl_2$ bubbling time) used during target processing with more $^{105}$Rh recovered with longer $Cl_2$ bubbling time. Additionally, $Cl_2$ is a toxic gas and should be avoided if possible. As an alternative, commercially available NaOCl can be used to oxidize $^{104}$Ru metal to $^{104}RuO_4$. Phelps has demonstrated the oxidation of $^{nat}$Ru metal using 12-15% NaOCl.[4] Therefore, this method can be applied for processing irradiated $^{104}$Ru metal target to separate $^{105}$Rh.

Potential preclinical and clinical translation of $^{105}$Rh-based radiopharmaceuticals will require the development of bifunctional analogues of ***222S$_4$diAcOH*** that are conjugated to suitable targeting molecules. The pendant carboxylic acid groups in ***222S$_4$diAcOH*** provide a suitable functional group for the formation of an amide bond with terminal amines in peptide molecules. Rhodium-105 labeling of the resulting bifunctional chelator can then be performed without the addition of ethanol or $SnCl_2$ as reducing agents, following the synthesis procedure that is reported in this work. Additionally, the microwave synthesis method reported here for the synthesis of non-radioactive Rh(III) complexes can also be applied for $^{105}$Rh labeling studies to decrease reaction time.

## 4.6. References


1. Grazman, B.; Troutner, D., Rh-105 as a potential radiotherapeutic agent. *Journal of Labelled Compounds and Radiopharmaceuticals* **1986,** *23* (10-12), 1371-1373.

2. Grazman, B.; Troutner, D., $^{105}$Rh as a potential radiotherapeutic agent. *International Journal of Radiation Applications and Instrumentation. Part A. Applied Radiation and Isotopes* **1988,** *39* (3), 257-260.

3. Venkatesh, M.; Goswami, N.; Volkert, W.; Schlemper, E.; Ketring, A.; Barnes, C.; Jurisson, S., An Rh-105 complex of tetrathiacyclohexadecane diol with potential for formulating bifunctional chelates. *Nuclear Medicine and Biology* **1996,** *23* (1), 33-40.

4. Phelps, T. Radionuclide Production and Separation Techniques for Radiopharmaceutical Development and Nuclear Waste Processing. Doctoral Dissertation, University of Missouri-Columbia, 2018.

5. Greenwood, N. N.; Earnshaw, A., *Chemistry of the Elements*. Elsevier: 2012.

6. Kruper Jr, W. J.; Fordyce, W. A.; Pollock, D. K.; Fazio, M. J.; Inbaskaran, M. N.; Muthyala, R., Functionalized polyamine chelants and rhodium complexes thereof for conjugation to antibodies. U.S. Patent No. 5,284,644: 1994.

7. Pillai, M.; John, C.; Troutner, D. E., Labeling of human IgG with rhodium-105 using a new pentadentate bifunctional ligand. *Bioconjugate Chemistry* **1990,** *1* (3), 191-197.

8. Li, N.; Struttman, M.; Higginbotham, C.; Grall, A. J.; Skerlj, J. F.; Vollano, J. F.; Bridger, S. A.; Ochrymowycz, L. A.; Ketring, A. R.; Abrams, M. J.; Volkert, W. A., Biodistribution of model $^{105}$Rh-labeled tetradentate thiamacrocycles in rats. *Nuclear Medicine and Biology* **1997,** *24* (1), 85-92.

9. Pillai, M.; Lo, J.; Troutner, D., Labeling of hematoporphyrin with $^{105}$Rh and binding studies with human gamma globulin. *International Journal of Radiation Applications and Instrumentation. Part A. Applied Radiation and Isotopes* **1990,** *41* (1), 69-73.

10. Pillai, M.; Lo, J.; John, C.; Troutner, D., Labeling of proteins using [$^{105}$Rh]Rh-4-(p-aminobenzyl)-diethylenetriamine. *International Journal of Radiation Applications and Instrumentation. Part B. Nuclear Medicine and Biology* **1990,** *17* (4), 419-426.

11. Efe, G. E.; Pillai, M.; Schlemper, E.; Troutner, D., Rhodium complexes of two bidentate secondary amine oxime ligands and application to the labelling of proteins. *Polyhedron* **1991,** *10* (14), 1617-1624.

12. Goswami, N.; Alberto, R.; Barnes, C. L.; Jurisson, S., Rhodium(III) complexes with acyclic tetrathioether ligands. Effects of backbone chain length on the conformation of the Rh(III) complex. *Inorganic Chemistry* **1996,** *35* (26), 7546-7555.

13. Goswami, N.; Higginbotham, C.; Volkert, W.; Alberto, R.; Nef, W.; Jurisson, S., Rhodium-105 tetrathioether complexes: radiochemistry and initial biological evaluation. *Nuclear Medicine and Biology* **1999,** *26* (8), 951-7.

14. Feng, Y.; Phelps, T. E.; Carroll, V.; Gallazzi, F.; Sieckman, G.; Hoffman, T. J.; Barnes, C. L.; Ketring, A. R.; Hennkens, H. M.; Jurisson, S. S., Chemistry and radiochemistry of As, Re and Rh isotopes relevant to radiopharmaceutical applications: high specific activity radionuclides for imaging and treatment. *Dalton Transactions* **2017,** *46* (42), 14677-14690.

15. Dame, A. Synthesis Design and Nuclear Medicine Applications for Radiometals, Beta and Gamma Emission, Chelated Complexes. Doctoral Dissertation, University of Missouri-Columbia, 2017.

16. Crenshaw, N. N. Characterization of Acyclic Rhodium Tetrathioether Ligand Systems for $^{105}$Rh (III). Masters Thesis, University of Missouri-Columbia, 2015.

17. Akgun, Z.; Engelbrecht, H.; Fan, K.-H.; Barnes, C. L.; Cutler, C. S.; Jurisson, S. S.; Lever, S. Z., The complexation of rhodium (III) with acyclic diaminedithioether (DADTE) ligands. *Dalton Transactions* **2010,** *39* (42), 10169-10178.

18. Carroll, V. N., *Development of a rhodium tetrathioether bombesin analogue and investigation of cyclic and acyclic ligand systems for $^{105}$Rh (III)*. University of Missouri-Columbia: 2013.

19. Rund, J. V.; Basolo, F.; Pearson, R. G., Catalysis of substitution reactions of rhodium (III) complexes. The reaction of aquopentachlororhodate (III) ion with pyridine. *Inorganic Chemistry* **1964,** *3* (5), 658-661.

20. Jurisson, S. S.; Ketring, A. R.; Volkert, W. A., Rhodium-105 complexes as potential radiotherapeutic agents. *Transition Metal Chemistry* **1997,** *22* (3), 315-317.

21. Llopis, J.; Vazquez, M., Passivation of ruthenium in hydrochloric acid solution. *Electrochimica Acta* **1966,** *11* (6), 633-640.

22. Forrester, J.; Ayres, G., Rhodium (III) in aqueous solutions. *The Journal of Physical Chemistry* **1959,** *63* (11), 1979-1981.

# Supplementary Information

## Supplementary Data - Chapter 2

**Table S2-1.** Efficiency of $^{59}Fe$ stripping from Pb-resin

| Column # | $^{59}FeCl_3$ (µCi) | Fe (µg)* | Pb (µg)** | Fraction 1 (µCi) | Fraction 2 (µCi) | Total $^{59}Fe$ recovery |
|---|---|---|---|---|---|---|
| 1 | 129 | 0 | 0 | 125.5 | 0 | 97% |
| 2 | 129 | 4.4 | 0 | 126 | 0 | 98% |
| 3 | 121.5 | 22.1 | 0 | 120.7 | 0 | 99% |
| 4 | 117.6 | 11.0 | 41.0 | 114.4 | 0.8 | 98% |
| 5 | 108.5 | 11.0 | 41.0 | 106.5 | 1.9 | 100% |
| 6 | 108.5 | 11.0 | 41.0 | 106.3 | 1.9 | 100% |
| 7 | 55.8 | 6.1 | 6.1 | 53.4 | 0.6 | 97% |
| 8 | 55.8 | 6.1 | 6.1 | 54 | 0.6 | 98% |
| 9 | 55.6 | 6.1 | 6.1 | 53.7 | 0.3 | 97% |

* from 0.54 mg/ml $FeCl_3.6H_2O$ solution
** from 0.64 mg/ml $Pb(NO_3)_2$ solution

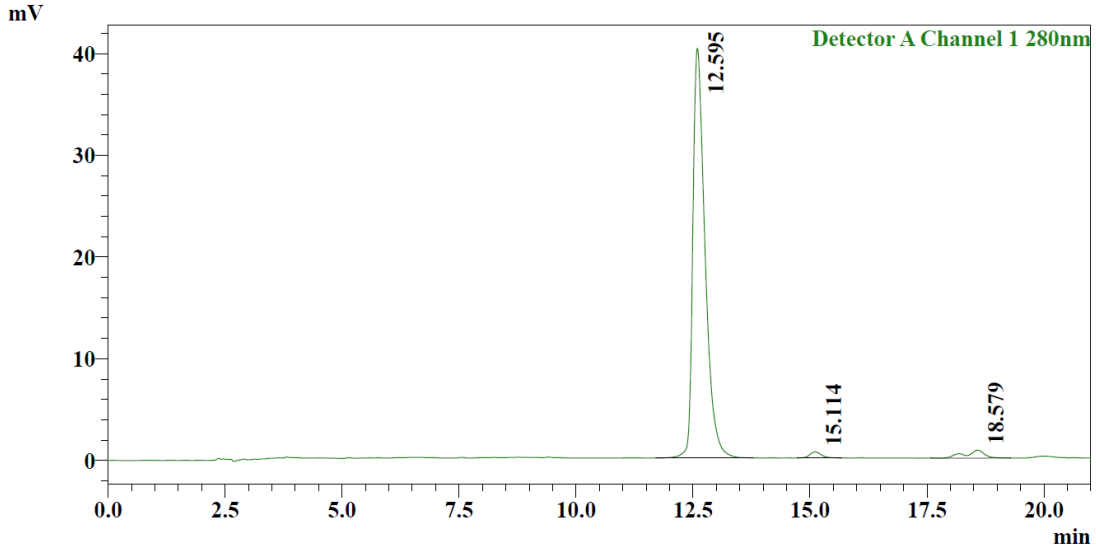


**Figure S2-1.** HPLC profile of Pb-RM2 (gradient = 22% ACN:$H_2O$ increased to 25% ACN:$H_2O$ over 19 minutes, followed by an additional 1 minute at 25% ACN:$H_2O$, then decreased to 22% ACN:$H_2O$ over 1 minute at a flow rate of 1.5 mL/min)

| Table S2-2. [$^{203}$Pb]$PbCl_2$ biodistribution in CF1 mice<br>Data shown as mean ± SD %ID (n = 5 mice per time point) | | | | |
|---|---|---|---|---|
| **Tissue** | **15 min** | **1 h** | **4 h** | **24 h** |
| **Blood** | 7.64 ± 0.97 | 6.70 ± 1.06 | 5.27 ± 0.98 | 3.64 ± 0.45 |
| **Heart** | 0.12 ± 0.04 | 0.07 ± 0.02 | 0.06 ± 0.02 | 0.03 ± 0.01 |
| **Lung** | 0.61 ± 0.08 | 0.54 ± 0.12 | 0.42 ± 0.23 | 0.18 ± 0.04 |
| **Liver** | 22.17 ± 2.07 | 22.79 ± 1.49 | 23.89 ± 1.36 | 16.53 ± 3.50 |
| **Stomach** | 0.47 ± 0.07 | 0.45 ± 0.14 | 0.65 ± 0.28 | 0.42 ± 0.34 |
| **Sm. Intestines** | 4.17 ± 0.40 | 4.35 ± 0.42 | 4.19 ± 0.38 | 1.70 ± 0.20 |
| **Lg. Intestines** | 1.53 ± 0.55 | 1.17 ± 0.07 | 2.70 ± 0.43 | 1.71 ± 0.23 |
| **Kidney** | 26.26 ± 3.10 | 28.52 ± 2.84 | 25.46 ± 2.10 | 18.97 ± 1.51 |
| **Spleen** | 0.13 ± 0.03 | 0.16 ± 0.05 | 0.18 ± 0.03 | 0.10 ± 0.06 |
| **Brain** | 0.07 ± 0.01 | 0.07 ± 0.02 | 0.08 ± 0.03 | 0.05 ± 0.01 |
| **Pancreas** | 0.83 ± 0.14 | 0.78 ± 0.13 | 0.65 ± 0.14 | 0.34 ± 0.06 |
| **Muscle** | 0.05 ± 0.01 | 0.05 ± 0.02 | 0.03 ± 0.02 | 0.03 ± 0.03 |
| **Bone** | 0.75 ± 0.16 | 0.95 ± 0.12 | 0.95 ± 0.10 | 1.29 ± 0.14 |
| **Urine (%ID)** | 0.95 ± 0.54 | 2.05 ± 0.32 | 4.63 ± 0.84 | 10.22 ± 2.86 |
| **Excretion (%ID)** | 0.95 ± 0.19 | 2.05 ± 0.19 | 4.63 ± 0.86 | 19.82 ± 4.61 |
| Note: Values for urine include radioactivity measured in cage paper | | | | |

**Table S2-3. [$^{203}$Pb]Pb-RM2 biodistribution in PC3 tumor-bearing mice.**
**Data shown as mean ± SD %ID (n = 5 mice per time point)**

| Tissue | 15 min | 30 min | 1 h | 2 h | 4 h | 24 h |
|---|---|---|---|---|---|---|
| **Blood** | 5.03 ± 1.55 | 2.57 ± 0.70 | 0.84 ± 0.28 | 0.13 ± 0.06 | 0.09 ± 0.02 | 0.05 ± 0.01 |
| **Heart** | 0.15 ± 0.04 | 0.07 ± 0.02 | 0.03 ± 0.01 | 0.01 ± 0.00 | 0.01 ± 0.00 | 0.00 ± 0.00 |
| **Lung** | 0.44 ± 0.13 | 0.24 ± 0.04 | 0.10 ± 0.01 | 0.03 ± 0.01 | 0.02 ± 0.00 | 0.01 ± 0.01 |
| **Liver** | 2.83 ± 0.81 | 1.39 ± 0.21 | 0.71 ± 0.12 | 0.33 ± 0.05 | 0.37 ± 0.07 | 0.26 ± 0.04 |
| **Stomach** | 0.55 ± 0.13 | 0.35 ± 0.08 | 0.21 ± 0.06 | 0.97 ± 1.86 | 0.07 ± 0.01 | 0.02 ± 0.01 |
| **Sm. Intestines** | 3.25 ± 0.66 | 2.55 ± 0.45 | 1.53 ± 0.21 | 3.80 ± 6.56 | 0.48 ± 0.22 | 0.26 ± 0.28 |
| **Lg. Intestines** | 1.04 ± 0.33 | 0.76 ± 0.20 | 0.36 ± 0.09 | 0.76 ± 0.19 | 1.90 ± 2.00 | 0.13 ± 0.05 |
| **Kidney** | 3.33 ± 0.73 | 2.22 ± 0.39 | 1.89 ± 0.15 | 1.47 ± 0.23 | 1.51 ± 0.27 | 0.88 ± 0.26 |
| **Spleen** | 0.06 ± 0.02 | 0.03 ± 0.01 | 0.01 ± 0.00 | 0.01 ± 0.01 | 0.01 ± 0.00 | 0.01 ± 0.00 |
| **Brain** | 0.06 ± 0.01 | 0.03 ± 0.01 | 0.02 ± 0.00 | 0.01 ± 0.01 | 0.01 ± 0.00 | 0.00 ± 0.00 |
| **Pancreas** | 4.24 ± 0.72 | 3.28 ± 0.68 | 1.44 ± 0.41 | 0.56 ± 0.25 | 0.12 ± 0.06 | 0.04 ± 0.00 |
| **Muscle** | 0.15 ± 0.05 | 0.09 ± 0.04 | 0.03 ± 0.01 | 0.01 ± 0.00 | 0.01 ± 0.01 | 0.01 ± 0.01 |
| **Bone** | 0.05 ± 0.01 | 0.03 ± 0.01 | 0.01 ± 0.00 | 0.01 ± 0.02 | 0.01 ± 0.00 | 0.01 ± 0.00 |
| **Tumors** | 1.44 ± 1.03 | 1.45 ± 0.49 | 2.20 ± 0.95 | 1.23 ± 0.39 | 1.57 ± 0.72 | 1.38 ± 0.79 |
| **Urine (%ID)** | 41.66 ± 0.27 | 57.42 ± 4.40 | 79.36 ± 1.25 | 86.75 ± 8.01 | 90.44 ± 2.92 | 92.32 ± 2.06 |
| **Excretion (%ID)** | 41.66 ± 0.27 | 57.42 ± 4.40 | 79.36 ± 1.25 | 86.75 ± 8.01 | 90.44 ± 2.92 | 94.59 ± 1.85 |

Note: Values for urine include radioactivity measured in cage paper

# Supplementary Data – Chapter 3

```
*****************************************************************************
*****        G A M M A   S P E C T R U M   A N A L Y S I S          *****
*****************************************************************************
```

**Pb-212 Generator Eluent**

```
Filename: DET01

Report Generated On              : 1/28/2019   2:29:47 PM

Sample Title                     : Sample title.
Sample Description               :
Sample Identification            :
Sample Type                      :
Sample Geometry                  :

Peak Locate Threshold            :  3.00
Peak Locate Range (in channels)  :     1 - 65535
Peak Area Range (in channels)    :     1 - 65535
Identification Energy Tolerance  :    1.000 keV

Sample Size                      :  1.0000E+00 Unit

Sample Taken On                  :
Acquisition Started              : 1/28/2019   2:07:25 PM

Live Time                        :     1200.0 seconds
Real Time                        :     1313.1 seconds

Dead Time                        :   8.62 %


              Energy Calibration Used Done On       : 1/28/2019
              Efficiency Calibration Used Done On   : ??????????
              Efficiency ID                         :
```

**Pb-212 Generator Eluent**

**********************************************************************

***** P E A K A N A L Y S I S R E P O R T *****

**********************************************************************

Detector Name: DET01
Sample Title: Sample title.
Peak Analysis Performed on: 1/28/2019 2:29:47 PM
Peak Analysis From Channel: 1
Peak Analysis To Channel: 8192

| | Peak No. | ROI start | ROI end | Peak centroid | Energy (keV) | FWHM (keV) | Net Peak Area | Net Area Uncert. | Continuum Counts | |
|---|---|---|---|---|---|---|---|---|---|---|
| | 1 | 80- | 92 | 86.65 | 24.80 | 1.79 | 9.048E+03 | 468.44 | 7.743E+04 | |
| M | 2 | 249- | 276 | 255.88 | 73.08 | 1.36 | 5.269E+04 | 383.34 | 1.350E+05 | Tl-208 |
| m | 3 | 249- | 276 | 262.77 | 75.05 | 1.36 | 2.172E+05 | 575.63 | 1.344E+05 | Pb-212 |
| m | 4 | 249- | 276 | 270.41 | 77.23 | 1.36 | 2.604E+05 | 608.49 | 1.245E+05 | Pb-212 |
| M | 5 | 291- | 320 | 297.61 | 84.99 | 1.56 | 4.376E+04 | 341.88 | 9.600E+04 | Pb-212 |
| m | 6 | 291- | 320 | 305.78 | 87.32 | 1.56 | 1.362E+05 | 473.70 | 1.020E+05 | Pb-212 |
| m | 7 | 291- | 320 | 314.71 | 89.87 | 1.56 | 4.500E+04 | 325.98 | 8.331E+04 | Pb-212 |
| | 8 | 402- | 403 | 403.40 | 115.18 | 0.29 | 3.042E+03 | 143.31 | 1.318E+04 | Pb-212 |
| | 9 | 831- | 836 | 834.00 | 238.04 | 1.15 | 6.368E+05 | 1002.90 | 2.070E+05 | Pb-212 |
| | 10 | 965- | 972 | 969.14 | 276.60 | 1.24 | 3.515E+04 | 285.21 | 2.299E+04 | Tl-208 |
| | 11 | 1003- | 1010 | 1006.58 | 287.29 | 1.29 | 5.194E+03 | 189.55 | 1.527E+04 | Bi-212 |
| | 12 | 1044- | 1052 | 1048.55 | 299.26 | 1.31 | 4.736E+04 | 316.09 | 2.463E+04 | Pb-212 |
| | 13 | 1141- | 1149 | 1145.53 | 326.93 | 0.92 | 1.378E+03 | 186.67 | 1.567E+04 | Bi-212 |
| | 14 | 1576- | 1587 | 1581.69 | 451.39 | 1.44 | 4.072E+03 | 171.41 | 1.009E+04 | Bi-212 |
| | 15 | 1777- | 1789 | 1783.68 | 509.02 | 1.64 | 9.271E+04 | 401.27 | 2.596E+04 | Tl-208 |
| | 16 | 2029- | 2043 | 2036.62 | 581.20 | 1.62 | 2.758E+05 | 613.59 | 3.501E+04 | Tl-208 |
| M | 17 | 2513- | 2548 | 2530.78 | 722.20 | 1.92 | 2.309E+03 | 97.79 | 5.018E+03 | Tl-208 |
| m | 18 | 2513- | 2548 | 2539.82 | 724.78 | 1.93 | 5.096E+04 | 249.59 | 5.596E+03 | Bi-212 |
| | 19 | 2657- | 2674 | 2665.74 | 760.71 | 1.63 | 4.625E+03 | 119.42 | 2.962E+03 | Tl-208 |
| | 20 | 2734- | 2751 | 2742.96 | 782.74 | 1.82 | 7.898E+03 | 133.78 | 3.077E+03 | Bi-212 |
| | 21 | 2864- | 2876 | 2869.10 | 818.73 | 1.90 | 2.529E+02 | 71.36 | 1.835E+03 | |
| | 22 | 2995- | 3014 | 3005.12 | 857.55 | 1.90 | 3.028E+04 | 213.69 | 4.393E+03 | Tl-208 |
| | 23 | 3110- | 3129 | 3119.89 | 890.30 | 1.95 | 2.473E+03 | 103.94 | 2.376E+03 | Bi-212 |
| | 24 | 3233- | 3249 | 3239.22 | 924.34 | 0.83 | 3.412E+02 | 78.71 | 1.866E+03 | Tl-208 |
| | 25 | 3314- | 3335 | 3325.01 | 948.82 | 1.68 | 1.222E+03 | 99.35 | 2.306E+03 | |
| | 26 | 3424- | 3442 | 3431.89 | 979.32 | 1.81 | 3.175E+02 | 86.44 | 2.115E+03 | Tl-208 |
| | 27 | 3756- | 3778 | 3767.27 | 1075.02 | 2.01 | 2.969E+03 | 112.91 | 2.525E+03 | Bi-212 |
| | 28 | 3810- | 3829 | 3819.77 | 1090.00 | 2.16 | 1.080E+03 | 90.69 | 2.040E+03 | Tl-208 |
| | 29 | 5270- | 5294 | 5284.19 | 1507.85 | 2.22 | 1.271E+03 | 108.73 | 2.557E+03 | Bi-212 |
| | 30 | 5366- | 5379 | 5372.05 | 1532.92 | 1.10 | -1.116E+01 | 61.56 | 1.378E+03 | |
| | 31 | 5548- | 5577 | 5562.64 | 1587.30 | 2.63 | 1.551E+04 | 184.02 | 3.859E+03 | 2nd escape peak |
| | 32 | 5646- | 5676 | 5661.32 | 1615.46 | 2.50 | 5.857E+03 | 158.28 | 3.936E+03 | Bi-212 |
| | 33 | 6295- | 6319 | 6309.38 | 1800.38 | 1.91 | 3.320E+02 | 115.79 | 3.165E+03 | |
| | 34 | 6556- | 6573 | 6562.06 | 1872.48 | 0.46 | 2.116E+02 | 86.58 | 2.238E+03 | |
| | 35 | 7332- | 7366 | 7349.52 | 2097.17 | 3.63 | 1.238E+04 | 211.31 | 6.005E+03 | 1st escape peak |

M = First peak in a multiplet region
m = Other peak in a multiplet region
F = Fitted singlet

Errors quoted at 1.000 sigma

**Figure S3-1.** Gamma spectrum peak analysis report for Pb-212 generator eluent

```
********************************************************************************
*****        G A M M A   S P E C T R U M   A N A L Y S I S          *****
********************************************************************************
```

**Purified Pb-212**

Filename: DET01

| | | |
|---|---|---|
| Report Generated On | : | 1/28/2019 2:00:35 PM |
| Sample Title | : | Sample title. |
| Sample Description | : | |
| Sample Identification | : | |
| Sample Type | : | |
| Sample Geometry | : | |
| Peak Locate Threshold | : | 3.00 |
| Peak Locate Range (in channels) | : | 1 - 65535 |
| Peak Area Range (in channels) | : | 1 - 65535 |
| Identification Energy Tolerance | : | 1.000 keV |
| Sample Size | : | 1.0000E+00 Unit |
| Sample Taken On | : | |
| Acquisition Started | : | 1/28/2019 1:38:49 PM |
| Live Time | : | 1200.0 seconds |
| Real Time | : | 1237.8 seconds |
| Dead Time | : | 3.05 % |

| | | |
|---|---|---|
| Energy Calibration Used Done On | : | 1/28/2019 |
| Efficiency Calibration Used Done On | : | ?????????? |
| Efficiency ID | : | |

**Purified Pb-212**

**********
***** PEAK ANALYSIS REPORT *****
**********

Detector Name: DET01
Sample Title: Sample title.
Peak Analysis Performed on: 1/28/2019 2:00:35 PM
Peak Analysis From Channel: 1
Peak Analysis To Channel: 8192

| | Peak No. | ROI start | ROI end | Peak centroid | Energy (keV) | FWHM (keV) | Net Peak Area | Net Area Uncert. | Continuum Counts | |
|---|---|---|---|---|---|---|---|---|---|---|
| | 1 | 22- | 34 | 28.91 | 8.32 | 1.76 | 3.078E+04 | 356.05 | 3.377E+04 | |
| M | 2 | 249- | 276 | 255.76 | 73.05 | 1.00 | 1.773E+04 | 204.08 | 3.860E+04 | Tl-208 |
| m | 3 | 249- | 276 | 262.47 | 74.97 | 1.00 | 1.175E+05 | 380.69 | 3.615E+04 | Pb-212 |
| m | 4 | 249- | 276 | 270.29 | 77.20 | 1.00 | 1.628E+05 | 434.51 | 3.167E+04 | Pb-212 |
| M | 5 | 291- | 320 | 297.30 | 84.90 | 1.20 | 1.627E+04 | 189.44 | 3.049E+04 | Pb-212 |
| m | 6 | 291- | 320 | 305.52 | 87.25 | 1.20 | 8.184E+04 | 323.79 | 2.785E+04 | Pb-212 |
| m | 7 | 291- | 320 | 314.84 | 89.91 | 1.20 | 2.560E+04 | 207.67 | 2.499E+04 | Pb-212 |
| | 8 | 402- | 403 | 403.39 | 115.17 | 0.29 | 3.385E+03 | 103.53 | 5.487E+03 | Pb-212 |
| | 9 | 511- | 514 | 513.00 | 146.45 | 0.29 | 2.581E+01 | 99.37 | 6.436E+03 | |
| | 10 | 753- | 758 | 756.00 | 215.79 | 0.29 | 1.252E+02 | 119.65 | 8.017E+03 | |
| | 11 | 831- | 836 | 833.96 | **238.03** | 0.99 | 5.404E+05 | 793.13 | 5.024E+04 | Pb-212 |
| | 12 | 965- | 972 | 969.14 | 276.61 | 1.04 | 8.447E+03 | 121.77 | 3.189E+03 | Tl-208 |
| | 13 | 1003- | 1010 | 1006.77 | 287.34 | 1.05 | 1.435E+03 | 83.09 | 2.723E+03 | Bi-212 |
| | 14 | 1044- | 1052 | 1048.63 | 299.29 | 1.10 | 3.519E+04 | 210.12 | 4.215E+03 | Pb-212 |
| | 15 | 1576- | 1587 | 1581.72 | 451.40 | 1.15 | 9.459E+02 | 71.01 | 1.635E+03 | Bi-212 |
| | 16 | 1777- | 1789 | 1783.71 | 509.03 | 1.37 | 1.906E+04 | 163.26 | 2.894E+03 | Tl-208 |
| | 17 | 2029- | 2043 | 2036.76 | **581.24** | 1.35 | 5.420E+04 | 245.73 | 2.147E+03 | Tl-208 |
| M | 18 | 2515- | 2548 | 2521.49 | 719.55 | 1.54 | 1.336E+02 | 22.69 | 5.466E+02 | Tl-208 |
| m | 19 | 2515- | 2548 | 2539.93 | 724.81 | 1.55 | 1.058E+04 | 105.73 | 6.377E+02 | Bi-212 |
| | 20 | 2658- | 2674 | 2665.92 | 760.76 | 1.41 | 8.835E+02 | 47.82 | 4.495E+02 | |
| | 21 | 2734- | 2751 | 2743.31 | 782.84 | 1.60 | 1.712E+03 | 56.17 | 4.435E+02 | Bi-212 |
| | 22 | 2791- | 2798 | 2794.06 | 797.32 | 0.76 | 9.269E+00 | 19.14 | 1.767E+02 | Tl-208 |
| | 23 | 2914- | 2923 | 2919.12 | 833.01 | 0.85 | 3.228E+01 | 22.30 | 2.057E+02 | |
| | 24 | 2996- | 3014 | 3005.51 | 857.66 | 1.59 | 5.467E+03 | 84.91 | 5.168E+02 | Tl-208 |
| | 25 | 3111- | 3130 | 3120.36 | 890.43 | 1.57 | 4.821E+02 | 44.72 | 4.319E+02 | Bi-212 |
| | 26 | 3318- | 3335 | 3325.13 | 948.86 | 1.90 | 2.404E+02 | 38.39 | 3.756E+02 | |
| | 27 | 3422- | 3441 | 3432.73 | 979.56 | 1.30 | 9.457E+01 | 36.21 | 3.454E+02 | Tl-208 |
| | 28 | 3609- | 3620 | 3613.56 | 1031.16 | 0.38 | 2.107E+01 | 22.79 | 1.959E+02 | |
| | 29 | 3760- | 3778 | 3767.73 | 1075.15 | 1.21 | 5.446E+02 | 42.12 | 3.634E+02 | Bi-212 |
| | 30 | 3809- | 3831 | 3820.70 | 1090.26 | 1.34 | 2.639E+02 | 40.97 | 3.651E+02 | Tl-208 |
| | 31 | 5094- | 5113 | 5102.73 | 1456.08 | 0.86 | 1.198E+02 | 38.62 | 3.892E+02 | |
| | 32 | 5276- | 5293 | 5284.32 | 1507.89 | 2.04 | 2.848E+02 | 34.50 | 2.772E+02 | Bi-212 |
| | 33 | 5551- | 5577 | 5563.40 | 1587.52 | 2.21 | 2.634E+03 | 71.19 | 5.473E+02 | 2nd escape peak |
| | 34 | 5647- | 5674 | 5662.43 | 1615.78 | 2.00 | 1.134E+03 | 61.93 | 6.006E+02 | Bi-212 |
| | 35 | 5729- | 5740 | 5734.38 | 1636.31 | 0.44 | -1.090E+01 | 24.59 | 2.439E+02 | |
| | 36 | 6302- | 6317 | 6310.13 | 1800.59 | 0.29 | 4.054E+01 | 32.82 | 3.445E+02 | |
| | 37 | 6810- | 6824 | 6817.69 | 1945.42 | 0.59 | 2.577E+01 | 31.40 | 3.332E+02 | |
| | 38 | 7133- | 7146 | 7139.99 | 2037.38 | 0.46 | 5.350E+01 | 27.85 | 2.625E+02 | |
| | 39 | 7332- | 7367 | 7350.27 | 2097.38 | 3.65 | 2.239E+03 | 87.07 | 9.714E+02 | 1st escape peak |

M = First peak in a multiplet region
m = Other peak in a multiplet region
F = Fitted singlet

**Figure S3-2.** Gamma spectrum peak analysis report for purified Pb-212

**Table S3-1. [$^{212}$Pb]Pb-RM2 biodistribution in PC3 tumor bearing mice**
**Data shown as mean ± SD %ID (n = 6 mice per time point)**

| Tissue | 15 min | 30 min | 1 h | 2 h * | 4 h* | 24 h | 48 h |
|---|---|---|---|---|---|---|---|
| **Blood** | 7.39 ± 2.94 | 3.36 ± 1.39 | 1.12 ± 0.54 | 0.17 ± 0.11 | 0.06 ± 0.07 | 0.03 ± 0.04 | 0.12 ± 0.19 |
| **Heart** | 0.17 ± 0.07 | 0.08 ± 0.03 | 0.02 ± 0.02 | 0.00 ± 0.01 | 0.01 ± 0.02 | 0.01 ± 0.02 | 0.03 ± 0.07 |
| **Lung** | 0.54 ± 0.24 | 0.29 ± 0.12 | 0.10 ± 0.05 | 0.03 ± 0.01 | 0.02 ± 0.02 | 0.02 ± 0.02 | 0.04 ± 0.08 |
| **Liver** | 4.44 ± 2.01 | 2.82 ± 1.44 | 1.56 ± 0.67 | 0.58 ± 0.09 | 0.32 ± 0.12 | 0.08 ± 0.04 | 0.08 ± 0.09 |
| **Stomach** | 0.68 ± 0.29 | 0.29 ± 0.12 | 0.31 ± 0.17 | 0.18 ± 0.19 | 0.07 ± 0.03 | 0.01 ± 0.03 | 0.06 ± 0.08 |
| **Sm. Intestines** | 4.05 ± 1.99 | 1.90 ± 0.99 | 1.49 ± 0.72 | 0.72 ± 0.55 | 0.27 ± 0.13 | 0.10 ± 0.05 | 0.06 ± 0.07 |
| **Lg. Intestines** | 1.34 ± 0.56 | 0.60 ± 0.25 | 0.45 ± 0.18 | 0.69 ± 0.18 | 0.68 ± 0.18 | 0.45 ± 0.34 | 0.13 ± 0.15 |
| **Kidney** | 6.96 ± 3.03 | 5.57 ± 2.24 | 4.98 ± 1.94 | 2.30 ± 0.52 | 1.42 ± 0.39 | 0.41 ± 0.17 | 0.17 ± 0.14 |
| **Spleen** | 0.10 ± 0.04 | 0.09 ± 0.04 | 0.03 ± 0.01 | 0.01 ± 0.01 | 0.01 ± 0.01 | 0.01 ± 0.01 | 0.03 ± 0.05 |
| **Brain** | 0.07 ± 0.03 | 0.04 ± 0.02 | 0.02 ± 0.02 | 0.00 ± 0.00 | 0.01 ± 0.02 | 0.00 ± 0.00 | 0.03 ± 0.06 |
| **Pancreas** | 7.03 ± 3.71 | 1.93 ± 1.00 | 1.42 ± 0.77 | 0.48 ± 0.44 | 0.07 ± 0.04 | 0.02 ± 0.02 | 0.01 ± 0.02 |
| **Muscle** | 0.16 ± 0.07 | 0.08 ± 0.04 | 0.02 ± 0.01 | 0.01 ± 0.01 | 0.01 ± 0.01 | 0.01 ± 0.01 | 0.05 ± 0.06 |
| **Bone** | 0.16 ± 0.07 | 0.08 ± 0.04 | 0.03 ± 0.02 | 0.01 ± 0.01 | 0.01 ± 0.01 | 0.01 ± 0.01 | 0.03 ± 0.04 |
| **Tumors** | 1.26 ± 0.44 | 1.28 ± 0.43 | 1.08 ± 0.42 | 1.31 ± 0.62 | 1.15 ± 0.51 | 0.75 ± 0.22 | 0.47 ± 0.24 |
| **Urine (%ID)** | 33.67 ± 11.23 | 62.93 ± 8.67 | 76.73 ± 2.16 | 89.87 ± 2.04 | 93.76 ± 1.40 | 92.92 ± 3.17 | 88.28± 10.58 |
| **Excretion (%ID)** | 33.67 ± 11.23 | 62.93 ± 8.67 | 76.73 ± 2.16 | 89.87 ± 2.04 | 93.76 ± 1.40 | 96.89 ± 0.38 | 98.11± 1.18 |

* n = 7
Note: Values for urine include radioactivity measured in bladder and cage paper

| **Table S3-2.** ICP-MS analysis of crude and purified $^{212}$Pb samples ** | | | | | |
|---|---|---|---|---|---|
| Sample ID | Date | Description | Fe (ng) | Zn (ng) | Pb (ng) |
| **Generator 3** | | | | | |
| T 1 | 09/19/2018 | 2M HCl | 6.00 | 0.50 | 3.46 |
| T 2 | 09/19/2018 | 0.5M NaOAc | <LOD | 0.71 | 0.30 |
| T 3 | 09/19/2018 | Crude Pb-212 | 113 | 20.7 | 50.9 |
| T 4 | 09/19/2018 | Purified Pb-212 | 6.12 | 7.20 | 40.0 |
| T 5 | 09/20/2018 | Crude Pb-212 | 65.2 | 40.6 | 90.7 |
| T 6 | 09/20/2018 | Purified Pb-212 | 1.77 | 14.7 | 32.0 |
| T 7 | 09/21/2018 | Crude Pb-212 | 22.2 | 24.4 | 82.4 |
| T 8 | 09/21/2018 | Purified Pb-212 | 1.30 | 13.2 | 28.6 |
| T 9 | 09/24/2018 | Crude Pb-212 | 37.7 | 27.3 | 5.06 |
| T 10 | 09/24/2018 | Purified Pb-212 | 1.70 | 8.44 | 16.5 |
| T 11 | 09/26/2018 | Crude Pb-212 | 18.3 | 29.0 | 17.3 |
| T 12 | 09/26/2018 | Purified Pb-212 | 1.02 | 8.25 | 48.1 |
| T 13 | 09/28/2018 | Crude Pb-212 | 17.5 | 24.4 | 4.83 |
| T 14 | 09/28/2018 | Purified Pb-212 | 1.93 | 7.18 | 9.51 |
| **Generator 4** | | | | | |
| T 18 | 10/10/2018 | Crude Pb-212 | 104 | 22.2 | 42.7 |
| T 19 | 10/10/2018 | Purified Pb-212 | <LOD | 2.43 | 30.1 |
| T 20 | 10/11/2018 | Crude Pb-212 | 121 | 23.1 | 14.5 |
| T 26 | 10/11/2018 | Purified Pb-212 | <LOD | 2.02 | 6.53 |
| T 27 | 10/12/2018 | Crude Pb-212 | 96.8 | 34.8 | 6.01 |
| T 28 | 10/12/2018 | Purified Pb-212 | <LOD | 3.28 | 4.80 |
| T 29 | 10/15/2018 | Crude Pb-212 | 243 | 28.0 | 2.58 |
| T 30 | 10/15/2018 | Purified Pb-212 | <LOD | 2.04 | 4.01 |
| T 31 | 10/16/2018 | Crude Pb-212 | 137 | 24.2 | 8.39 |
| ** Each sample contains 200 μL | | | | | |

# Supplementary Data – Chapter 4

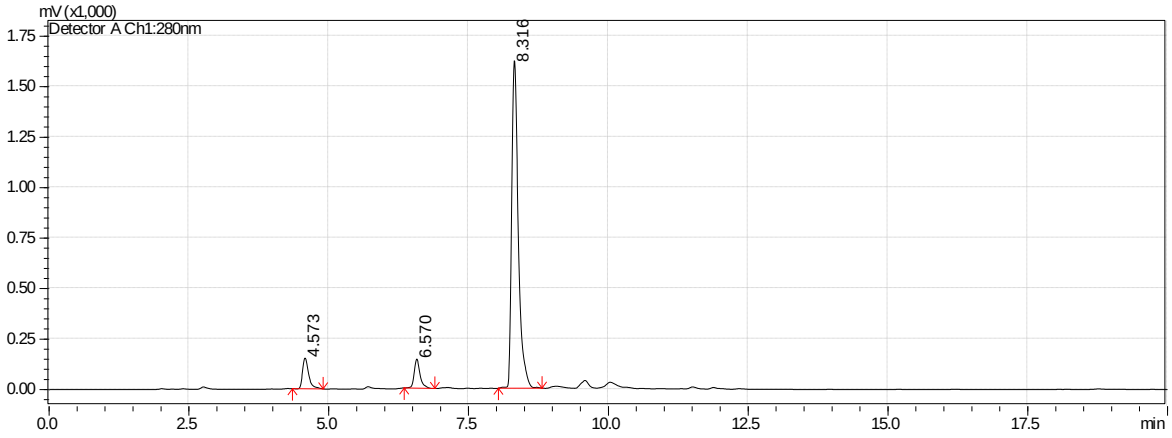


**Figure S4-1A.** HPLC spectrum for reaction 1

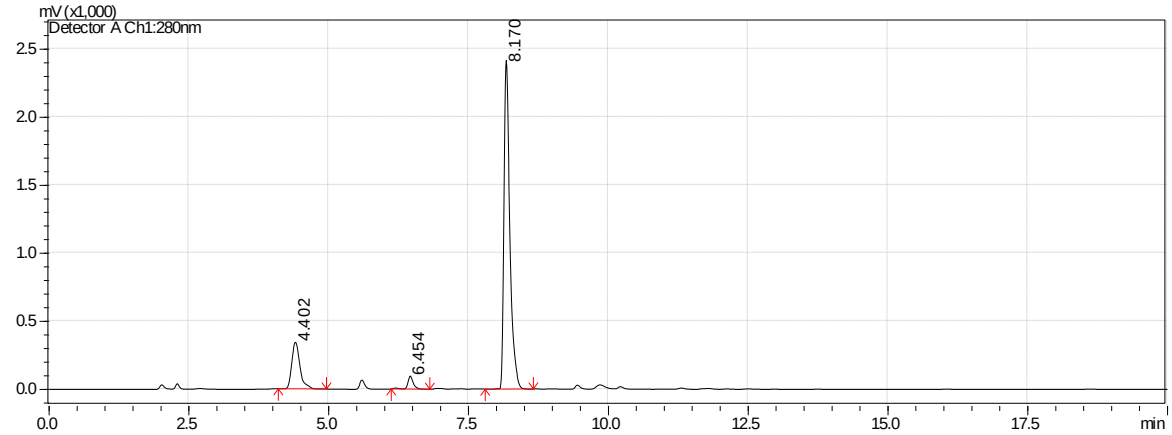


**Figure S4-1B.** HPLC spectrum for reaction 2

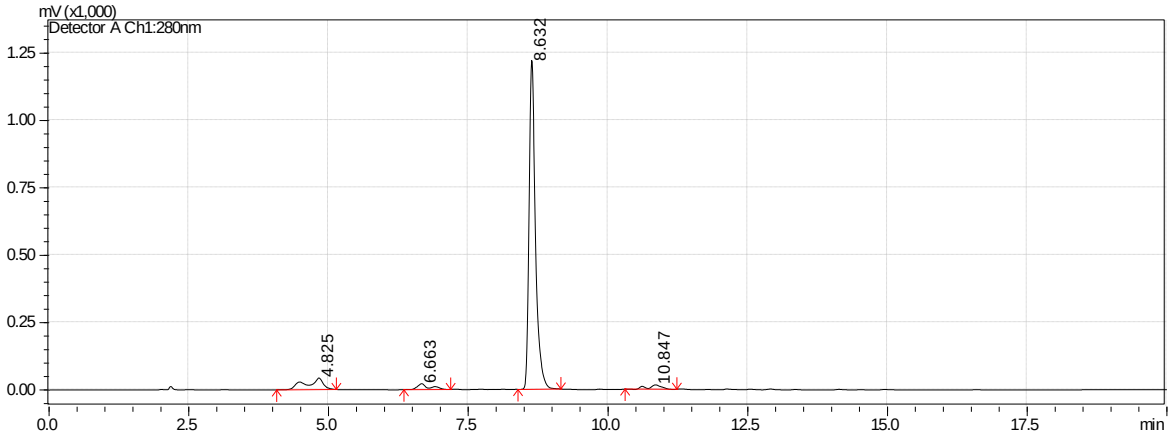


**Figure S4-1C.** HPLC spectrum for reaction 3

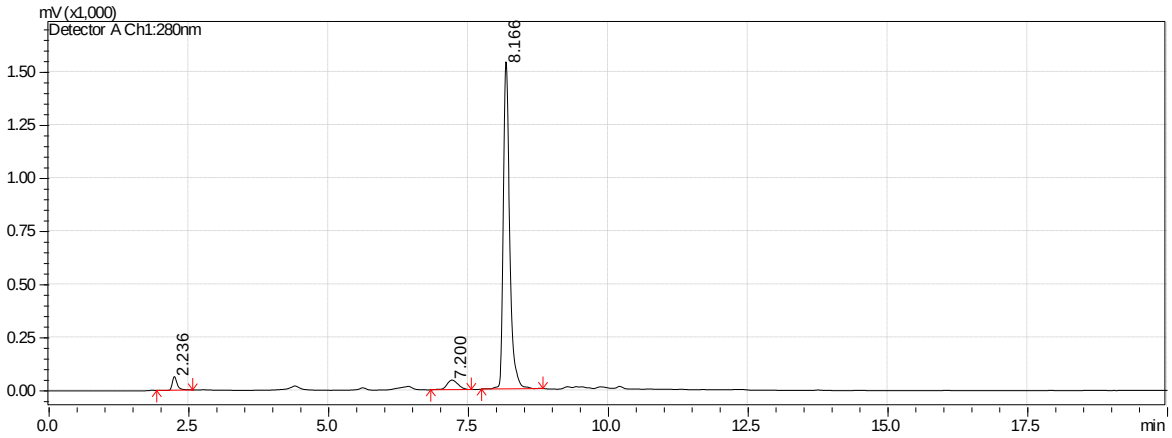


**Figure S4-1D.** HPLC spectrum for reaction 4

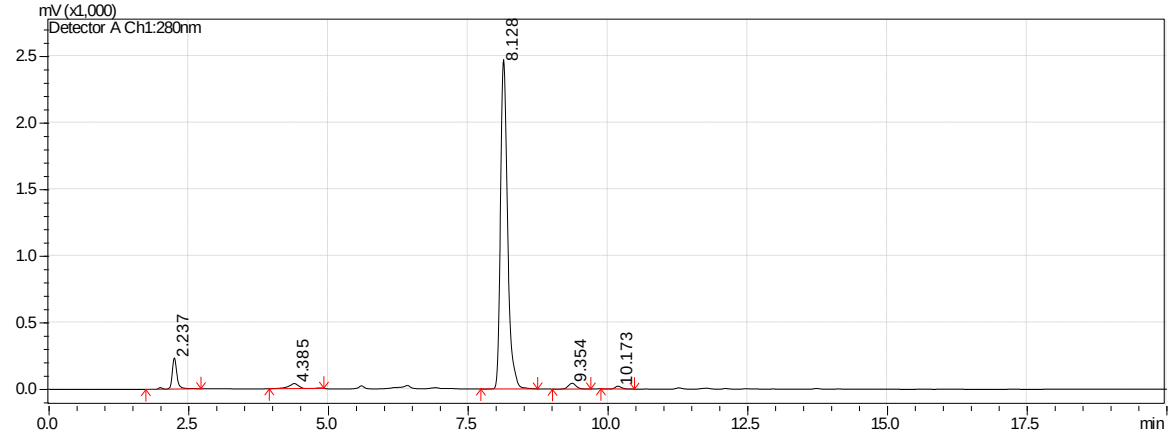


**Figure S4-1E.** HPLC spectrum for reaction 5

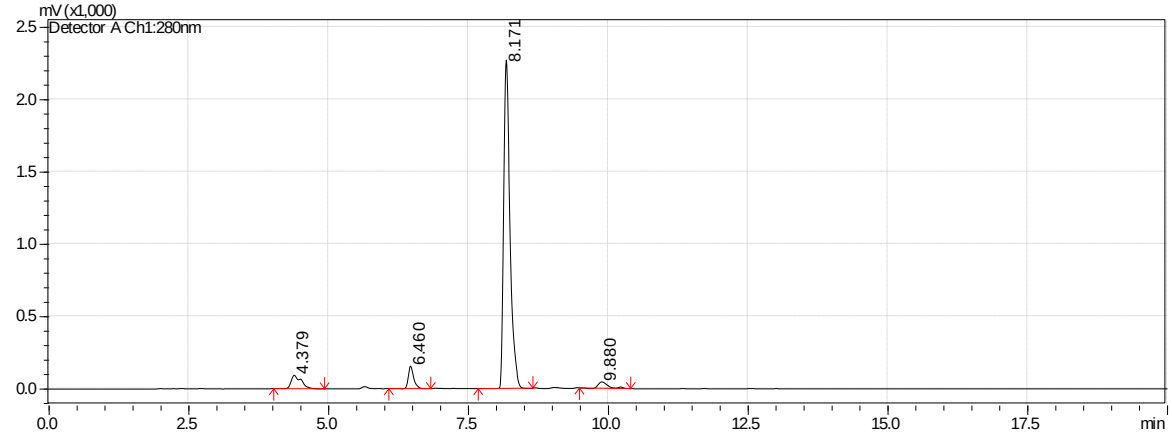


**Figure S4-1F.** HPLC spectrum for reaction 6

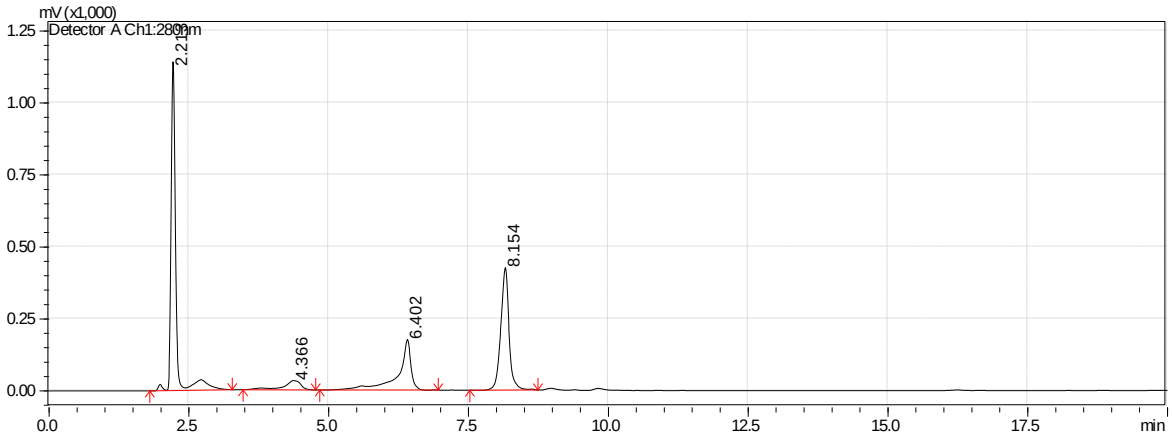


**Figure S4-1G.** HPLC spectrum for reaction 7

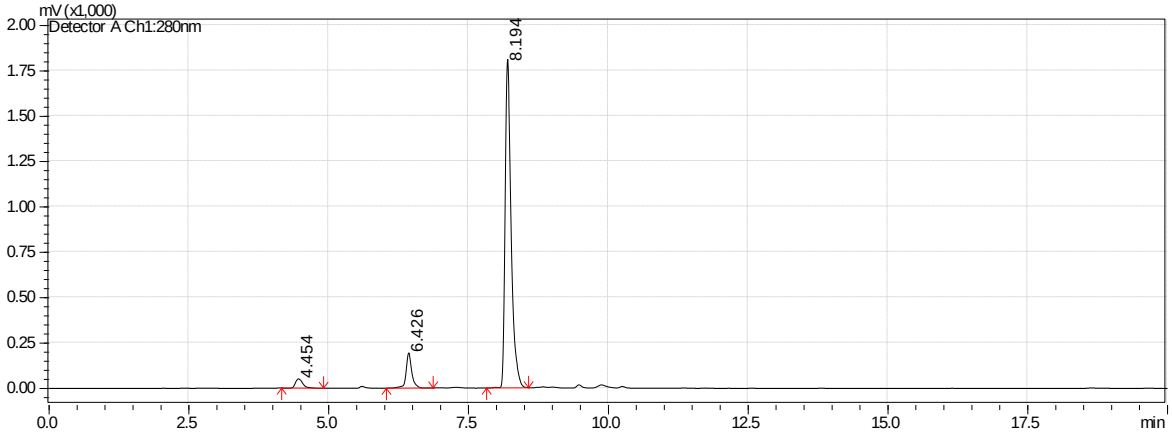


**Figure S4-1H.** HPLC spectrum for reaction 8

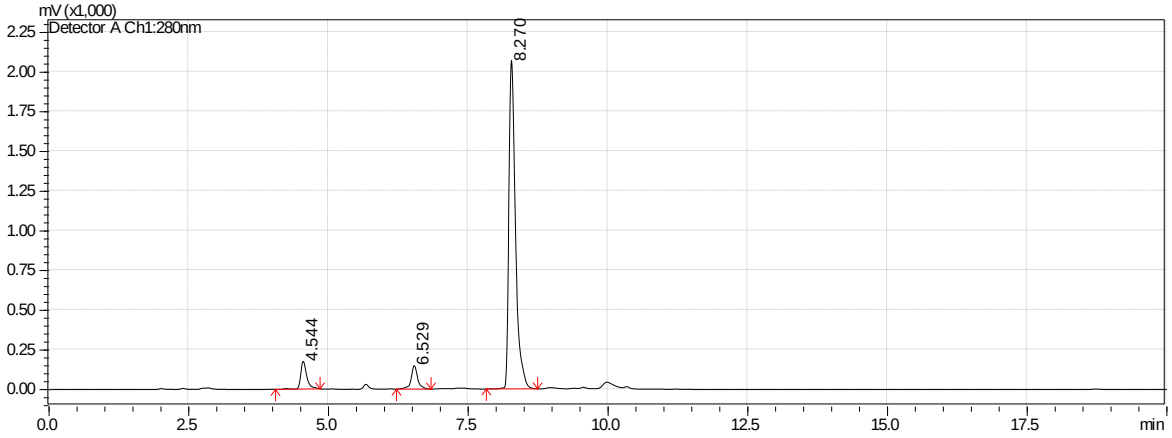


**Figure S4-1I.** HPLC spectrum for reaction 9

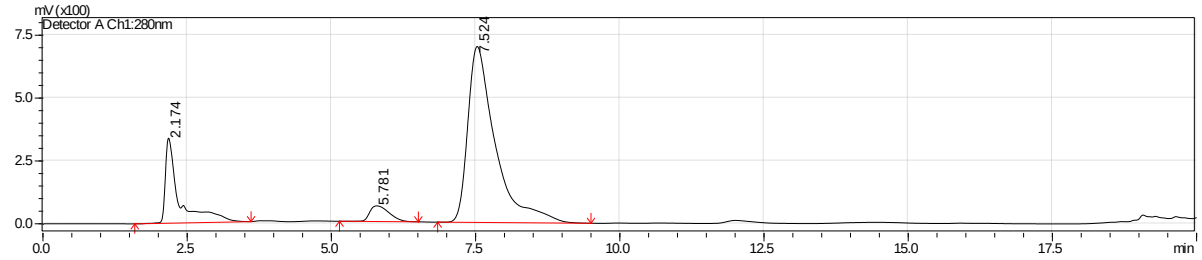


**Figure S4-2A.** HPLC spectrum for reaction 10

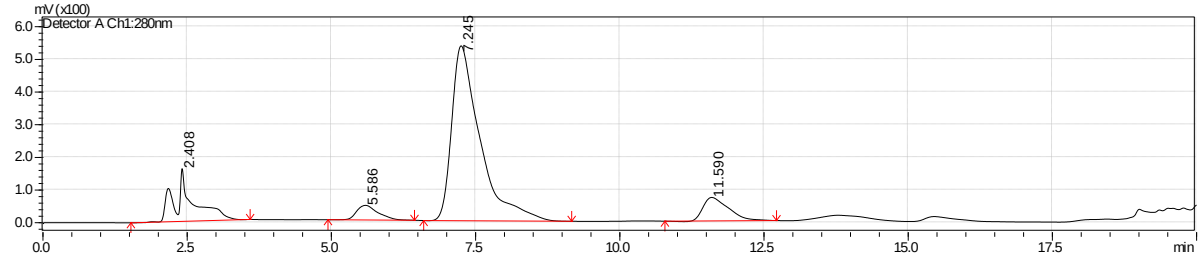


**Figure S4-2B.** HPLC spectrum for reaction 11

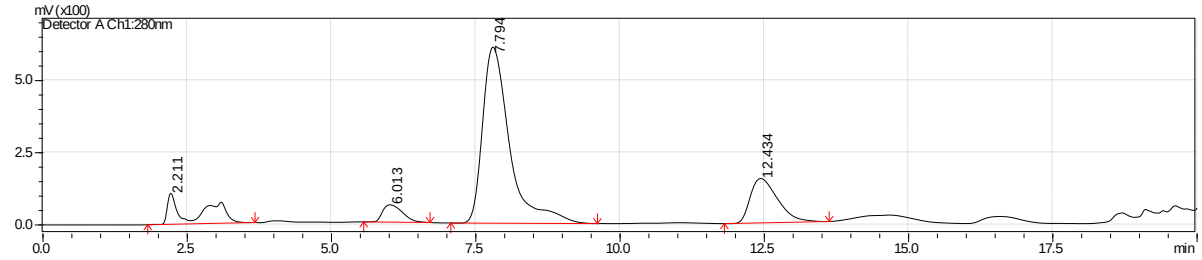


**Figure S4-2C.** HPLC spectrum for reaction 12

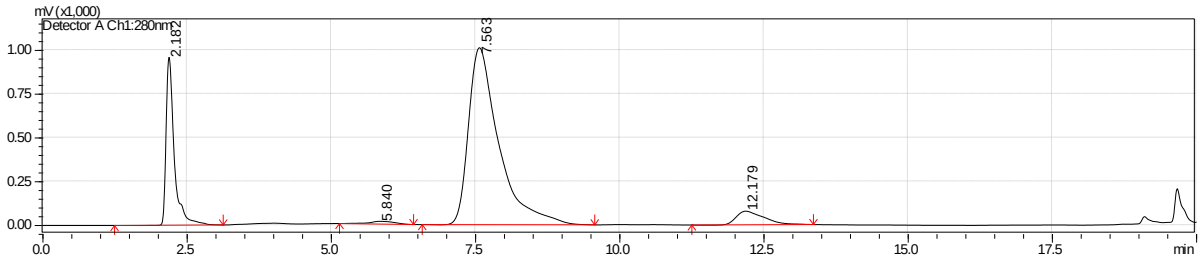


**Figure S4-2D.** HPLC spectrum for reaction 13

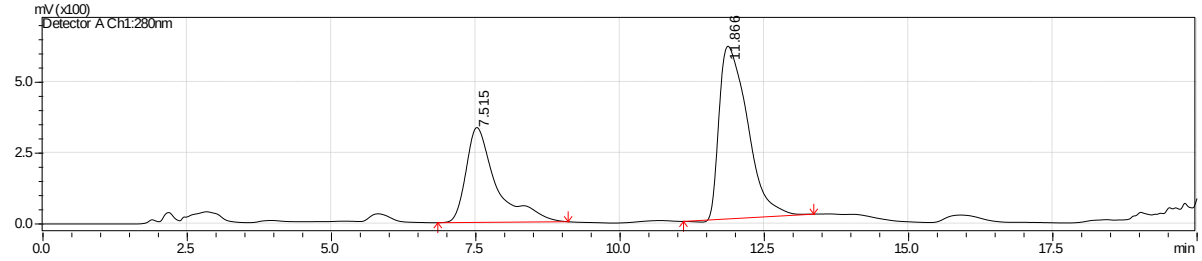


**Figure S4-2E.** HPLC spectrum for reaction 14

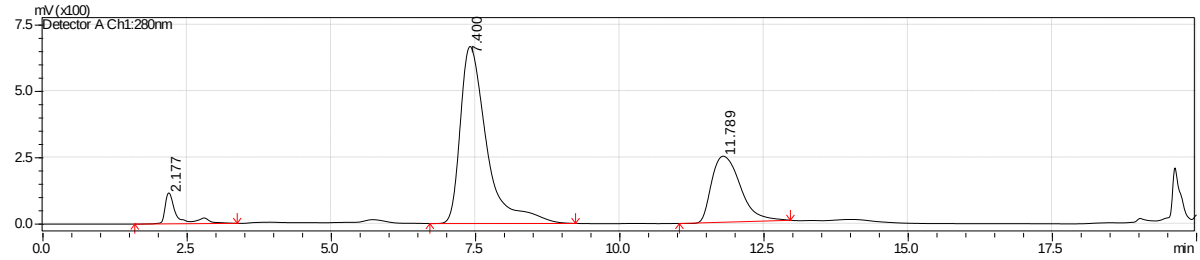


**Figure S4-2F.** HPLC spectrum for reaction 15

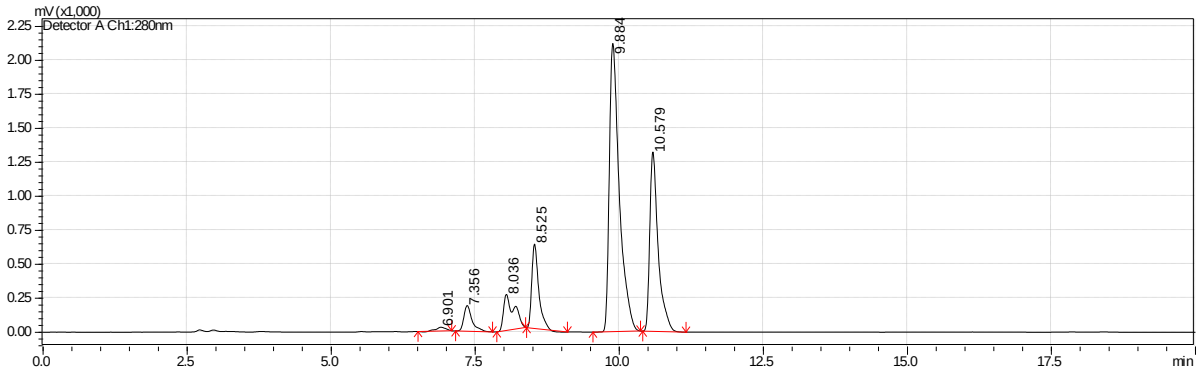


**Figure S4-3A.** HPLC spectrum for reaction 16

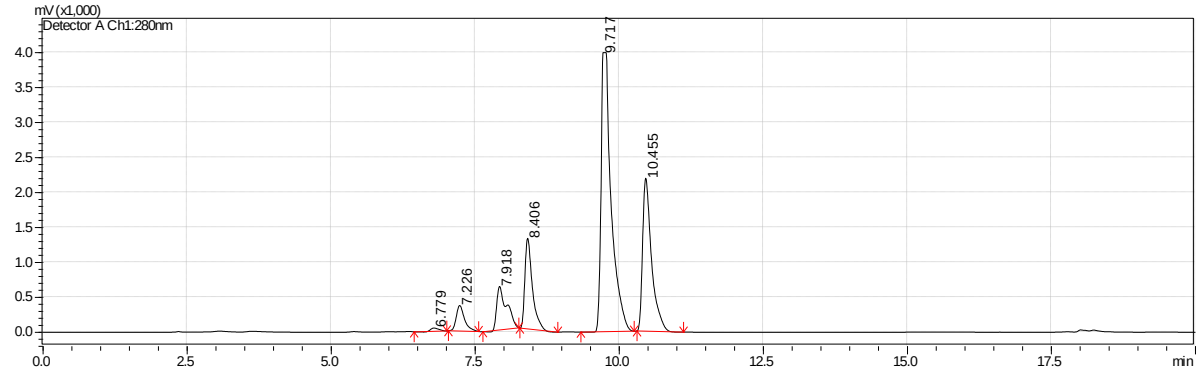


**Figure S4-3B.** HPLC spectrum for reaction 17

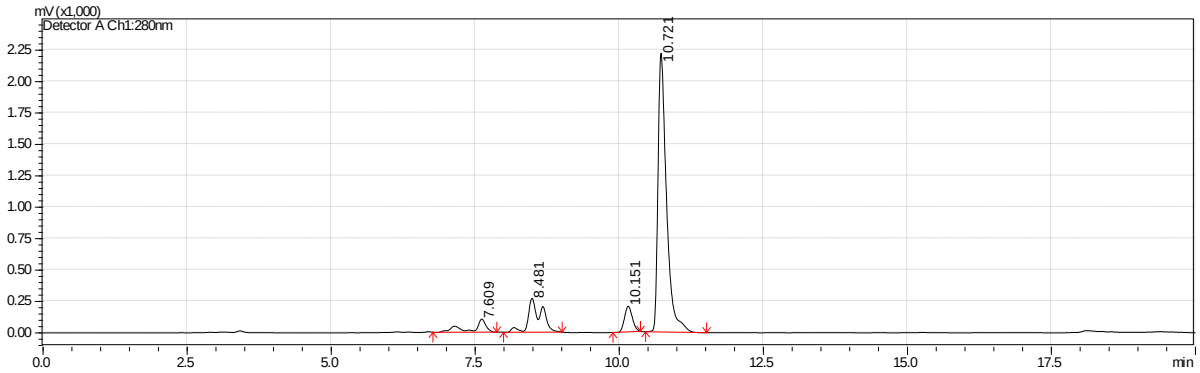


**Figure S4-3C.** HPLC spectrum for reaction 18

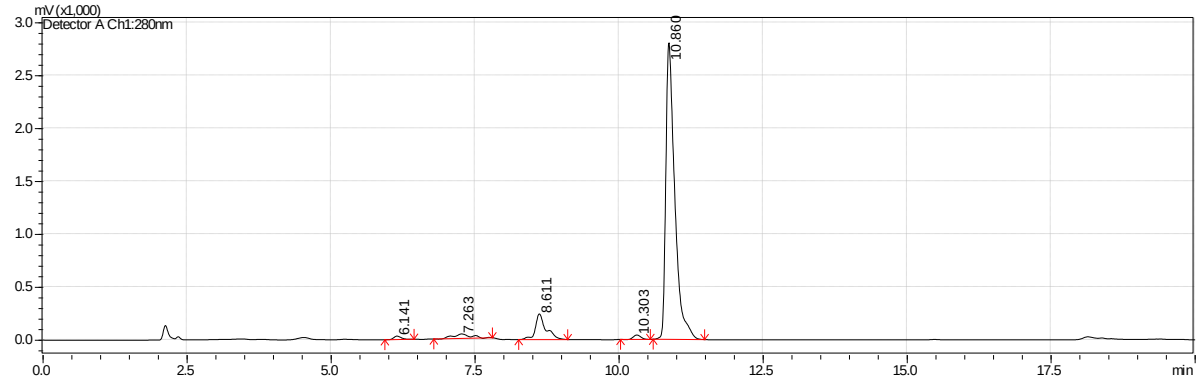


**Figure S4-3D.** HPLC spectrum for reaction 19

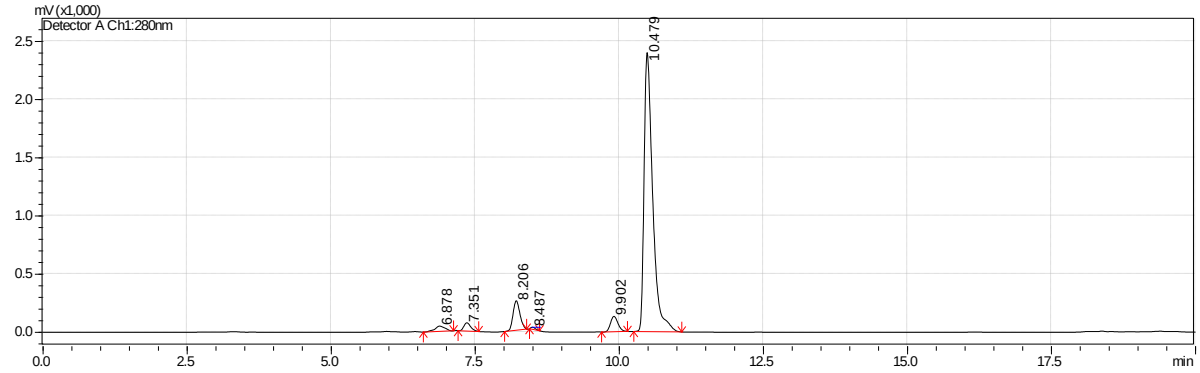


**Figure S4-3E.** HPLC spectrum for reaction 20

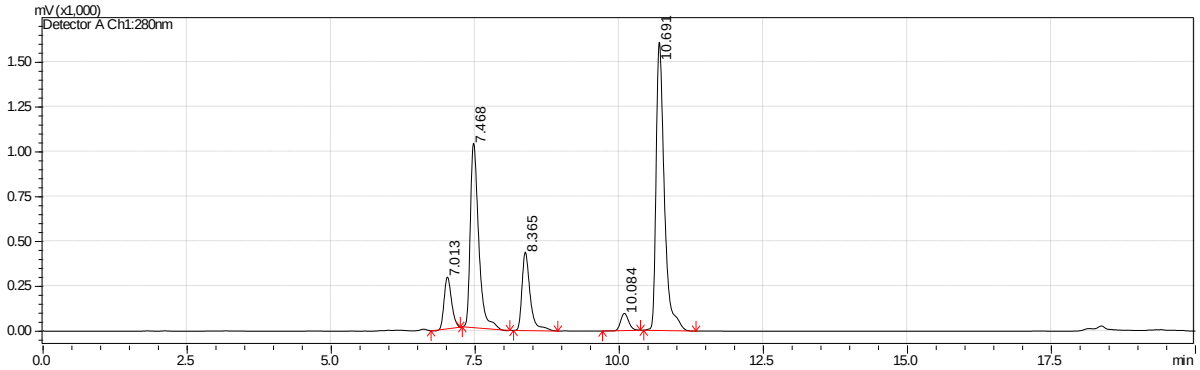


**Figure S4-3F.** HPLC spectrum for reaction 21

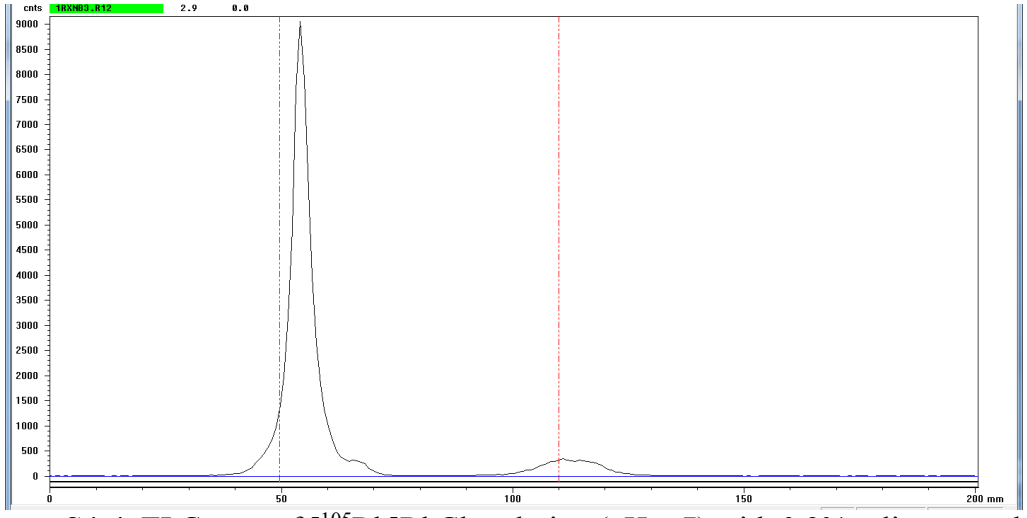


**Figure S4-4.** TLC scan of [$^{105}$Rh]$RhCl_3$ solution (pH > 7) with 0.9% saline as mobile phase

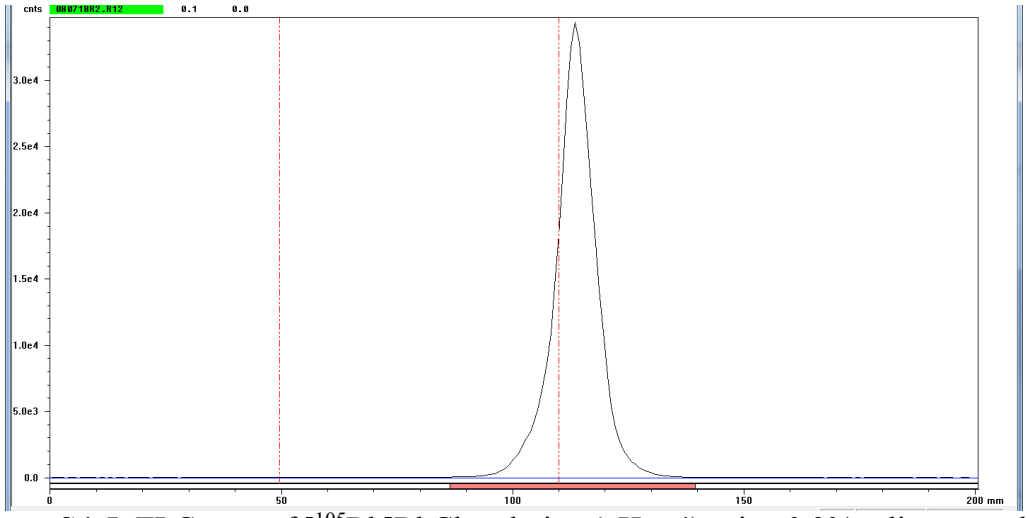


**Figure S4-5.** TLC scan of [$^{105}$Rh]$RhCl_3$ solution (pH ~ 4) using 0.9% saline as mobile phase

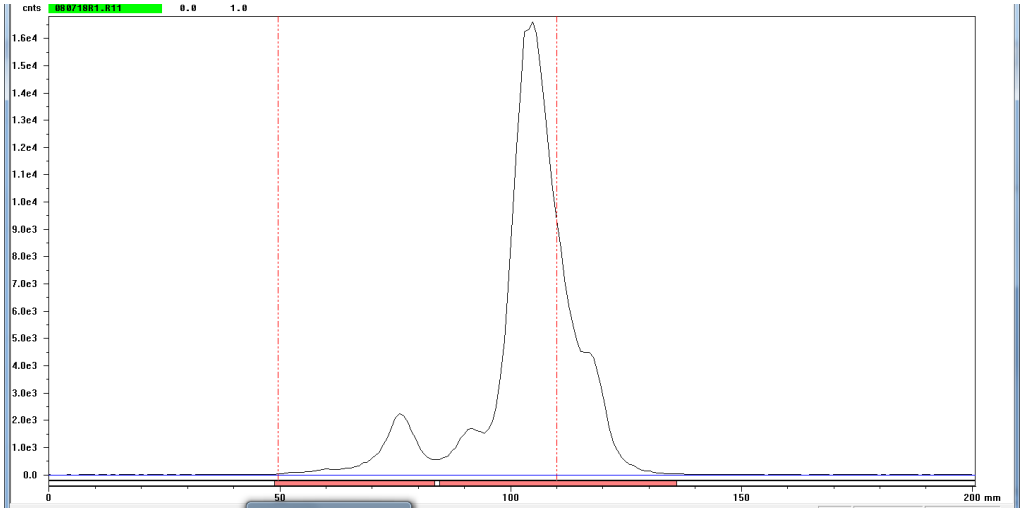


**Figure S4-6.** TLC scan of [$^{105}$**Rh]RhCl$_2$-*222S$_4$diAcOH*** using 0.9% saline as mobile phase

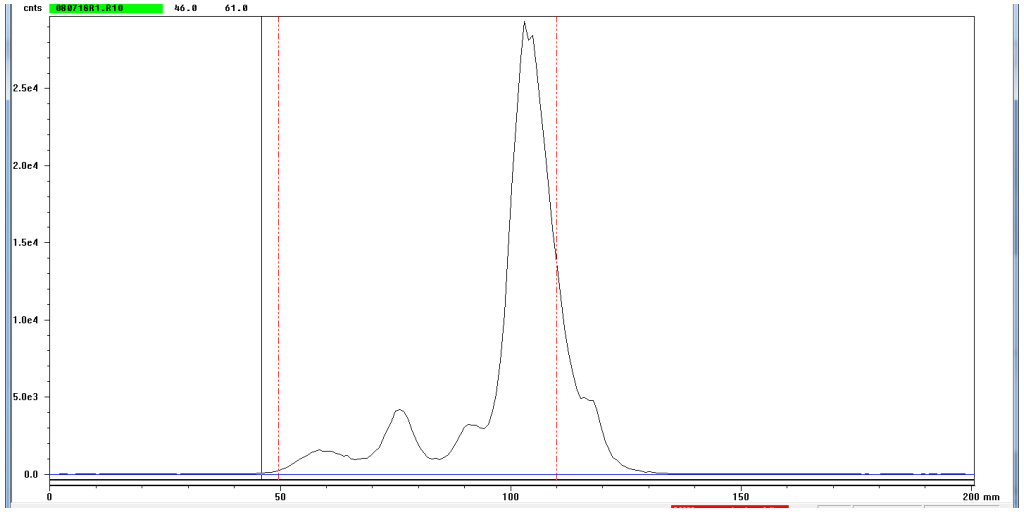


**Figure S4-7.** TLC scan of [$^{105}$**Rh]RhCl$_2$-*222S$_4$diAcOMe*** using 0.9% saline as mobile phase

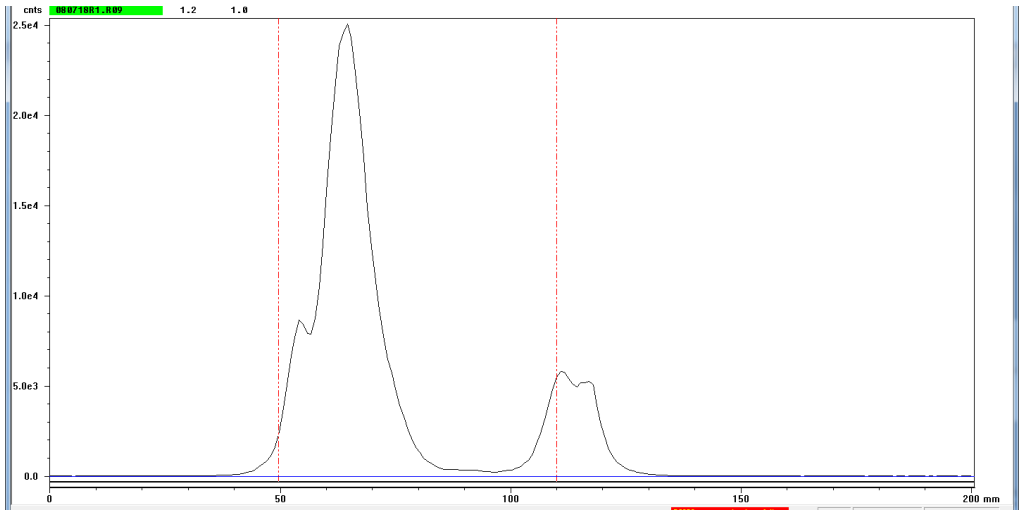


**Figure S4-8.** TLC scan of [$^{105}$**Rh]RhCl$_2$-*16S$_4$diol*** using 0.9% saline as mobile phase

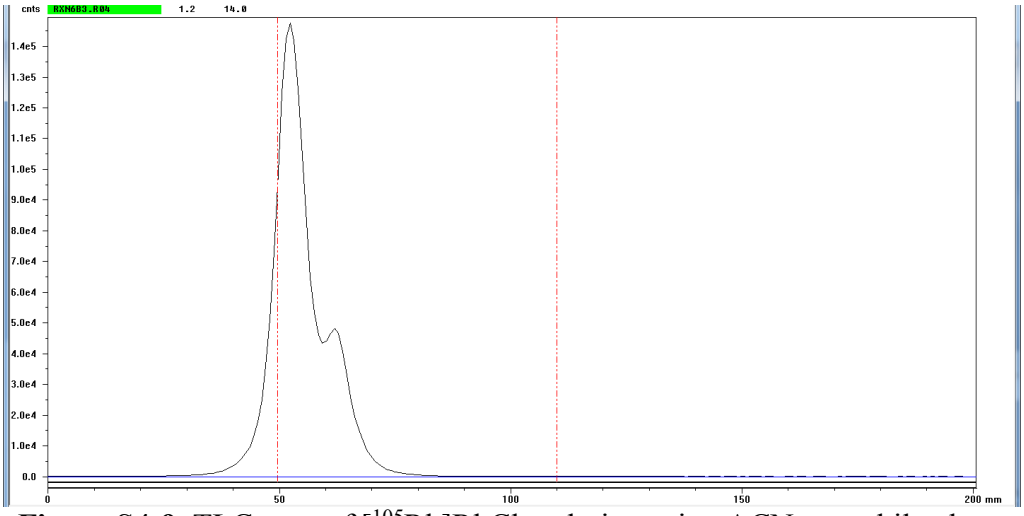


**Figure S4-9.** TLC scan of [$^{105}$Rh]RhCl$_3$ solution using ACN as mobile phase

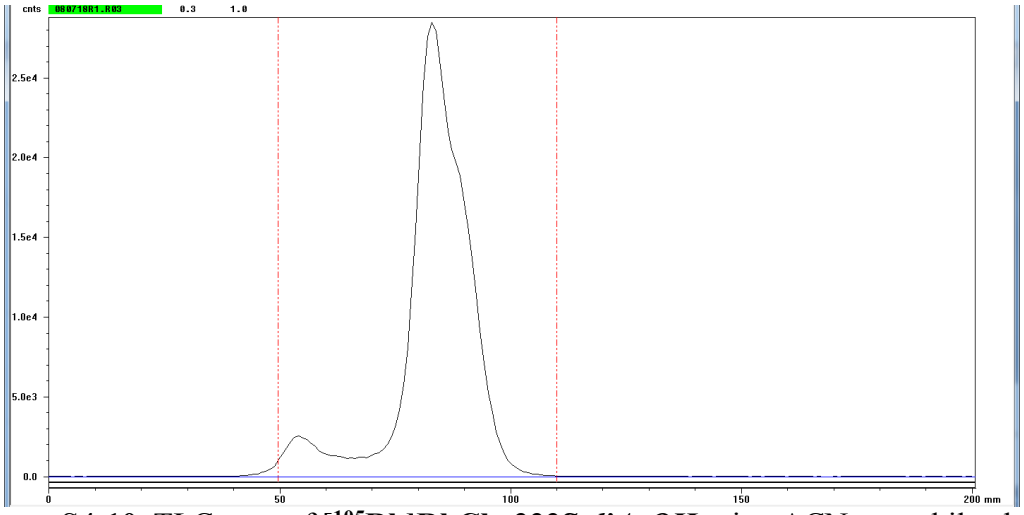


**Figure S4-10.** TLC scan of [$^{105}$**Rh]RhCl$_2$-*222S$_4$diAcOH*** using ACN as mobile phase

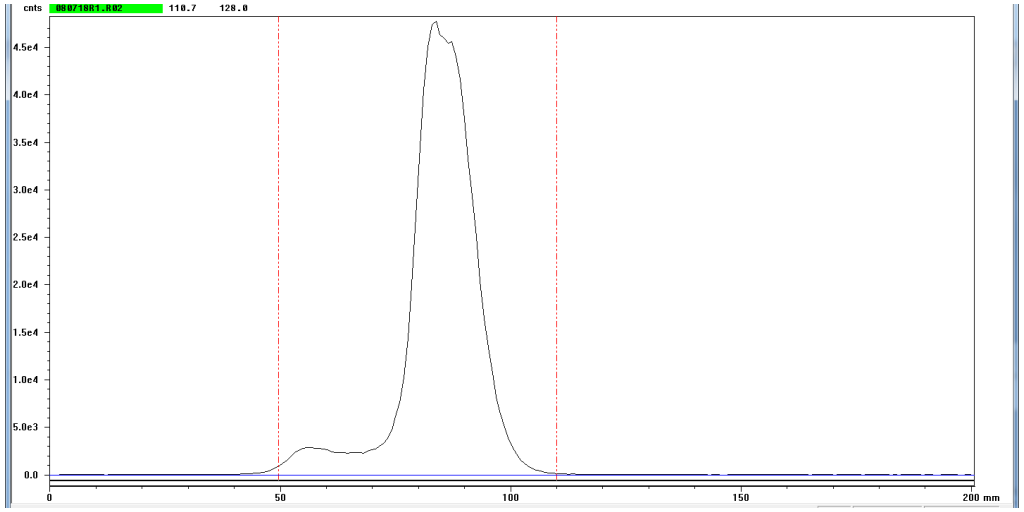


**Figure S4-11.** TLC scan of [$^{105}$**Rh]RhCl$_2$-*222S$_4$diAcOMe*** using ACN as mobile phase

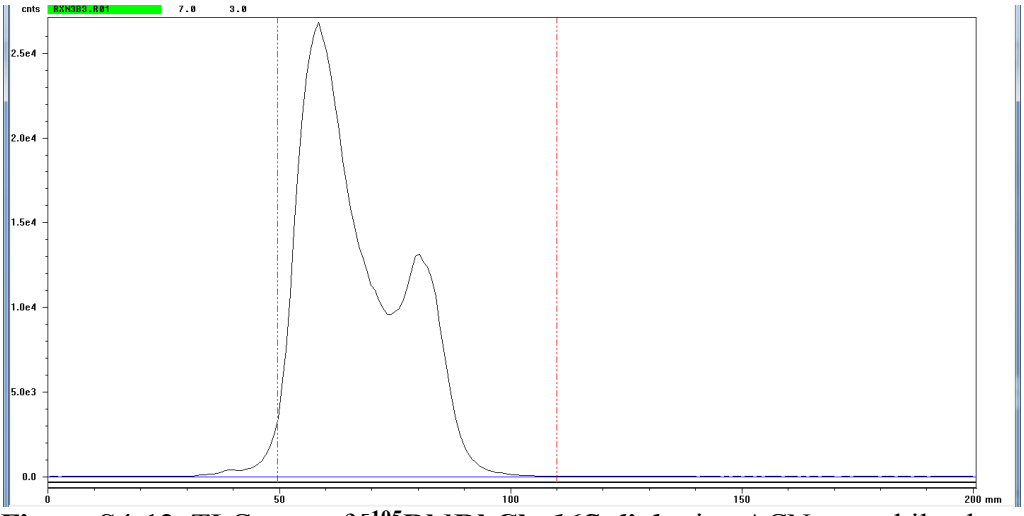


**Figure S4-12.** TLC scan of [$^{105}$**Rh]RhCl$_2$-*16S$_4$diol*** using ACN as mobile phase

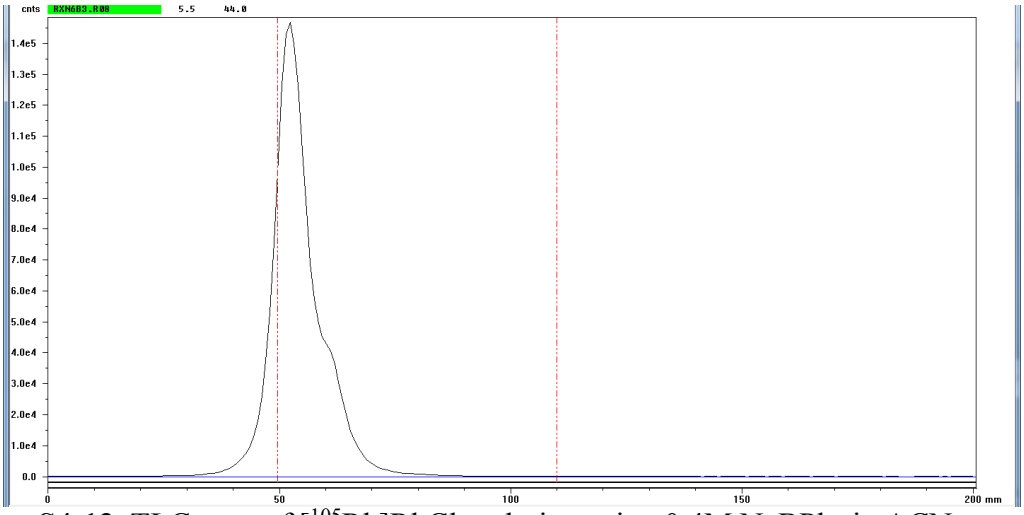


**Figure S4-13.** TLC scan of [$^{105}$Rh]RhCl$_3$ solution using 0.4M NaBPh$_4$ in ACN as mobile phase

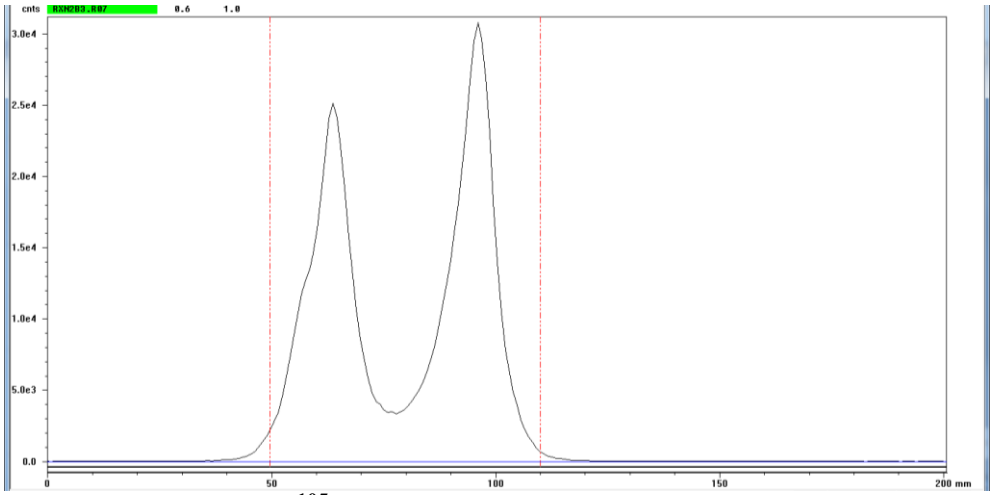


**Figure S4-14.** TLC scan of [$^{105}$**Rh]RhCl$_2$-*222S$_4$diAcOH*** using 0.4M $NaBPh_4$ in ACN as mobile phase

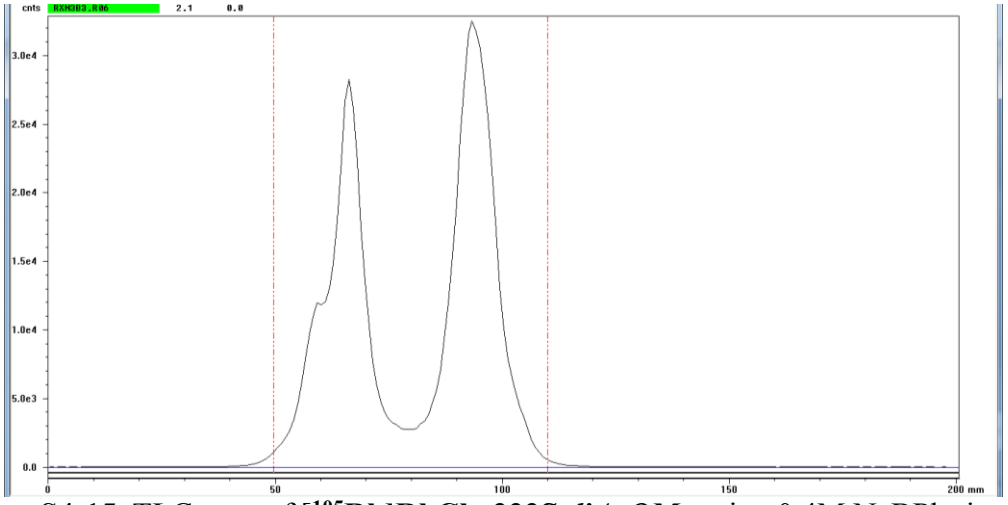


**Figure S4-15.** TLC scan of [$^{105}$**Rh]RhCl$_2$-*222S$_4$diAcOMe*** using 0.4M $NaBPh_4$ in ACN as mobile phase

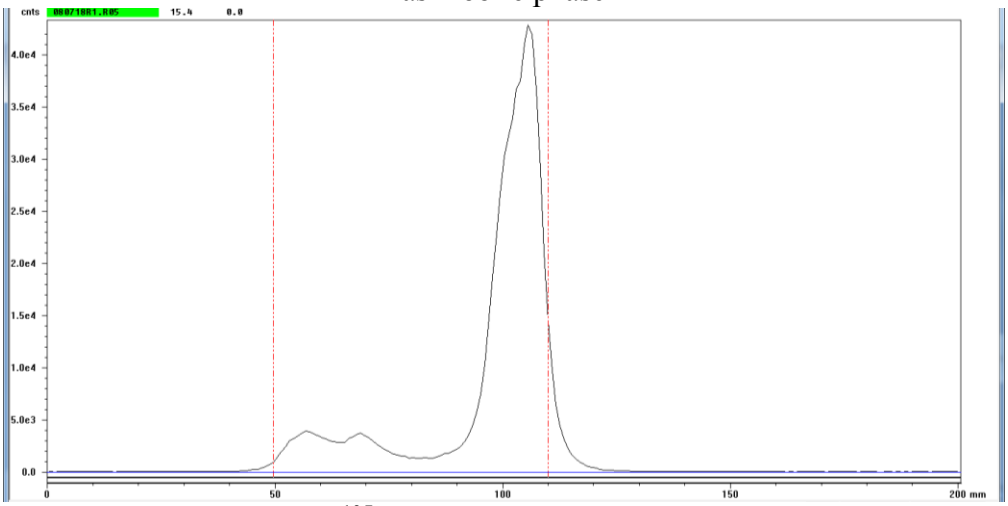


**Figure S4-16.** TLC scan of [$^{105}$**Rh]RhCl$_2$-*16S$_4$diol*** using 0.4M $NaBPh_4$ in ACN as mobile phase

# VITA

Nkemakonam Chukwuebuka Okoye was born on February 26, 1992 in Aba, Abia State, Nigeria to the family of Sir Josiah Okoye and Lady Charity Okoye. He attended Dority International Secondary School where he completed the West African Senior School Certificate Examination in 2009. Nkem moved to the United States of America in August 2010 on a full academic scholarship to attend South Carolina State University (SCSU) in Orangeburg South Carolina. Nkem was involved in undergraduate research in the environmental radiochemistry laboratory at SCSU under the mentorship of Dr. Zheng Chang and subsequently earned his Bachelor of Science degree in Chemistry (with honors) in May, 2014.

Nkem joined the chemistry Ph.D program at the University of Missouri-Columbia in August 2014. Under the supervision of Dr. Silvia S. Jurisson and Dr. Timothy J. Hoffman, Nkem conducted his graduate research on the synthesis and preclinical evaluation of targeted diagnostic and therapeutic radiopharmaceuticals using a range of radiometals including $^{212}$Pb, $^{203}$Pb, $^{177}$Lu, $^{68}$Ga, and $^{105}$Rh. Nkem's academic and research accomplishments were recognized by his award of the 2018 Bradley-Alavi Student Fellowship from the Society of Nuclear Medicine and Molecular Imaging, the 2018 David E. Troutner Radiochemistry Fellowship and the 2019 Breckenridge/Lyons Award for Outstanding Graduate Research both from the University of Missouri Department of Chemistry. In May 2019, Nkem earned his Doctor of Philosophy degree in chemistry with a specialization in radiopharmaceutical chemistry.

Nkem has accepted a postdoctoral fellowship in clinical chemistry at the University of Utah Department of Pathology / ARUP Laboratories. He is excited to broaden his knowledge in radiopharmaceutical chemistry to include other clinical diagnostic systems that analyze changes in a patient's biochemical and physiological function in order to facilitate better medical decisions by clinicians.